LEVEL II

12

AFTAC-TR-80-37

PRELIMINARY RESULTS OF THE VELA SEISMOLOGICAL CENTER RESEARCH PROGRAM IN FY 80 (U)

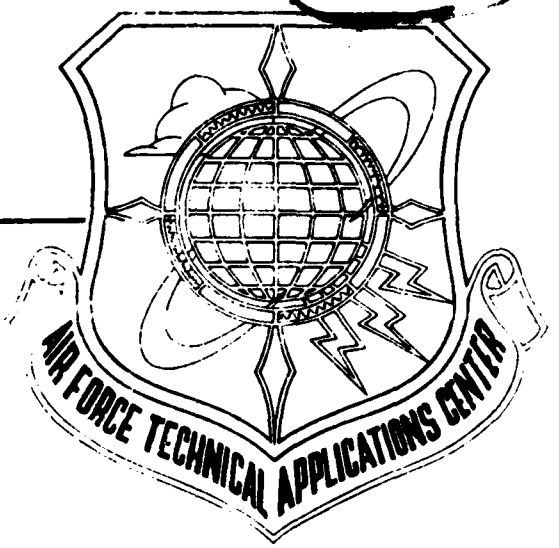

VELA Seismological Center
312 Montgomery Street
Alexandria, Virginia 22314

11 AUGUST 1980

Interim Report. 1 October 1979 - 15 July 1980.

Approved for Public Release; Distribution Unlimited.

AIR FORCE TECHNICAL APPLICATIONS CENTER
HEADQUARTERS UNITED STATES AIR FORCE
PATRICK AIR FORCE BASE, FLORIDA 32925

Unclassified
SECURITY CLASSIFICATION OF THIS PAGE (When Data Entered)

REPORT DOCUMENTATION PAGE

READ INSTRUCTIONS BEFORE COMPLETING FORM

1. REPORT NUMBER: AFTAC-TR-80-37
2. GOVT ACCESSION NO: AD A090 736
3. RECIPIENT'S CATALOG NUMBER:

4. TITLE (and Subtitle): Preliminary Results of the VELA Seismological Center Research Program in FY 80,
5. TYPE OF REPORT & PERIOD COVERED: Interim / 1 Oct 79 - 15 Jul 80,
6. PERFORMING ORG. REPORT NUMBER:

7. AUTHOR(s):
8. CONTRACT OR GRANT NUMBER(s):

9. PERFORMING ORGANIZATION NAME AND ADDRESS:
VELA Seismological Center
312 Montgomery Street
Alexandria VA 22314

10. PROGRAM ELEMENT, PROJECT, TASK AREA & WORK UNIT NUMBERS:

11. CONTROLLING OFFICE NAME AND ADDRESS:
Air Force Technical Applications Center/TD
Patrick Air Force Base FL 32925

12. REPORT DATE: 11 August 1980
13. NUMBER OF PAGES: 265

14. MONITORING AGENCY NAME & ADDRESS (if different from Controlling Office):

15. SECURITY CLASS. (of this report): Unclassified
15a. DECLASSIFICATION DOWNGRADING SCHEDULE:

16. DISTRIBUTION STATEMENT (of this Report)
Approved for Public Release, Distribution Unlimited.

17. DISTRIBUTION STATEMENT (of the abstract entered in Block 20, if different from Report)

18. SUPPLEMENTARY NOTES

19. KEY WORDS (Continue on reverse side if necessary and identify by block number)

Seismic Research	Discrimination
Seismology	Location
VELA UNIFORM	Evasion
Underground Nuclear Explosion	Yield Estimation
Detection	Earthquakes

20. ABSTRACT (Continue on reverse side if necessary and identify by block number)
This report provides a summary of preliminary results of research conducted under the sponsorship of the VELA Seismological Center (VSC) during FY80. Contractors, in preparing this document, were instructed to outline the objectives of each of their research tasks and provide brief summaries of their accomplishments as of July 1980. Final reports which will include detailed discussions of each of the research tasks will be available for Projects VT/0702, VT/0706, VT/0709, VT/0710 and VT/0712 in early FY81. Reports discussing results under other projects will be available later in FY81.

DD FORM 1 JAN 73 1473 EDITION OF 1 NOV 65 IS OBSOLETE

Unclassified
SECURITY CLASSIFICATION OF THIS PAGE (When Data Entered)

The organization of this report is identical to the "VELA Research Program for FY 80" which was submitted to the Defense Advanced Research Projects Agency on 31 May 79. Air Force funded research, although not included in the VELA Research Program, has been inserted at appropriate places within this document so that all VSC funded research is included.

TABLE OF CONTENTS

Lg Wave Propagation in Eurasia

by

Svein Mykkeltveit and Eystein S. Husebye

Project VT/0702/B/PMP

Contractor: NTNF/NORSAR
Post Box 51
N-2007 Kjeller, Norway

Task 1: Regional and Near-field Discrimination

Objective

Using data from Fennoscandian and Asian stations: study the propagation characteristics of seismic waves from events within the USSR to distances of 30^{o}, evaluate the detection capability of the stations in question at these distances, attempt to define a reliable set of seismic event detection and discrimination parameters from the data base and continue research on statistical decision criteria.

Accomplishments

There is considerable interest in the potential usefulness of observations at regional distances in the context of seismic event discrimination. This is the motivation for our study of the relative propagation efficiency of phases like P_g, P_n, S_g, S_n, Lg, (Li) and Rg across various parts of Central Asia and Western Russia with objectives as stated above.

Observational data and analyzing procedures

For obvious reasons, the choice of observational data was limited to mostly record copies from WWSSN stations in southern and western Asia and Fennoscandia. Likewise, the events subjected to analysis are mainly presumed underground explosions in Kazakh, Caspian Sea area, Western Russia and Novaya Zemlya in addition to Central Asian earthquakes (see Fig. 1). Furthermore, the Fennoscandian observations constituted a

W. Russia/Baltic Shield population while the remainder of the data constituted a Eurasian population.

The data analysis was based on reading of all prominent phases in addition to the first onset P-waves within the 5.0-2.5 km s^{-1} group velocity window, with arrival times corresponding to the wave packet onset time. Amplitudes and periods, however, were read for the maximum amplitude-to-period ratio within the same wavepacket. With the data extracted from the WWSSN records we can calculate travel times, group velocities, event magnitudes, amplitude decays and also which component(s) are most prominent as regards higher mode surface wave recordings.

Group velocity observations

Initially, the group velocities associated with all 'local' amplitude maxima were determined both from SP and LP records. The LP observations appear to be mainly of the S_n and Rg types and at that are of the fundamental and the first few higher modes. The general SP observations are somewhat messy exhibiting a roughly continuous distribution of group velocities in the range 4.60 - 3.35 km s^{-1}. This situation is much improved by considering only the most energetic arrival of each seismogram as shown in Fig. 2a for the Baltic Shield/Western Russia region.

The main results are: the Lg stands out rather clearly and with a velocity of about 3.5 km s^{-1}. It is the most likely observable phase of the surface wave type for distances exceeding 18-20 deg. S_n (and Li) is only occasionally the strongest phase. LP records are dominated by Rg phases with velocities slightly below 3.0 km s^{-1}.

Similarly, the Eurasian group velocity data shown in Fig. 2b gave that the Lg (ca 3.50 km s^{-1}) and the S_n (4.20-4.50 km s^{-1}) dominate the SP records whereas Li is never the strongest phase. The LP records are again dominated by Rg arrivals and also slow Lg arrivals. In essence, the only two phases consistently observed were Lg on SP records and Rg on LP records.

Distribution of dominant signal frequencies

The following characteristic features have been observed: i) In the SP records the peak amplitudes are associated with frequencies in the range 0.8-1.2 Hz with the highest frequencies for paths across Western Russia/Baltic Shield. ii) In the LP records, the peak amplitudes are associated with periods in the range 3-7 sec, with a notable difference as regards Rg phases from earthquake and explosions, respectively.

Propagation efficiency/Event detectability

Analysis of short period phase amplitudes is difficult, in particular when the data at hand are a mix of different event/receiver combinations. In our case, the problem is twofold, namely: i) average propagation efficiency of higher mode surface waves as a function of distance and ii) event detectability or how to compare Lg and S_n amplitudes with those of P. Our preference was to tie the scaling of the individual observation to estimates of the amplitude-distance factor in the magnitude formula, using ISC or NOAA reportings for the 'true' event m_b-magnitude.

Amplitude decay across the Baltic Shield and Western Russia

Using the ISC-reported body wave magnitude for the events in question, the corresponding estimates for the magnitude distance factor $B(\Delta)$ for both P and Lg waves are plotted in Fig. 3a, and estimates of $B(\Delta)$ for S_n in comparison with $B(\Delta)$ for Lg are given in Fig. 3b. The analysis was restricted to max. amplitudes of wavelets in the S_n and Lg group velocity windows and all maxima were read on the vertical short period component. In Fig. 3a, we clearly see that P is the strongest phase for distances beyond 10^{o}. A notable exception here is a presumed explosion on the Kola peninsula - where Lg waves are significantly stronger than the P-waves. There is a notable scarcity of observations below 10 deg because there are few observations available and because it is hopeless to read accurately strong signals on analog WWSSN records. Finally, a comparison of vertical amplitude readings with corresponding horizontal ones gave that the latter were larger by a factor of 0.1-0.2 m_b units.

Amplitude decay across Central Asia and the Himalayas

Fig. 4 shows the magnitude distance factor for P and Lg waves as a function of distance for events in the Eurasian data base. The down-pointing arrows indicate a maximum possible value for log(A/T) for Lg. In fact, for these cases there is no sign of clear wave onsets within the appropriate time interval and thus the mentioned arrows indicate the general coda or noise level.

A study of Fig. 4 reveals a very high attenuation/scattering level for the Central Asia/Himalayas region in comparison with the Baltic Shield/ Western Russia area both for P and Lg waves. The average amplitude difference amounts to about half a magnitude unit for both types of waves, and the above remarks on nondetections are liable to increase this difference for Lg waves, keeping in mind that all Baltic Shield/Western Russia observations given are made for readable onsets within the specified group velocity window. For an account of this relatively high attenuation level, we are in favor of a general explanation in terms of complex tectonics and sedimentary covers.

Results/summary

Manual analysis of analog WWSSN station records of earthquakes/explosions in Central Asia and Western Russia gave the following results. P waves (P_g, P_b or P_n) are generally among the very strongest in the SP records. S waves and/or higher mode Love-Rayleigh waves have velocities around 4.5 km s^{-1} (S_n waves), and 3.35-3.54 km s^{-1} (Lg waves). In SP records Lg waves are the most prominent for distances below 10 deg and occasionally for even larger distances. Beyond 15 degrees their amplitudes decrease rapidly. The most efficient transmission paths for Central Asian/W. Russian events appear to be westward towards Fennoscandia, whereas propagation is less efficient towards India, Pakistan and Iran. Irrespective of source type, S_n (approx. 4.5 km s^{-1}) and fundamental mode Rayleigh waves besides occasional P phases dominate the LP records. That high frequency Lg waves should have good event discrimination power is

not obvious from the data analyzed here. We remark, however, that Rg waves exhibit marked differences in periods for earthquakes vis-a-vis explosions.

Concluding remarks

The research report here is somewhat hampered by the lack of digital data from relatively broadband instrumentation. It should suffice to refer to similar studies based on NORSAR data where wave types and propagation effects can be effectively studied by using particle-motion and high-resolution techniques. Similarly, the frequency band 2-10 Hz may prove crucial for surveillance capabilities at the regional distances. Presently, even a comprehensive noise study for this range is lacking. Finally, in future studies more attention should be given to very detailed mapping as regards tectonic regimes.

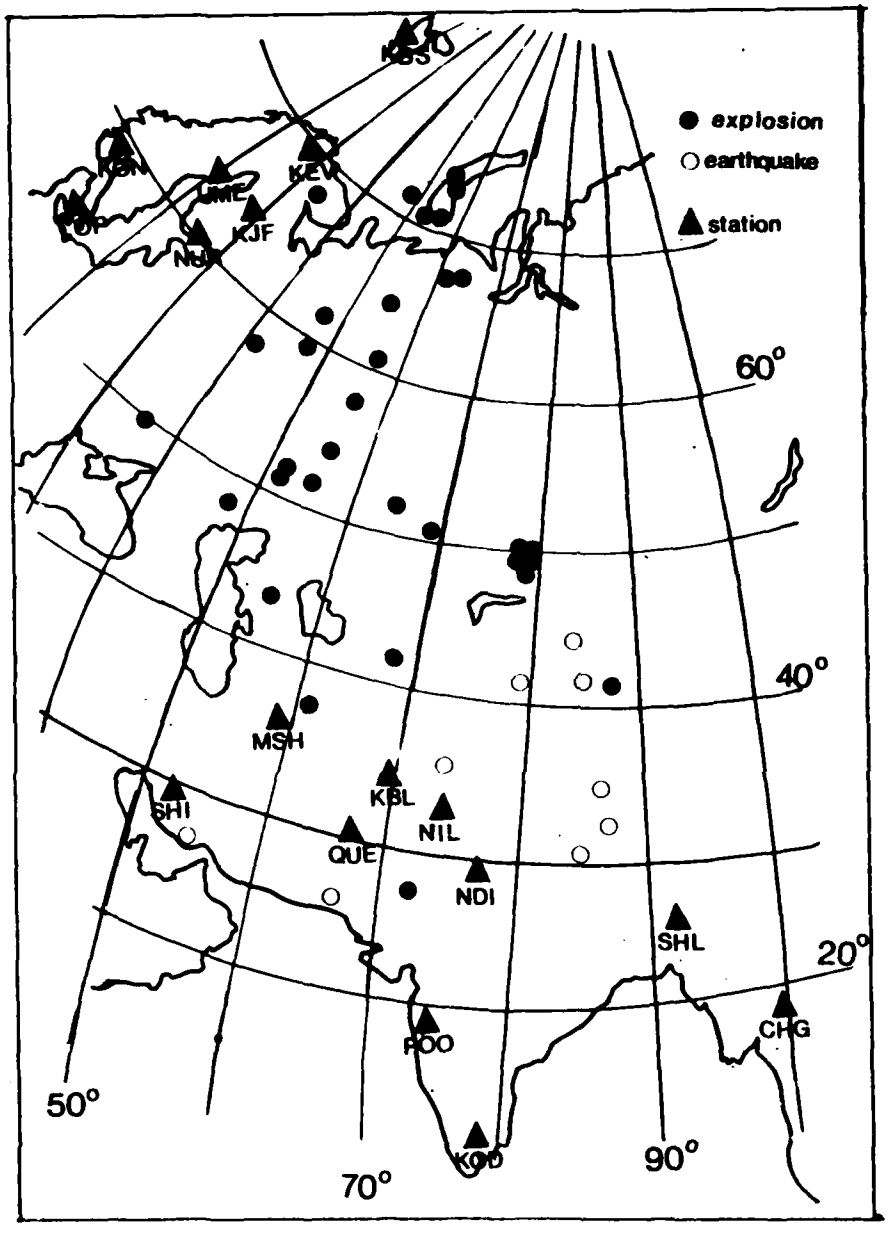

Fig. 1 Events and stations used in this analysis.

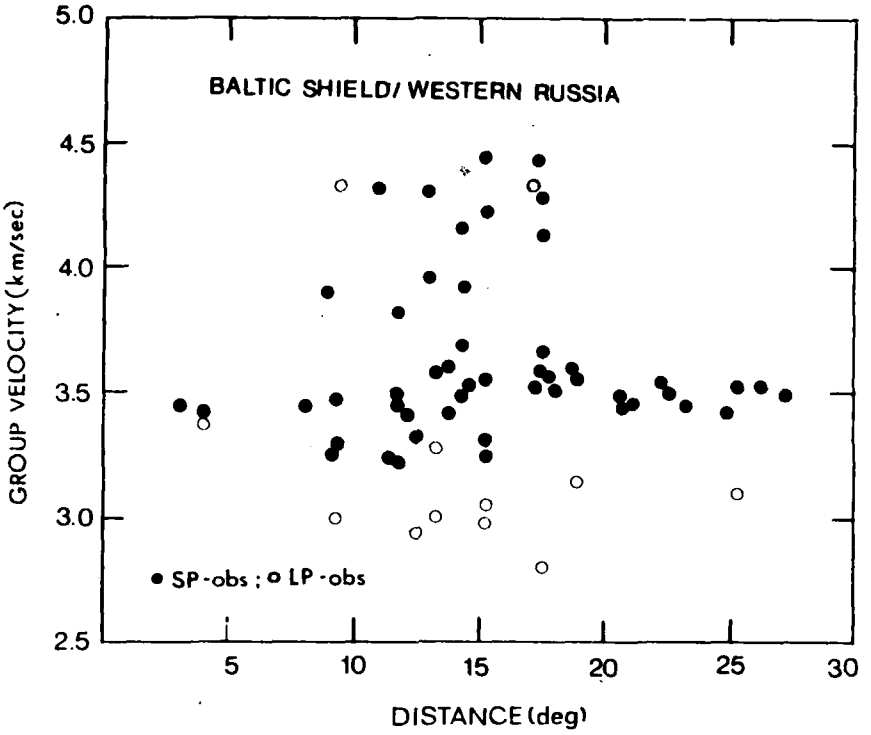

Fig. 2a Group velocity as a function of epicentral distance for the strongest phase within the group velocity window (2.8-5.0) km/s for each seismogram, as recorded by stations in Fennoscandia.

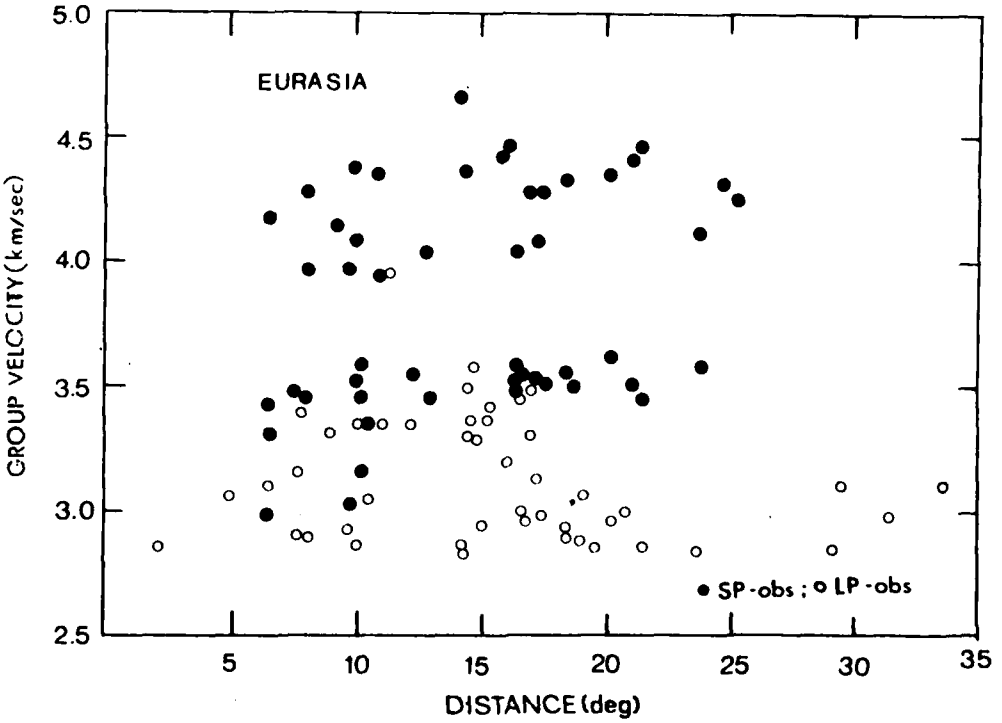

Fig. 2b Same as Fig. 2a for stations in Central Asia.

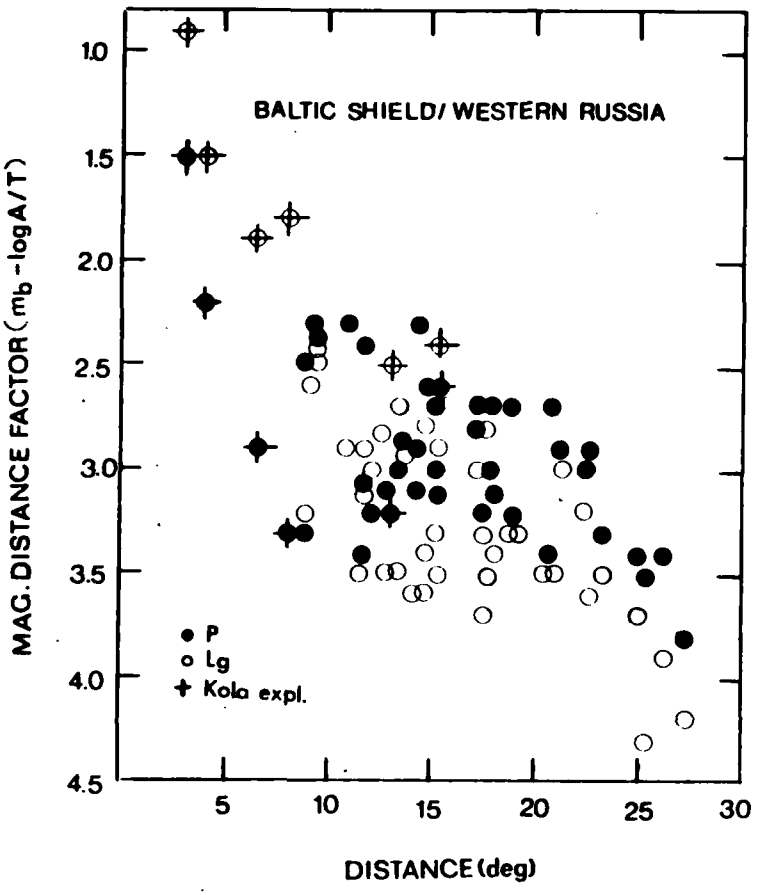

Fig. 3a Magnitude distance factor B(Δ) for P and Lg waves for Fennoscandian stations.

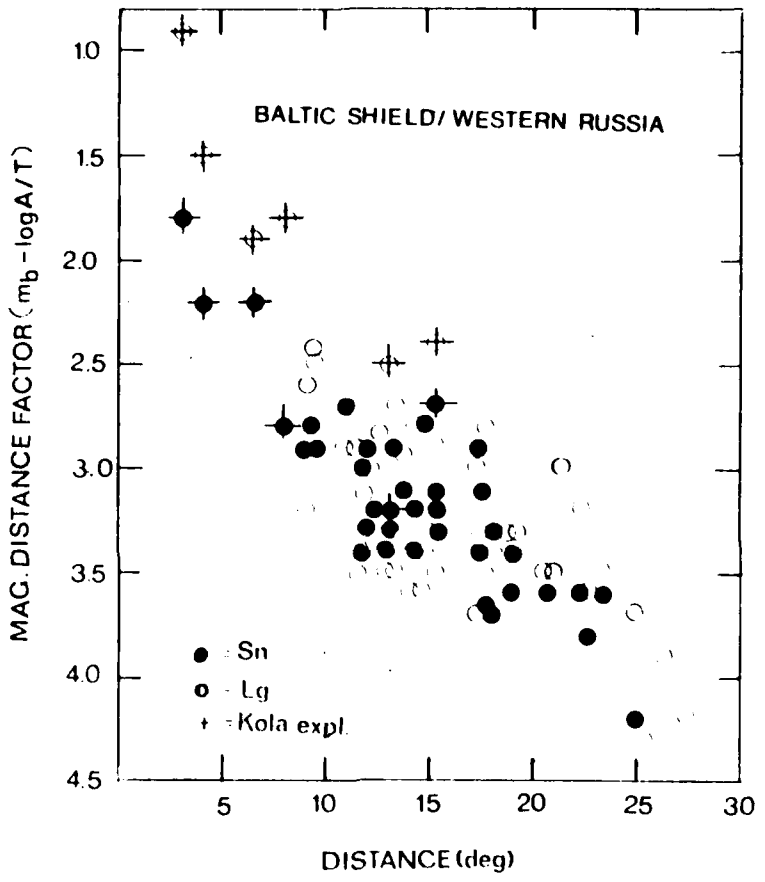

Fig. 3b Same as Fig. 3a for Lg and S_n waves.

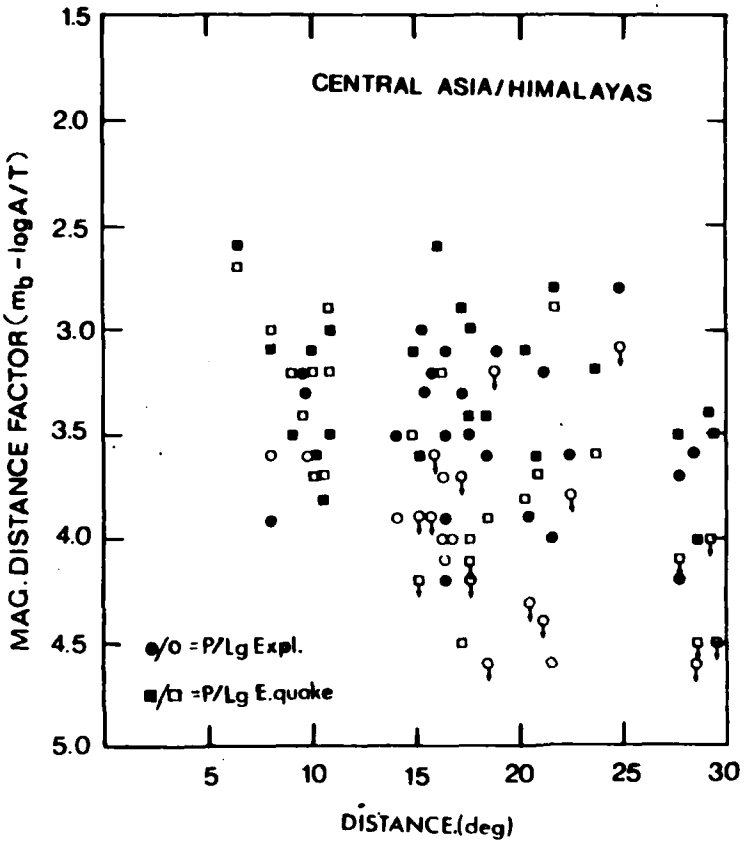

Fig. 4 Magnitude distance factor B(Δ) for P and Lg waves for stations in Central Asia.

Frequency dependent attenuation of short period P and Lg waves in the distance range 0-15° from NORSAR

by

Frode Ringdal and Svein Mykkeltveit

Project VT/0702/B/PMP

Contractor: NTNF/NORSAR
Post Box 51
N-2007 Kjeller, Norway

Task 1: Regional and near-field discrimination

Objective

Using NORSAR data and data from other Scandinavian seismic stations: study the propagation characteristics of seismic waves from events within the USSR to distances of 30°, evaluate the detection capability of the stations in question at these distances, attempt to define a reliable set of seismic event detection and discrimination parameters from the data base and continue research on statistical decision criteria.

Accomplishments

NORSAR short period data from 7 subarrays for explosions and earthquakes within 15 degrees (Fig. 1) have been analyzed to determine attenuation characteristics and signal-to-noise ratios for P and Lg waves at various frequencies. The earthquakes are either felt or classified as earthquakes by various reporting agencies, and the explosions are associated with refraction profiling investigations or reported mining/hydroelectrical power plant activity.

Fig. 2 shows the logarithm of the Lg to P ratio for subarray average amplitude values as a function of epicentral distance for five frequency windows. It is found that Lg is generally larger than P up to about 10 degrees. However, the assessment of the full detection potential of the Lg phase is left for further study. Dominant frequency of P is almost always higher than that of Lg, the differences being most pronounced

beyond 10 degrees. Typical dominant frequencies are 3-5 Hz or higher for P and 1-3 Hz for Lg. These points are illustrated in Fig. 3, where records for two subarrays are shown for a presumed explosion at a distance of 11.7 degrees.

Discrimination on the basis of Lg to P amplitude ratio seems difficult. The explosions in our data base generate surprisingly large Lg waves, and no clear separation between P to Lg amplitude ratios for earthquakes on one side and explosions on the other can be found in any of the five frequency bands.

The data base has recently been extended with additional near events, without changing the conclusions above. However, an interesting observation is that earthquakes originating near the U.K. and in the North Sea at distances greater than 500 km from NORSAR give consistently very small Lg signals recorded at NORSAR. This is most likely due to a strong attenuation across the paths in question. Noting that the crustal structure is of continental type (i.e., no oceanic structures are involved), this attenuation may be due to the thick sedimentary layers with strong lateral inhomogeneities under the North Sea, in combination with crustal effects. This observation may therefore have relevance to the expected Lg wave amplitudes in parts of the USSR characterized by thick sedimentary deposits.

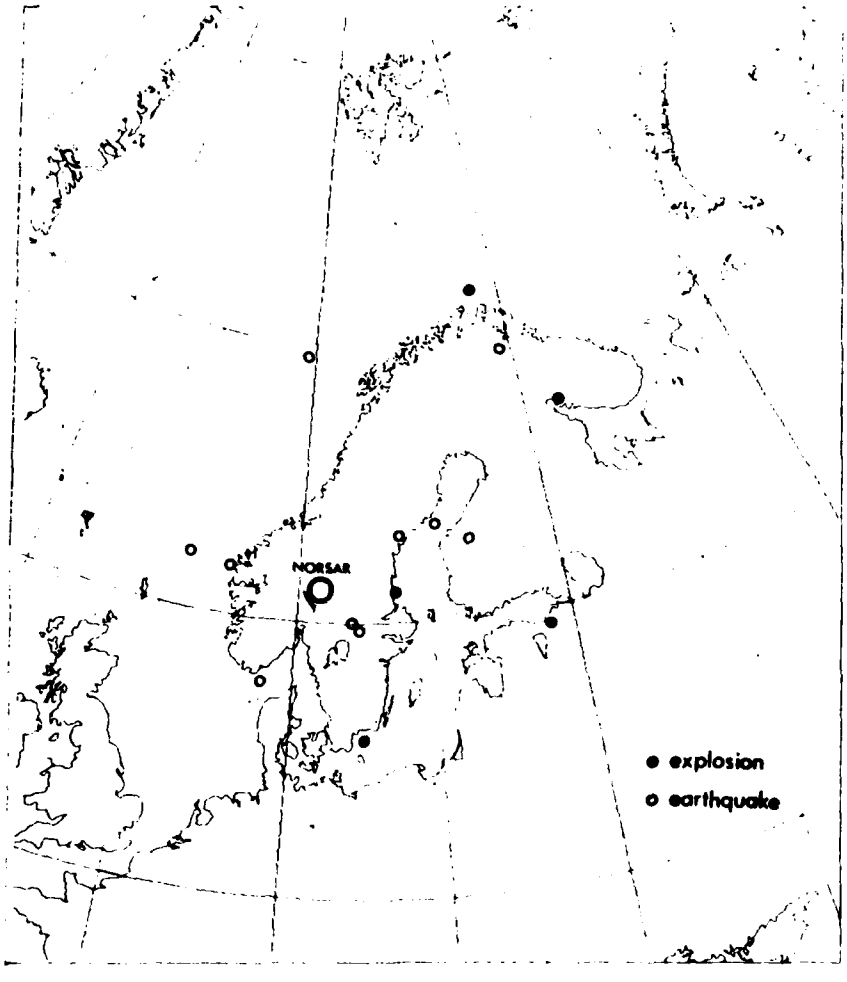

Fig. 1 Earthquake and explosion locations for events analyzed.

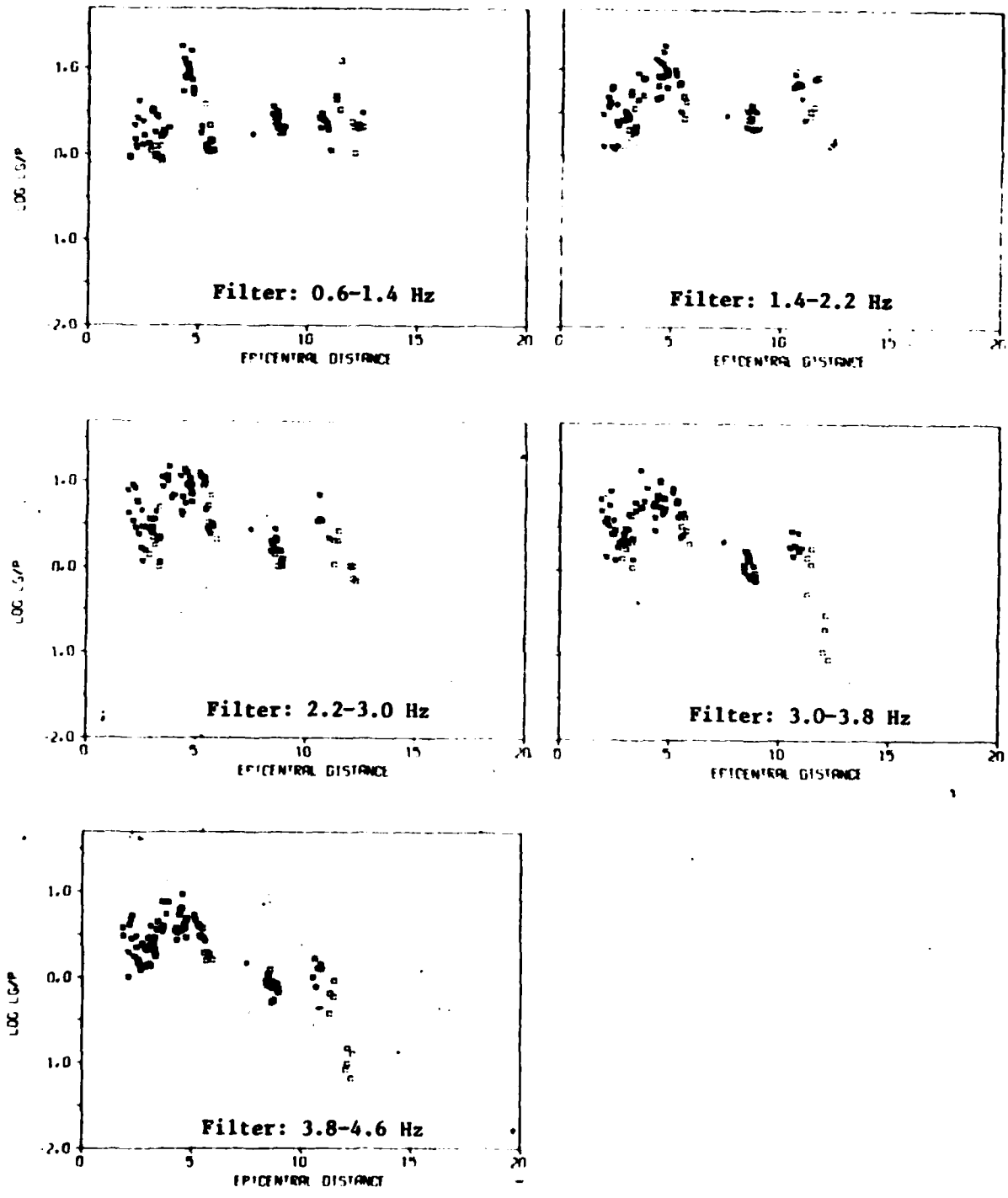

Fig. 2 Lg to P amplitude ratios for five frequency intervals as a function of epicentral distance. Squares indicate explosions; stars denote earthquakes. Each symbol represents an average subarray value.

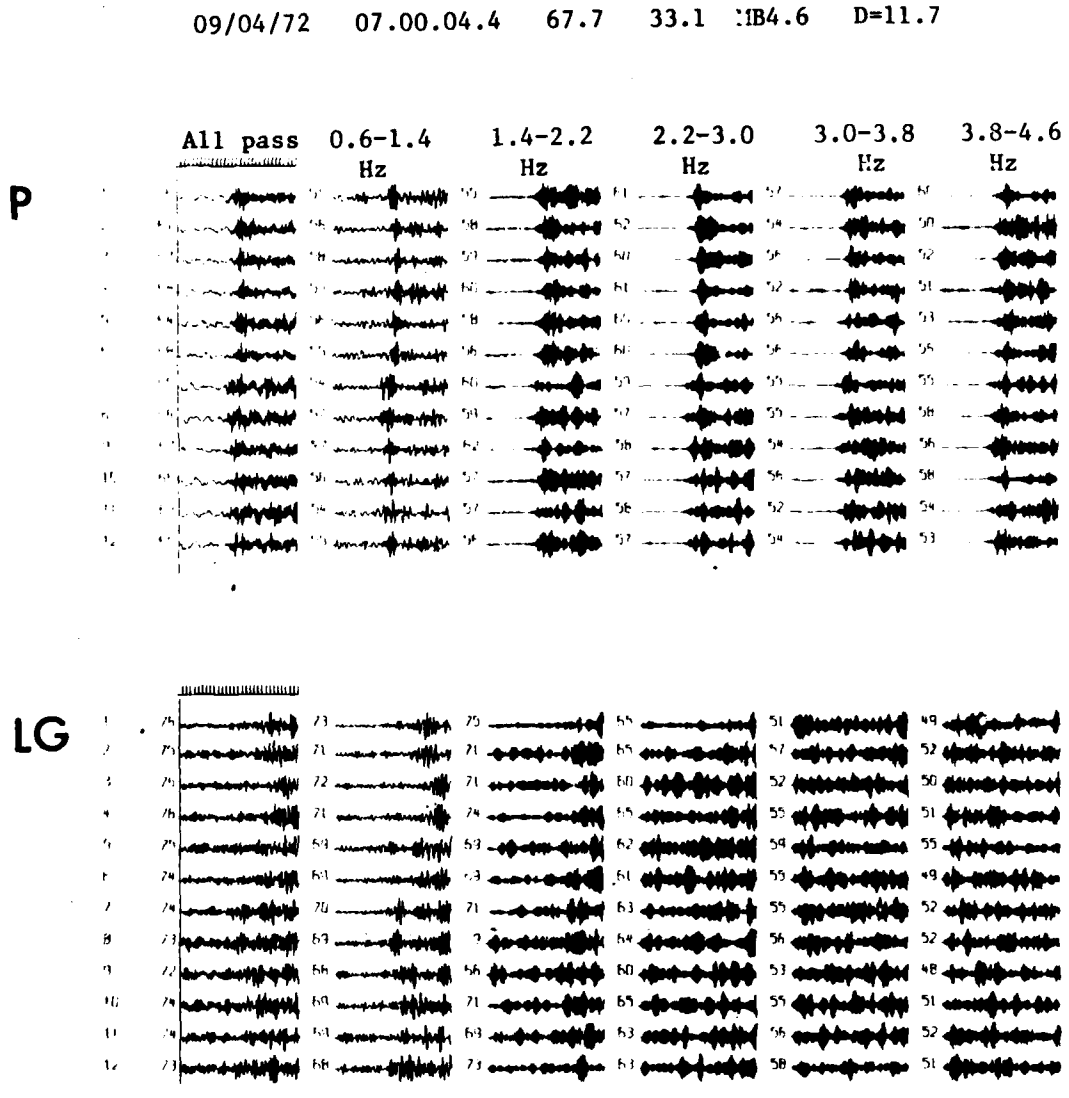

Fig. 3 NORSAR filtered records for subarrays 01A and 01B for a presumed explosion in the Kola peninsula 4 Sept 1972, distance 11.7 degrees from NORSAR. A 30 s interval is covered for both P and Lg wave main arrivals, and the number in front of each trace represents its maximum amplitude in dB relative to 1 quantum unit. Note the rapid falloff of signal-to-noise ratio with increasing frequency for the Lg phase, as compared to P.

PROPAGATION IN SHIELDS (A)

Amplitude-Distance Relationships for Regional Phases in Shield Regions

I. N. Gupta and J. A. Burnetti

Project VT/0709 Contractor: Teledyne Geotech

Task 4.1.1 Propagation in Shields (A)

Objective

By a special survey of the literature, particularly the Soviet literature, and analysis of selected data, determine amplitude-distance relations for regional phases in shields. These are of use for discrimination and for yield estimation.

Accomplishments

We first carried out a detailed review of available Soviet literature on regional phases. Analysis of Russian data on amplitude-distance relationships was performed in order to understand the effects of frequency and propagation path. Data on regional phases from seismographic stations bordering the USSR was also investigated and the results compared with those from other regions. Both earthquake and explosion sources were considered and the usefulness of regional phases for source discrimination was examined. We also examined data on regional phases from earthquakes in the shield areas of Canada which has geological conditions similar to those in the stable platform areas of the Soviet Union.

Review and Interpretation of Soviet Data:

Perhaps the most useful single source of Russian data on regional phases is the monograph by Antonova et al (1978). Other principal sources used in this study are Nersesov and Rautian (1964), Ruzaikin et al (1977), Piwinskii and Springer (1978), and Shishkevish (1979). Most of the data in these studies came from seismographic stations in and near the Tien Shan region and in the region east of 70°E, bordering China and Mongolia. These regions are seismically active and have fairly rugged terrain (Tapponier and Molnar, 1979) and should perhaps be classified as tectonic rather than shield. Most of this area has generally been recognized as one of efficient propagation of L_g (Gupta et al, 1980; Piwinskii and Springer, 1978; Ruzaikin et al, 1977).

The amplitude-distance curves of all regional phases (P_n, P_g, S_n and L_g) are highly variable from one region to another and even from one direction to another (Nersesov and Rautian, 1964; Antonova, 1971). Amplitude-distance relationships for different frequency bands also show significant variations with both azimuthal direction and average passband frequency (Antonova et al, 1978). The amplitude variations in all these studies are relatively the least for the phases L_g and P_g although scatter by a factor of about 2 is rather common even for these two phases. The most stable and the largest amplitude phase is generally L_g, observed to distances of 3000 km or greater. The next most stable and large amplitude arrival is P_g recorded to a distance of only about 1000 km.

Task 4.1.1 Propagation in Shields (A)

Accomplishments continued

Figure 1 shows average amplitude curves of L_g, P_g, S_n and P_n from 40 crustal earthquakes originating in North Tien Shan and recorded by instruments in the same region. The two largest-amplitude phases are L_g and P_g and, on the average, L_g is about three times as big as P_g.

L_g may be regarded as a higher-mode surface wave traveling with minimum group velocity (Nuttli, 1973) so that the time-domain amplitude, A varies with distance, Δ as

$$A = K\Delta^{-1/3} (\sin \Delta)^{-1/2} e^{-\gamma\Delta} \quad (1)$$

where Δ is in degrees, γ is the coefficient of anelastic attenuation and K is a constant. Taking logarithms, equation (1) leads to

$$\log A + f(\Delta) = \log K - \gamma\Delta \log e \quad (2)$$

where $f(\Delta)$ is a known function of Δ. Equation (2), a linear equation suitable for least-squares curve fitting, yielded a γ value of about 0.27 per degree for the L_g amplitudes in Figure 1.

Recent data suggest that P_g may also be regarded as a dispersed surface wavetrain so that equation (1) may be applicable (e.g. Nuttli, 1980a). Using data on P_g amplitudes in Figure 1, a mean value of $\gamma = 0.30$ per degree was obtained. Therefore the attenuation coefficients for L_g and P_g, based on data in Figure 1, are nearly equal.

Data on amplitude-distance curves of L_g and P_g for different frequency bands (Antonova et al, 1978) provide valuable insight into the generation, propagation and spectral characteristics of these two important regional phases. Recordings of earthquakes by a seven-channel ChISS station located at Talgar (approximately 43°N and 77°E) near Alma Ata in northern Tien Shan were used in these studies. The epicentral locations of earthquakes were divided amongst four azimuthal directions relative to the Talgar station: Northeast, East, South, and West. Data from about 800 earthquakes were processed and normalized to a magnitude 5 earthquake.

Amplitude-distance curves of L_g and P_g along different directions show several interesting features. Perhaps the most notable feature is the strong directional dependence of the attenuation coefficient for both P_g and L_g. It may be noted that azimuthal dependence of the efficiency of L_g propagation has been observed for the southeastern United States by Jones et al (1977) and for the western South America by Chinn et al (1980). Assuming the validity of equation (1), the absorption coefficient, γ and the quality factor, Q were obtained for the amplitude-distance curves of L_g and P_g. The results suggested the following inferences: (1) Q increases substantially with frequency for both P_g and L_g, for $\Delta \leq 1000$ km, (2) $Q(P_g)$ is less than $Q(L_g)$ by a factor of 2 to 3 for a given frequency and direction of propagation, (3) $Q(L_g)$ increases substantially for $\Delta > 1000$ km, and (4) L_g travels more efficiently (higher Q) along the Northeast direction than along the West direction whereas P_g is less efficient for propagation along the Northeast direction than along the West direction; this effect is more pronounced for higher frequencies.

Task 4.1.1 Propagation in Shields (A)

Accomplishments continued

A strong increase in Q with frequency has previously been noted for L_g by Molnar et al (1976) for the region between Talgar and Lake Baykal. Using data from underground nuclear explosions at Nevada Test Site, Press (1964) reported Q values for L_g greater than for P_g by a factor of 2 to 3. Rautian et al (1978) pointed out that Soviet scientists have often observed Q for S waves to be greater than Q for P waves; as this is opposite to observations of attenuation in the upper mantle, it is a puzzling result. $Q(L_g)$ increasing with epicentral distance is, probably due to deeper penetration of the crust. The opposite directional effects suggesting that an increased efficiency of L_g may be accompanied by a decreased efficiency of P_g and vice versa is very hard to explain. However, the presence of strong L_g and weak P_g in EUS and weak L_g and strong P_g in WUS are perhaps manifestations of the same puzzling feature of P_g and L_g phases.

Data on amplitude-distance curves of L_g, P_g, and P or P_n for different frequency bands (Antonova et al, 1978) were used to obtain L_g/P_{max} versus Δ curves for three different frequency bands. Results are shown in Figure 2 for the Northeast direction and in Figure 3 for the West direction. Both figures show that L_g/P_{max} decreases with frequency and this ratio is larger and more stable for dominant frequency of 0.35 Hz or period about 3 sec. Instruments with peak response in the neighborhood of 3 sec may therefore be more suitable for source discrimination on the basis of L_g/P_{max} than the conventional short-period instrument (such as the WWSSN instrument) with peak response at about 0.7 sec.

Analysis of Data from Stations Outside USSR:

Previous studies of the spatial attenuation of regional phases from earthquakes in Russia, based on data recorded outside the Soviet Union, have been very few and not very successful. For example, North and Lande (1978) attempted to obtain amplitude-distance curves for regional phases from Soviet PNEs recorded at WWSNN stations but "the results were uniformly hopeless." Nuttli (1980b) studied the attenuation of L_g waves in western and central Asia and found the anelastic attenuation coefficient to vary over a very large range, 0.04/deg to 0.50/deg.

We first examined regional phases on records from both earthquake and explosion sources in western USSR. However, the amplitude-distance plots showed too much scatter to yield reliable attenuation relationships. Furthermore, no clear separation was evident between the earthquake and explosion populations. The lack of a uniform attenuation relationship for L_g is not surprising in view of the existence of paths of efficient and inefficient propagation of L_g in this region (Gupta et al, 1980; Piwinskii and Springer, 1978; Ruzaikin et al, 1977).

Data from paths within the region of efficient propagation of L_g were next considered. Results from 7 earthquakes and 9 explosions are shown in Figure 4 wherein data from only four stations are included. L_g paths to only KBL and MSH lie within the region of efficient propagation and the earthquake and explosion data from these two stations show significant discrimination.

Task 4.1.1 Propagation in Shields (A)

Accomplishments continued

Earthquake data suggest an attenuation coefficient, γ of about 0.1/deg. Data from the other two stations, SHI and QUE, show much greater attenuation of L_g, in agreement with the earlier results of Gupta et al (1980).

The results from KBL and MSH, as shown in Figure 4, appear encouraging from the viewpoint of source discrimination. However, the data are limited in the number of both sources and recording stations considered. Both KBL and MSH lie in regions of complex geology wherein the local attenuation of L_g is known to be high (Nuttli and Springer, 1978; Nuttli, 1980a). Recently, Nuttli (1980b) considered the attenuation of L_g in the western and central parts of the Soviet Union and concluded that, although the amplitude ratios of L_g to P on the average are larger for earthquakes than for explosions, there is much overlap so that the ratio appears not to be a useful discriminant between earthquakes and explosions. A large number of L_g propagation paths in Nuttli's study are, however, through regions of known inefficient propagation of short-period L_g, see, for example, Piwinskii and Springer (1978, Figure 1) and Gupta et al (1980, Figure 2). The areas investigated in the two studies are not the same. There is only one event (explosion of 24 November 1972 in West Kazakhstan) common to both studies and it is interesting to note that in Nuttli's study, its path to MSH indicated a value of $\gamma = 0.12$/deg, nearly the same as in this study. It is recommended that data from additional sources and stations should be examined before the usefulness of L_g as a source discriminant can be established.

Results from the Canadian Shield Region

Short-period vertical-component records of 7 earthquakes in the Canadian Shield region were obtained. The quality of data was generally poor and only four earthquakes provided usable data for amplitude-distance relationships. Results for L_g amplitudes are shown in Figure 5. There is considerable scatter in the data but the least-squares regression yielded an attenuation rate of r^{-n} where $n = 1.79 \pm 0.35$. This rate is only slightly smaller than the rate of r^{-2} for L_g in EUS (Blandford et al, 1980). The level of L_g excitation and fall-off with distance for EUS, based on Nuttli (1973), is also indicated in Figure 5. It is interesting to note that, in spite of the scatter in data, L_g amplitudes in Canadian Shield appear to be somewhat larger and/or the spatial attenuation is somewhat smaller than in EUS. These results are consistent with the limited data on attenuation of L_g in published literature (e.g. Horner et al, 1978, Figure 14).

References

Antonova, L. V. (1971). Investigations of the field of dynamic features of seismic oscillations, Experimental Seismology, Publishing House "Nauka", Moscow, 107-112.

Antonova, L. V., F. F. Aptikayev, R. I. Kurochkina, I. L. Nersesov, A. V. Nikolayev, A. I. Ruazykin, E. N. Sedova, A. V. Sitnikov, F. S. Tregub, L. D. Fedorskaya and V. I. Khalturin (1978). Experiment Seismic Studies of the Earth's Interior, Institute of Physics of the Earth, USSR Academy of Sciences, Nauka, Moscow, 155 pp.

Task 4.1.1 Propagation in Shields (A)

References continued

Blandford, R. R., R. Hartenberger and R. Naylor (1980). Regional amplitude-distance relations, discrimination and detection, SDAC-TR-80-6, Teledyne Geotech, Alexandria, Virginia, (in preparation).

Chinn, D. S., B. L. Isacks and M. Barazangi (1980). High-frequency seismic wave propagation in western South America along the continental margin, in the Nazca plate and across the Altiplano, Geophys. J. R. Astr. Soc., 60, 209-244.

Gupta, I. N., B. W. Barker, J. A. Burnetti and Z. A. Der (1980). A study of regional phases from earthquakes and explosions in Western Russia, Bull. Seism. Soc. Am., 70, 851-872.

Horner, R. B., A. E. Stevens, H. S. Hasegawa and G. LeBlanc (1978). Focal parameters of the July 12, 1975 Maniwaki, Quebec earthquake - an example of intraplate seismicity in eastern Canada, Bull. Seism. Soc. Am., 68, 619-640.

Jones, F. B., L. T. Long and J. H. McKee (1977). Study of the attenuation and azimuthal dependence of seismic-wave propagation in the southeastern United States, Bull. Seism. Soc. Am., 67, 1503-1513.

Molnar, P., I. L. Nersesov, A. I. Ruzaikin and V. I. Khalturin (1976). L_g waves and their propagation in Central Asia, Collection of Articles on Soviet - U. S. Investigations on Earthquake Prediction, Publishing House "Donish", Dushambe - Moscow (in Russian).

Nersesov, I. L. and R. G. Rautian (1964). Kinematics and dynamics of seismic waves to distance of 3500 km from the epicenter, Akad. Nauk. SSSR, Trudy Inst. Fiziki Zemli, 32(199), 63-87.

North, R. G. and L. C. Lande (1978). Crustal phases from Soviet PNEs recorded at WWSSN stations, Seismic Discrimination, Semi-annual Technical Summary Report, 1 Oct. 1977 to 31 Mar. 1978, Lincoln Lab, M.I.T., Lexington, Massachusetts, 7.

Nuttli, O. W. (1980a). The excitation and attenuation of seismic crustal phases in Iran, Bull. Seism. Soc. Am., 70, 469-485.

Nuttli, O. W. (1980b). On the attenuation of L_g waves in western and central Asia and their use as a discriminant between earthquakes and explosions, presented at the VSC meeting at Buffalo, New York, May 1980.

Nuttli, O. W. (1973). Seismic wave attenuation and magnitude relations for eastern North America, J. Geophys. Res., 78, 876-885.

Piwinskii, A. J. and D. L. Springer (1978). Propagation of L_g waves across Eastern Europe and Asia, Report UCRL-52494, Lawrence Livermore Laboratory, Livermore, California.

References continued

Press, F. (1964). Seismic wave attenuation in the crust, J. Geophys. Res., 69, 4417-4418.

Rautian, T. G., V. I. Khalturin, V. G. Martinov and P. Molnar (1978). Preliminary analysis of the spectral content of P and S waves from local earthquakes in Garm, Tadjikistan region, Bull. Seism. Soc. Am., 68, 949-971.

Ruzaikin, A. I., I. L. Nersesov, V. I. Khalturin and P. Molnar (1977). Propagation of L_g and lateral variations in crustal structure in Asia, J. Geophys. Res., 82, 307-316.

Shishkevish, C. (1979). Propagation of L_g seismic waves in the Soviet Union, Report N-1014-ARPA, Rand Corporation, Santa Monica, California.

Tapponnier, P and P. Molnar (1979). Active faulting and cenozoic tectonics of the Tien Shan, Mongolia, and Baykal regions, J. Geophys. Res., 84 3425-3459.

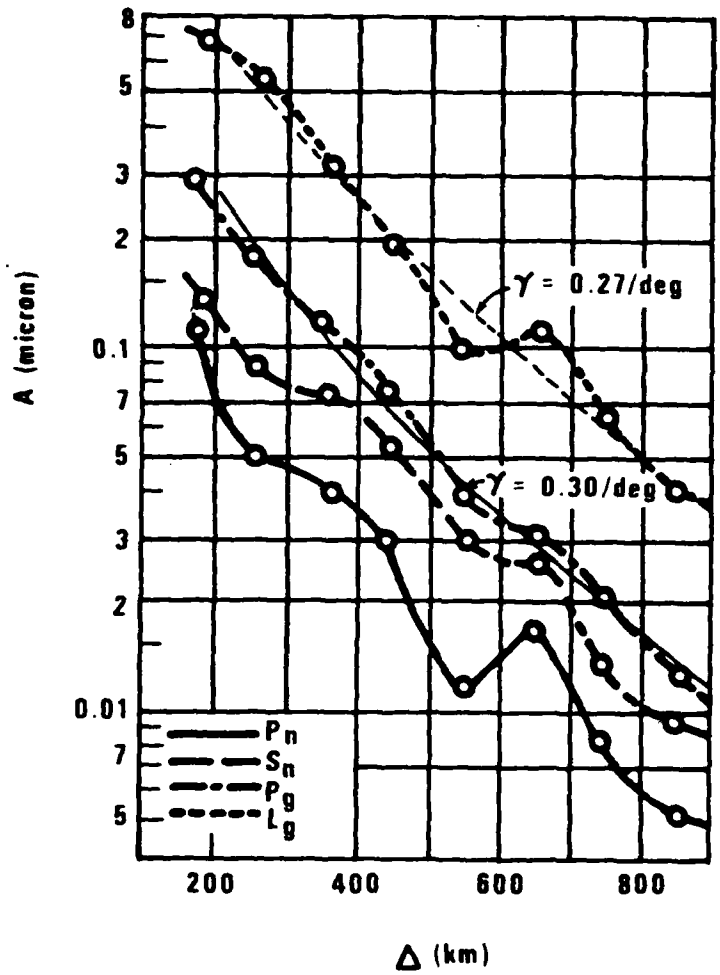

Figure 1. Average amplitude, A versus distance, Δ curves of regional phases L_g, P_g, S_n, and P_n for the North Tien Shan region (after Figure 9, Shishkevish, 1979). The two thin-line curves represent theoretical least-squares fit to the observed data.

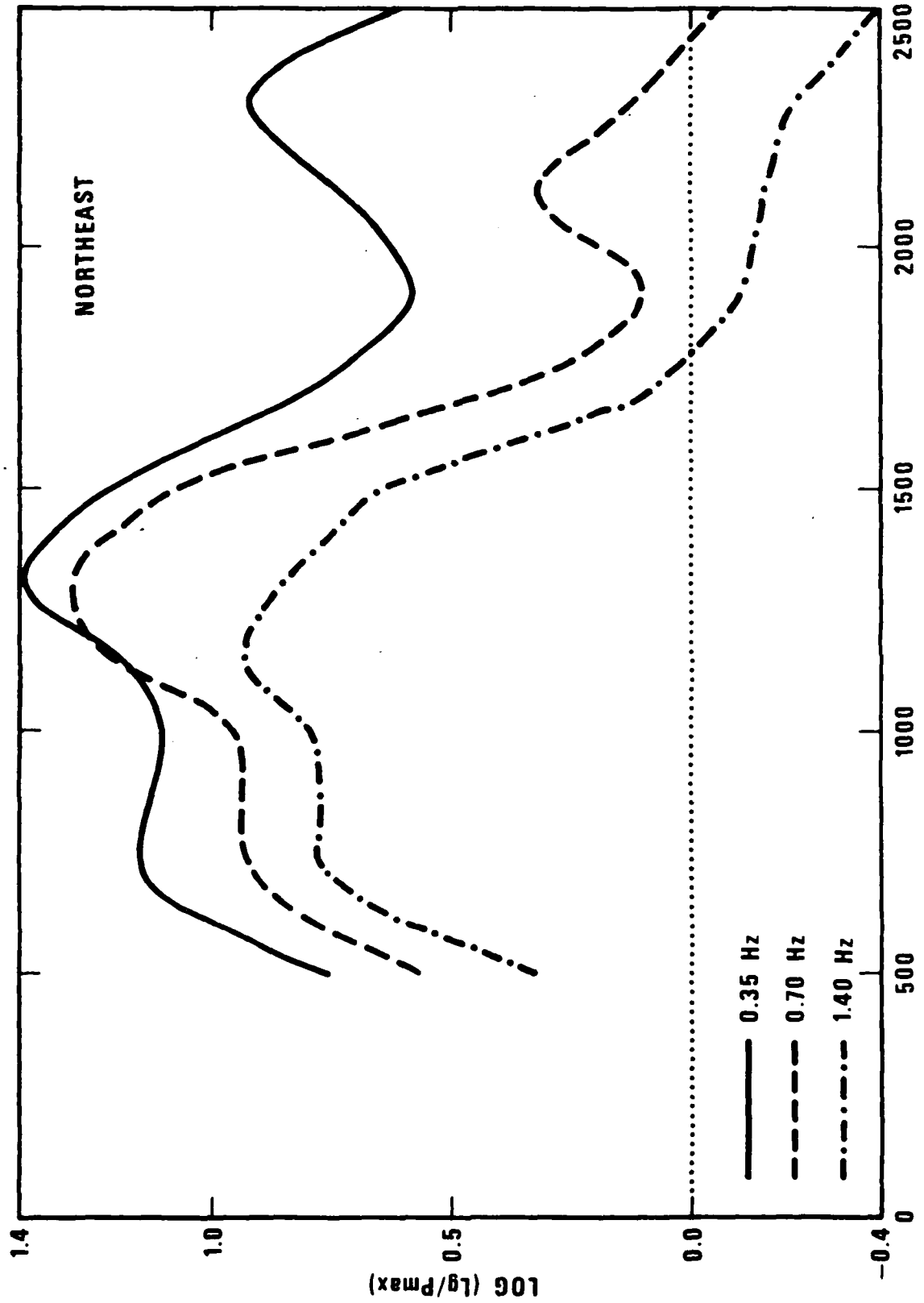

Figure 2. Amplitude-distance curves of Lg/P_{max} for three frequency bands for the Northeast direction, based on Antonova et al (1978).

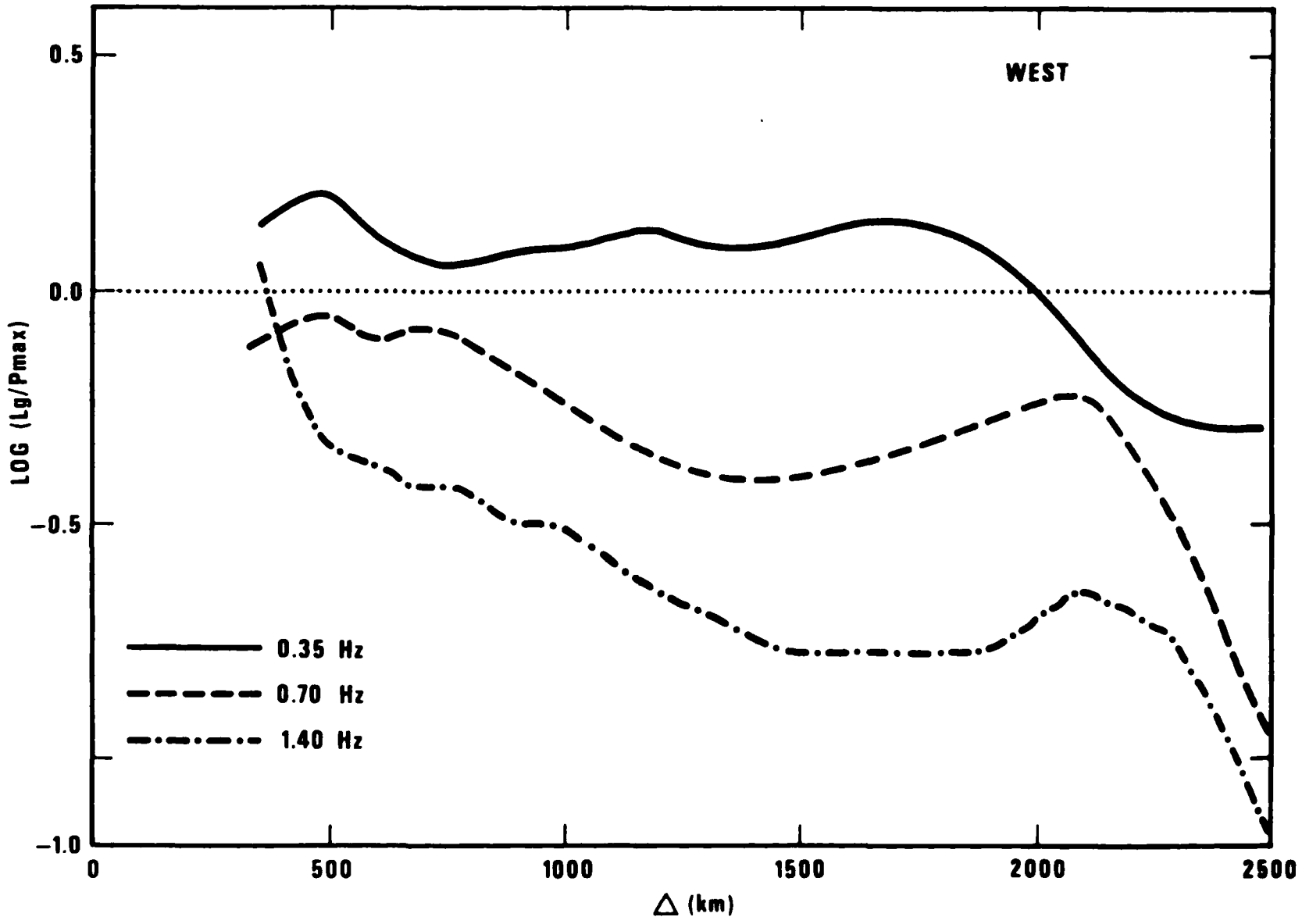

Figure 3. Amplitude-distance curves of L_g/P_{max} for three frequency bands for the West direction, based on Antonova et al (1978).

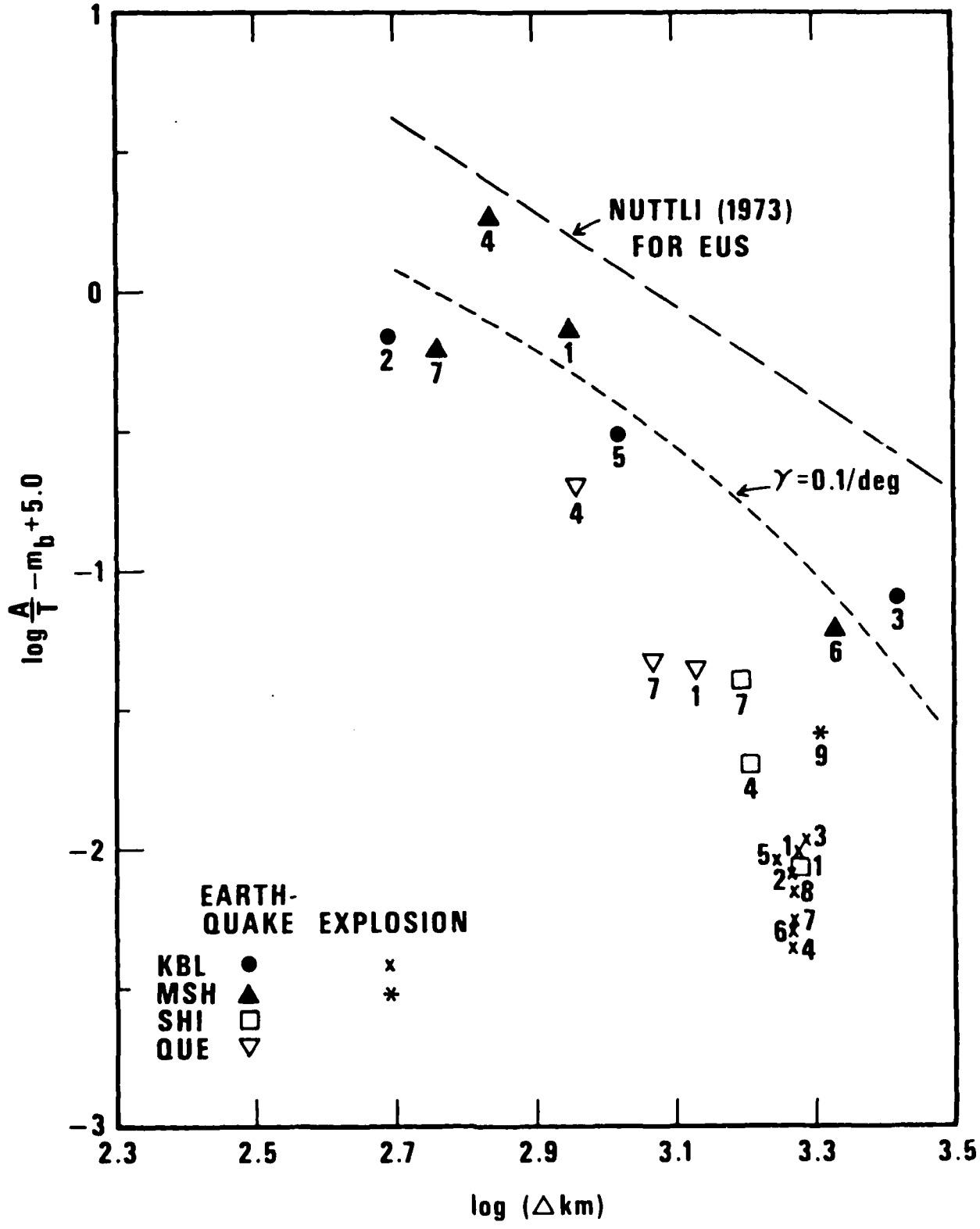

Figure 4. Normalized L_g amplitude-distance data from four stations outside the USSR. L_g paths from 7 earthquakes and 9 explosions to KBL and MSH are through regions of efficient propagation of L_g and to SHI and QUE are partly through regions of inefficient propagation of L_g. Earthquake data from KBL and MSH suggest attenuation coefficient, γ of about 0.1/deg. Nuttli's (1973) curve for L_g in EUS is also shown for comparison.

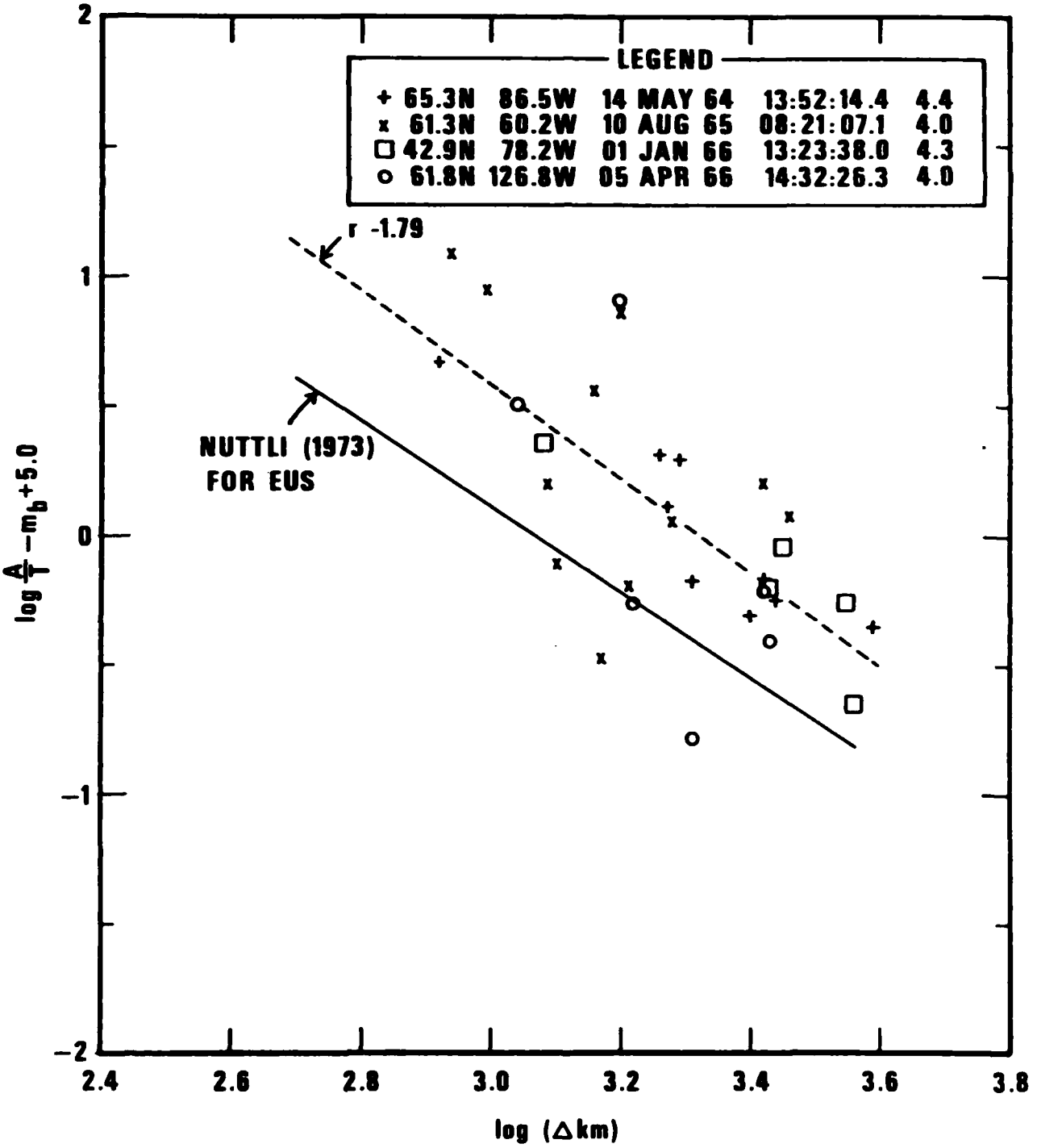

Figure 5. Normalized L_g amplitude-distance data from four earthquakes in the Canadian Shield region with the four different symbols denoting the four events. The least-squares regression line with slope of -1.79 is shown along with Nuttli's (1973) L_g attenuation curve for EUS.

PROPAGATION IN SHIELDS (B)

Site Effects on Regional Phases

Z. A. Der, A. O'Donnell, M. Marshall, and D. W. Rivers

Project VT/0709 Contractor: Teledyne Geotech

Task 4.1.1 Propagation in Shields (B)

Objective

The objective of this section is to understand the effects of site geology on regional phase amplitudes and coda shapes. These measurements are crucial for yield determination and discrimination.

Accomplishments

In our previous work at NTS we have shown that at sites underlain by low velocity materials the amplitudes of the regional phases P_g and L_g were amplified by factors up to 10, and the envelope shapes of both phases also changed, resulting in a prolongation of wavetrains at those sites (Barker et al, 1980). The observed site effect for L_g and P_g appears, therefore, to be several times greater than that for teleseismic P and would seriously affect any yield estimates based on measurements on these phases. The sites at NTS were closely spaced such that differences in paths, as manifested in multipathing, source radiation patterns and varying geophysical properties along the paths, should not seriously affect the conclusions about site effects.

To further investigate site effects we have undertaken the analysis of regional phase amplitudes at LRSM stations located in the north-central region of the US and some adjoining regions of Canada. The stations analyzed thus far are shown in the enclosed map (Figure 1) showing the events used. Amplitudes of all identifiable regional phases were read at each station. In addition, for L_g the envelope shape was characterized by noting the time of the onset of the phase, the time at the maximum, and finally, where the envelope decreased to one-half of the maximum. The L_g amplitudes used in the estimation of site effects were at the maximum of the magnitude.

The L_g amplitudes were corrected to a common distance of 500 km using the Δ^{-2} fall-off rate appropriate to the EUS. The station sites were subdivided into two groups: hardrock sites and sedimentary sites. Hardrock sites were defined as stations resting on granitic or consolidated lower Paleozoic rocks having no more than 50 m of overlying unconsolidated rock cover. All sites not satisfying these criteria were classified as sedimentary sites. This subdivision is indicated in Figure 1. The distance corrected amplitudes were also corrected for event magnitude by dividing them with the average of the hardrock site amplitudes. Histograms of these reduced amplitudes of L_g for the two types of sites (Figure 2), clearly show the effect of site amplification. The average of the sedimentary site amplitudes is larger by a factor of 1.55 (about .19 amplitude units). This contrast is considerably less than at NTS. This is explainable by the fact that the sedimentary sites we examined do not have the thick, extremely low-velocity sediments or volcanics present at Pahute Mesa and Yucca Flats, and many sedimentary sites actually rest on fairly well consolicated rocks.

Task 4.1.1 Propagation in Shields (B)

Accomplishments continued

The P_n and P_g amplitudes were reduced by the regional fall-off rate written as (Alsup, 1972) $\Delta^{-2} \exp(-\pi f(\Delta/8.1) \cdot (1/Q))$ where the values f = 3 Hz and 2.5 Hz and for P_n and P_g were used together with Q = 1000.

The frequencies used were determined by measuring the records. After correcting for event magnitudes we obtained histograms for the two types of sites; these are shown in Figures 3 and 4, respectively. The site effect due to sediments appears to be quite large, .36 magnitude units for P_g and .27 for P_n. The scatter in all histograms is less for the hardrock group, a fact explainable by the more restrictive criteria applied in their selection, while sedimentary sites contain structures with a wide variation in the thickness of sediments. The differences between the "hardrock" and sedimentary groups is highly significant statistically, at least at the 95% level.

In addition to effects on amplitudes, the envelope shapes of L_g are also changed by sediments and possible multipathing effects. The envelope shapes characterized by the arrival times of L_g maxima and the 1/2 max points were examined by plotting these times as functions of distance for all the events. The first observation one can make is that sedimentary sites tend to have longer codas and tend to have late arrivals for the maximum of the L_g. This tendency, however, is not clear on all the plots. Another observation that may be more important is the similarity in coda characteristics for events that come from the same source region. The effect often overshadows the site geology effect. For instance, for a group of events at Baffin Bay there are some remarkable similarities in the coda characteristics at common stations (Figure 5). The most likely explanation for these similarities is that lateral focusing and multipathing patterns are likely to be similar for events coming from the same source region. The above findings indicate that time domain envelope shapes of L_g are quite fragile and cannot be used to derive details of source characteristics unless their behavior is better understood. The stations analyzed in this study cover a wide area, unlike NTS, and, therefore, lateral focusing plays a great role. These findings are similar to those of von Seggern (1980).

References

Alsup, S. A. (1972). Estimation of upper mantle Q beneath the United States from P_n amplitudes, Ph.D. Thesis, George Washington University, Washington, D.C.

Barker, B. W., Z. A. Der and C. P. Mrazek (1980). The effect of crustal structure on the regional phases P_g and L_g at NTS, Stuides of Seismic Wave Characteristics at Regional Distances, AL-80-1, Teledyne Geotech, Alexandria, Virginia.

von Seggern, D. (1980). Source, path and station effects on L_g propagation in North America, Trans. Am. Geophys. Union (EOS), 61, 307.

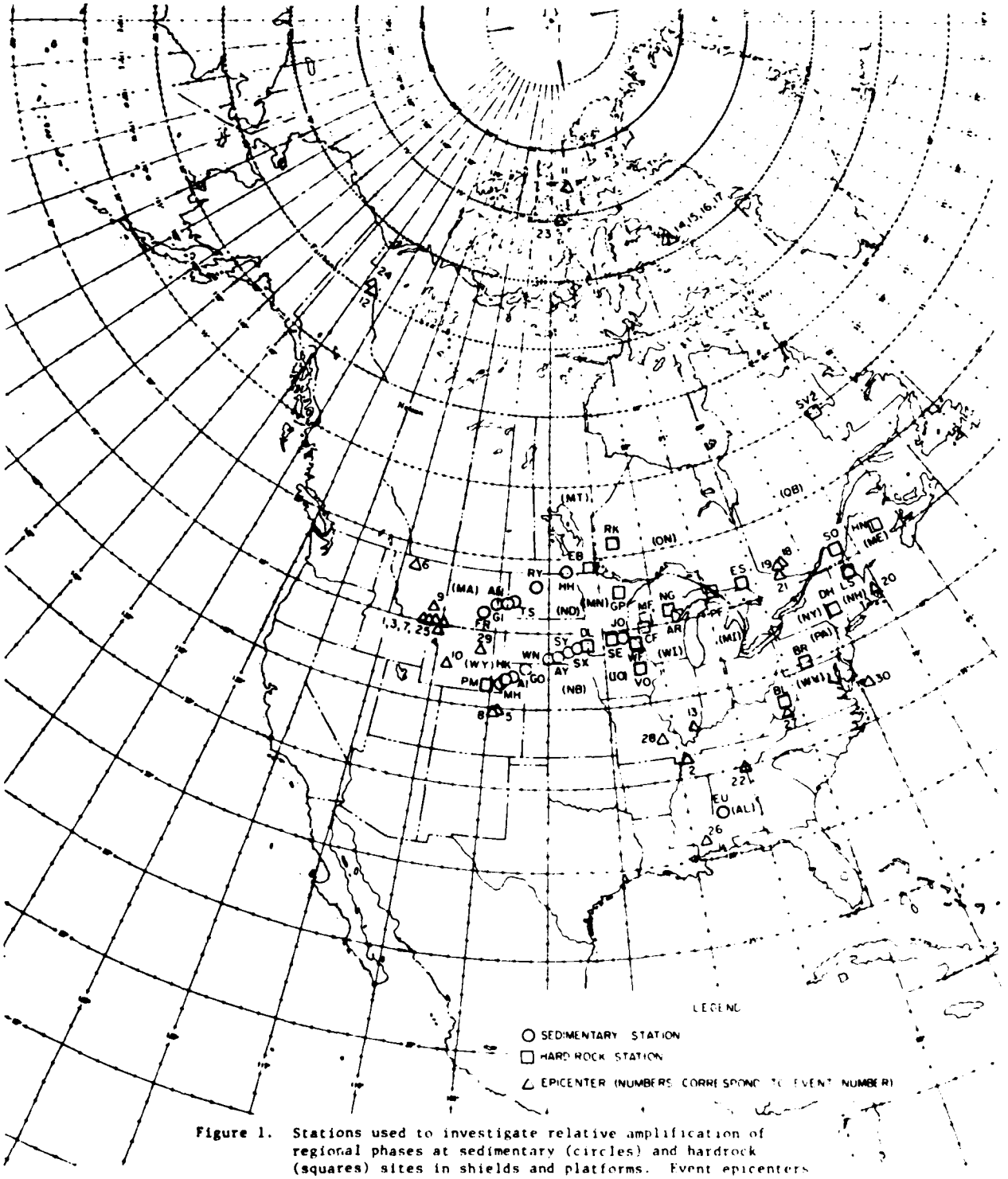

Figure 1. Stations used to investigate relative amplification of regional phases at sedimentary (circles) and hardrock (squares) sites in shields and platforms. Event epicenters (triangles) are also indicated.

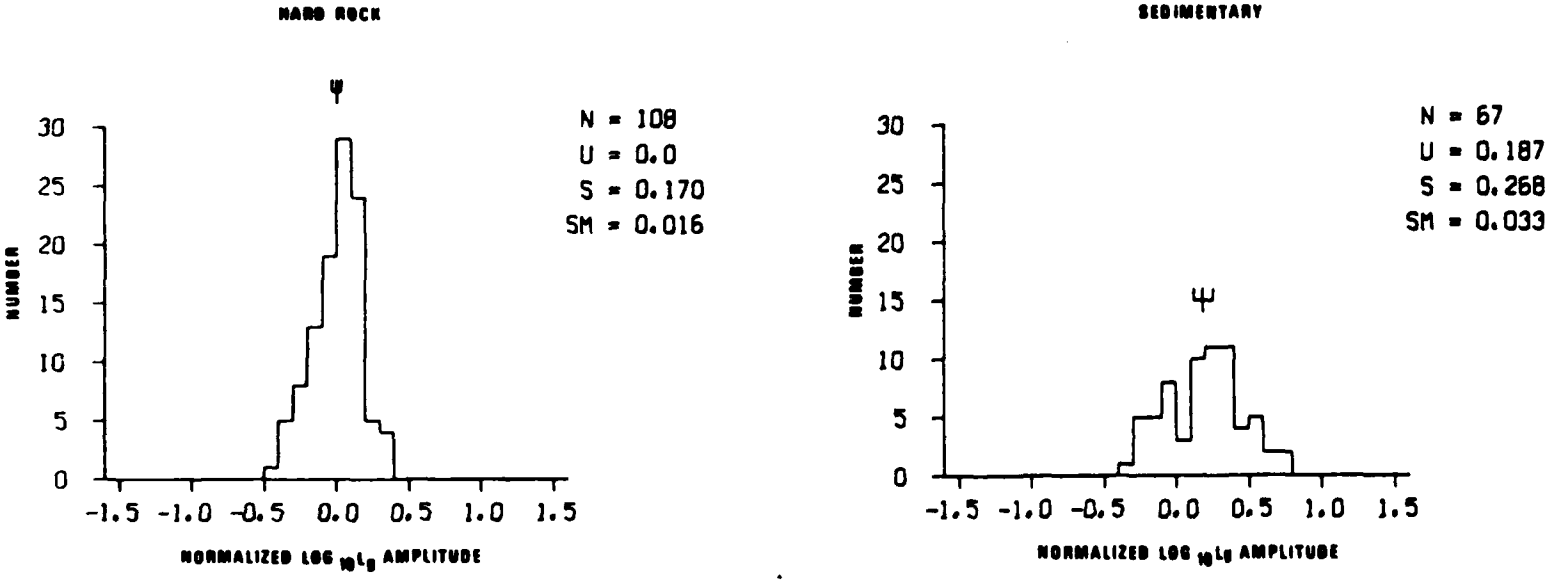

Figure 2. Difference in station magnitudes between hardrock and sedimentary sites for L_g.

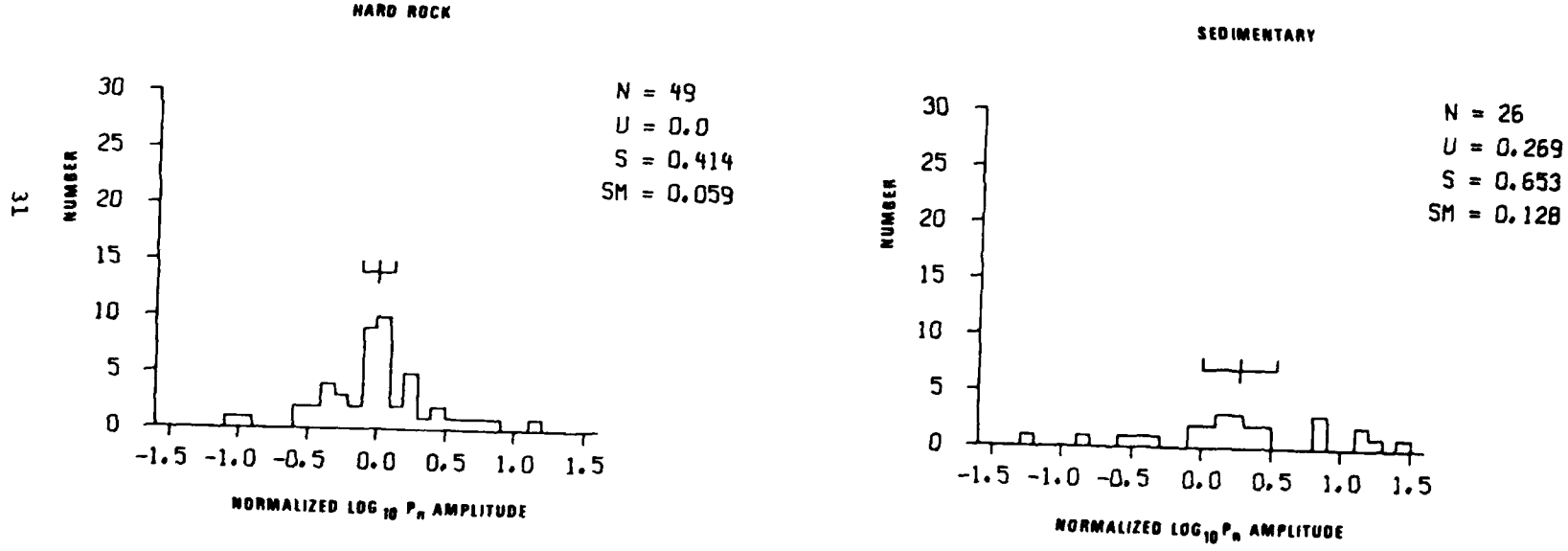

Figure 3. Difference in station magnitudes between hardrock and sedimentary sites for P_n.

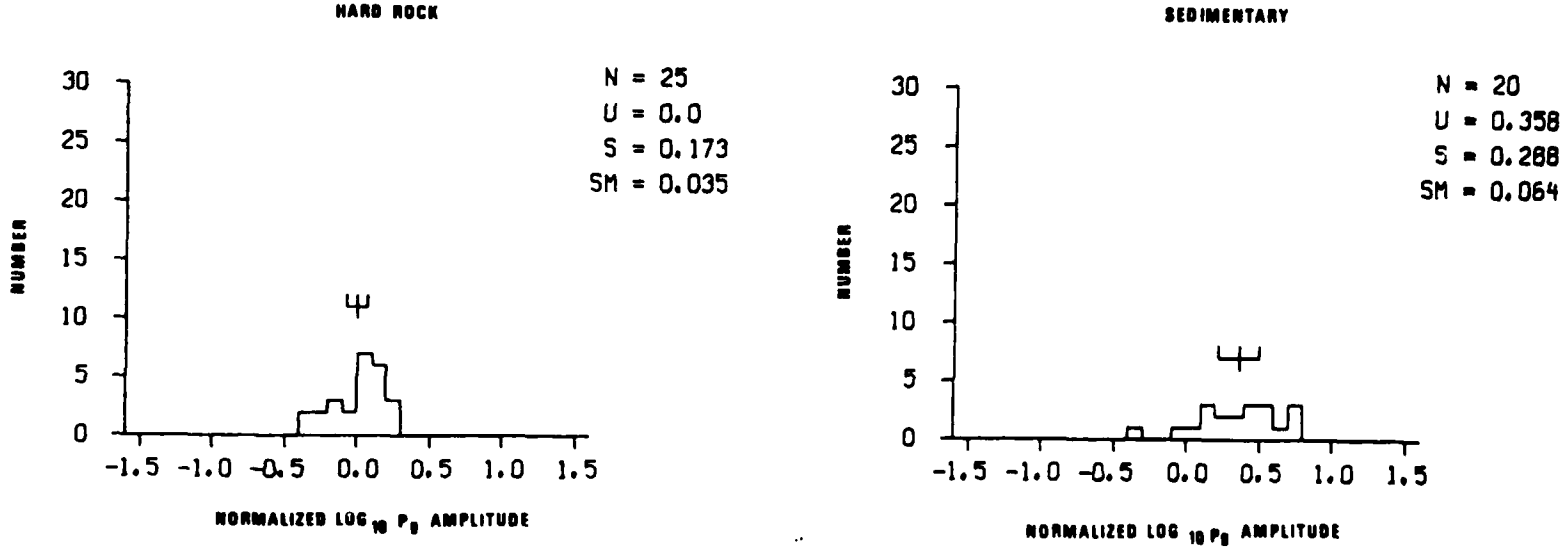

Figure 4. Difference in station magnitudes between hardrock and sedimentary sites for P_g.

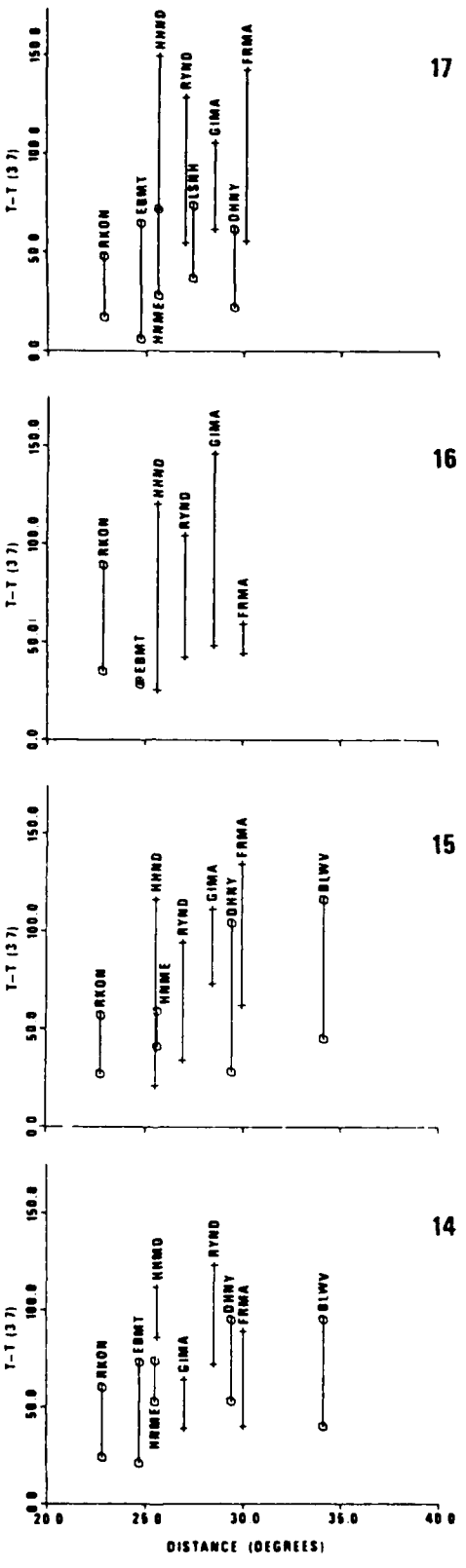

Figure 5. Length of coda as a function of distance and station for events 14, 15, 16, 17, a group of events from Baffin Bay. Note the consistent relationships between coda lengths. Coda length is measured by time interval between maximum amplitude and 1/2 maximum amplitude measured on the smoothed envelope.

PROPAGATION IN SHIELDS (C)

Phase Velocity Versus Depth

Z. Der, P. Klouda, D. W. Rivers

Project VT/0709 Contractor: Teledyne Geotech

Task 4.1.1 Propagation in Shields (C)

Objective

Study the relation between phase velocity of regional phases and the depth of the source. If depth can be determined by this method, it will serve as a discriminant.

Accomplishments

In an early study, Barley (1978) showed that apparent phase velocities measured across the Yellowknife array tended to increase with increasing source depth. A ray theory explanation of this phenomenon is that deep sources are associated with rays of deeper penetration in the earth, with correspondingly higher apparent velocities along the surface. Another manifestation of this idea, the change of L_g envelope shapes with depth, deeper rays being associated with faster group velocities was demonstrated by Noponen and Burnetti (1980). To test this idea, we have measured apparent phase velocities of L_g across the Alaskan array BFAK. Although the amount of data processed is small, it tends to confirm Barley's findings. In Figure 1 we show some phase velocity measurements versus source depth. The phase velocities were taken from F-K spectra, with fairly high F values (indicating good coherence across the array). Figure 2 shows some phase velocities computed from synthetic seisomgrams computed from various source depths, also showing the same tendency. We are in the process of collecting a much larger data set and investigate the stability of the method observationally as well as theoretically. Clearly, in order to be usable, the sensitivity of the method of various crustal structures and source mechanisms must be known.

Synthetic seismogram work simulating various source mechanisms has shown that the phase velocity method would be relatively insensitive to source mechanism and it depends mostly on depth. The difficulty in applying the method is the low coherence of L_g across most arrays. While synthetic array seismograms are very coherent and show well defined peaks on F-K plot, in spite of the many modes included in the synthetic seismograms, F-K plots generated from real data show low coherence (F-statistics). Analysis of L_g data at the four stations at Yucca Flats did not show any coherence between the L_g traces recorded at the various stations. This indicates that the low coherences are due to lateral inhomogeneities. It is possible that the method can be made to work only at arrays located over fairly homogeneous structures such as the Yellowknife and Gauribidanur, India, array where the intersensor coherences were reported to be high. We are attempting to obtain data from these arrays.

Task 4.1.1 Propagation in Shields (C)

References

Barley, B. J. (1978). On the use of seismometer arrays to locate sources of higher mode Rayleigh waves, AWRE, Blacknest, England.

Noponen, I. and J. Burnetti (1980). Alaskan regional data analysis, Studies of Seismic Wave Characteristics at Regional Distances, AL-80-1, Teledyne Geotech, Alexandria, Virginia.

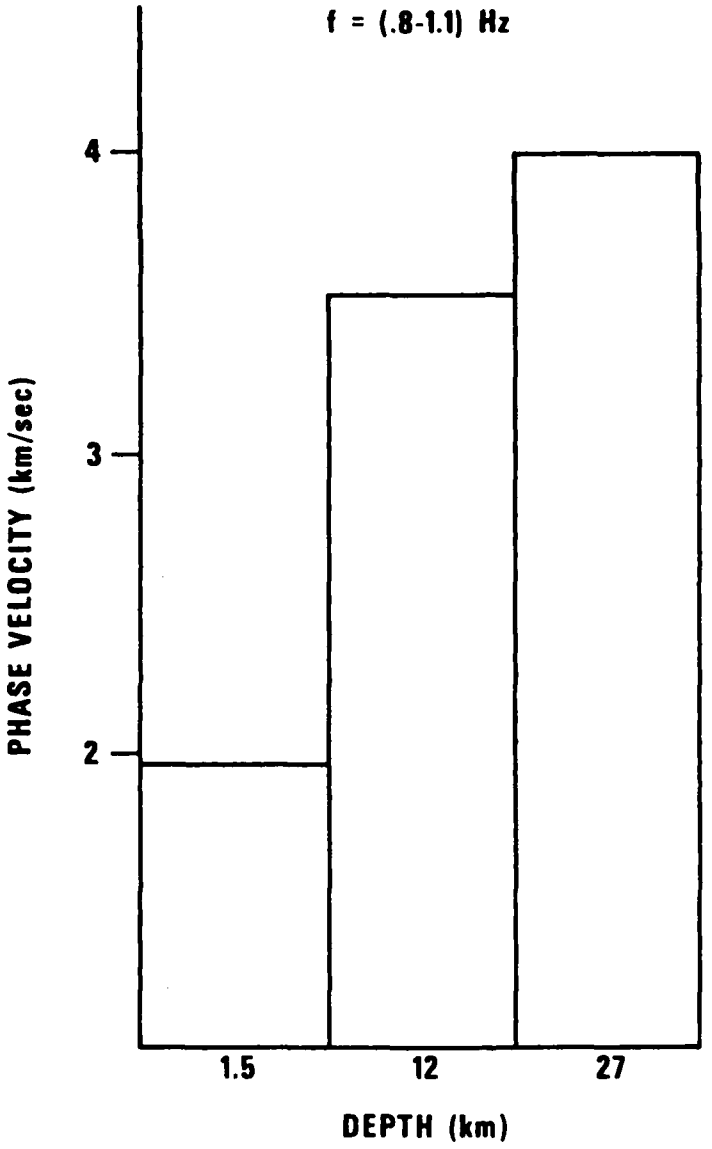

Figure 1. Apparent phase velocities in vertical component L_g at the Alaskan array BFAK as a function of source depth.

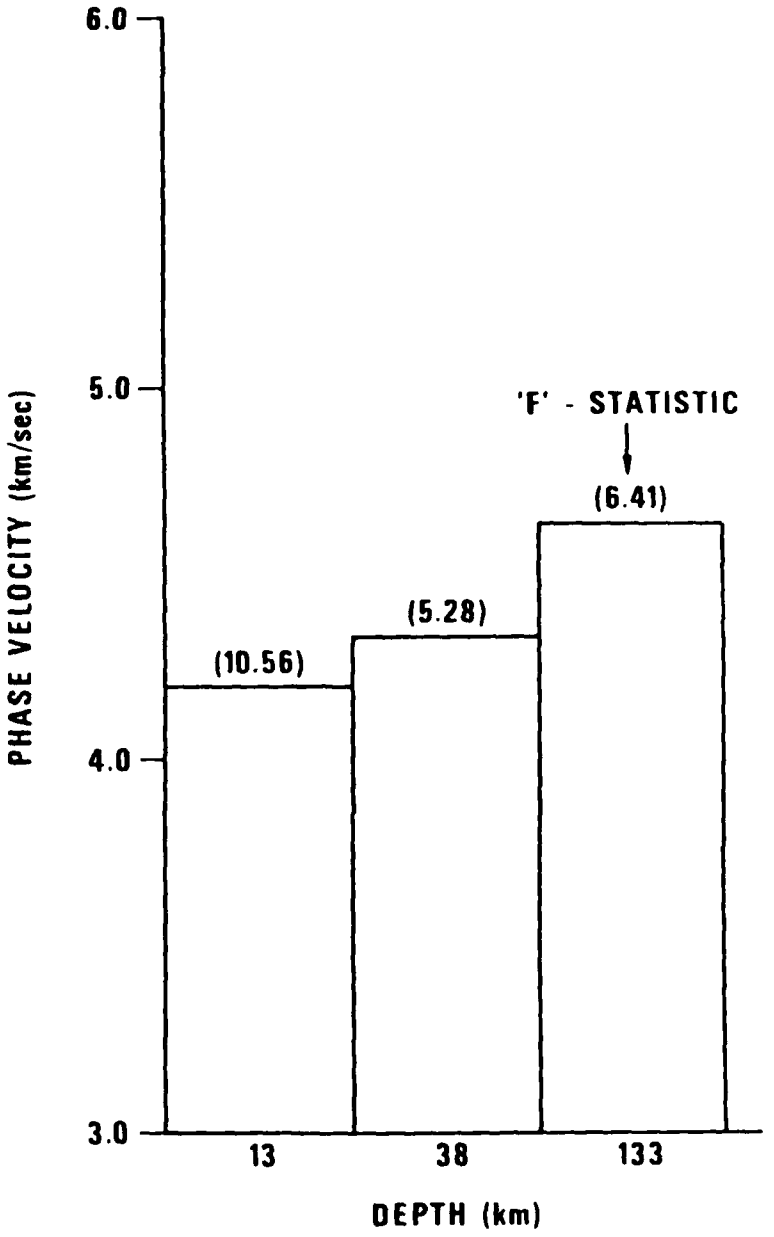

Figure 2. Apparent phase velocities (c) of synthetic L_g (transverse) seismograms versus source depth illustrating the principle of dependence of c on source depth. This figure is not directly comparable to Figure 1 since the component of motion as well as the applicable crustal structure is different.

PROPAGATION IN SHIELDS (D)

Scattering and Q Effects

Z. A. Der, A. O'Donnell, and T. W. McElfresh

Project VT/0709 Contractor: Teledyne Geotech

Objective

The objective of this section is to understand the effects and sources of scattering and Q on the frequency content, amplitude, and coda shape of regional phases. These measurements are crucial for yield determination and discrimination.

Accomplishments

Envelope shapes of L_g are likely depth discriminants. Amplitudes and envelope shapes of L_g are also affected by resonances in local two and three dimensional geological structures and by scattering at near surface inhomogeneities. The relative importance of these effects must be understood.

Codas of near earthquakes have been described in terms of backscattering from random inhomogeneities, Aki (1969) and Aki and Chouet (1975). In our previous work, we described the site amplification and coda lengthening in terms of resonance in a basin filled with low-velocity sediments.

Recently Aki's scattering coda theory has found increasing application in measuring Q in the crust (Herrmann, 1980; Rautian and Khalturin, 1978; Tsujiura, 1978), and has great importance in investigating the detectability and attenuation of seismic waves at regional distances. The theory assumes that the coda consists of waves scattered from crustal inhomogeneities and that this loss mechanism is dominant for crustal S waves (Aki, 1980). The loci of scatterers contributing to the coda at a given time depend on the source and receiver location and the relative velocities U and u of the primary and scattered waves. If the two velocities are equal the loci are on ellipses the foci of which are at the source and receiver. Aki's (1969) formulas are however valid only under some special conditions that may not be valid for events at regional distances. These formulas presuppose that the primary and scattered waves are the same kind with the same effective Q. It is quite conceivable however that since the upper crust is extremely inhomogeneous laterally due to topography and the presence of sedimentry structures (Baker et al 1980) that most of the scattering occurs near to the surface. In this case much of the scattered waves would be converted lower modes, including the fundamental, with considerably lower Q than the primary wave. We are presently exploring such a model.

For instance, if the primary and scattered waves have different velocities the curves for distant events again become ellipses or half hyperbolas with one of the foci at the receiver. Figure 1 shows the loci of scatterers for $U = 3.6$ km/sec and $u = 3$ km/sec. Assuming that the Q of primary waves is considerably larger than the scattered waves figure 2 shows the cumulative scattered energy contribution as a function of distance from

Task 4.1.1 Propagation in Shields (D)

Accomplishments continued

Accomplishments continued

the station at various times in the coda using a Q = 100 for the scattered waves. These curves show that the coda is influenced predominantly by the region a hundred km from the station in this case. The theory is also extremely robust with respect to any directionality in the scattering process. The scattering mechanism results in the dependence of coda length on frequency, since the late part of the coda comes from greater distances resulting in a diminuation of high frequency content. This can be matched by crustal Q values as is shown in Figure 3 where NTS data is matched using Q = 100. The dependence of coda decay rate on frequency is apparent in this figure. We have processed a large amount of data using this technique. Measurements at RKON indicate a larger Q in the crust that seems to agree with the high frequency content of many regional phases (frequencies in the 6 to 10 Hz range).

We must make a very important point here with regards to some recent work by Herrmann (1980) and Nuttli (1980). These authors have used Aki's (1969) formulas without allowing for the fact that Q values thus derived may apply to the vicinity of the station and not to the path as a whole as applied by Nuttli to derive distance decay rates. Some of his negative results about regional discrimination may possibly be attributed to this application of a formula valid only with some restrictive assumptions. The possibility that a large part of L_g may be locally scattered is supported by the observation of extremely low coherence in L_g across arrays (Mrazek et al, 1980). If a large part of the scattered L_g coda would be coming from scattering near the source the L_g phases would have considerably higher coherence across arrays.

References

Aki, K. (1969). Analysis of the seismic coda of local earthquakes as scattered waves, J. Geophys. Res., 74, 615.

Aki, K. and B. Chouet (1975). Origin of coda waves, source attenuation and scattering effects, J. Geophys. Res., 80, 3322.

Aki, K. (1980). Scattering and attenuation of shear waves in the lithosphere, (manuscript), (submitted to the J. Geophys. Res.).

Herrmann, R. B. (1980). Q estimates using the coda of local earthquakes, Bull. Seism. Soc. Am.

Mitchell, B. J. (1979). Frequency dependence of Q_β in the continental crust, (manuscript), Semi-annual Report for AFOSR, 1 Oct. 1978 - 31 Mar. 1979, Saint Louis University, Saint Louis, Missouri.

Mrazek, C. P., Z. A. Der, B. W. Barker and A. O'Donnell, (1980) Seismic array design for regional phases. In "Studies of Seismic wave characteristics at regional distances". Teledyne Geotech, AL-80-1.

Rautian, T. G. and V. Khalturin (1978). The use of coda for determination of the earthquake source spectra, Bull. Seism. Soc. Am., 68, 923-948.

Tsujiura, M. (1978). Spectral analysis of coda waves from local earthquakes, Bull. Earthq. Res. Inst., Tokyo, 53, 1-48.

von Seggern, D. (1980). Source, path and station effects on L_g propagation in North America, Trans. Am. Geophys. Union (EOS), 61, 307.

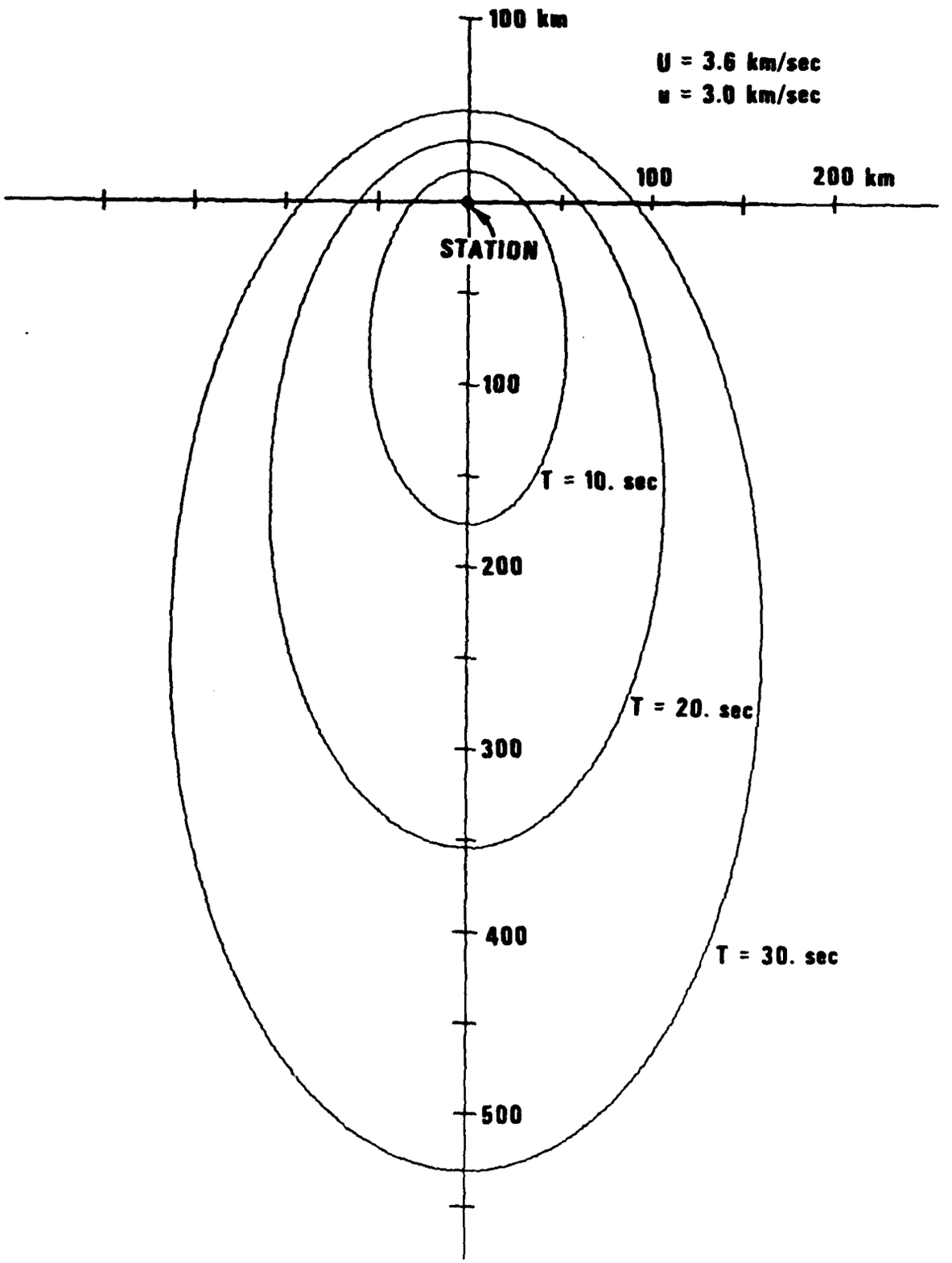

Figure 1. Location of scatterers at various times after arrival of primary wave. U = 3.6 km/sec, u = 3 km/sec.

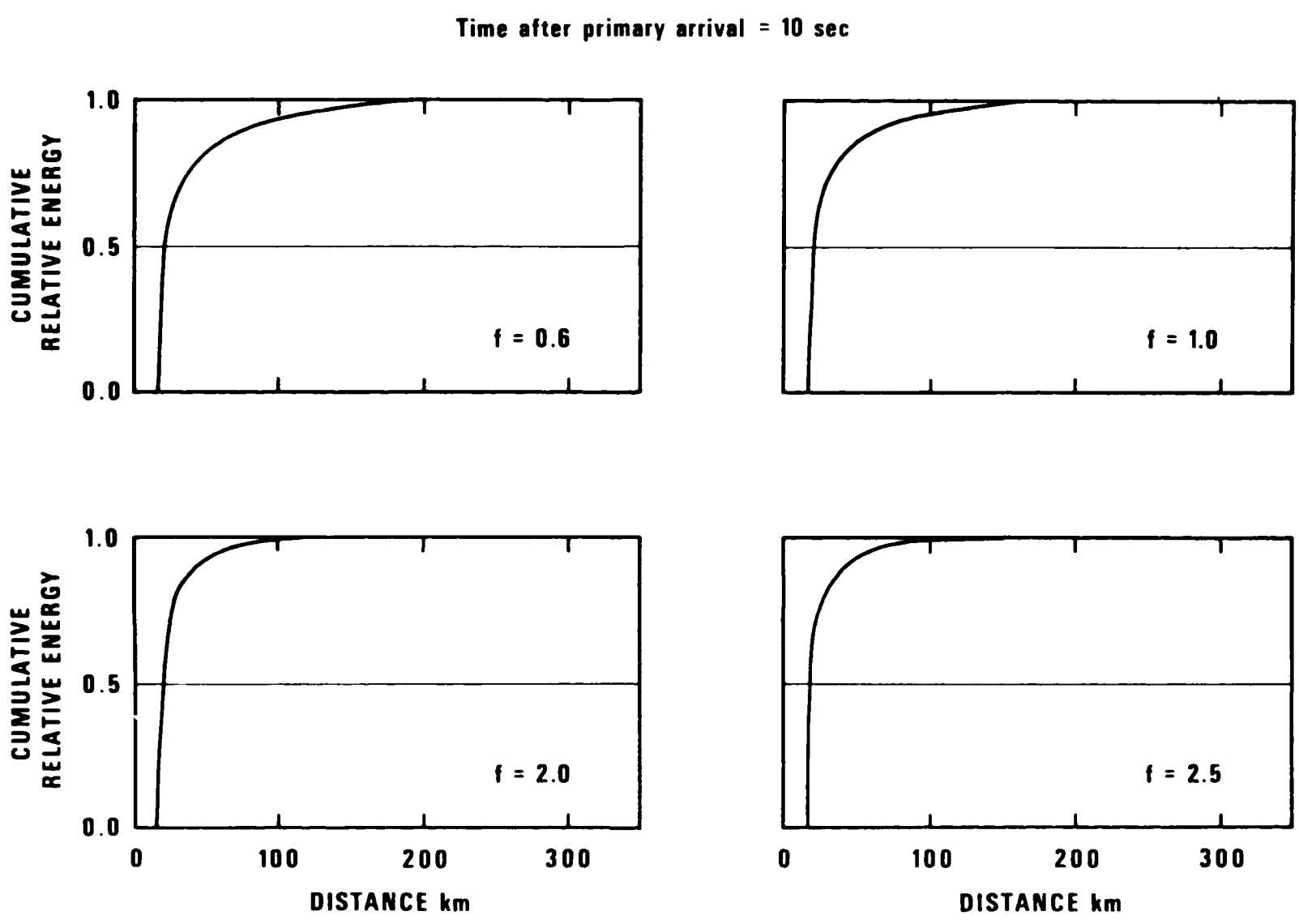

Figure 2a. Cumulative scattered energy contribution to the coda at 10 seconds after the primary arrival as a function of distance to the scatterer contributing the energy.

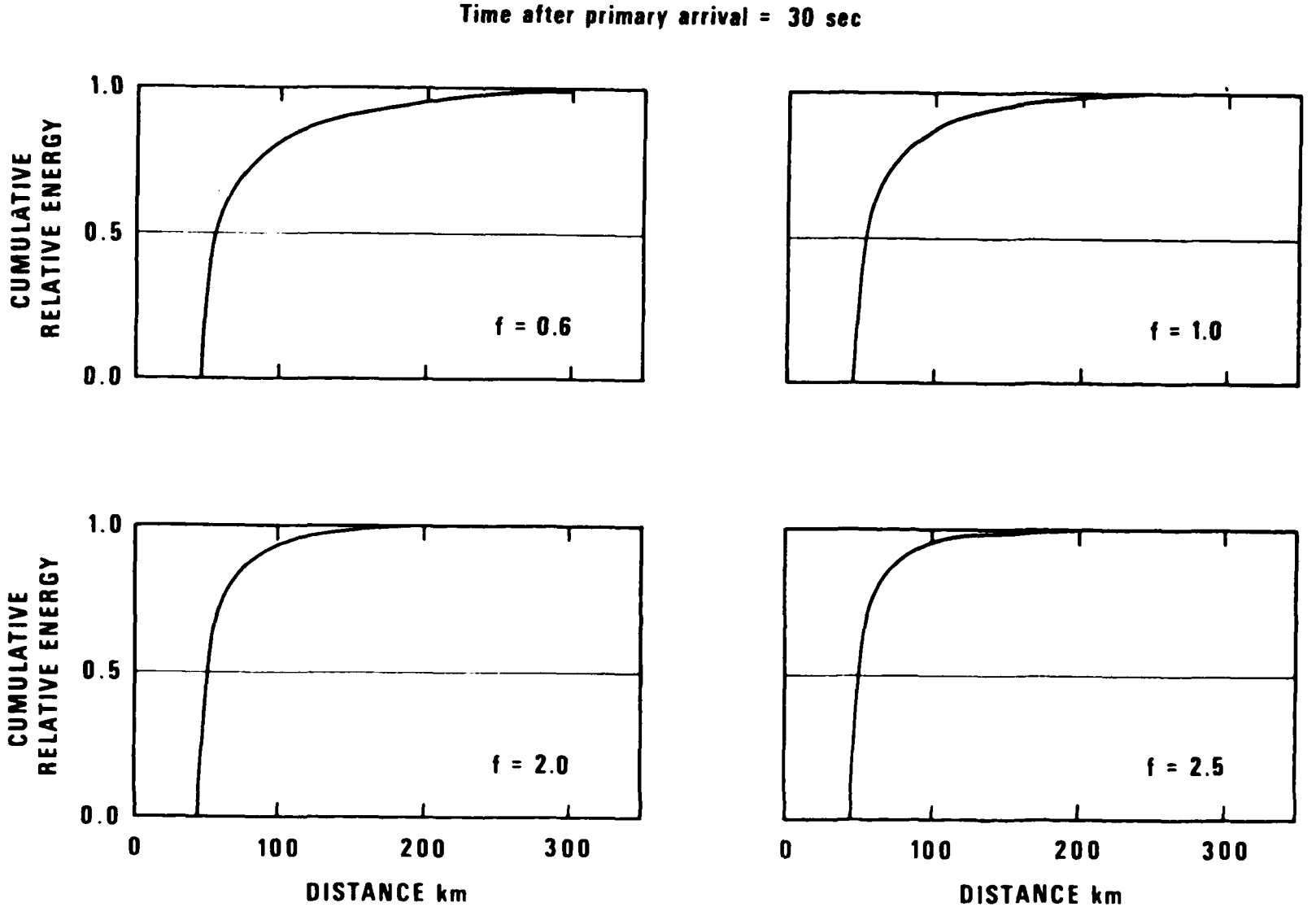

Figure 2b. Cumulative scattered energy contribution to the coda at 30 seconds after the primary arrival as a function of distance to the scatterer contributing the energy.

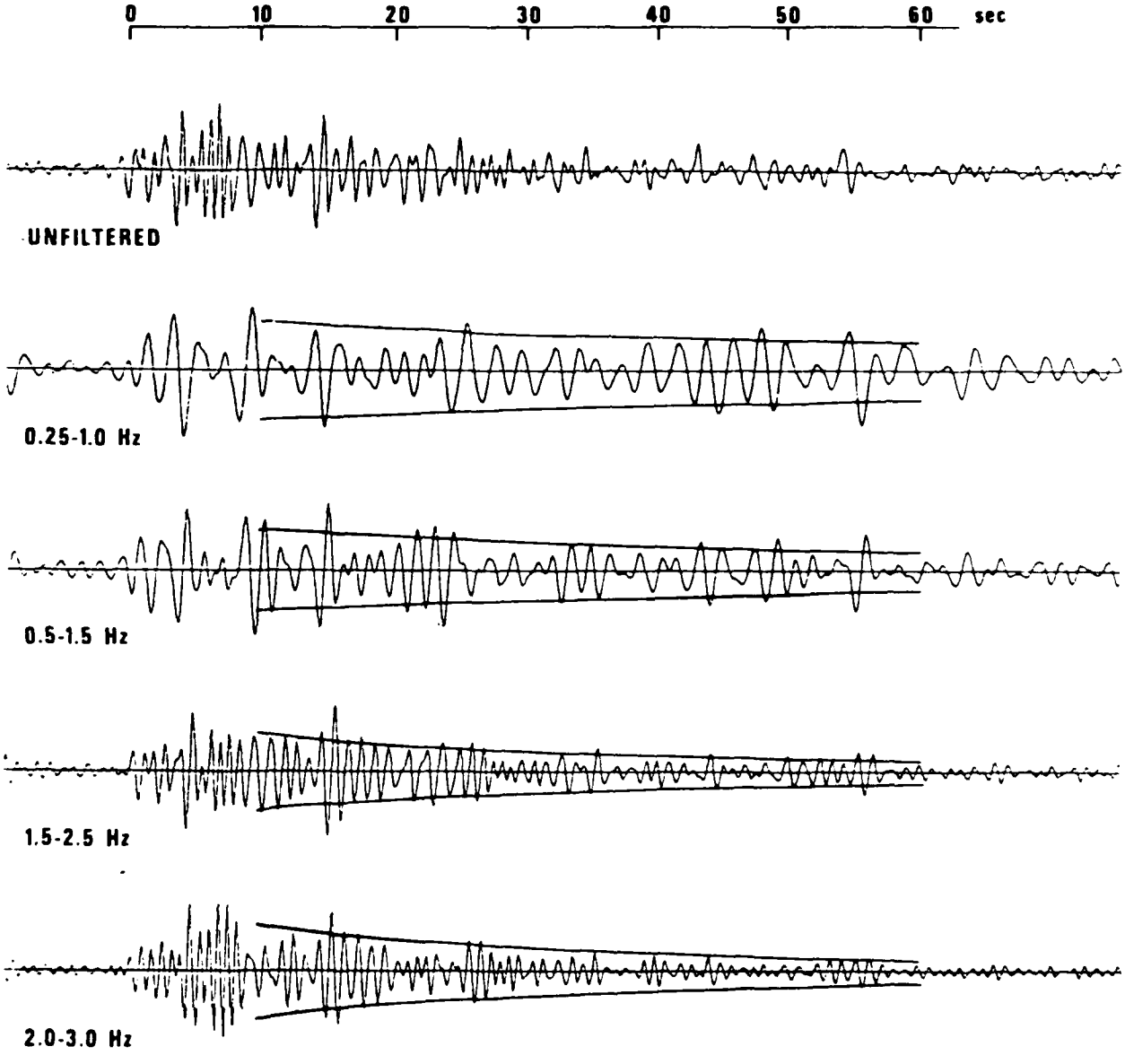

12 Sep 77 S. California
06:17:42.6 m_b = 3.2
Station: OB2NV Δ = 346 km
Q = 100 U = 3.6 u = 3.0

Figure 3. NTS coda decay waveforms matched using a Q = 100 for the scattered wave according to the theory by Aki.

PROPAGATION IN SHIELDS (E)

Effects of Crustal Structure

D. W. Rivers and D. H. von Seggern

Project VT/0709 Contractor: Teledyne Geotech

Task 4.1.1 *Propagation in Shields (E)*

Objective

Theoretical L_g seismograms will be generated for an earth model of a shield structure both with and without sedimentary cover. Measurements will be made on the synthetic seismograms in order to determine theoretical amplitude versus distance and phase velocity versus depth relations for L_g. The synthetic waveforms are to be compared with the envelopes of L_g traces recorded at stations on the Canadian Shield.

Accomplishments

A basic understanding of the mechanisms of propagation and the generation of regional phases is necessary for improving location, yield estimation and discrimination using regional phases. Due to the multi-modal structure of such signals, mode theory in layered media needs to be used.

Ever since the identification by Press and Ewing (1952) of the short-period surface wave Lg as a distinct seismic phase (or, more properly, a sequence of phases), an effort has been concentrated on understanding its origin and the effects of earth structure on its propagation and attenuation. In particular, it was necessary to explain why L_g was apparently unable to travel through even small segments of oceanic lithosphere and to determine whether, as it was sometimes conjectured, L_g was a channel wave whose occurrence indicated the existence of a high-velocity lid trapping energy in a low-velocity zone (LVZ). A major step towards understanding the nature of L_g was taken by Oliver and Ewing (1957), who noted that the group velocities of prominent maxima in the L_g wavetrain correspond to those of higher-mode Love waves. This identification of L_g as a superposition of short-period higher-mode Love waves was reinforced convincingly by Knopoff et al (1973), who demonstrated by means of synthetic seismograms that realistic seismic source mechanisms and earth structures could produce higher-mode Love waves of sufficient amplitude at the proper frequencies to account for the observations of L_g, at least to first order.

We have undertaken to expand upon the modal superposition technique in order to answer some questions about L_g propagation which ought to be understood if L_g is to be used in a program of seismic discrimination at regional distances. In particular, it is well known that L_g not only fails to propagate through the ocean but also attenuates rapidly in certain continental regions. It is also known that the amplitude of L_g, as well as its group velocity, is strongly influenced by surficial geology. In order to interpret observations of L_g in terms of the source mechanism, as well as to choose the best sites for locating future seismic stations, it is important to have a quantitative estimate of these path effects. We should also like to know, for a given source-to-receiver earth model, how large a variability in the characteristics of L_g can be anticipated from earthquakes of different source

Task 4.1.1 Propagation in Shields (E)

Accomplishments continued

mechanisms and of different depth. It is especially important to know whether certain earthquakes have some L_g signal characteristics which can be used as diagnostics in discrimination studies. Our study of L_g synthetic seismograms has been aimed at investigating these questions.

In order to produce the synthetic seismograms by modal superposition, it is necessary first to assume a flat, plane-parallel earth model and to calculate the dispersion relation (i.e., phase velocity as a function of frequency) for every Love-wave mode of this model. The results of a typical calculation are shown in the accompanying Figure 1. The high-velocity cut-off is the shear-wave velocity at the Moho, since higher velocities correspond not to L_g but to the mantle channel wave S_n (Stephens and Isacks, 1977). In the interest of computational efficiency, synthetics were sampled at five points per second, and thus no frequencies greater than the folding frequency of 2.5 Hz were considered; this cut-off results in the inclusion of twenty-six Love-wave modes for this particular earth model (Canadian shield with no surficial sediments). Also shown are the particle displacements as a function of depth for certain modes at a particular frequency in Figure 2. It is seen that most of the energy in the fundamental mode is confined to the top few kilometers of the crust, a phenomenon which will be important in considering the effect of a surficial layer of low-velocity sediments. For certain frequencies and certain modes, the displacement (and the tangential stress) eigenfunctions are not well behaved in the bottom layer of propagation above the attenuating half-space. This behavior is due to computational inaccuracy in the cumulative multiplication of propagator matrices, a phenomenon well known to all investigators in this field. Finally, there is shown an example of the superposition of the twenty-six Love-wave modes to produce L_g in Figure 3.

Synthetics have been produced for a variety of double-couple source mechanisms located at various depths and observed at various distances in earth models of a shield structure both with and without a sedimentary cover. An especially significant case which has been treated is that of a linear array of closely spaced instruments. Such an array is capable of measuring L_g phase velocity by means of frequency-wavenumber processing (Mrazek et al, 1980). For the hard-rock model, it was found that the phase velocity is about 1 km/sec greater (at a given frequency) for events at 40 km depth than for those near the surface, since deeper events preferentially excite the higher, faster modes. Although this result indicates that L_g phase velocity might be useful as a depth discriminant, it was also found that the simple relation of phase velocity increasing with depth was complicated by a large scatter in the data (about 0.5 km/sec) introduced by varying the orientation of the double-couple source mechanism. The relation was also less simple for the shield model which was overlain by a veneer of low velocity sediments. Because the veneer is characterized by a low value of the anelasticity parameter Q, the lower order modes, which are confined close to the surface, attenuate rapidly with distance. For shallow events, which preferentially excite the lower order modes, it was thus found that the phase velocity was dependent not only on the depth of the source but also on the distance from the source to the detecting station. These complications should be born in mind before attempting to use L_g phase velocity as a depth discriminant.

Task 4.1.1 Propagation in Shields (E)

Accomplishments continued

Synthetics generated for single sites, rather than for arrays, have been used to study the theoretical decay with distance of the L_g envelope. The decay of the maximum amplitude has been measured for distances in the 300 km to 1800 km range. Empirical fits to the data have been made using both log-log (i.e., amplitude versus distance) and semi-log (magnitude versus distance) plots. The gross behavior of the decay with distance within the hard-rock structure is slightly dependent upon the depth of the focus, since the envelopes of deeper events appear to decay slightly faster than do those of shallow events. Work is underway to see whether this slight trend may be masked by larger fluctuations introduced by variations in the focal mechanism and in the radiation pattern. Although the decay may be fit assuming a constant decay rate with distance, better results are obtained by subdividing the 1800 km-long path into 600 km-long segments in which the amplitude appears to fall off as first Δ^{-1}, then Δ^{-2}, and finally Δ^{-3}. At short distances the situation is rather more complicated in the structure with the sedimentary veneer, since the low Q associated with the sedimentary layer causes a very rapid decay of the lowest order modes, which are confined to the top layers of the crust. This effect is less pronounced for deeper events, since they preferentially excite only the higher order modes. The higher order modes nevertheless do attenuate rapidly, since they consist largely of high-frequency oscillations and since the attenuating layer acts as a low-pass filter.

Attempts have been made to fit the synthetic seismograms to observed waveforms. The observed signals could not be fit using synthetics generated from either of the two models described previously, since the first motion of the synthetics correspond to higher group velocities ($\simeq$ 3.8 km/sec) than are customarily observed for L_g. This situation was largely alleviated, although not completely rectified, by replacing the crust of the shield model by a thicker crustal model corresponding to the structure which has been determined at station WNSD. There are two principal differences between the synthetic and observed waveforms: the carrier signal (as opposed to the envelope) is characterized by sharper spikes for the synthetics, and the envelope decays much faster for the synthetic seismograms. The spikes are due to strongly defined Airy phases, which are blurred out in the observed seisomgrams by inhomogeneities along the propagation path. The observed envelope fall-off gives credence to the theory that the L_g coda is created by scattered energy, since the synthetics contain no provision for scattering or for the resulting conversion from Love-wave to (slower) Rayleigh-wave modes. Work continues on attempting to fit the observed signals better, at least with respect to the signal arrival time. The fact that much of the energy in the L_g wavetrain appears to have undergone scattering and mode conversion may have some effect on any attempt to use the L_g phase for seismic source identification.

Task 4.1.1 Propagation in Shields (E)

References

Knopoff, L., F. Schwab, and E. Kausel (1973). Interpretation of L_g, Geophys. J., 33, 389-404.

Mrazek, C. P., Z. A. Der, B. W. Barker, and A. O'Donnell (1980). Seismic array design for regional phases, AL-80-1, Teledyne Geotech, Alexandria, Virginia.

Oliver, J. and M. Ewing (1957). Higher modes of continental Rayleigh waves, Bull. Seism. Soc. Am., 47, 187-204.

Press, F. and M. Ewing (1952). Two slow surface waves across North America, Bull. Seism. Soc. Am., 42, 219-228.

Stephens, C. and B. L. Isacks (1977). Toward an understanding of S_n: normal modes of Love waves in an oceanic structure, Bull. Seism. Soc. Am., 67, 69-78.

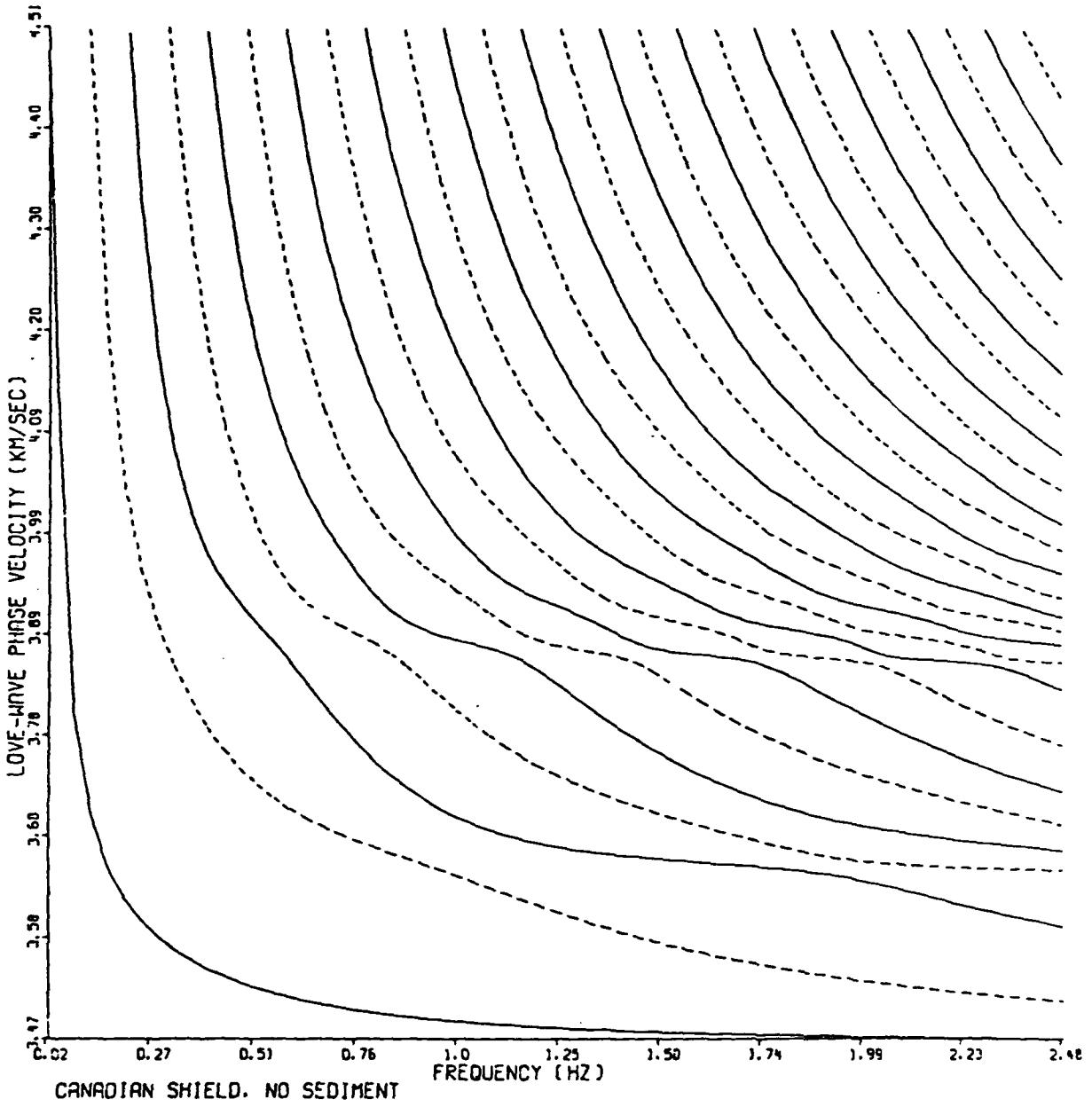

Figure 1. Dispersion relations for 26 Love-wave modes.

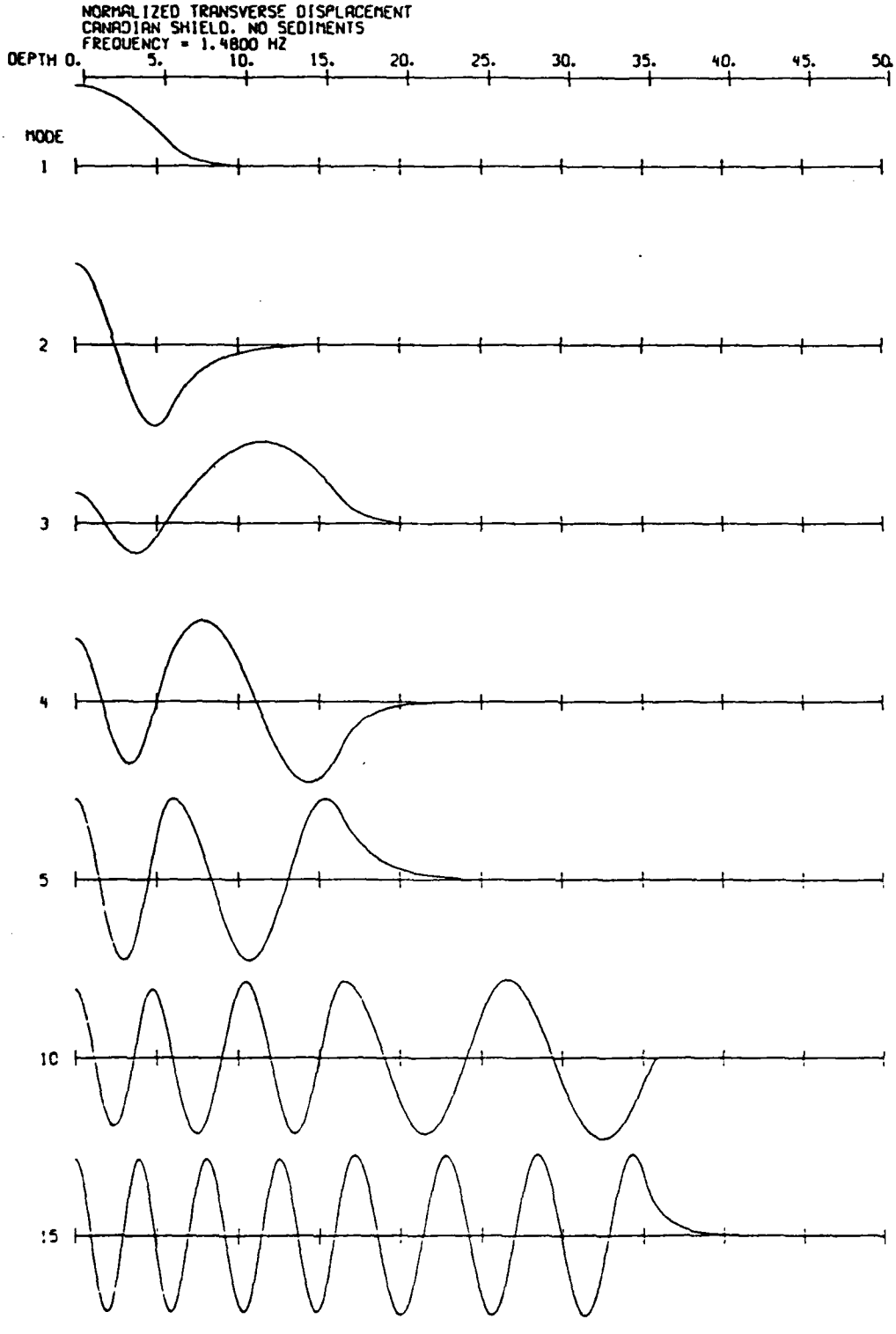

Figure 2. Particle displacement (normalized to the surface displacement) as a function of depth for seven selected Love-wave modes at a particular frequency.

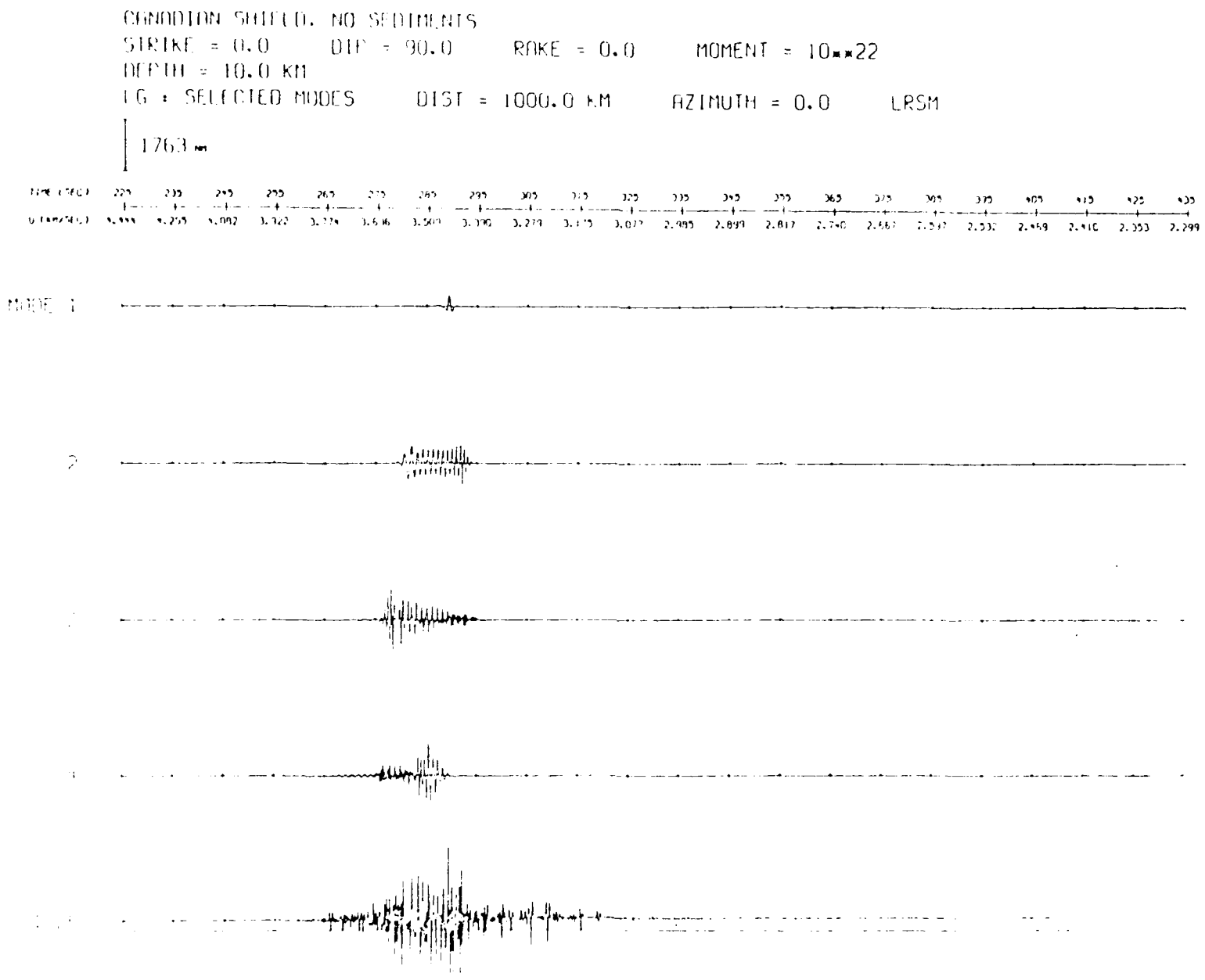

Figure 3. Synthesis of L_g for a particular double-couple mechanism and a particular source-to-receiver distance. The first four modes are shown separately along with the superposition of all twenty-six modes.

IMPROVED LOCATION WITH REGIONAL PHASES (A)

Use of P_n Arrivals in the HYLO Method

A. C. Chang, H. Sproules, J. A. Burnetti

Project VT/0709 Contractor: Teledyne Geotech

Task 4.1.3 Improved Location with Regional Phases (A)

Objective

To evaluate the P_n location accuracy of the HYLO method reported by Herrin and Taggart (1962).

Accomplishments

The location accuracy of the modified HYLO method was tested with the same 12 nuclear explosions used by Chang and Racine (1980). Comparison of location errors as shown in Table I indicates that results from the HYLO method are not significantly different from results using the Herrin '68 model in a standard location program. Possible reasons for this are that it is likely that P_n velocity variations are more complex than shown in Figure 1, and furthermore, that lateral crustal thickness variations are significant and even more complex. The method is applicable only to P_n arrivals, and to the areas where P_n variations are well known. We conclude that the original HYLO method is not clearly effective.

References

Chang, A. C. and D. P. J. Racine (1979). Evaluation of location accuracy using P_n and P_g arrivals, SDAC-TR-79-4, Teledyne Geotech, Alexandria, Virginia, (in press).

Herrin, E. and J. Taggart (1962). Regional variations in P_n velocity and their effect on the location of epicenters, Bull. Seism. Soc. Am., 52, 1037-1046.

Julian, B. (1973). Extension of standard event location procedures, Seismic Discrimination SATS, Lincoln Laboratory, M.I.T., 30 June 1973, 4-9.

McCowan, D. W. and R. E. Needham (1978). The use of crustal phases in locating explosion epicenters, Seismic Discrimination SATS, Lincoln Laboratory, M.I.T., 9 June 1978, 1-2.

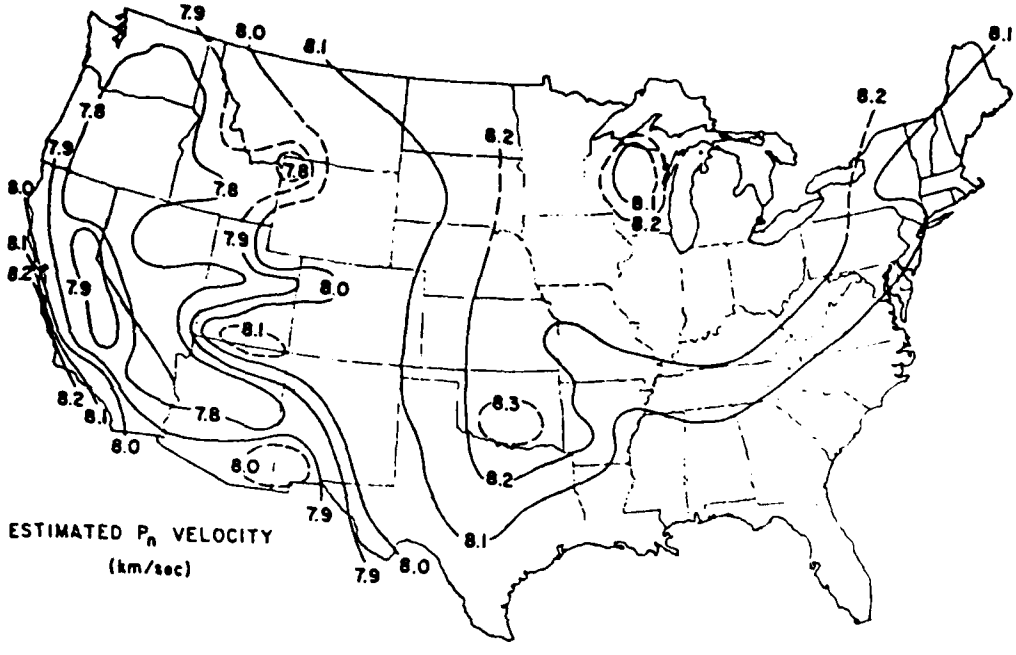

Figure 1. Estimated P_n velocity in the United States, based on data from deep seismic soundings, underground nuclear explosions, and earthquakes (compiled by E. Herrin and J. Taggart).

TABLE I

COMPARISON OF LOCATION ERRORS

	HERRIN Pn only		HERRIN(Pn + Pg)				HYLO			
	DEPTH REST		DEPTH REST		DEPTH FREE		DEPTH REST		DEPTH FREE	
	LOC E	OT E	LOC E*	OT E//	LOC E	OT E	LOC E	OT E	LOC E	OT E
Faultless	18.3	1.5	15.04	1.3	15.04	1.4	12.32	0.2	12.32	-1.8
Rullson	7.3	0.5	1.58	0.3	1.58	-0.1	3.63	1.3	3.72	1.0
Passaic	N/A	N/A	4.08	-0.4	4.08	-0.4	11.17	0.8	11.17	0.8
Rockville Dam	5.1	1.5	5.18	1.3	5.18	1.3	5.59	0.6	5.59	-0.4
Dormouse	N/A	N/A	9.09	-0.2	9.09	0.2	10.47	-0.8	10.47	-1.4
Klickitat	7.0	0.4	6.53	0.0	6.53	0.0	9.56	-0.5	9.64	0.6
Bandicoot	12.9	0.7	1.01	0.8	1.34	0.6	7.09	-0.6	7.09	-1.8
Shoal	5.9	0	5.18	0.1	5.18	4.1*	11.26	-0.7	11.26	0
Merrimac	10.3	0.3	9.58	0.2	9.58	1.0	10.99	-0.2	10.89	4.7
Gasbuggy	5.2	0.6	11.43	0.4	11.43	0.4	5.60	1.1	5.81	0.4
Piledriver	4.0	0.3	12.98	-0.4	12.98	1.2	24.54	-0.4	24.54	0.9
Roanoke	8.3	0.4	8.15	0.4	8.24	1.5	2.68	-0.6	3.68	0.4
Average	8.4		7.49		7.52		9.68		9.68	

HYLO METHOD

* LOC E: Error of location vector, in km

// OT E: Error of origin time estimates, $T_{est} - T_{true}$, in sec.

IMPROVED LOCATION WITH REGIONAL PHASES (B)

The Method of Successive Determinations

A. C. Chang and J. A. Burnetti

Project VT/0709 Contractor: Teledyne Geotech

Task 4.1.3 Improved Location with Regional Phases (B)

Objective

Evaluate the method of successive approximations as applied to regional locations.

Accomplishments

The successive determinations method uses the Herrin crustal model to compute a preliminary location. Then the program computes P_n and P_g velocities using the obtained preliminary location. These estimated velocities are then used to relocate the event. The method is applicable to any phase and any area without previous knowledge of the area's crustal structure.

In order to account for heterogeneous structures, an option has been included in the location programs to separate arrival data into two groups while computing the velocities. The results in Table I show that we have successfully reduced the average location error from 7.52 km to 4.35 km. This accuracy is comparable to the accuracy obtainable with accurate travel time residual corrections.

TABLE I

COMPARISON OF LOCATION ERRORS

SUCCESSIVE DETERMINATIONS METHODS
DEPTH FREE

	HERRIN			SUCCESSIVE DETERMINATIONS		
	LOC E.[1]	OT. E.[2]	DEPTH[3]	LOC. E.	OT. E.	DEPTH
Faultless	15.04	1.4	0.0	3.96	1.0	3.6
Rulison	1.58	0.0	0.0	3.39	2.6	0.0
Passaic	4.08	-0.2	0.0	2.14	-0.6	0.0
Rockville Dam	5.18	1.5	0.0	2.07	3.9	13.0
Dormouse Prime	9.09	0.2	0.0	9.87	0.7	4.3
Klickitat	6.53	0.1	0.0	2.78	0.7	8.1
Bandicoot	1.34	0.6	7.8	4.58	0.0	0.0
Shoal*	5.18	0.0	0.0	2.34	-0.9	0.0
Merrimac	9.58	0.3	0.0	5.16	0.2	15.9
Gasbuggy	11.43	0.6	0.0	10.04	2.0	0.0
Piledriver	12.98	0.0	0.0	1.66	-0.1	8.9
Roanoke	8.24	1.3	7.9	4.20	1.1	28.1
Average	7.52			4.35		

* Depth restricted

1. LOC. E.: Error of location vectors in km
2. OT. E.: Error of origin time estimates, $T_{est} - T_{true}$, in sec
3. when depth is zero, the depth is restricted to 0 km

IMPROVED LOCATION TECHNIQUES WITH REGIONAL PHASES (C)

Method of Simultaneous Inversions

D. W. Rivers

Project VT/0709 Contractor: Teledyne Geotech

Task 4.1.3 Improved Location Techniques with Regional Phases (C)

Objective

Algorithms for event location using P_n and/or P_g arrival times will be revised so that no *a priori* knowledge of the precise travel-time relationships for these phases is required. The particular technique developed under this subtask, the method of simultaneous inversion, may be used as an alternative to the method of successive determinations which was developed under subtask B.

Accomplishments

The method of simultaneous inversion is similar to the method of successive approximation except that the answer is determined by matrix inversion rather than by iteration.

In order to implement the method, the standard location program LOCATION has been rewritten to solve for eight, rather than four, unknowns. The revised program was tested using the same data set as was used for testing the method of simultaneous determinations. (There were a few small changes from the data used in subtask B.) A comparison of the absolute errors resulting from the application of the two different techniques is presented in the accompanying table. The simultaneous inversion results should be compared with those obtained by running the successive determinations program in both the depth-free and depth-restrained modes. The reason for this is that although the simultaneous inversions program was run in the depth-free mode, the use of only regional phases rendered the depth indeterminate (except indirectly through the parameters ap_n and ap_g), and hence the results are perhaps more nearly analogous with those obtained from the successive techniques run in the depth-restrained mode. In the table parentheses are placed around the absolute errors for certain cases of the method of successive determinations run in the depth-free mode; these are cases for which the depth was found to be negative at the end of at least one iteration and was then restrained to zero depth at the start of the next iteration. The table shows that for both methods the addition to the data base of P_g arrival times usually results in a smaller error than results from the use of P_n arrivals; this improvement was found not to occur in previous investigations which used conventional location techniques. Although one or the other of the two methods gives better results for particular events, on the whole the results obtained by the two different methods are comparable.

The coefficients a_{P_n}, b_{P_n}, a_{P_g}, and b_{Pg} are the same for all events with epicenters close to each other. They may thus be determined more accurately if data from nearby events are inverted simultaneously, a process known as joint epicenter determination (JED). The use of data from n events then results not in n systems of equations in eight unknowns but rather in a single system of equation in $4n + 4$ unknowns. The table also shows the absolute errors which

Task 4.1.3 Improved Location Techniques with Regional Phases (C)

Accomplishments continued

result when JED and the method of simultaneous inversion are applied to eight explosions at NTS. As might be expected, the locations of some events are improved relative to the locations found without JED, and the locations of other events are worsened.

In general, we conclude that successive determination and simultaneous inversion are equivalent to each other, and both are superior to standard location techniques.

Absolute errors (km) resulting from the application of two location techniques to a common data set.

Successive Determinations

Event	no. P_n	no. P_g	P_n only, depth free	P_n and P_g, depth free	P_n only, restrained	P_n and P_g, restrained
FAULTLESS	5	5	18.64	(3.95)	18.64	4.05
RULISON	10	7	restr.	restr.	2.65	3.38
PASSAIC	4	3	(2.66)	restr.	2.66	2.14
ROCKVILLE DAM	9	8	restr.	(2.07)	2.55	1.90
DORMOUSÉ	3	4	diverges	(9.39)	diverges	10.70
KLICKITAT	13	12	diverges	(3.11)	4.34	4.11
BANDICOOT	5	4	4.18	restr.	4.18	4.37
SHOAL	12	0	diverges	no P_g	2.34	no P_g
MERRIMAC	8	0	restr.	no P_g	5.17	no P_g
GASBUGGY	12	12	10.51	restr.	10.51	10.02
PILEDRIVER	5	5	diverges	(1.83)	10.41	2.56
ROANOKE	4	4	(4.41)	ignores P_g	4.38	4.24
SALMON	5	0	diverges	no P_g	33.00	no P_g
GNOME	18	1	restr.	restr.	7.10	7.06

Simultaneous Inversion

Event	P_n only	P_n and P_g		J.E.D.
FAULTLESS	22.35	18.46	-	19.16
RULISON	1.78	0.69	+	
PASSAIC	2.66	2.75	0	1.45
ROCKVILLE DAM	2.59	4.42	-	2.08
DORMOUSÉ	insuf. P_n	8.25		
KLICKITAT	0.97	0.63	+	1.44
BANDICOOT	11.14	8.67	-	5.01
SHOAL	1.88	no P_g		
MERRIMAC	5.17	no P_g		13.00
GASBUGGY	10.56	10.07		
PILEDRIVER	8.81	5.67	+	6.37
ROANOKE	4.00	4.11		9.48
SALMON	31.77	no P_g		
GNOME	7.15	7.15		

LOCATION WITH REGIONAL DATA

D. W. Rivers, A. Chang, and J. Burnetti

Project VT/0709 Contractor: Teledyne Geotech

Task 4.1.4 Location with Regional Data

Objective

The surface-wave processor developed by Smart (1977) will be applied to three-component short-period digital seismograms in order to determine the back azimuth of the event as seen at the station. The location algorithm will be revised to utilize this information along with the conventional measurements of signal arrival times.

Accomplishments

The traditional determination of hypocenters and origin times of seismic events involves finding the best values of the coordinates (latitude, longitude, depth, origin time) such that at a network of detecting stations the signal arrival time differences $\delta t = t_{observed} - t_{calculated}$ are minimized in a least-squares sense. In order to carry out the location, it is necessary to have measured arrival times at four or more stations in order that each of the four coordinates of the hypocenter can be determined uniquely. An accurate location, i.e., one for which the "error ellipsoid" formed by the confidence limits surrounding the calculated hypocenter is small, would obviously require several more than four measurements of arrival time. In practice, this requirement may be difficult to meet. One case in which it may not be met is that of a weak event for which the P-wave signal cannot be observed at teleseismic distances. Unless the area around the epicenter is densely populated by seismographic stations, it is unlikely that enough detections will be reported by stations at only regional distances to permit an accurate determination of the event location to be carried out. Another case in which the location may suffer from an insufficient number of arrival time measurements is that rather common instance in which, within some given time interval, several stations in a network have measured arrival times for P-waves, but the signals are from two or more different events (including local ones), and it is impossible to associate unambiguously each signal with the appropriate event.

These shortcomings of conventional location may be circumvented, or at least alleviated, by the use of more information than just the arrival time measurements. Smart (1977) has developed a surface-wave processor which enables three-component data to be inverted to yield the back azimuth of the epicenter at the detecting station. The back-azimuth measurements made by this processor are an excellent supplement to the arrival-time data. Even if no teleseismic measurements are available for an event, the surface-wave processor may still be used since, at regional distances, the amplitude of L_g is comparable to that of P. In the case in which the P-wave detections cannot be associated unambiguously with a particular event, measurement of the back azimuth will in many cases resolve the ambiguity. In particular, arrival time and back azimuth measurements at only two stations would be sufficient to determine the hypocenter. Although this determination would be crude, it should serve as an adequate trial value to permit the proper association of other signals with it. Back azimuth measurements are thus useful for event location, and we therefore have revised our standard location program LOCATION to use azimuth as well as arrival time data.

Task 4.1.4 Location with Regional Data

Accomplishments continued

In the revised version of LOCATION, an initial trial value of the hypocenter and origin time is used to calculate the predicted signal arrival time and back azimuth at each station in a given network. Residuals are calculated by subtracting the predicted values from the observed values, and these residuals are then expressed in the form of a Taylor series about the trial coordinates. For a data base consisting of m arrival time measurements and n back-azimuth measurements, this process results in m equations of the form

$$\delta t = dT + \frac{\partial t}{\partial x} dx + \frac{\partial t}{\partial y} dy + \frac{\partial t}{\partial h} dh$$

and n equations of the form

$$\delta \zeta = \frac{\partial \zeta}{\partial x} dx + \frac{\partial \zeta}{\partial y} dy$$

where δt and $\delta \zeta$ are the arrival time and back azimuth residuals and dT, dx, dy, and dh are the corrections which are to be added to the trial value of the origin time, east, north, and depth coordinates. The partial derivatives in the arrival time equation may be calculated in the usual manner from travel-time curves, and those in the back azimuth equation may be determined by a straightforward solution for the appropriate spherical triangles. The resulting system of m+n equations may then be solved for the four unknowns, dT, dx, dy, and dh; these values are then added to the assumed hypocentral coordinates, yielding an improved location. This location is then used as a new trial value, and the process may be repeated through several iterations until the location converges. In practice, every residual δt ought to be weighted by the standard deviation of the appropriate arrival time measurement (e.g., 0.2 sec for P, 1.0 sec for P_n, 3.0 sec for P_g, etc.) and every residual $\delta \zeta$ ought to be weighted by the standard deviation of a back azimuth measurement, which Smart (1977) finds to be 7 degrees. Since the intersection of circles of radius corresponding to arrival times of t±1.0 sec around each station comprises a much smaller area than does the intersection of sectors of angle ζ+7 degrees from each station, it is seen that the use of back azimuth data will offer very little improvement in the location beyond that which would be obtained by the use of several measurements of only the arrival time. Nevertheless, the back azimuth data will be helpful when a few arrival times were measured; in fact, the epicenter, but not the depth or origin time, may be calculated (crudely) from two back azimuth measurements alone. It may thus be possible to use this technique for locating "lonesome L_g" events.

The two accompanying figures show the results of two epicenter determinations in which only back azimuth measurements (i.e., no arrival times) were used. The locations obtained using the techniques developed in this task are indicated by means of a triangle. The more accurate locations indicated by a circle were obtained using a maximum likelihood method based on the theory of Bernoulli tirals (Smart, 1977). This latter technique (which does not encompass the use of arrival time data) gives better results since it is less strongly influenced by outlying data points. The vulnerability of the epicenter determination to faulty measurements is a general feature of the weighting scheme employed by the program LOCATION and not of the particular algorithm which uses the back azimuth data.

Task 4.1.4 Location with Regional Data

Accomplishments continued

When both arrival time and azimuth data were used, the location found for GNOME was essentially the same as that which was found using only arrival times, a result which was anticipated on account of the previously discussed superiority of arrival time data. When arrival times were added to the SALMON data base, however, the resulting location still lay far to the south of the true epicenter, indicating that the results were still heavily influenced by the azimuth measurements. The explanation of this discrepancy is that the error in the epicenter was offset by an error in the calculated value of the origin time, so the erroneous four-dimensional hypocenter was in fact consistent with the measured arrival times. This error point out a deficiency in the method, namely a susceptibility to bias introduced by the use of stations within an insufficiently large range of azimuths.

A data base of three-component, digital, short-period seismograms is being compiled so that this technique may be further tested with various combinations of back azimuth and arrival time measurements.

Reference

Smart, E. (1977). A three-component, single-station, maximum-likelihood surface wave processor, SDAC-TR-77-14, Teledyne Geotech, Alexandria, Virginia.

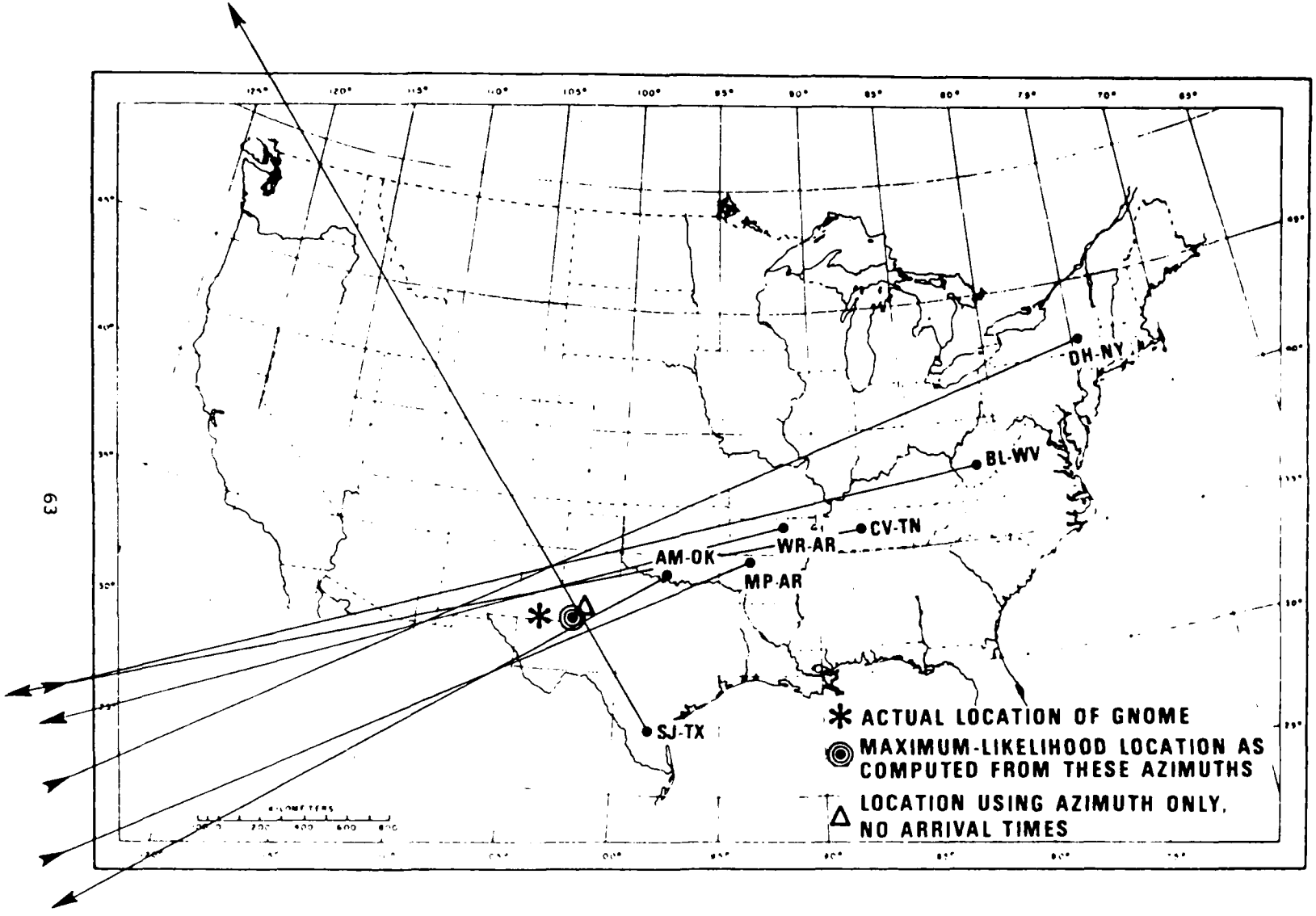

Figure 1 Automatic signal azimuth estimates of L_g surface waves from GNOME as seen at several LRSM stations.

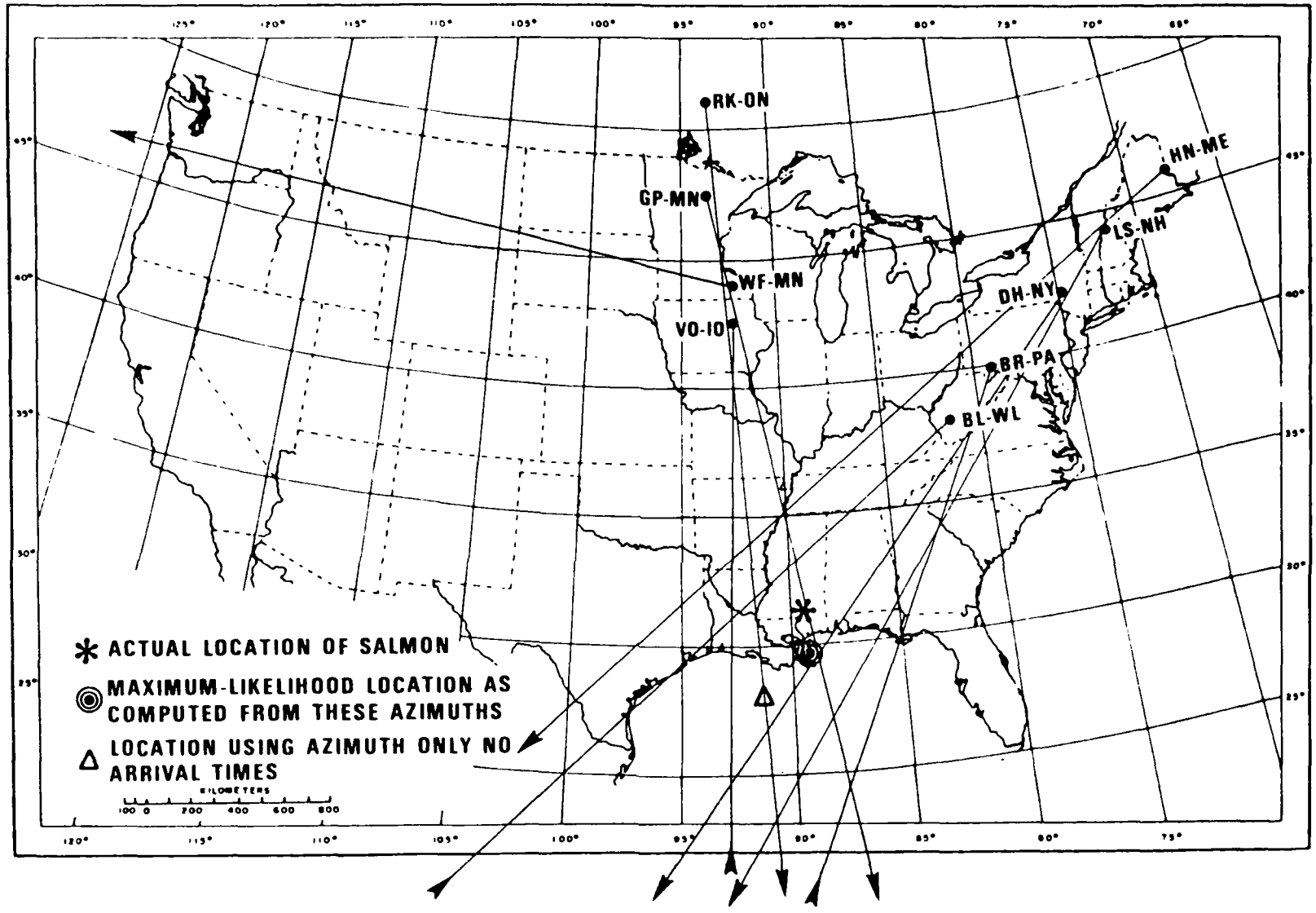

Figure 2 Automatic signal azimuth estimates of L_g surface waves from SALMON as seen at several LRSM stations.

TITLE OF EXECUTIVE SUMMARY: "Regional Discrimination Research"

AUTHORS: T. J. Bennett, J. R. Murphy and J. M. Savino

Project: VT/0701 Contractor: Systems, Science and Software

Task 4.1 Task title from Statement of Work: "Regional Phase Characterization"

Objectives

The objectives of this task are to develop a systematic procedure for evaluating excitation differences of regional phases from underground explosions and earthquakes and to define the dependence of these differences on focal depth. In particular, the procedure is being applied to data from a variety of tectonic environments, including available U.S.S.R. data, in an attempt to develop regional phase discriminants for different regions of the U.S.S.R.

Accomplishments

This project was initiated in May, 1980 and the effort to date has focused primarily on the identification of the available regional data and the selection of subsets of that data which are suitable for achieving the task objectives. In addition, we have been compiling and reviewing literature dealing with regional phases with particular emphasis on those studies applied to discrimination and to characterizing regional phase transmission properties within and on the borders of the U.S.S.R.

Our effort to acquire the data base needed to determine source related excitation differences for regional phases is proceeding on several fronts. We have initiated a computer search to identify events in a 2° x 2° area surrounding the Nevada Test Site for the period from 1962 to 1975. We anticipate using the records from these events at TFO and at selected other regional stations to determine the relative excitation of various regional phases for earthquake and explosive sources. To supplement these data for the purpose of studying the depth dependence of regional phase excitation, we have identified and requested digital data from Nevada Test Site

station (SDCS) recordings of seven southern California earthquakes with focal depths in the range from 5 to 16 km. A preliminary look at records for these events suggested that at least some of the deeper events were producing clear P_g phases not apparent on records for the shallower events from the same area.

In our survey of regional phase literature we have reviewed several reports dealing with the propagation characteristics of various regional phases and their application to the discrimination problem. Among the primary sources of this type of information are the technical reports for several DARPA/AFOSR contracts in recent years. Wave groups which have been given the greatest attention in these studies are L_g, R_g, P_n, P_g and S_n. The propagation characteristics of these phases have been established using recordings of regional earthquakes (cf. Shishkevish, 1979; Nuttli, 1979). However, nuclear explosion data for the U.S. (cf. Evernden, 1967; Baker, 1970; Blandford and Hartenberger, 1978) and, in some cases, presumed nuclear explosion data for the U.S.S.R. recorded outside the country (cf. Pomeroy, 1978b; Gupta, 1979; Gupta et al., 1980) have also been used.

Results of preliminary discrimination studies using regional phases are somewhat mixed. Blandford and Hartenberger (1978), based on a comparison of recorded regional phases from the Salmon nuclear explosion and earthquakes in the eastern U.S., found that the ratio of the amplitude in the time window following S_n (presumably L_g) to that in the P wave time window (P_n and P_g) was greater for earthquakes than for the explosion. Gupta (1979) and Gupta et al., (1980) reported similar findings for southern Asia where the amplitude ratios of various time windows for several earthquakes in the U.S.S.R. border region were compared with those for presumed nuclear explosions inside the U.S.S.R. Pomeroy (1978a) reported differences in the excitation of early and late phases within the L_g window between the Salmon explosion and earthquakes in the eastern U.S. which he attributed to depth of focus differences. However, for earthquakes and presumed nuclear explosions in the western U.S.S.R. Pomeroy (1978b) found a wide scatter in

the ratio of early to late time $L_g(Z)$ excitation which did not permit discrimination. Furthermore, for the western U.S.S.R. data set Pomeroy (1978b) found no distinguishable differences in the ratios of $L_g(Z)$ to P wave amplitudes between the earthquakes and explosions. In a still more recent study, Pomeroy (1979) found no clear separation in the L_g/P amplitude ratios for explosions in southern Russia compared to similar amplitude ratios for the Gazli earthquake of April, 1976. It should be noted, however, that Pomeroy (1979) and Gupta et al., (1980) suggest that local or regional differences may be contributing to the lack of a clearer separation in the proposed discriminant. We plan to continue to review reports as they become available from on-going studies of regional phase propagation. In addition, we are continuing our literature review to identify regional differences in the propagation characteristics of the various regional phases within the U.S.S.R.

REFERENCES

Baker, R. G. (1970), "Determining Magnitude from L_g", BSSA, 60, pp. 1970-1919.

Blandford, R. R. and R. A. Hartenberger (1978), "Regional Discrimination Between Earthquakes and Explosions", Paper presented at the 1978 Fall Meeting of the AGU.

Evernden, J. F. (1967), "Magnitude Determination at Regional and Near-Regional Distances in the United States", BSSA, 57, pp. 591-639.

Gupta, I. N. (1979), "Discrimination Studies Based on Regional Data from Western U.S.S.R.", Presented by the DARPA/AFOSR Program Review Conference on Regional Seismic Detection and Discrimination.

Gupta, I. N., B. W. Barker, J. A. Burnetti and Z. A. Der (1980), "A Study of Regional Phases from Earthquakes and Explosions in Western Russia", BSSA, 70, pp. 851-872.

Nuttli, O. W. (1979), "Excitation and Attenuation of Short-Period Crustal Phases in Southern Asia", Presented at the DARPA/ AFOSR Program Review Conference on Regional Seismic Detection and Discrimination.

Pomeroy, P. W. (1978a), "An Investigation of Seismic Wave Propagation in Eastern North America", Rondout Associates, Semi-Annual Technical Report Under Contract F49620-78-C-0043.

Pomeroy, P. W. (1978b), "An Investigation of Seismic Wave Propagation in Western U.S.S.R.", Semi-Annual Technical Report No. 2 Under Contract F49620-78-C-0043.

Pomeroy, P. W. (1979), "Regional Seismic Wave Propagation", Rondout Associates, Semi-Annual Technical Report No. 3 Under Contract F49620-78-C-0043.

Shishkevish, C. (1979), "Propagation of L_g Seismic Waves in the Soviet Union", N-1014-ARPA.

TITLE OF EXECUTIVE SUMMARY: "Regional Discrimination Research"

AUTHORS: J. M. Savino, J. R. Murphy and T. J. Bennett

Project: VT/0701 Contractor: Systems, Science and Software

Task 4.2 Task title from Statement of Work: "Development of Regional Discriminants"

Objective

The objective of this task is to synthesize all the information on characterization of regional phases obtained under Task 4.1 of this contract and develop a tentative set of discrimination techniques that will be applicable to events recorded at regional distances. The set of source discriminants to be considered will include techniques that use regional body and surface waves jointly and separately. Data for preliminary testing will include events in the United States and Eurasia recorded at SDCS, SRO and AEDS stations. We will conclude this phase of the work with a plan for more comprehensive testing of the proposed set of source discriminants.

Accomplishments

A proposed source discriminant that will receive particular attention during the course of work under Task 4.2 is the variable frequency magnitude (VFM) technique (Savino et al., 1979; 1980a and 1980b). During the recent VSC sponsored discrimination experiment, the VFM technique, which is based on narrow band filtering of seismic signals, was applied to digital recordings of short period P waves from 133 Eurasian events. These events were recorded at a globally distributed network of seismograph stations. While the majority of VFM discrimination results were for teleseismic P waves, preliminary results from several Asian stations that recorded regional P waves from both earthquakes and explosions indicated that, at least for some source-receiver combinations, the VFM technique provides very effective discrimination of events at epicentral distances less than 20 degrees.

Figure 1 shows the locations of 18 shallow earthquakes (open circles) and ten presumed explosions (closed circles) relative to the

Seismic Research Observatory (SRO) station at Kabul, Afghanistan (KAAO). The epicentral distance range of these events to KAAO is 15 to 23 degrees, with the nine presumed explosions in eastern Kazakhstan at approximately 17 degrees. The VFM results for these 28 events, which are based on analysis of short period P waves only, are given in Figure 2. As seen in this figure, the presumed explosions separate from the shallow earthquakes over the entire event magnitude range. In particular, using the VFM technique we find that we can discriminate between shallow earthquakes (Events 80, 162, 163 and 272) and nearby explosions. The implication here is that differences in propagation paths are minimized and we are seeing differences in the explosion and earthquake source spectra.

VFM results from a short period sensor located at the site of the Iranian Long Period Array (ILPA) are shown in Figure 3 for events in the distance range 6.9 to 19 degrees. Several of the shallow earthquakes mapped in Figure 1 are included here. Deep focus events are indicated by the open squares ($50 < h \cdot 250$ km) and open triangles ($h > 250$ km). The presumed explosion, Event 22, is approximately 12.5 degrees from ILPA. Event 22 was the only presumed explosion in this distance range from ILPA for which digital recordings were available. The VFM results in Figure 3 are primarily based on P_g for the shallow earthquakes included within the solid line and mantle P waves for all the other events. While the presumed explosion separates extremely well from earthquakes at equal or greater distances, the separation between it and the six earthquakes at closer distances to ILPA is much less. This is probably a result of more efficient high frequency P_g propagation for the earthquakes in the distance range 6.9 to 9.2 degrees.

Because of the small number of stations and regional events, particularly explosions, analyzed to date, the VFM results discussed above must be considered preliminary. Thus, during the first phase of this contract we have concentrated on identifying a more substantial data set, both in terms of numbers of events and improved geographical distribution. This new data base will include L_g waves since we will be extending the VFM technique to include all the principal regional

wave types. To date we have reviewed the large Eurasian discrimination data base for digital recordings of regional phases at the AEDS, SRO and ASRO stations. A list of available digital seismograms for P_n, P_g, and L_g waves has been compiled and is being used as a starting point for identifying additional events needed for analysis.

REFERENCES

Savino, J. M., J. F. Masso and C. B. Archambeau (1979), "Discrimination Results from the Priority 1 Stations (U)", Systems, Science and Software Interim Report Submitted to the Advanced Research Projects Agency, SSS-CR-79-4026, May. (S).

Savino, J. M., C. B. Archambeau and J. F. Masso (1980a), "Discrimination Results from the Priority 2 Stations", Systems, Science and Software Technical Report (Draft) Submitted to the Advanced Research Projects Agency, SSS-R-80-4566, July.

Savino, J. M., C. B. Archambeau and J. F. Masso (1980b), "Discrimination Results for Eurasian Events Using the Priority 1 and Priority 2 Stations (U)", Systems, Science and Software Technical Report (Draft) Submitted to the Advanced Research Projects Agency, SSS-CR-80-4570, July. (S).

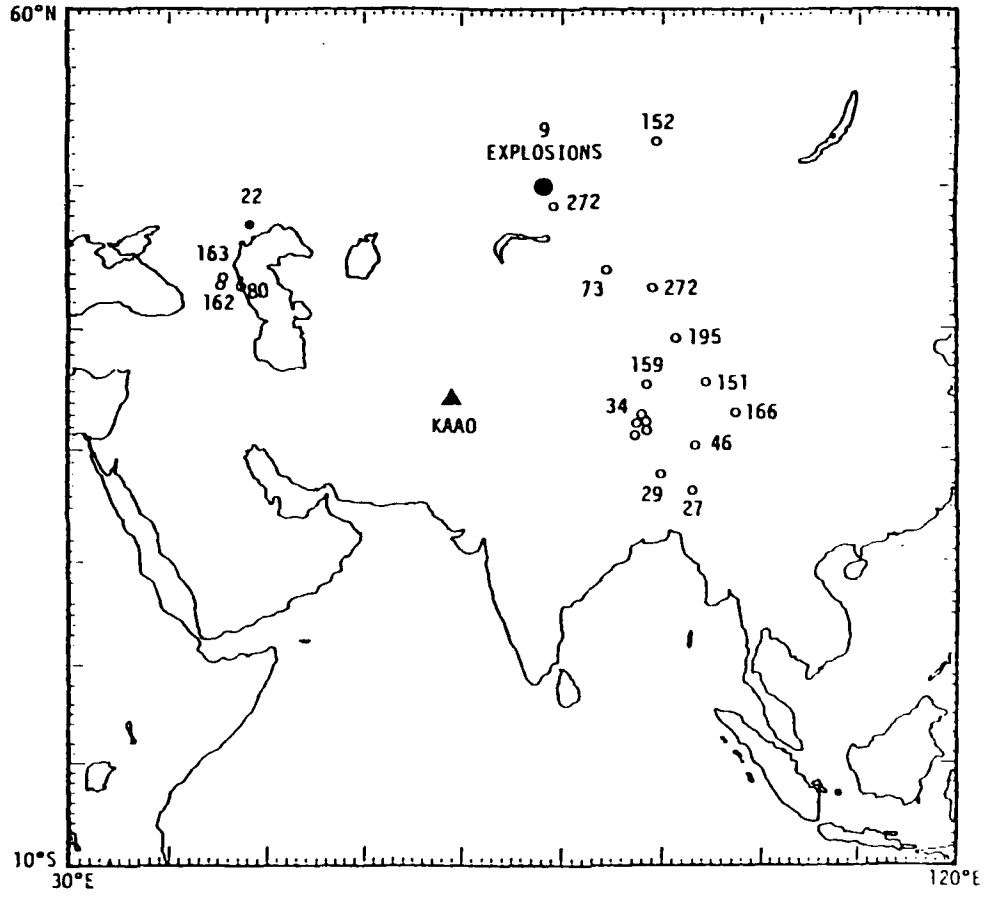

Figure 1. Map of Eurasian Earthquakes (Open Circles and Presumed Explosions (Closed Circles) Located Between 15 and 23 Degrees From the SRO Station at Kabul, Afghanistan (KAAO).

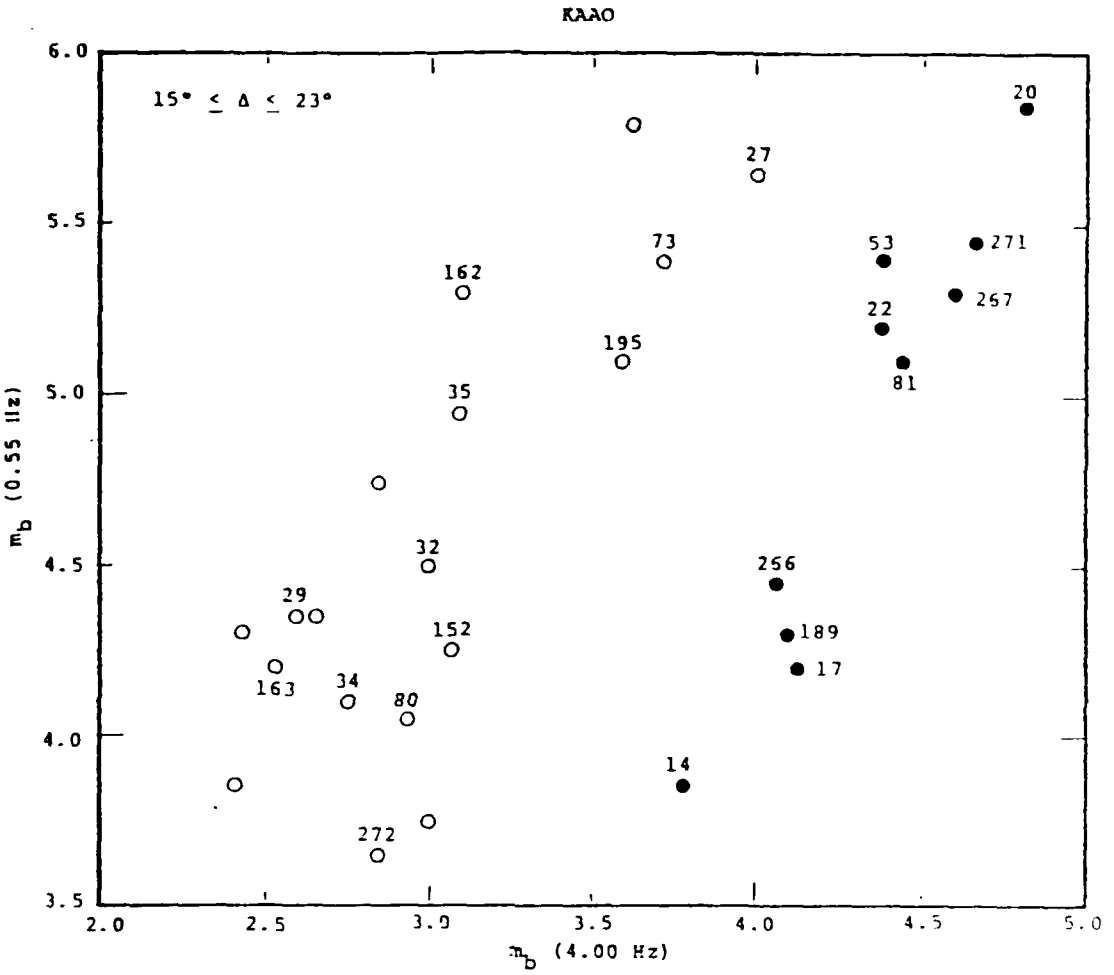

Figure 2. VFM Discrimination Results for Kabul, Afghanistan (KAAO) for the Earthquakes (Open Circles) and Presumed Explosions (Closed Circles) Mapped in Figure 1. These Events are Located Between 15° and 23° from KAAO. Frequency Dependent Magnitudes at 4.00 Hz are Plotted Along the Abscissa, Magnitude Estimates at 0.55 Hz Along the Ordinate. These Magnitudes are Based on the Amplitudes of Envelope Functions Obtained From the Outputs of Narrow Band Filters Applied to the Event P Waves.

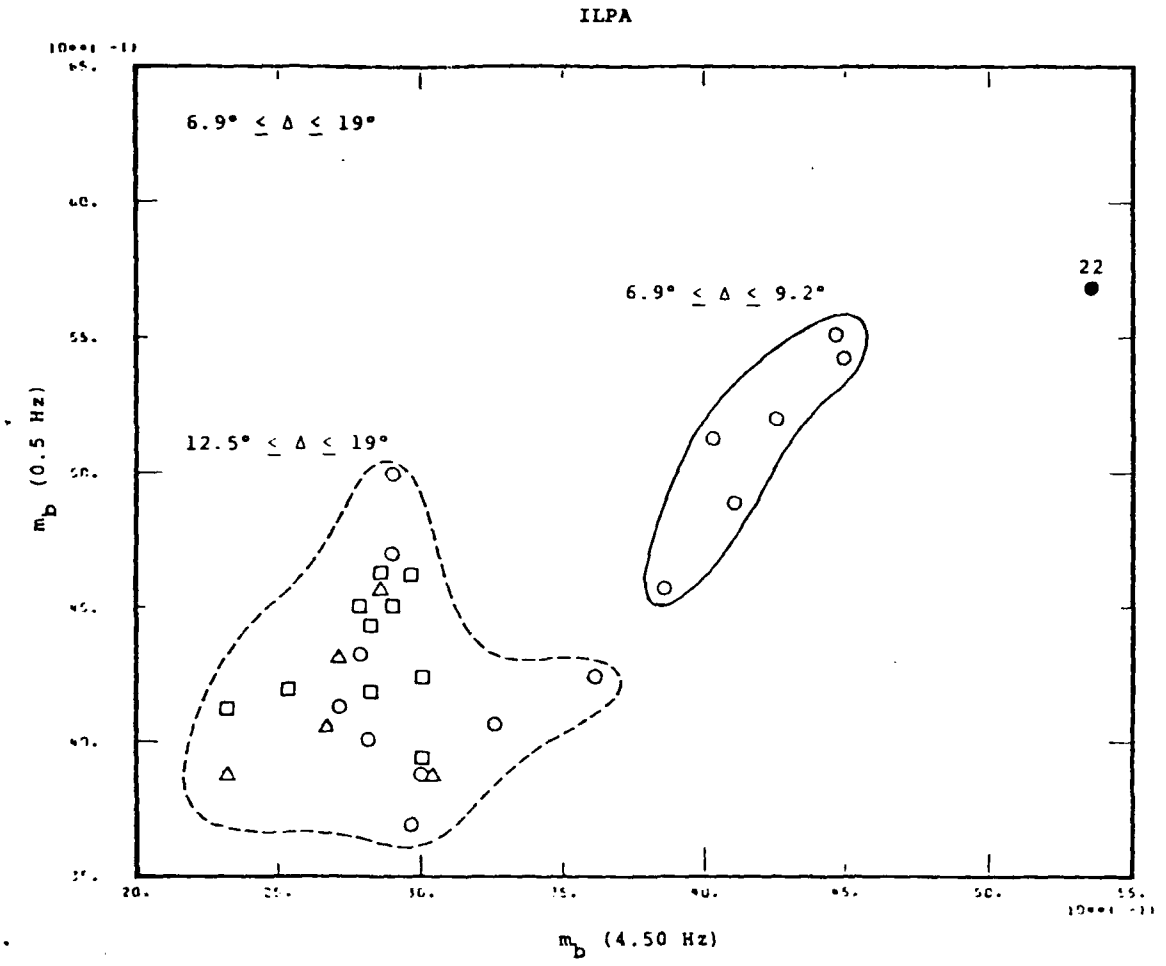

Figure 3. VFM Results for Regional Events Recorded at ILPA. The Dashed and Solid Curves Group Events in the Two Epicentral Distance Ranges. The Epicentral Distance of the Presumed Explosion, Event 22, to ILPA is 12.5 degrees. For the Earthquakes, the Open Squares Indicate Focal Depths Between 50 and 250 km, Open Triangles for Depths Greater Than 250 km.

CONTRIBUTION OF TWO-DIMENSIONAL SOURCE EFFECTS TO THE FAR-FIELD SEISMIC SIGNATURES OF UNDERGROUND NUCLEAR EXPLOSIONS

T. C. Bache
T. G. Barker
N. Rimer
J. T. Cherry

Project VT/0712

Contractor: Systems, Science and Software

Tasks 4.2: Regional Seismology
4.1.1: Seismic Source Calculations

Objective

As the contract evolved, the objective of Task 4.2 became to study the far-field seismic waves from a series of two-dimensional explosion calculations done under Task 4.1.1. The purpose was to determine the importance of nonlinear interaction with the free surface (including spallation) and the depth-dependence of overburden pressure and material properties. While the potential importance of these two-dimensional effects has long been acknowledged, previous attempts to model the seismic signatures of underground explosions have almost all employed spherically symmetric point source representations. A quantitative understanding of the potential influence of higher order source effects is important for delineating the validity of this convenient approximation.

Accomplishments

The results summarized here are extracted from a 1980 Systems, Science and Software report by Bache, Barker, Rimer and Cherry. The report presents a detailed analysis of the seismic waves from eleven two-dimensional finite difference calculations of underground nuclear explosions in granite. Seven were 150 KT explosions at depths from 159 to 1000 meters done by J. Trulio and N. Perl of Applied Theory, Inc. (ATI).

The other four calculations were done at S-Cubed with one intended to model the PILEDRIVER event. The constitutive model and source geology (three layers) were chosen for this particular event. As described by Rimer, et al. (1979), the computed and observed ground motions were compared at some twenty-five near-field gauge locations, where the agreement was quite good, except that the calculation overpredicted the amount of cracking (spallation). This turns out to be important when comparing synthetic and observed far-field seismograms. The other three S-Cubed calculations were the same, except that the depth and yield were varied. The four calculations were as follows:

DEPTH (meters)	YIELD (KT)
463	60 (PILEDRIVER)
1000	150
1000	20
400	20

The main results of the study may be summarized by plots of M_S and m_b versus source depth and yield. The observed values for the United States granite explosions PILEDRIVER, SHOAL and HARDHAT provide a standard for comparison.

In Figure 1 the M_S for all eleven calculations are plotted versus source depth. For this plot all M_S, including the observed value for PILEDRIVER, have been scaled to 150 KT by adding log (150/W).

In Figure 2 the M_S values are plotted versus yield. ALso shown are the M_S from seismograms computed with reduced displacement potential (RDP) sources. The RDP calculations were done at S-Cubed for two depths (460 and 1000 meters) with the same constitutive models used for the two-dimensional (2-D) calculations. Thus, comparing seismograms from the RDP and 2-D calculations directly displays the influence of two-dimensional effects.

The m_b data from the ATI and S-Cubed source calculations are plotted versus source depth in Figure 3 and versus yield in Figures 4 and 5. Again, the values for comparable RDP sources are shown to directly display the two-dimensional effects predicted by the S-Cubed calculations.

The most important result of this study is that the S-Cubed calculations show M_S to be a strong function of depth. The shallow S-Cubed calculations have surface wave amplitudes that are a factor of two or three larger than those from a comparable one-dimensional source calculation. This effect is probably exaggerated because the free surface interaction effects are too large in the S-Cubed calculations, but would remain important even with increased strength in the near-surface material. On the other hand, the ATI calculations show no strong dependence of M_S on depth, even though the shallow ATI sources cratered. We do not know why the two sets of calculations give such different results.

Comparison of waveforms, as well as the magnitude data in the plots, leads to the following conclusions:

ATI Calculations

- Neither m_b nor M_S are strongly dependent on depth. The most effect was on M_S at shallow depths.

- Compared to the semi-empirical RDP source of Mueller and Murphy (1971), depth dependence in both amplitude and corner frequency is less for the ATI sources.

- The pP phase appears to be smaller than expected from elastic theory.

S-Cubed Calculations

- Two-dimensional effects are not very important for the two deep explosions (20 KT and 150 KT at 1000 meters). Both m_b and M_S are little different from the values estimated from an RDP source computed with the same constitutive model at the same depth.* It is gratifying that these two very different and complex procedures arrive at the same results. This is true even though considerable cracking and spallation occur in the two-dimensional calculations.

- For body waves the first arriving P wave is essentially the same for one- and two-dimensional sources.*

- The two-dimensional effects enhance the surface wave amplitudes for the shallow events (60 KT at 463 meters and 20 KT at 400 meters) by a factor of two or three. We must qualify this by pointing out that these shallow calculations have very strong surface interaction effects. Comparison with PILEDRIVER data indicates that the free surface interaction is overpredicted, at least for that event. Less free surface interaction would presumably give less enhancement of the surface wave amplitudes.

- For the shallow events, the m_b is different than predicted with an RDP source, though by less than 1.2 units.

* These results are essentially tests of the entire computational procedure.

- Analysis of the spectra show that in no case is pP a spectral shadow of P, as it is for an RDP source and elastic propagation.

- Phases that seem to be associated with spall closure can be seen on the shallow source body wave records. However, they are not easily associated with identifiable crack closure patterns in the source calculation.

- Comparison of observed and calculated body and surface waves for PILEDRIVER leads to the conclusion that the two are in rather good agreement. This conclusion is subject to the qualifications one often faces in this kind of comparison. For the surface waves, it is the need to account for the non-axisymmetric component, usually attributed to tectonic stress release. Adding a recent estimate for this component by Rivers and von Seggern (1979) to our solution, we get good agreement with the data. However, if the strike-slip solution of Toksöz and Kehrer (1972) is correct, the synthetic surface waves are about a factor of six too small.

- For body waves the comparison is complicated by the apparent presence of strong azimuthal effects in the radiated short period energy (Hadley and Hart, 1979). Our conclusion is that the computed PILEDRIVER source (in one- or two-dimensions) has about the right direct P amplitude. However, the two-dimensional source calculation appears to include too much non-linear interaction with the free surface. The later portion of the P waveform does not match the data, apparently because pP is too greatly suppressed and because the seismic energy from spall closure is too large or is timed incorrectly. This "overprediction" of surface interaction effects is expected since comparison of theoretical and observed near-field motions and plots of the cracking near the source indicate that there was too much spallation in the calculation.

- The constitutive models used by S-Cubed (in spherically symmetric source calculations) lead to RDP source functions that are strongly peaked, with the value near 1 Hz a factor of five or more larger than the value at long

periods. The peaking is due to the incorporation of an effective stress law and the choice of unconfined compressive strength (0.75 kbar), based on laboratory data for fractured granite and results of comparison with near-field ground motion observations.

- While we do not have RDP source functions for the ATI granite, comparison of M_S and m_b for the ATI two-dimensional calculations indicates that the RDP peaking is probably less than a factor of two. Due primarily to this difference, the m_b for the S-Cubed calculations is about 0.5 units higher than that for ATI calculations of the same yield. The ATI M_S values fall between those for the shallow and deep S-Cubed calculations.

REFERENCES

Bache, T. C., T. G. Barker, N. Rimer and J. T. Cherry (1980), "Contribution of Two-Dimensional Source Effects to the Far-Field Seismic Signatures of Underground Nuclear Explosions," Systems, Science and Software Topical Report SSS-R-80-4569 submitted to ARPA/VSC, July.

Hadley, D. M. and R. S. Hart (1979), "Seismic Studies of the Nevada Test Site," Sierra Geophysics Quarterly Technical Report submitted to VSC/ARPA, SGI-R-79003, June.

Mueller, R. A., and J. R. Murphy (1971), "Seismic Characteristics of Underground Nuclear Detonations Part I: Seismic Spectrum Scaling," Bull. Seism. Soc. Amer., 67, pp. 1675-1692.

Pert, N., F. J. Thomas, J. Trulio and W. L. Woodie (1979), "Effect of Burial Depth on Seismic Signals, Volume I," Pacific Sierra Research Technical Report submitted to DNA/ARPA, PSR Report 815, May.

Perl, N. and J. Trulio (1979), "Effect of Burial Depth on Seismic Signals, Volume II," Pacific Sierra Research Technical Report submitted to DNA/ARPA, PSR Report 815, May.

Rimer, N., J. T. Cherry, S. M. Day, T. C. Bache, J. R. Murphy and A. Maewal (1979), "Two-Dimensional Calculation of PILEDRIVER, Analytic Continuation of Finite Difference Source Calculations, Analysis of Free Field Data from MERLIN and Summary of Current Research," Systems, Science and Software Quarterly Technical Report submitted to VSC/ARPA, SSS-R-79-4121.

Rivers, W. and D. H. von Seggern (1979), "Effect of Tectonic Strain Release on Surface-Wave Magnitudes," to be published as Teledyne Geotech Technical Report SDAC-TR-79-6, submitted to VSC/ARPA.

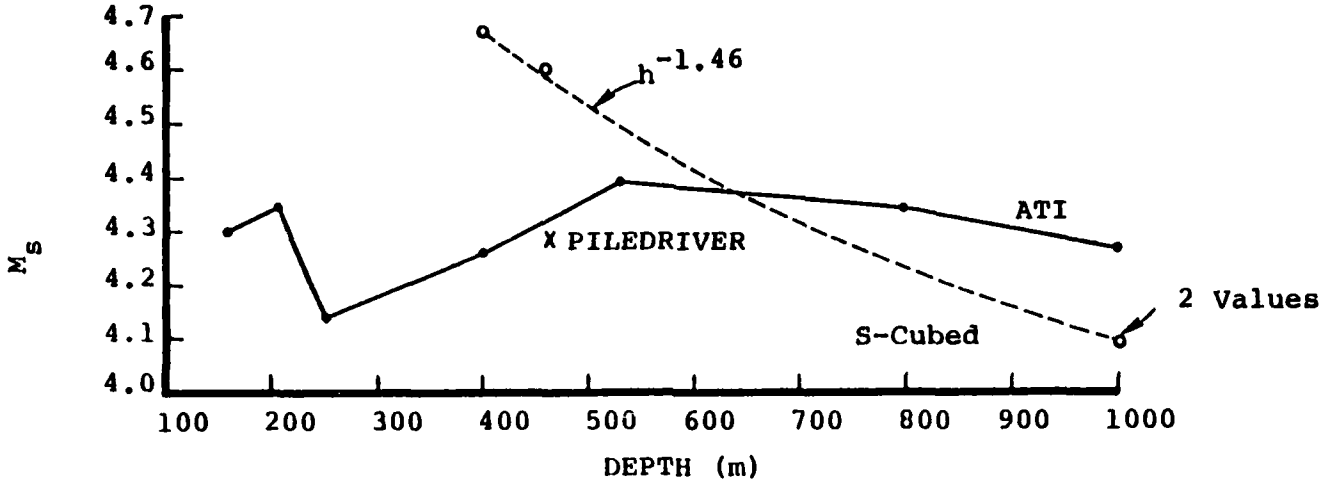

Figure 1 The M_S values for all the two-dimensional calculations are plotted versus source depth. The observed value for PILEDRIVER is also shown. All magnitudes have been scaled to 150 KT.

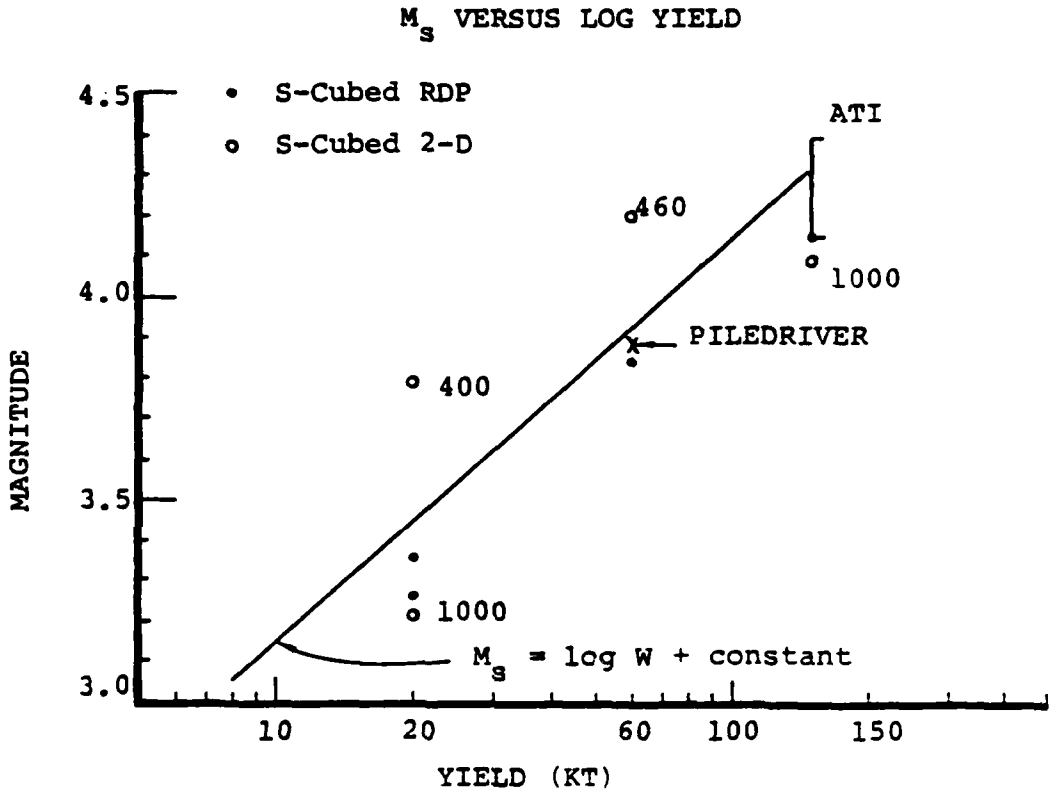

Figure 2. The M_s values for the S-Cubed RDP and two-dimensional source calculations are plotted versus explosion yield. The PILEDRIVER observed value and the range of M_s for the seven 150 KT ATI sources are also shown. The source depth of the S-Cubed two-dimensional calculations is noted with the M_s.

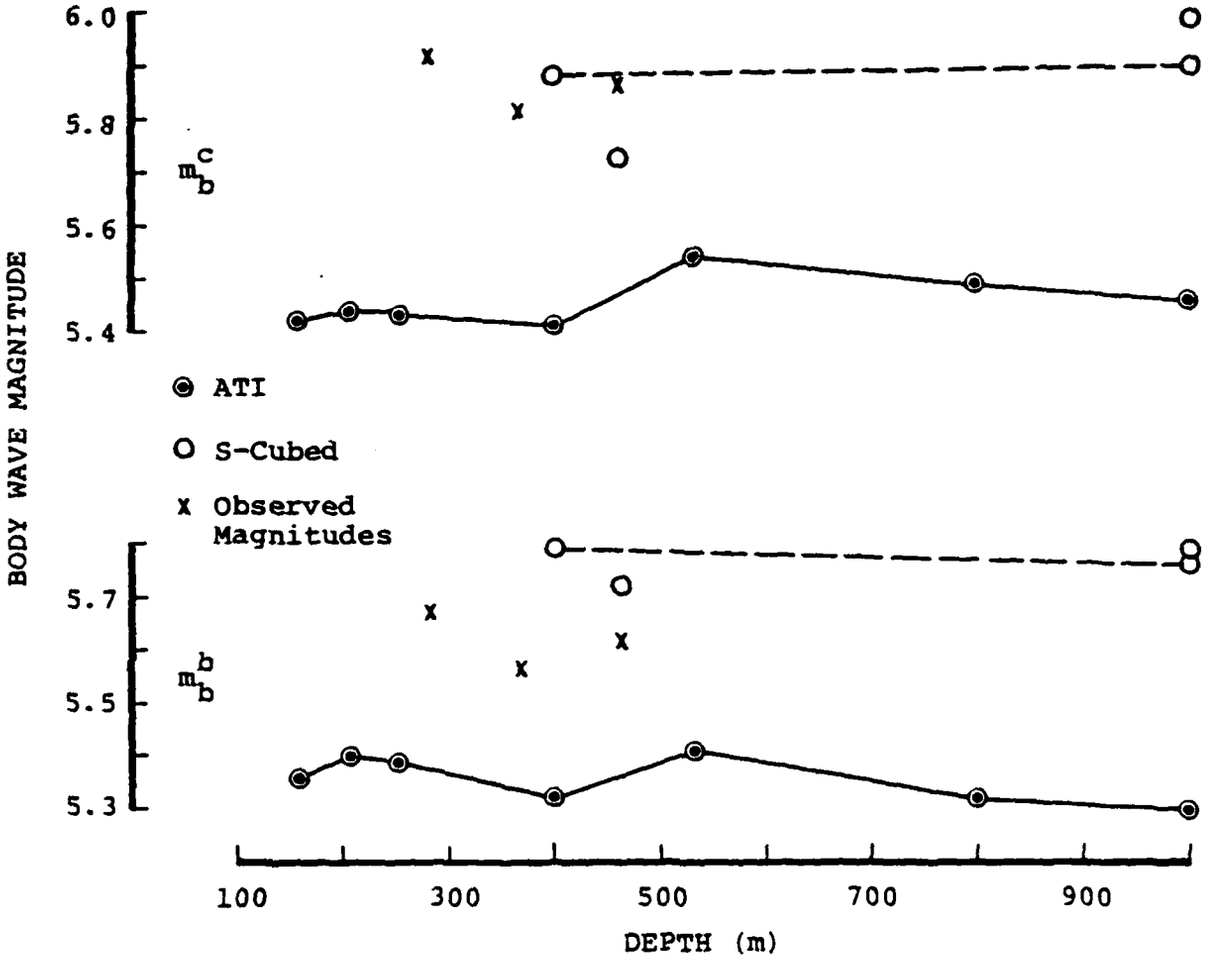

Figure 3 The m_b values for all the two-dimensional calculations are plotted versus source depth. The S-Cubed calculations at the same yield are connected with a dashed line. The observed values for HARDHAT, SHOAL and PILEDRIVER are also plotted with $m_b^b = m_b^c - 0.25$. All magnitudes have been scaled to 150 KT.

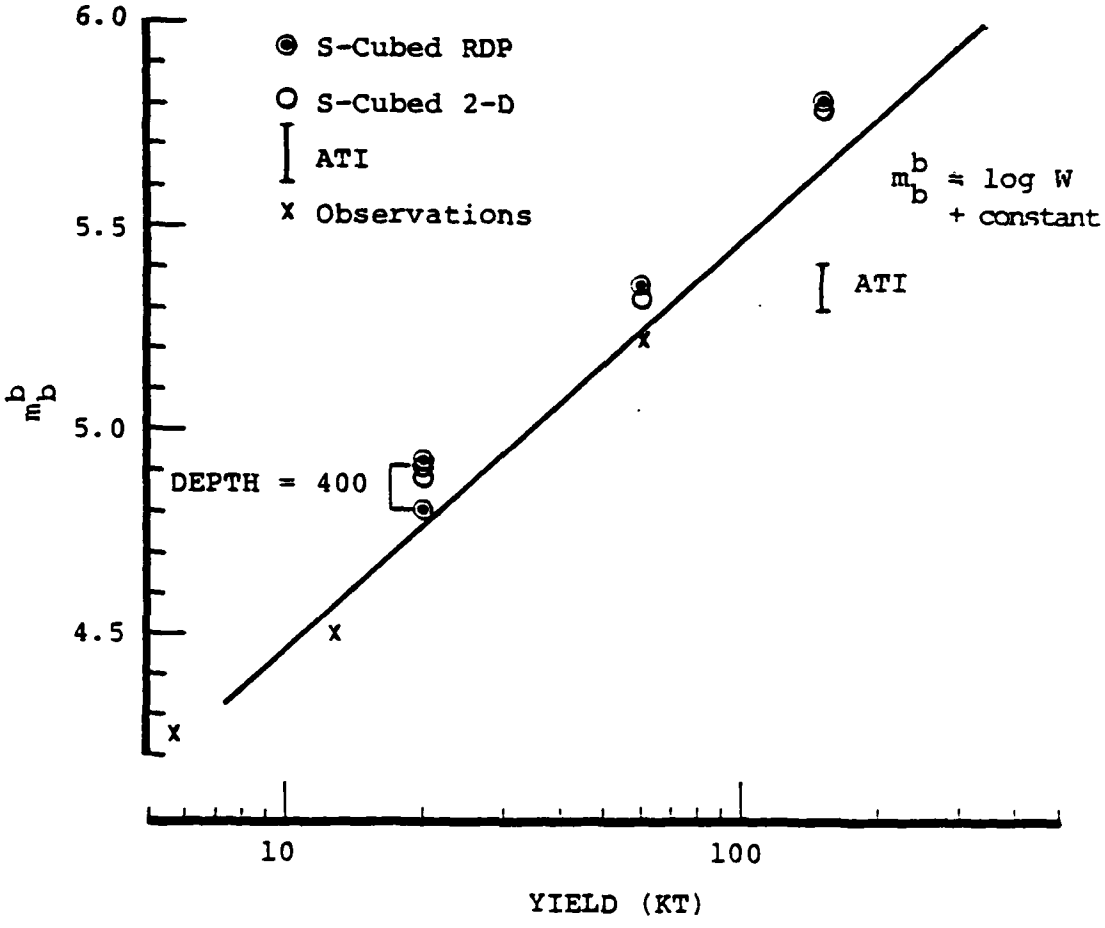

Figure 4 The b phase magnitude, m_b^b, is plotted versus yield. The values for the ATI calculations fall within the indicated range. The observed values are the published m_b^c minus 0.25 for HARDHAT, SHOAL and PILEDRIVER.

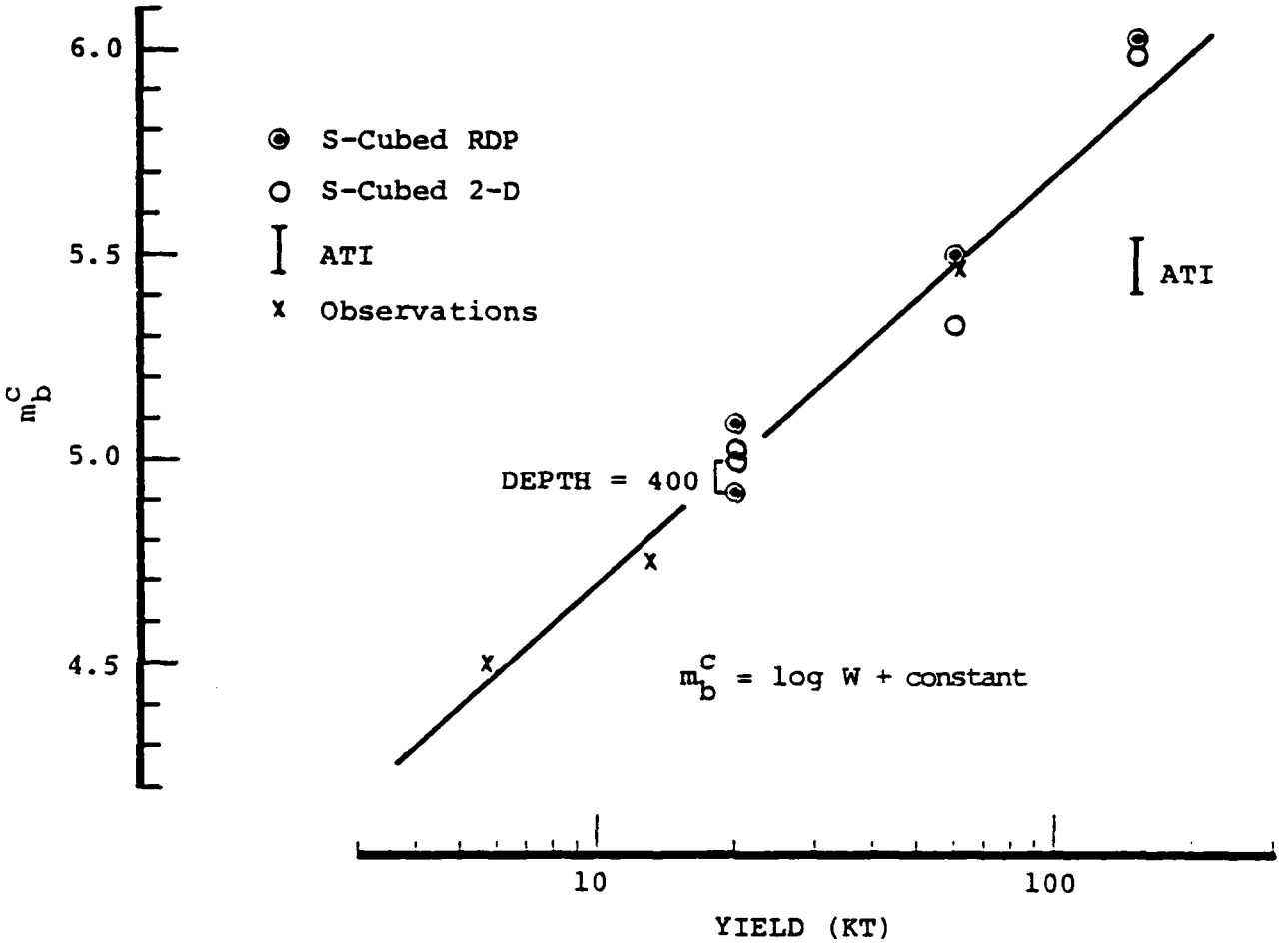

Figure 5 The c phase magnitude, m_b^c, is plotted versus yield. Published (network average) magnitude values for HARDHAT, SHOAL and PILEDRIVER are also plotted.

DETECTION OF REGIONAL PHASES

E. Smart and H. Sproules

Project VT/0709 Contractor: Teledyne Geotech

Task 4.1.2 Detection of Regional Phases

Objective

The purpose of this study was to apply the technique known as the Smart processor, developed at the SDAC (Smart, 1977), to identify and determine the propagation direction of regional seismic phases, operating on a comprehensive data set.

Accomplishements

The Smart single-station maximum-likelihood surface-wave processor and variants thereof, all relying on 3-component particle-motion analysis, demonstrated in this study their utility for automatic signal azimuth determination. For the test data set the average azimuthal error was 6.7° for the L_g signals and 6.0° for the P arrivals. Moreover, the results strongly suggest that the particle-motion analysis can further be made to automatically yield good distance determinations simultaneously with the azimuth measurements. One source location determination could thus be made for each recording station picking up an event.

As noted above, the purpose of this study was to develop a regional event processor based upon the fundamental-mode surface-wave technique developed by Smart (1977). The study has enabled us to explain the past success of the technique as an azimuth estimator when applied to L_g phases.

A test data set of 32 events was collected at RKON, well distributed azimuthally about that station, Figure 1. Signal and noise spectra were computed for all the L_g phases. The noise spectra were found not to vary significantly over the seasons, contrary to expectations. Figure 2 shows the spectra of four events, the two highest frequency and the two lowest frequency spectral maxima in the data set. It also shows composite noise spectra by seasons. It can be seen that the noise spectra peak below 0.4 Hz, whereas all signal spectral peak at or above that frequency. In general, the low-frequency signals were those which transversed complex mountainous regions on their way to RKON, e.g., events from California, Oregon, Washington, and British Columbia.

A modified version of the Smart processor was used which estimates particle motion ellipticity as well as azimuth and waveform. Previously ellipticity had been an input parameter. The frequency band examined was 0.5 and 3.0 Hz. The L_g window for each case was hand picked by an analyst. Good back azimuths were obtained in general: the average error was 6.7°. Some of the low-frequency events yielded the least accurate estimates.

We attempted to find a parameter for detection, i.e., one which separated signals from the noise. The parameters investigated were: the F-statistic, the mean recurrence period, and the derivative $\partial^2 E/\partial \phi^2$, where E = error and ϕ = back azimuth (see Smart, 1977). The rms excursions for the model in the

Task 4.1.2 Detection of Regional Phases

Accomplishments continued

vertical, radial, and transverse directions, denoted by Z, R, and T, were also examined.

The derivative did not follow a discernible pattern. The F-statistic and mean recurrence period were consistently low for both noise and signal and did not separate them (see Figure 3 for F-statistic histogram). The best discriminator was the ratio T/R, but the separation of the populations was not complete enough to make it a useful detection parameter (Figure 4). It was observed that $T/R < 2.0$, when it occurred, accompanied poor azimuthal estimates, i.e., error > 10°, and that the smaller T/R, the larger the azimuthal error.

These observations suggested that the figure traced by the particle motion in the horizontal plane might serve to indicate signal azimuth. An algorithm was coded to find in each time window the orientation in the horizontal plane in which the rms excursion, in the frequency band of interest, was minimized. The azimuth of that orientation was, on the average, as good an estimate of surface wave origin as the back azimuth from the original coherent processor. Moreover, it was more stable. In low signal-to-noise records, where T/R fell below 2.0, the estimated azimuth was more accurate than that of the coherent processor. All this appears to explain why the Smart processor has been successful for estimating L_g azimuths, but unsuccessful for detecting L_g arrivals. The azimuth estimations have been controlled by the dominant transverse Love component, but the F-statistics have been kept low by the incoherence between the vertical and radial components, incoherence resulting from the mixing of Rayleigh modes, the fundamental with higher modes. Thus, the Smart processor operating on L_g waves actually functions as an incoherent processor.

The results suggested another use of the elongation of the figure described by particle motion, that is, to flag the arrival of P-waves and indicate their azimuths. 6.4 second time windows--an order of magnitude smaller than those for the L_g waves--were used to search in the vicinity of the expected P arrivals. The principal axis of the elongated figure was taken to indicate back azimuth, and the amount of elongation, that is, the ratio of the principal long axis to the short axis, was taken as the index of signal presence. Taking that ratio at 2.4 as the detection threshold, in the band 0.9 to 6.0 Hz, 80% of the signals were detected with a false alarm rate of 28 per hour. The average azimuthal error was 6.0 degrees, and in the case of the low-frequency, low signal-to-noise events these P azimuthal estimates were markedly more accurate than those from the L_g waves. Thus, in spite of the high L_g/P ratios, the P wave proved more useful for signal detection and for azimuth estimation than L_g, within the restraints of the present investigation.

The limitations of this study have not permitted the conclusion of the research. The optimum frequency band, the optimum signal flag, and the most useful combination of P and L_g information have not been determined. Two additional detection criteria have suggested themselves during this work.

Task 4.1.2 Detection of Regional Phases

Accomplishments continued

One is the observed stability of orientation, over several time windows, of the elongated particle-motion envelope, both in the P-wave portion of the record and in the L_g portion. The other is the observed ninety degree rotation of the envelope as the P-wave passes and the L_g wavetrain arrives. These items demand further study.

Finally, it appears from the research carried out thus far, that the principal utility of particle-motion processing lies not in signal detection, where the simple power detector is so successful, but in azimuth and distance determination. Of the missed signals in the P-wave detection trials discussed earlier, the P-wave processor estimated the back azimuth of half of them to within 5 degrees of their true back azimuth, even though it did not "detect" them. One of these signals was not visible even to the analyst. Moreover, the elongation of the figure traced by the reference particle has not been fully exploited in this study. The orientation of the elongation, measured in 3 dimensions and not just in the horizontal plane, will yield not only azimuth but emergence angle as well which indicates the source distance and thus fixes location. The time between P and L_g, measured from the power rise at the signal onset down to the point where the particle-motion orientation rotates 90 degrees, also yields a distance estimate. Particle motion processing can also be exploited for picking phases. All of this potential must be addressed in future research.

Reference

Smart, E. (1977). A 3-component single-station maximum-likelihood signal processor, SDAC-TR-77-14, Teledyne Geotech, Alexandria, Virginia.

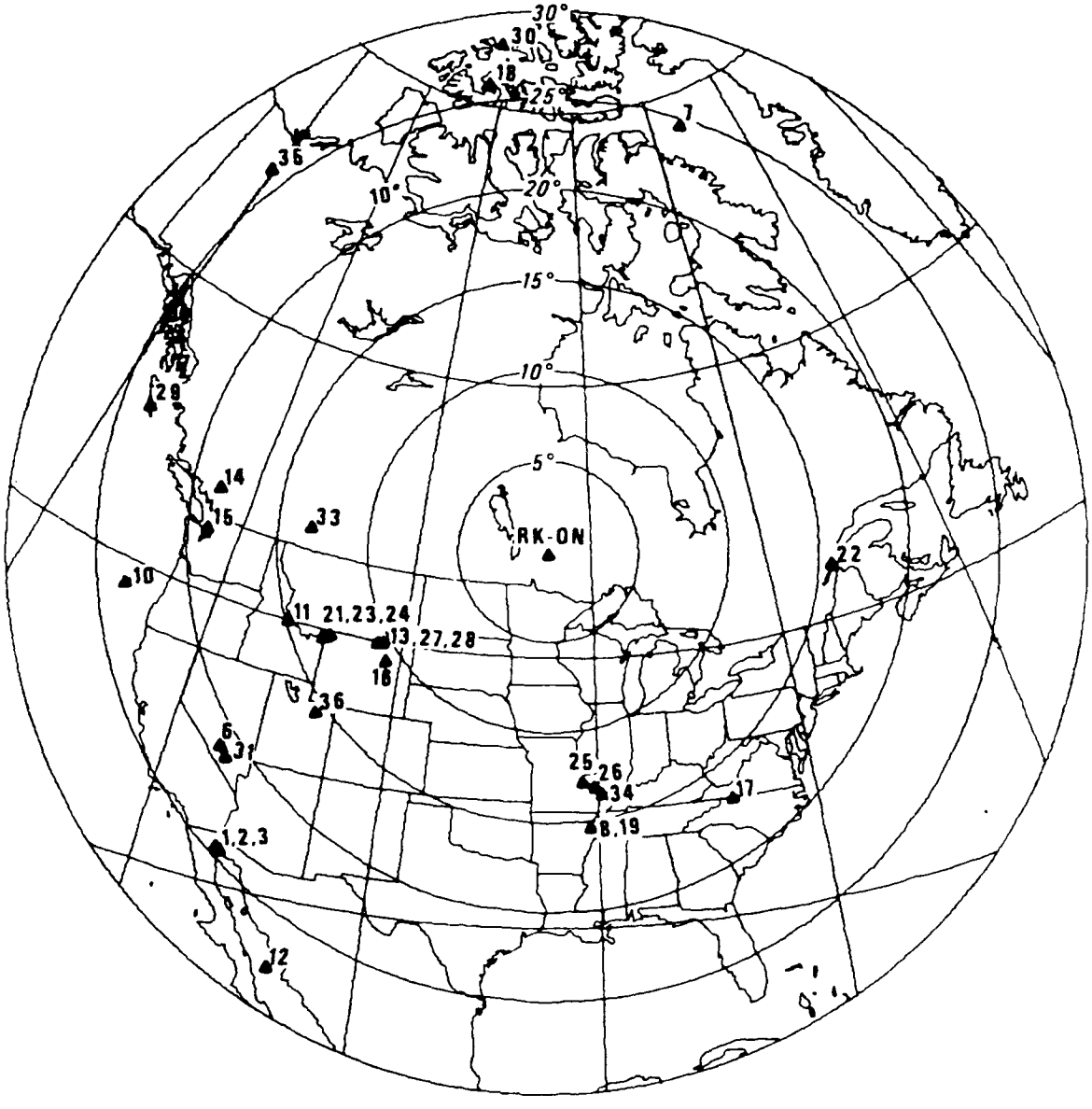

Figure 1. Map showing the location of RKON and of the events used in this study.

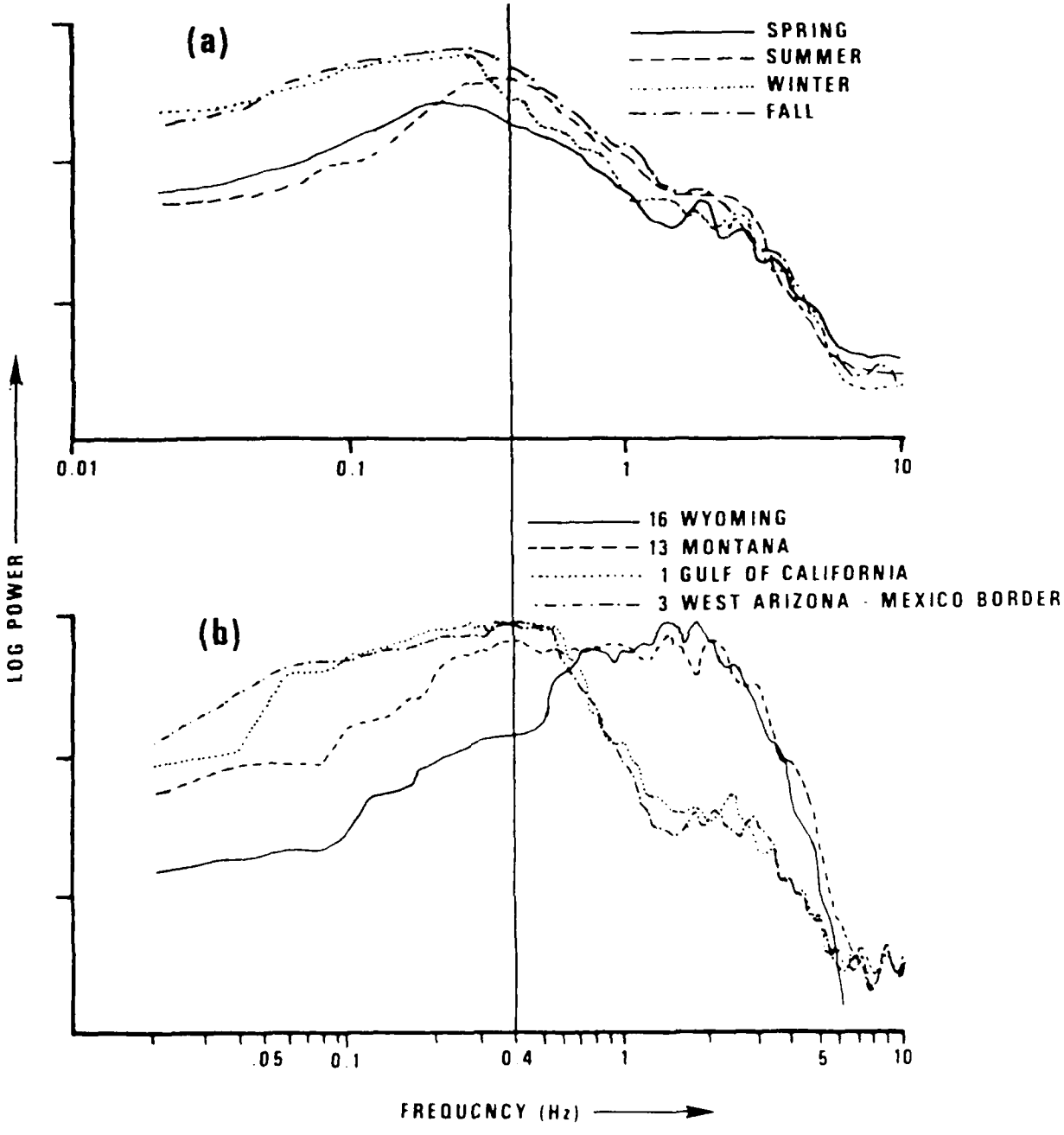

Figure 2. (a) Composite noise spectra for RKON, for four seasons.
(b) Peak-normalized spectra of the lowest- and highest-frequency events nos. 1, 3, 13 and 16.

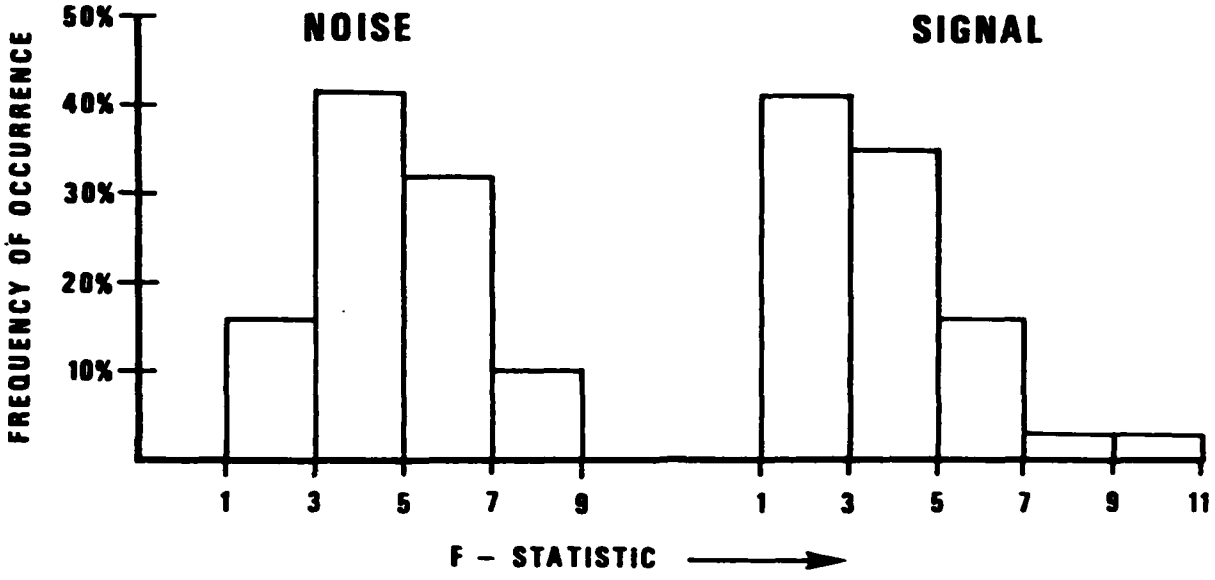

Figure 3. F-statistic for noise and L_g's for the frequency band 0.1 to 6.0 Hz show negligible separation of populations.

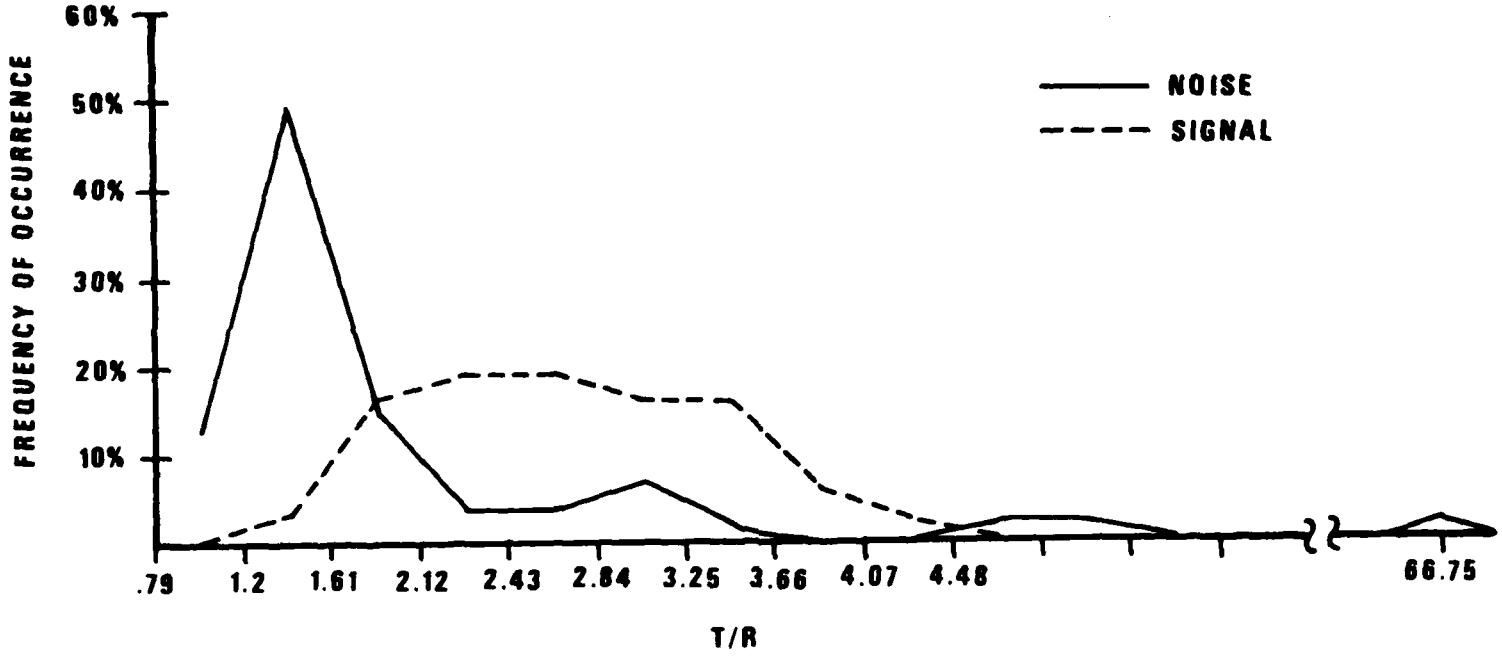

Figure 4. Separation of noise and signal by T/R.

REGIONAL EVENT LOCATION EXPERIMENT

J. Martin, A. Whitaker, R. Baumstark, R. Blandford

Project VT/0706 Contractor: Teledyne Geotech

Task 4.5.4 Regional Event Location Experiment

Objective

Procure equipment for and design and implement an environment to conduct regional event location studies. The system will be similar in function and include the capabilities of the NEP system but will emphasize the ability to modify algorithms and conduct experiments relating to improving techniques, algorithms, and methods of locating and evaluating seismic signals from regional distances.

Accomplishments

For the most part the effort on this task was devoted toward equipment selection. Special consideration needed to be given for selecting hardware for the analyst station. The requirements for a large graphic screen and many vectors were met by the supplier, Vector Automations. Two color alphanumeric screens were configured with the system as well.

Function specifications are well underway and personnel are familiarizing themselves with the hardware, operating system and program language. Preliminary file structure for the RELS processing have been defined and coordination begun with the project office and other members of the staff.

DETECTION PROCESSING

R. Blandford, A. Hill, A. Whitaker, R. Romine, D. Racine

Project VT/0706 Contractor: Teledyne Geotech

Task 4.5.3 Detection Processing

Objective

To procure equipment for and design and implement system software to support researchers conducting detection experiments and to recommend, test, and report results of detection algorithms run in this environment.

Accomplishments

Two parallel efforts were actually conducted for this task. Computers and processing systems were evaluated which resulted in recommendations for an upgrade to the SDAC systems. Conceptional planning for data flow, recording, and file structures was also begun in support of this task.

Concurrently, a detection experiment was conducted using the on-line data stream. The detections were made off-line using the data recorded by the DPS system.

This new detector implemented on the DEC PDP-11/70 provided much insight into the capabilities of this computer and its UNIX operating system. Also many improvements were made to the detector in a scientific or geophysical sense.

- Reprogramming the entire program in FORTRAN to facilitate program maintenance, and to eliminate program bugs which could not be found in the machine language version.
- Adding a FFT algorithm for identification of analog a spikes.
- Using a FFT output for identifying local events.
- Adding a data dropout algorithm.
- Improving the detection start time algorithm.
- Adding ability to easily modify run time parameters.
- Identifying AI detections for NORSAR.
- Adding the capability to get on-line plots of detection windows.

In general terms, the net result of these enhancements is a detector which is truly useful and reliable and which has gained the confidence of the analysts. Missed signals are always weak and difficult even for the analyst to detect. Spikes and locals are generally properly identified and thus properly handled by AA. No longer does the analyst feel the need to scroll to find missed detections. Almost every detection shows signs of being a plausible signal. Start times are typically accurate to 0.3 seconds.

Another project under this task was to supply test data for evaluation of detectors by various contractors. VSC Technical Note No. 38, "Experimental Design for Detector Evaluation: Single Channel Detectors," was written by R. Blandford. The abstract reads:

Task 4.5.3 Detection Processing

Accomplishments continued

"A suggested experimental design for automatic single channel detectors is to bury approximately 30 signals at 4 gain levels each in 24 hours of noise from single elements at NORSAR and PWY. The noise is to be real noise except that random phases will be assigned to the Fourier components so that researchers may be confident that false alarms are not weak signals. The detectors to be tested on this data base include an STA/LTA detector working on rectified and squared data; a detector working on the squared STA transformed into a unit normal distribution; a detector working in the frequency domain and looking for coincident detections; and two detectors designed to work on microprocessors, one of which uses for the STA a sum of the squared signal and squared first derivative, and the other of which uses the Walsh transform."

The data tapes have been produced and distributed to the interested researchers. The standard STA/LTA algorithm has been run on the optimally prefiltered data and the results distributed with the tapes as a benchmark. Tests on the tapes have shown that a 10-second window is perhaps 0.05 mu better in detection than the 3-second window, and that there are small advantages to detecting with the appropriate window length in general. However, the advantages to detecting with several windows are very small or even negative because of the additional false alarms generated. A carefully selected bandpass filter seems to be equal in practical terms in capability to the optimum filter.

Work under way at this time involves testing other detectors and creating a 3-component data base on which to test 3-component detection and location.

Analysis of Regional P-wave Attenuation Characteristics and Station Detection Procedure using ISC Data Files

by

Frode Ringdal and Jan Fyen

Project VT/0702/B/PMP

Contractor: NTNF/NORSAR
Post Box 51
N-2007 Kjeller, Norway

Task 6: Earthquake Detectability and Magnitude Studies

Objective

Conduct a detectability study of International Seismic Centre reporting stations for regional events. Analyze P-wave amplitude decay as a function of epicentral distance. The results of this study will be used to improve the currently used magnitude-distance correction factors.

Accomplishments

A study has been undertaken to derive the global attenuation characteristics of P-waves based upon data files from the International Seismological Centre (ISC). The main motivation behind the study has been the failure of commonly accepted attenuation relations to provide good magnitude estimates at epicentral distances below 20 degrees. In fact, using the Gutenberg and Richter (1956) or Veith and Clawson (1972) amplitude-distance curves at close distances usually leads to an overestimation of earthquake magnitudes (m_b), sometimes by a full magnitude unit or more, relative to teleseismically derived m_b estimates.

For the study presented here, 136 globally distributed seismograph stations were selected. Most of these were WWSSN stations, and all of them are stations with fairly consistent reporting of amplitudes and periods of P-phases of detected seismic events. Altogether 6 years of data (1971-76) were included in the data base, giving a total of about 214,000 log A/T observations in the distance range $0\text{-}90^{\circ}$.

The observed values of log A/T - m_b(ISC) are plotted versus epicentral distance in Fig. 1, and compared to the Veith-Clawson (1972) and Gutenberg and Richter (1956) relationships. In the plot all data within each 1 degree interval have been averaged to obtain a fairly smooth curve. The following major points may be noted:

a) Below 20 degrees the observed averages generally lie at least 0.5 m_b units higher than the conventional correction factors, thus confirming the bias effects mentioned earlier.

b) Although there is a local maximum between 15 and 20 degrees, this is not by far as pronounced as indicated in the conventional attenuation relations.

We also did some studies to investigate the effects of possible error sources in the data base, and preliminary conclusions are as follows:

1. Possible ISC m_b bias at low or high magnitudes. We first note that all ISC values are based on stations only at epicentral distances at least 20 degrees, so that the bias effects at closer distances should be relatively small. Nonetheless, we compared, for one year, the attenuation curves obtained using ISC and NORSAR reference m_b, respectively. As shown in Fig. 2, the resulting effect is only a baseline shift (independent of distance), thus this problem would not cause a change in the shape of the attenuation relationship.

2. Effects of instrument saturation and 'clipping'. This is potentially a serious problem, since, for large events, it may result in close-in stations reporting too low magnitudes. To investigate this, we subdivided all reference events into magnitude bins of 0.5 m_b units, and plotted the resulting curves separately as shown in Fig. 3. It is seen that there are indeed significant differences, although the main conclusions a) and b) remain unaltered. However, this problem will be subjected to further investigation.

There may also be other sources of bias effects, such as the lack of consistency in station reports and possible effects of frequency-dependent attenuation, but we have at this stage little possibility to investigate

these further. Our main conclusion is that the conventionally used P-wave attenuation relationships should be revised for short distances, and we believe that this study will provide a useful first step for such a revision.

An attempt to extend the methods of Ringdal et al (1977) to estimate the detectability of ISC-reporting stations at distances 0-30 degrees has so far had only limited success, due to the lack of 'reference events' within this distance range for the stations of most interest. It appears that the most reliable approach in this respect would be to adjust the 50 per cent estimates given by Ringdal et al (1977) for teleseismic distance ranges to nearer distances simply by compensating for the distance-dependent attenuation in accordance with the diagram of Fig. 1.

References

Gutenberg, B., and C.F. Richter (1956): Magnitude and energy of earthquakes Ann. Geofisica, 9, 1-15.

Ringdal, F., E.S. Husebye and J. Fyen (1977): Earthquake detectability estimates for 478 globally distributed seismograph stations, Phys. Earth Planet. Inter., 15, P24-P32.

Veith, K.F., and G.E. Clawson (1972): Magnitude from short-period P-wave data, Bull. Seism. Soc. Amer., 62, 435-452.

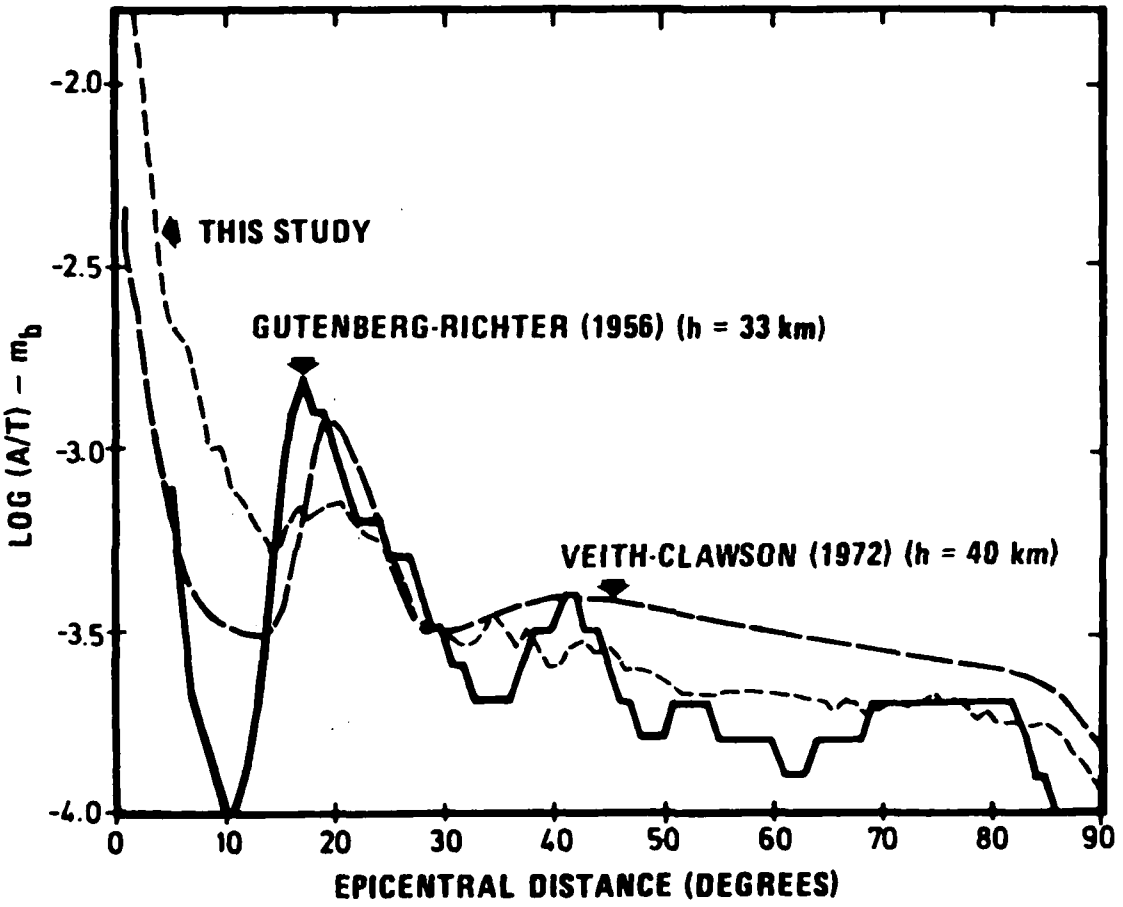

Fig. 1 Average observed magnitude correction factors based on ISC data for 23,198 events and 136 stations. Averages have been computed and plotted within each 1 degree distance interval. Note the considerable deviations from 'standard' curves at distances below 20 degrees.

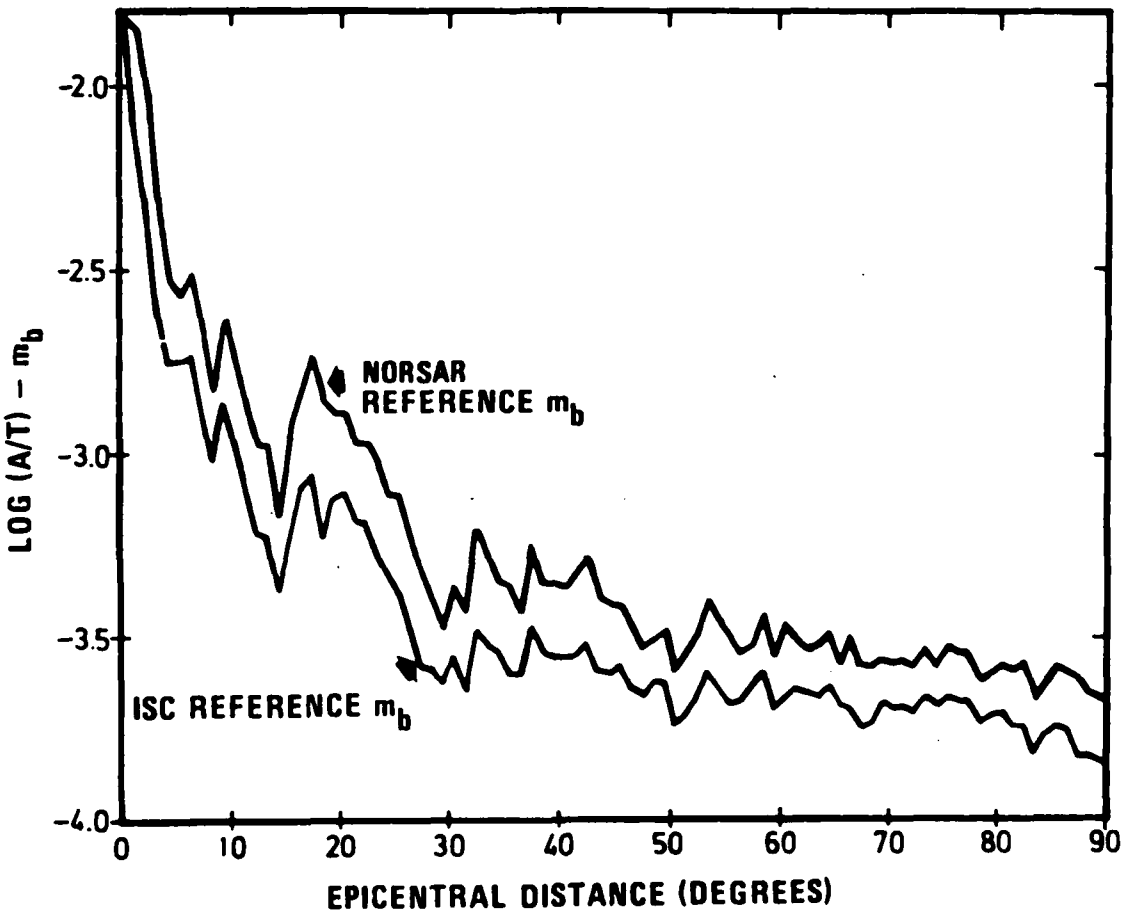

Fig. 2 Comparison of observed magnitude correction factors using NORSAR and ISC m_b values as a reference. The bias effect of about 0.2 m_b units is independent of distance.

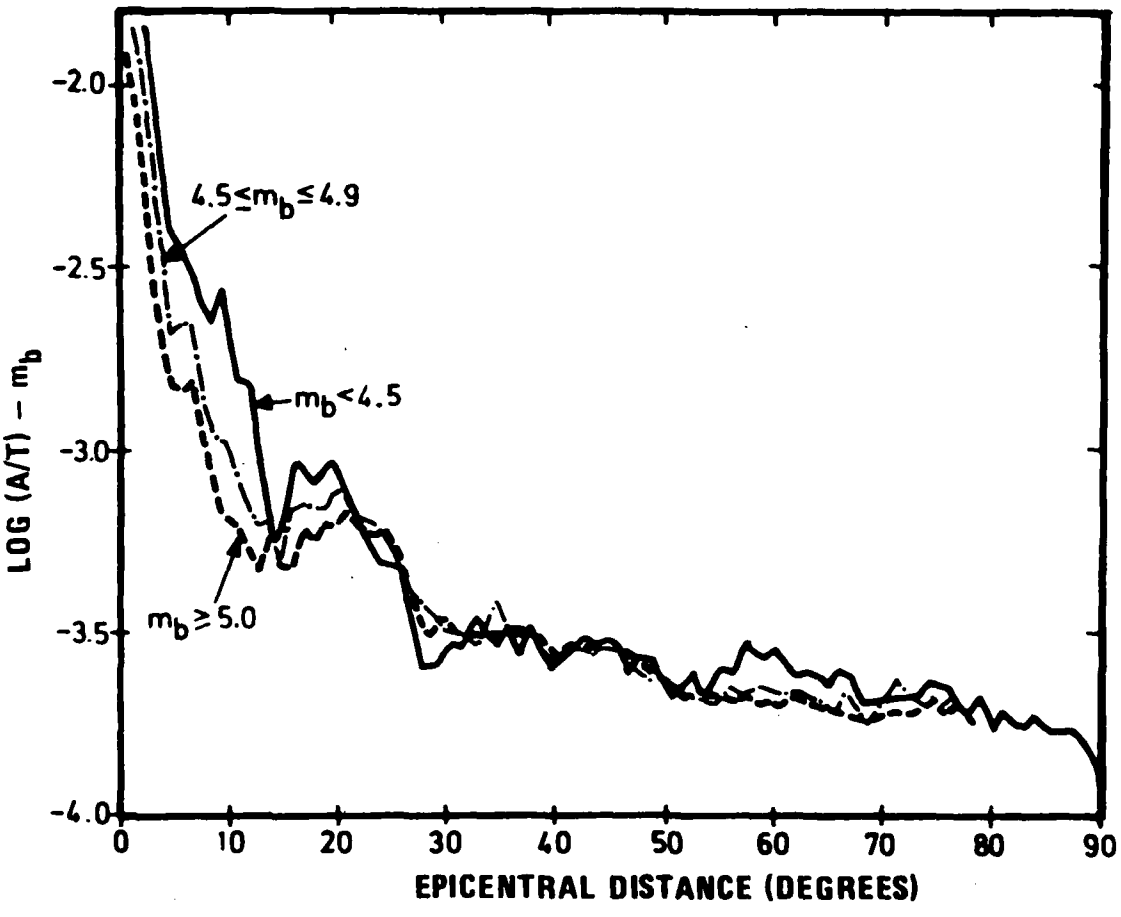

Fig. 3 Comparison of observed magnitude correction factors using as a data base events of different magnitudes. Using small reference events (m_b<4.5) results in higher correction factors within 20 degrees distance than using larger events.

MARS SEISMIC EVENT DETECTION

W. E. Farrell
R. C. Goff
J. Wang

Project VT/0712

Contractor:Systems, Science and Software

Task 4.3.1 Automatic Signal Processing: The MARS event detector

Objective

The objective of this Task was to optimize the MARS-based signal detection algorithm and evaluate it in an off-line mode on data supplied by VSC.

Accomplishments

The principal accomplishment has been the development of an efficient code which has been tested on four hour noise samples from NORSAR and Pinedale, and on the 24 hour NORSAR and Pinedale test tapes supplied by VSC. Results from both test tapes, which contained over 30 signals at each of 4 different amplitude levels, were comparable to the VSC benchmark run; that is, at similar false alarm rates, about the same pattern of events was detected. On the UNIVAC 1100/81 the algorithm runs at 40 times real time on the 10 sample/second NORSAR data. As with the VSC detector, most of the time (80 percent) is consumed by Fourier transforms.

As an example of the current state of the MARS detector, Figure 1 shows the first ten NORSAR signals extracted from the 24 hour test tape. Each signal was buried in noise at four distinct amplitude levels, which Blandford refers to as "raw signal-to-noise ratio 1/2, 1/4, 1/8, 1/16." We refer to these four scaled copies as signal classes A, B, C and D. Thus, the plot shows 10 A class events, those with raw SNR of 1/2. Furthermore, the seismograms shown in this figure are not the actual data present on the tape, but they have been high-pass filtered through a filter with a 1 Hz corner frequency. This is to attenuate the long period energy which contains mostly noise power and very little signal power. The events are much less obvious in the broad band data (see Figure 4). For each seismogram we have shown the times at which "events" were detected by the MARS processor. Events labeled A were detections found in the A class seismograms, just the records shown here. Events labeled B were found on the B class seismograms, and so on.

The most important point to be made about these results is that the principal objective in the work to date has been to optimize the speed of the code and to calibrate the false alarm behavior. Thus, we have not "educated" it to look for specific

signal types, nor to pick "first motion." Thus, the narrow band, long period motion in event 2, is ignored in favor of later, broad band energy. Seismogram 3 is easily found at all four signal levels, but the peak in the broad band power falls well back in the L_g wave train.

It should be emphasized that no pre-processing or signal conditioning (e.g., optimum band-pass filtering) precedes the MARS analysis. Instead, the raw data is at the very first stage decomposed into a multiplicity of band pass channels. The signal amplitude in each channel changes dynamically as the background noise power rises and falls, as the shape of the noise spectrum changes with time, and as true seismic events come and go. By keeping a running history of noise amplitude in each channel, the MARS process then flags significant short term excursions, and finally searches for a pattern across the many frequency bands.

Among the subsidiary accomplishments in this automatic signal processing task, the most important are the following:

- A tenfold or more acceleration in processing speed was obtained by incorporating a heterodyne and decimate operation in the construction of the narrow band envelope function. Implementation of this feature was based on the observation that the spectrum of a narrow band signal is band limited, and practically vanishes outside a narrow region about the center frequency. The heterodyne operation is a signal processing device which shifts the center frequency down to zero frequency. But now the signal spectrum drops to a negligible value at frequencies much less than the Nyquist frequency. Then the inverse transform back to the time domain can be accurately found with a new and much smaller Nyquist frequency.

- An extensive study was made of the statistical properties of narrow band seismic noise. This study was performed on the continuous envelope functions, rather than the envelope maxima catalog actually used by MARS, in order to be able to relate the experimental results with classical statistical theory. It was found, for example, that the envelope probability density function closely follows the Rayleigh law, which is expected if narrow band envelopes are extracted from Gaussian noise whose spectrum is not too ragged. Further, the joint statistics of multiple envelope functions were studied to estimate the cross-correlation between two envelope functions generated by different filters. This work was necessary to quantify the possibility of cross-correlation in envelope maxima, and to give

objective guidance both to the construction of the comb of filters, and to the significances of envelope alignments. Preliminary work was undertaken in multiple envelope correlation, using the Bernoulli trial model, but we have not yet obtained definitive results.

- Working still with noise records, we know how to tune the MARS false alarm rate by adjusting the three key parameters: amplitude (normalized with respect to the noise in each band), bandwidth and dispersion. Figure 2 shows a cube in this parameter space, each cell of which contains a number related to the False Alarm Rate. The bigger this number, the poorer the detector. In our terminology, the bandwidth parameter is called k; it gives the number of envelope maxima (out of twenty possible) required before an event is called. The amplitude parameter, also referred to as normalized amplitude cutoff in the third figure, expresses how large extrema must be before an envelope peak is to be included in the search for events. We refer to this as a normalized amplitude because each envelope function in the time window currently being processed is scaled by the mean envelope amplitude of the previous N windows. There is, then, a floor on the minimum instantaneous signal spectrum required before an event is called. The floor is just some multiple of the preceding noise spectrum. Finally, the dispersion parameter specifies how broad a time swath one permits the k peaks to fall within.

  Figure 3 shows a specific result selected from our noise study. It is a slice along the k = 6 plane for a two-hour section of NORSAR data. The figure shows that the lower left hand corner is good, but that the upper right hand corner is bad. But we do not want to be too far down in the lower left hand corner. That gives great noise rejection, but concomitantly requires an extremely large and impulsive arrival to trigger. Thus, this part of the parameter space would show a low probability of detection for easily seen signals. To capture weak, moderately dispersed signals, one wants to site the detector parameters somewhere in the hatched region.

- New graphical display procedures have been implemented for showing the time-frequency structure of seismograms. These have been found to be extremely powerful tools in our research studies, and should be equally useful at seismic analyst stations for operational detection and discrimination. Figure 4 displays the pre-bandpass filtered version of seismogram 5 from

Figure 1, along with its associated time-frequency decomposition. This is a true amplitude plot at each frequency, which clearly indicates the dominance of the long period noise, as does the comparison between this version of the seismogram and the bandpassed version in Figure 1. It can be seen, for example, that the best signal amplitude occurs over the 2 to 3.5 Hz frequency band. There is also significant signal power out to 5 Hz, but the noise there is so low, it is not possible to get an accurate estimate of the signal-to-noise ratio.

Another type of display is shown in Figure 5. This display is similar to the sonogram display, long used in acoustic signal processing, but these figures were generated by digital rather than analog signal analysis methods. In this display, high power points in the time-frequency plane are shown as black zones, small amplitude regions shade down through various gray levels towards pure white. Unlike the previous display, these data have been scaled according to the "peak" power in each frequency band. This tends to "whiten" any signals present, and make more visible these frequency bands with good signal-to-noise ratio.

The extra frequency dimension in Figures 4 and 5 tells much more about the nature of the seismic events than does the seismogram itself. Event 9, for example, is barely visible in Figure 1, but on Figure 5, it shows up as the dark band between 2 and 3 Hz, slightly later than 9 minutes. One does see, of course, bands of similar length elsewhere in the figure, but they are not surrounded by the long gray zone, indicating they are most likely noise signals.

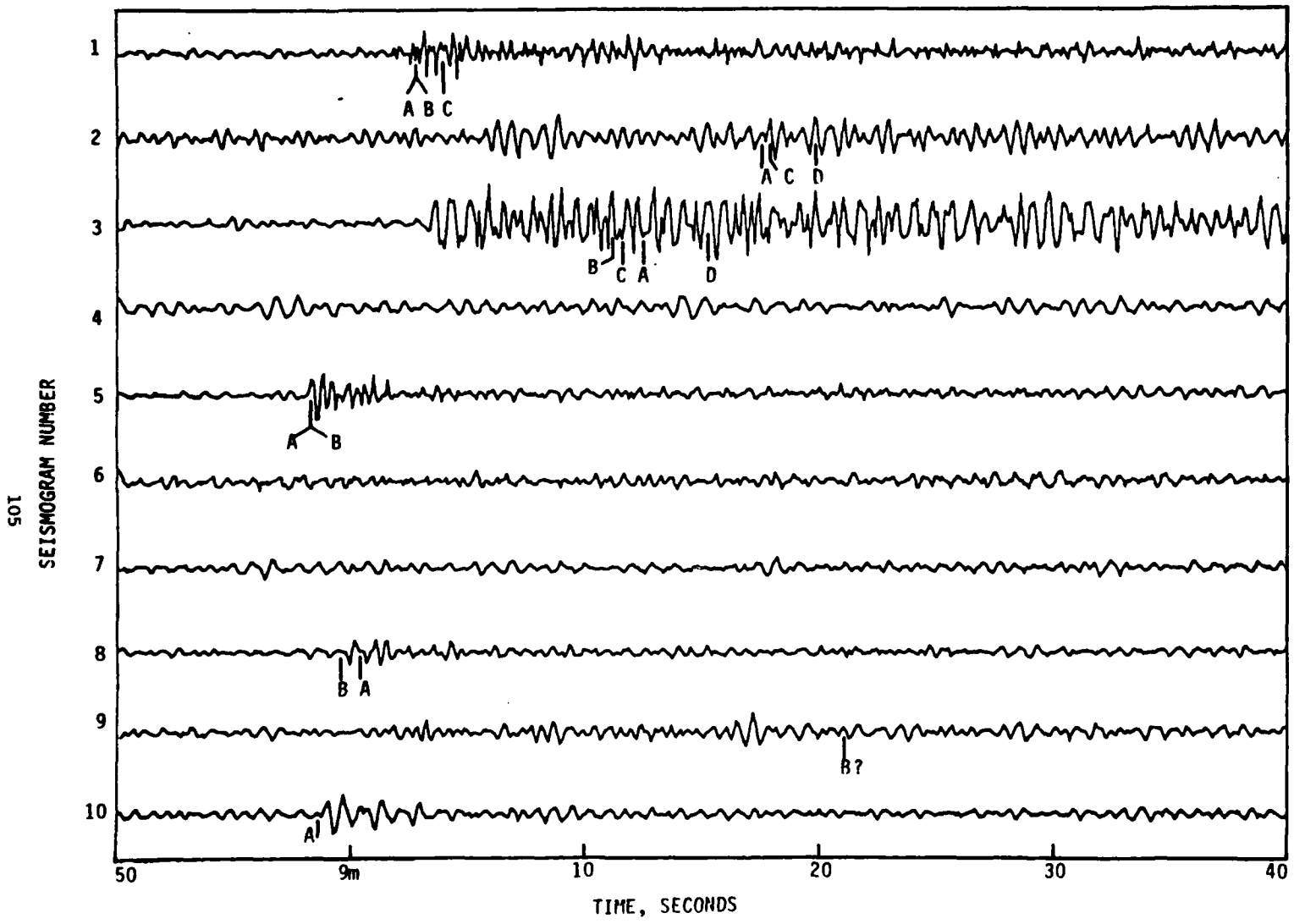

Figure 1. Events 1 to 10 from VSC 24 hour NORSAR test tape, high pass filtered. Letters A, B, C and D denote times of detection on signals with "raw signal-to-noise ratio 1/2, 1/4, 1/8, 1/16" respectively. There were 165 false alarms for this run over the 24 hour tape.

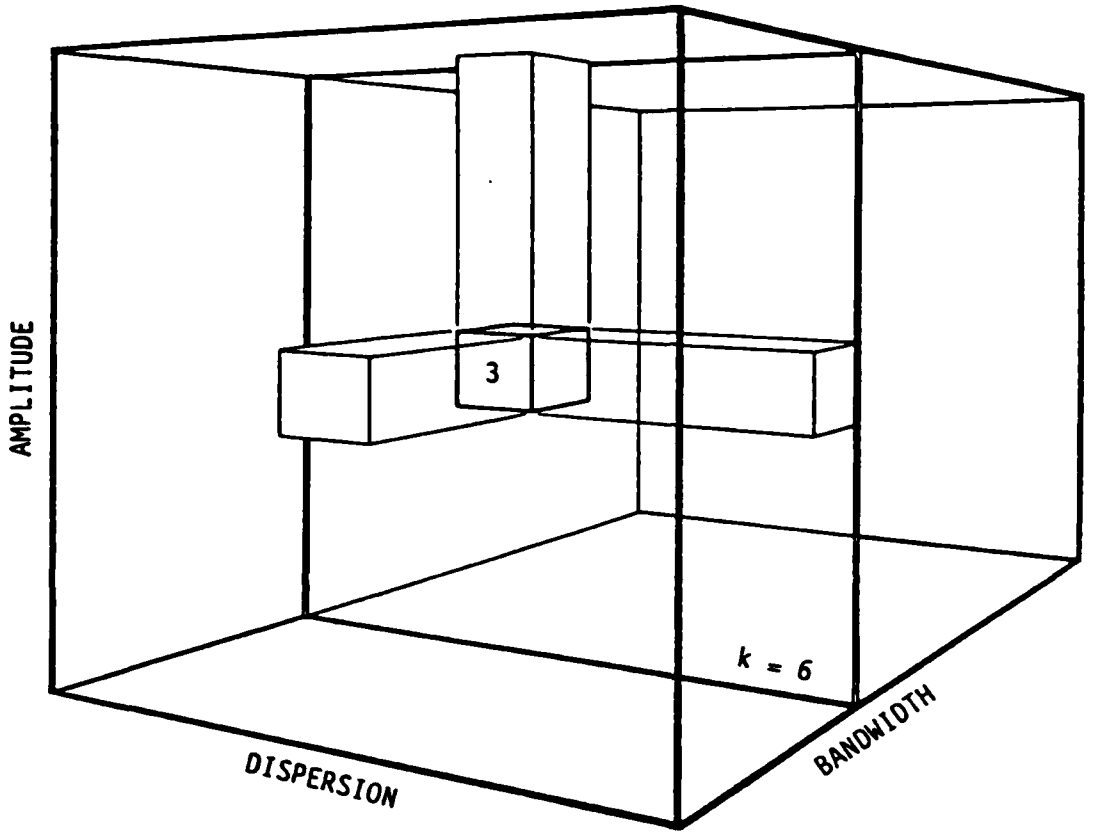

Figure 2. Schematic representation of the three-dimensional parameter space spanned by the key MARS (Multiple Arrival Recognition System) detection parameters. Each cell within this cube contains a number giving the false alarm rate when the algorithm operates on pure noise.

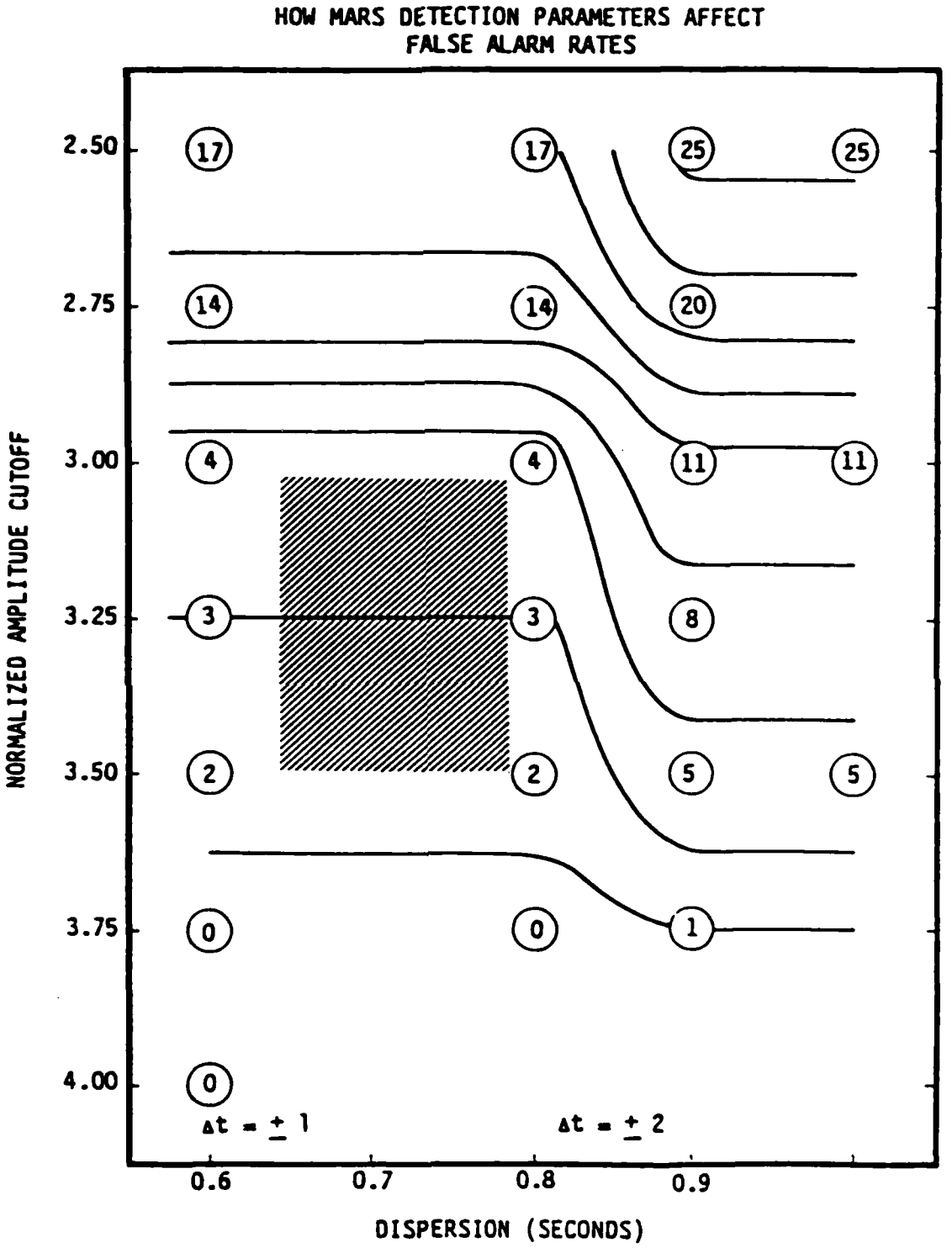

Figure 3. Contour plot giving number of false alarms in two hours of NORSAR data when k = 6 peaks are required to flag an event. Best region of operation is the hatched zone.

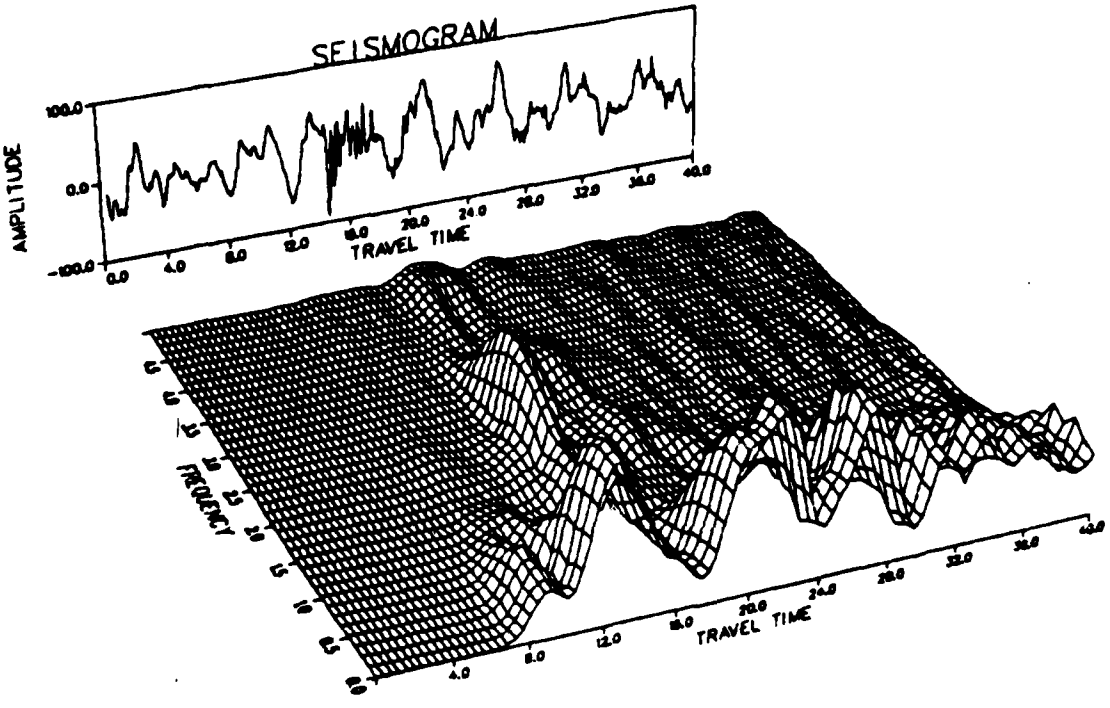

Figure 4. Seismic event 5 (see Figure 1) and its associated time-frequency decomposition. The fin at 16 sec (this time is arbitrary) and 2.5 Hz is the same event which appears at 56 seconds, 2.5 Hz in the middle panel of Figure 5. In this figure the true amplitude in each frequency band is preserved. This makes the predominance of the long period noise obvious. In Figure 5, the data has been "whitened" by scaling according to the largest amplitude in each band. This emphasizes frequency bands with good signal-to-noise ratio.

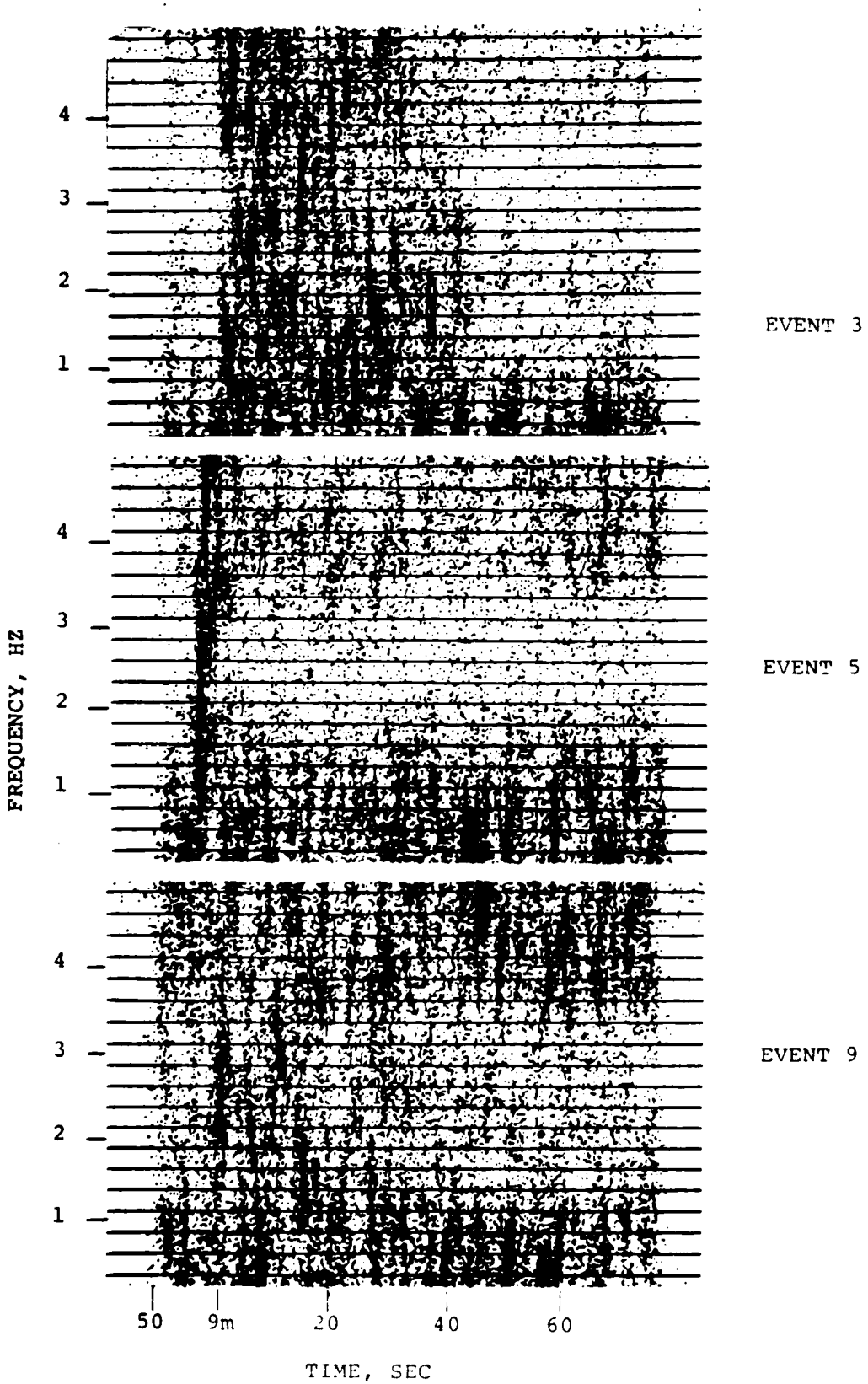

Figure 5. "Sonograms" for seismic events 3, 5 and 9 which are also displayed in Figure 1.

DETECTION STATE-OF-THE-ART

J. Berger

Project VT/0712

Contractor: Systems, Science and Software

Task 4.3.3 Automatic Signal Processing: Review of Seismic Event Detectors

Objective

The objective of this review study was to identify all pertinent automatic signal detection algorithms by equation, mathematical derivation and usage history, including algorithms currently under development and scheduled to be validated by October, 1981.

Accomplishments

A draft report entitled "Seismic Detectors: The State-of-the-Art" has been prepared and submitted to VSC. In this report, the following detection algorithms were reviewed:

1. IBM
2. Z
3. Deflection
4. Analytic Envelope
5. Allen
6. Stewart
7. Walsh
8. MARS

General conclusions reached were:

1. All detectors reviewed in this report are based on a comparison between some form of variance estimate of the signal calculated over a time period approximately equal to the duration of an expected seismic event, and the normal (or long term) variance.

Possible exceptions to this general form are the phase detector described by Unger (1978) and the similar part of MARS. The former did not work because the short period phase fluctuations were so rapid that they could not reliably be predicted; the latter has not been implemented.

2. Ad hoc detection algorithms such as Allen's and Stewarts' (1977) offer a hope of some improvement in the detection process. These methods, after having made the basic detection statistic test and having made a tentative identification, are followed by a further process that is designed to:

a. reduce the false alarm rate,

b. improve the timing capability, and

c. speed the recovery of the detection algorithm after an event is encountered.

How much these algorithms can be expected to offer significant improvements depends upon the noise environment in which they are operating. If the SNR is such that a high probability of detection is achieved with a tolerable FAR, then little improvement can be expected. If, however, the SNR is poor, so that the probability of detection is low for a given FAR, then significant improvement may be achieved by such two-stage algorithms.

3. Testing of the detectors described in this report was not carried out in a uniform manner on the same or even similar data sets. Thus, no definitive statement about their relative performance may be made. However, it appears that no one detector is obviously superior to all others. Some have been optimized for teleseismic detection using a moderately large computing facility. Some have been designed for operation in microprocessor controlled field recording units, typically used in the near field or at least at regional distances. These applications stress ease of implementation in microprocessors. Some algorithms stress timing ability as this may be another object of the algorithm.

4. Little theoretical advance has been achieved since Frieberger's 1963 work in which he "solved" the problem for detection of a Gaussian signal in Gaussian noise. The influence of this work has rightly guided the design and implementation of many of the detectors used today. However, it must not be thought that the "real problem" has been solved. The "real problem" is the detection of certain non-Gaussian signals in the presence of non-Gaussian noise. Frieberger discovered the optimum detector for an approximate model of the actual situation, but, other algorithms may work significantly better on "real" data. Further, considerations such as timing ability, recovery of the algorithm after an event, and immunity to highly non-Gaussian noise such as line spikes and data dropouts may dictate very different approaches.

As a result of the review, the following recommendations were made:

- Uniform testing of all viable detectors should be conducted with

  a. a realistic synthetic data set;

  b. all detectors coded for and running on the same or similar machines;

  c. ROC curves produced for each detector comparing them with the theoretical performance of the detector for a completely known signal.

- Theoretical and experimental research in phase sensitive detectors should be supported as this is an area where it may be possible to exploit signal information not used in energy or power detectors.

- Research should be encouraged to test if matched filters for specific types of signals (station/source pairs) improves detector performance.

- Further development of hybrid detection algorithms, that combine high probability of detection with a high FAR and then are followed by a post processing to reduce the FAR should be undertaken.

- New algorithms, designed specifically for use with the new generation of three component broad band seismographs, should be developed and tested.

- In view of data rates from these new data sources, dedicated microprocessors to run the detection algorithms on a one processor per channel (or seismic station) basis should be considered.

PRINCIPAL REFERENCES

Allen, R. V. (1978), "Automatic Earthquake Recognition and Timing from Single Traces," Bull. Seism. Soc. Amer., 68, pp. 1521-1532.

Berger, J. (1980), "Seismic Detectors: The State-of-the-Art," Systems, Science and Software Technical Report SSS-R-80-4588 submitted to AFTAC/VSC, July.

Farnbach, J. S. (1975), "The Complex Envelope in Seismic Signal Analysis," Bull. Seism. Soc. Amer., 65, pp. 951-962.

Frieberger, W. F. (1963), "An Approximate Method in Signal Detection," Quarterly Appl. Math., 20, pp. 373-378.

Goforth, T. and E. Herrin (1980), "Semiannual Technical Report," Air Force Office of Scientific Research, Contract No. F49620-76-C-0030, Dallas Geophysical Laboratory, Southern Methodist University.

Shensa, M. J. (1977), "The Deflection Detector, Its Theory and Evaluation on Short-Period Seismic Data," Report TR-77-03, Texas Instruments, Alexandria, VA.

Stewart, S. W. (1977), "Real-Time Detection and Location of Local Seismic Events in Central California," Bull. Seism. Soc. Amer., 67, pp. 433-452.

Swindell, W. H. and N. S. Snell (1977), "Station Processor Automatic Signal Detection System. Phase 1: Final Report, Station PRocessor Software Development," Texas Instruments Report No. ALEX(01)-FR-77-01, AFTAC Contract No. F08606-76-C-0025, Texas Instruments, Incorporated, Dallas, Texas.

Unger, R. T. (1978), "Automatic Detection, Timing and Preliminary Discrimination of Seismic Signals with the Instantaneous Amplitude, Phase and Frequency," Texas Instruments Report No. ALEX(01)-TR-77-04, AFTAC Contract No. F08606-77-C-0004, Texas Instruments, Incorporated, Dallas, Texas.

Vanderkulk, W., F. Rosen and S. Lorenz (1965), "Large Aperture Seismic Array Signal Processing Study," IBM Final Report, ARPA Contract SD-296, International Business Machines, Rockville, Maryland.

SEISMIC DATA PROCESSING RESEARCH

(ongoing effort)

Project VT/0704/B/PMP Contractor: ENSCO, Inc.

Task 4.1: Automated Signal Measurement Research

Objective

Our objective is to transfer existing array-processing software, three-component software, and automatic single-sensor processing software from the IBM 360/44 to the PDP-11/70 system at the VSC. The newly transferred software will then be tested to verify that it is operating correctly.

The Adaptive Beamformer (ABF) and the three-component-adaptive Polarization Filter (PF) will perform the function of extracting weak signals from array or three-component records containing signals from events of known location. The ABF program package is viewed as a sub-system in the VSC system data flow which transforms array records of events into single-channel estimates of signals. Similarly, the PF program package transforms three-component records into single-channel estimates of some specified type of signal such as P-waves, S-waves, or Rayleigh waves. These single-channel estimates of signals, together with other single-sensor records, are then considered as potential inputs to a third sub-system element in the VSC data flow. This third sub-system performs the functions of correcting the system response to produce ground motion records of signals and to perform algorithms which automatically time and measure the seismic signals.

Finally, we will define and document the work which needs to be done to perform detection, timing, and signal measurement in an acceptable manner by evaluating and defining the status of existing programs which perform these functions. Specifically, the automatic detector will be designed to effectively detect and accurately time signals. We envision that this detector will be a modification of Unger's analytic detector.

Accomplishments

To date, a Research Objective Plan has been submitted to the VSC for approval and work has begun on three subtasks:

Subtask 4.1.1: Automatic Signal Processing Algorithms
Subtask 4.1.2: Adaptive Beamforming
Subtask 4.1.3: Polarization Filtering.

Below is a brief overview of what we intend to accomplish under each subtask.

Subtask 4.1.1: Automatic Signal Processing Algorithms

The input to the Automatic Signal Processing (ASP) package will be single-channel records possibly containing signals which are to be extracted and measured. These single-sensor records may be output traces of the ABF or PF program package which are in a format compatible with the VSC data flow. Alternatively, the input to ASP may be other single-sensor records of events of known location which have been edited by the VSC system.

The purpose of ASP is to automatically time signals and to perform measurements on those signals. The following functions of ASP will be developed, implemented, and tested:

- Time-domain system response corrections of short-period (SP) records
- Time-domain system response corrections of long-period (LP) records.

The output of this function will be signal displacement, velocity, and acceleration records. An off-line program will be written to test and validate this system response function prior to implementing it into the data flow of the VSC system.

Unger's detector was selected for study because of its proven accuracy in timing signals. This capability was demonstrated by Unger (1978) and was verified by Sax, et al. (1979), who described some of its advantages and disadvantages. Unger's detector was tested by automatically timing signals on records analyzed for the 1979 VSC Event Identification Experiment. The design modifications we envision for this detector should correct the obvious design deficiencies which were uncovered by our exhaustive test of its performance capabilities.

Finally, a study will be made of the following parameters:

- Pulse frequency
- Phase standard deviation
- Gated energy measurements.

These measurements are expected to be performed on signals detected by the automatic detector, and should be incorporated in the ASP at a later date (such a task is not part of the current work).

Subtask 4.1.2: Adaptive Beamforming

The ABF package is viewed as a sub-system of the VSC system. It provides an option to process input array records of signals of known location. It outputs single-channel estimates of a signal for a given azimuth and velocity. Presently the ABF is combined with a constant false alarm rate 'Z' detector (DET) developed by Swindell and Snell (1977). The ABF lists 'Z' statistics together with short-term averaged estimates of signal magnitudes. In its present form, this list provides a means of comparing detections produced by this automatic detector to those obtained visually using plots of the ABF output. That output provides plots and the corresponding 'Z' statistic listing for a representative single-sensor of the array, the conventional beamformed signal estimate, and the adaptive beamformed signal estimate. In last year's work, we re-programmed Shen's ABF algorithm (see Shen, 1979) in FORTRAN; as such, the transfer to the PDP-11/70 system should be relatively uncomplicated.

Subtask 4.1.3: Polarization Filtering

The PF package is viewed as a sub-system of the VSC system. It provides an option to process three-component records of known location. The three-components which are input to the PF have been rotated into the radial and transverse direction to the source. Presumably, this will have been done by another sub-system element in the VSC data flow. If such a sub-system is available it will be utilized; otherwise, we will insert it into the VSC system.

Presently, the PF is not implemented with an automatic detector. We will combine the PF with a constant false alarm rate 'Z' detector developed by Swindell and Snell (1977). This will produce a 'Z' statistic listing of each signal estimate channel for flagging possible signal arrivals and providing magnitude measurements.

In previous year's work, the FORTRAN PF program has been applied to both short-period and long-period data in either the regional or teleseismic distance range. Transfer of this program from the IBM 360/44 to the PDP-11/70 system should be relatively uncomplicated.

References:

Sax, R. L., A. G. R. Bell, and D. L. Dietz, 1979; Event Identification Experiment: Priority I Data Set (U), Technical Report No. 1, ENSCO Report No. SAR(01)-TR-79-01, AFTAC Contract Number F08606-79-C-0014, ENSCO, Inc., Alexandria, VA (Classified Report).

Shen, W. W., 1979; A Constrained Minimum Power Adaptive Beamformer with Time-Varying Adaptation Rate, Geophysics, 44, No. 6, 1088-1096.

Swindell, W. H., and N. S. Snell, 1977; Station Processor Automatic Signal Detection System, Phase I: Final Report, Station Processor Software Development, TI Report No. ALEX(01)-FR-77-01, AFTAC Contract Number F08606-76-C-0025, Texas Instruments Incorporated, Dallas, TX.

Unger, R., 1978; Automatic Detection, Timing and Preliminary Discrimination of Seismic Signals with the Instantaneous Amplitude, Phase and Frequency, Technical Report No. 4, TI Report No. ALEX(01)-TR-77-04, AFTAC Contract Number F08606-77-C-0004, Texas Instruments Incorporated, Dallas, TX.

MODEL 44000 SEISMOMETER DEVELOPMENT PROGRAM

STAN MONROE

Project VT/8711/B/PMR Teledyne Geotech

Task 4.3 Phase II Prototype Task

Objective

The 44000 development program includes the design, engineering development and development testing of the Model 44000 Long-Period Borehole Seismometer System. The design objectives for the Model 44000 system are: match or exceed the performance of the Teledyne Geotech KS36000 system; not exceed the cost of the KS36000; design to install in a 4-inch inside diameter borehole up to 15° off vertical; design to reduce complexity of installation, operation and maintenance procedures; and take maximum advantage of design concepts already developed for the KS36000 system.

Phase II of the program consists of engineering development and includes refinements and changes to the designs based on evaluation of the engineering model constructed during Phase I; preparation of test procedures for bench tests, initial borehole test and final performance evaluations; generation of prototype level documentation; and the fabrication and initial testing of two prototype units. The objectives for FY80 include only the prototype design and documentation.

Accomplishments

The 44000 system contains two (orthogonal) horizontal and one vertical force feedback transducers. Earth accelerations transmitted through a holelock at the base of the instrument are converted to electrical signals by the transducers and their associated "loop-electronics." The elements of this force feedback system are shown in figure 1. The suspension is a mass of 250 grams constrained to move in only one direction. The horizontal suspensions are simple pendulums and the vertical is a mass on an unastaticized spring. The position of each mass is determined by the capacitance bridge of figure 2. Two variable capacitors are formed by the mass and two parallel plates. A bridge circuit is formed from these two capacitors and two reference capacitors. As the mass moves from its center position, an AC output voltage is produced with an amplitude proportional to the distance and of a phase (0 to 180°) corresponding to the direction.

The AC output is amplified and demodulated, and the resulting DC (relative to the 15625 Hz carrier frequency) voltage is used to produce a negative feedback force on the mass. The position feedback results in an addition to the mechanical "spring constant" of the suspension and is used to set the corner frequency of the seismometer. The velocity feedback is used to control the damping of the suspension.

The electrostatic transducer consists of the capacitor plates used in the output bridge and associated feedback voltage conditioning circuits. First the feedback signal is split into two paths, one for each plate. Then, after one voltage is inverted, they are summed with a positive offset voltage and applied to the transducer capacitor plates at the points labeled FEEDBACK in figure 2. The need for an offset voltage results from the fact that only charges induced by the plate voltages will be present on the grounded mass, and thus each plate can exert only an attractive force on the mass. By adding and subtracting the feedback voltage from some offset voltage, the plates will exert equal but opposite forces on the mass in its center position (feedback voltage equal to zero, both plate voltages equal to the offset voltage). As the mass moves away from the center, the force from one side is lowered (offset voltage minus feedback voltage) and increased on the other side (offset voltage plus feedback voltage) to produce a net force on the mass.

During Phase I of the development program, an engineering model was constructed based on the principles briefly described above. In January of 1980, the instrument was installed at a depth of 200 feet in a four-inch borehole at Garland, Texas. Data were recorded using long-period filters (Teledyne Geotech Model 38840) and a three pen Helicorder. Comparisons were made to data being taken in a nearby borehole with a KS36000 system using the same type uphole filters and recording equipment. Much larger long-period signals from train traffic near the test site were observed in the 44000 records than in the 36000 records. Non-linearities in the 44000 system were suspected, and linearity test data taken in the borehole during February confirmed this fact. It was found that the downhole system non-linearity was on the order of 1%, not 0.1% as previously predicted.

An analysis of the force feedback transducer was made using an ideal parallel plate capacitor model. This derivation was submitted as an informal technical note in April. The study showed that although the output transducer is fundamentally linear, the feedback transducer is intrinsically non-linear. Furthermore, it was shown that the non-linear component at any mass position is proportional to the ratio of the feedback voltage to the DC offset voltage. Because these voltages are also involved in total feedback force, there is only one value of offset voltage satisfying the system parameters for each non-linear component value.

Calculations using this model and the 7.5 volt offset, ± 5 volt feedback values of the initial engineering model design predicted a non-linear component of 0.8% due to the force feedback as compared to the 1% measured for the system.

The feedback circuits were redesigned using a reasonable offset voltage (about 20 volts) with a predicted non-linear component of less than 0.1%. Because of long delivery times on precision components, "close" values were chosen and the vertical and north/south horizontal loop circuits were modified. When the linearity tests were rerun, the non-linear components were found to be 0.35% for the vertical, 0.045% for the north/south and 1.2% for the east/west. These results verified the analysis and new circuit boards have been laid out so that the circuits can be tested with low-noise, good-quality hardware.

Another question arose during Phase I and has been studied during Phase II. The spacing between the mass and each capacitor plate is nominally 0.003 inches. Such a small spacing allows air between the mass and the plates to contribute significantly to the damping coefficient of the suspension and results in a lower mechanical Q. Because suspension noise is inversely proportional to the Q, a high Q is desirable. Noise calculations predict that a Q of at least a few hundred must be maintained to meet system requirements.

The suspension is contained in a case which is normally baked at 100°C for two weeks while a vacuum pump continuously removes the baked out gases. The system is then sealed under vacuum, and will have a mechanical Q of 10,000 or higher. It was observed during Phase I that after an initial drop in the Q to about 500 in 2 to 3 months, there was a slower reduction to about 50 a year later.

Studies conducted during Phase I indicated that the case seal was not leaking, so trapped gas inside the module case was suspected. The assembly was reviewed and spaces which could trap gases (e.g.: the area behind a screw) were vented to the main body of the module. The modules were then reassembled using a different sealing procedure and evacuated during the summer of 1979. In early July of 1980, about one year later, the mechanical Q's were still on the order of 150 to 200. These results are encouraging and it is believed that the vacuum requirements can be met by additional reductions in the volumes of trapped gas and by improving the assembly and evacuation procedures.

The holelock and the holelock installation tool have been tested and found to be satisfactory. The seismometer has been installed and operated in a borehole and seismic data has been recorded.

Figure 3 contains records from the Model 44000 seismometer and comparison records from an adjacent KS36000. The responses of these systems are not yet matched, so comparisons at the longer periods cannot be made; however, the results illustrated in figure 3 are what was expected. The filters in the 44000 system are to be modified to match the response of the Model KS36000.

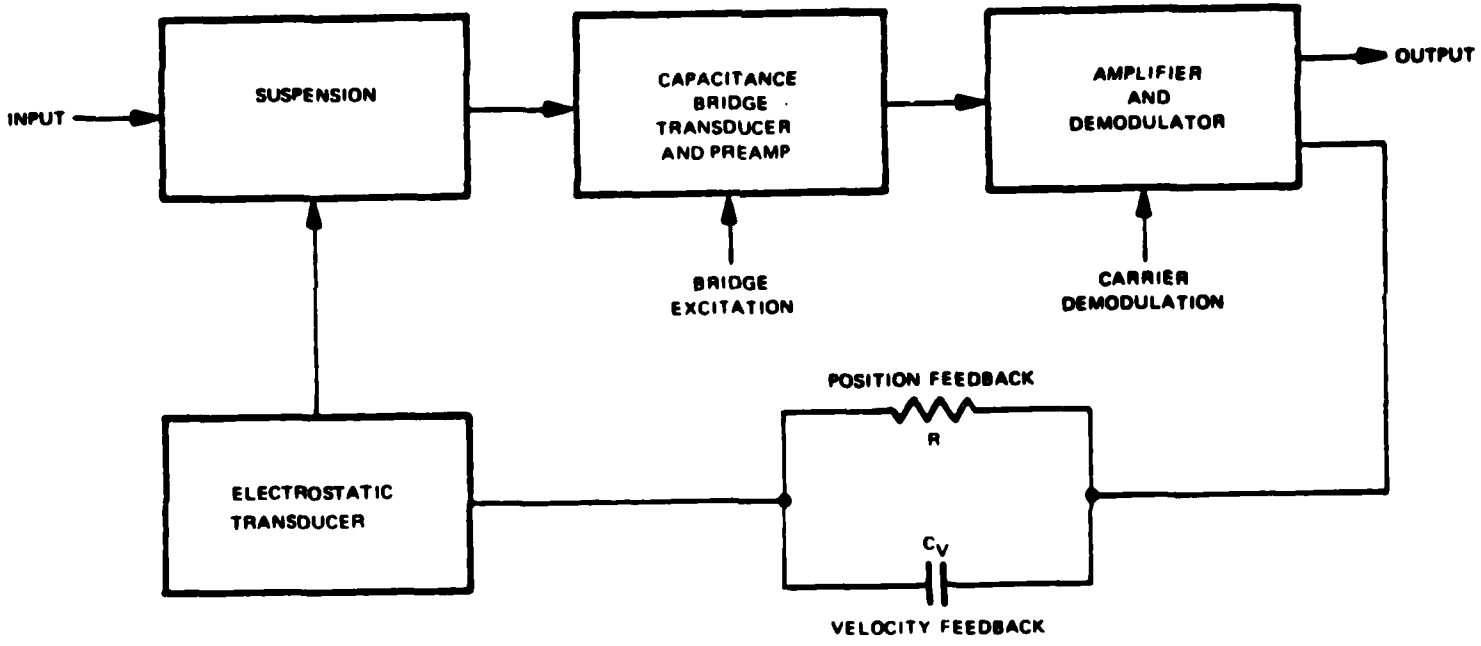

FIGURE 1. SEISMIC SIGNAL ELECTRONICS
MODEL 44000 SEISMOMETER

FIGURE 2.

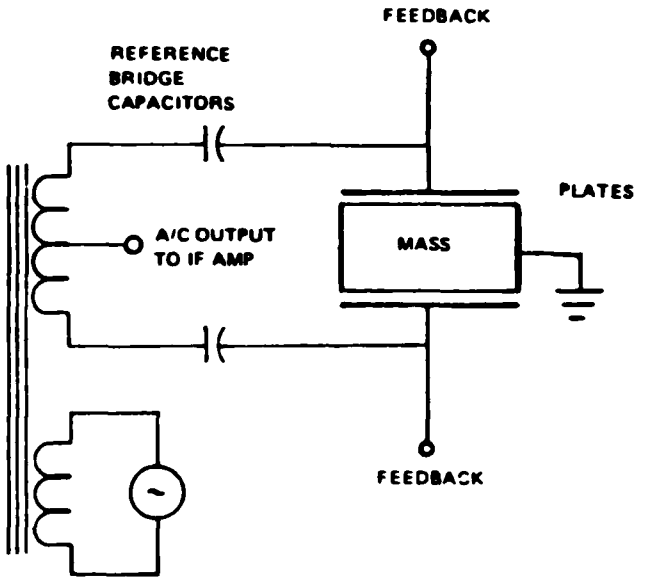

EQUIVALENT SCHEMATIC OF CAPACITIVE BRIDGE

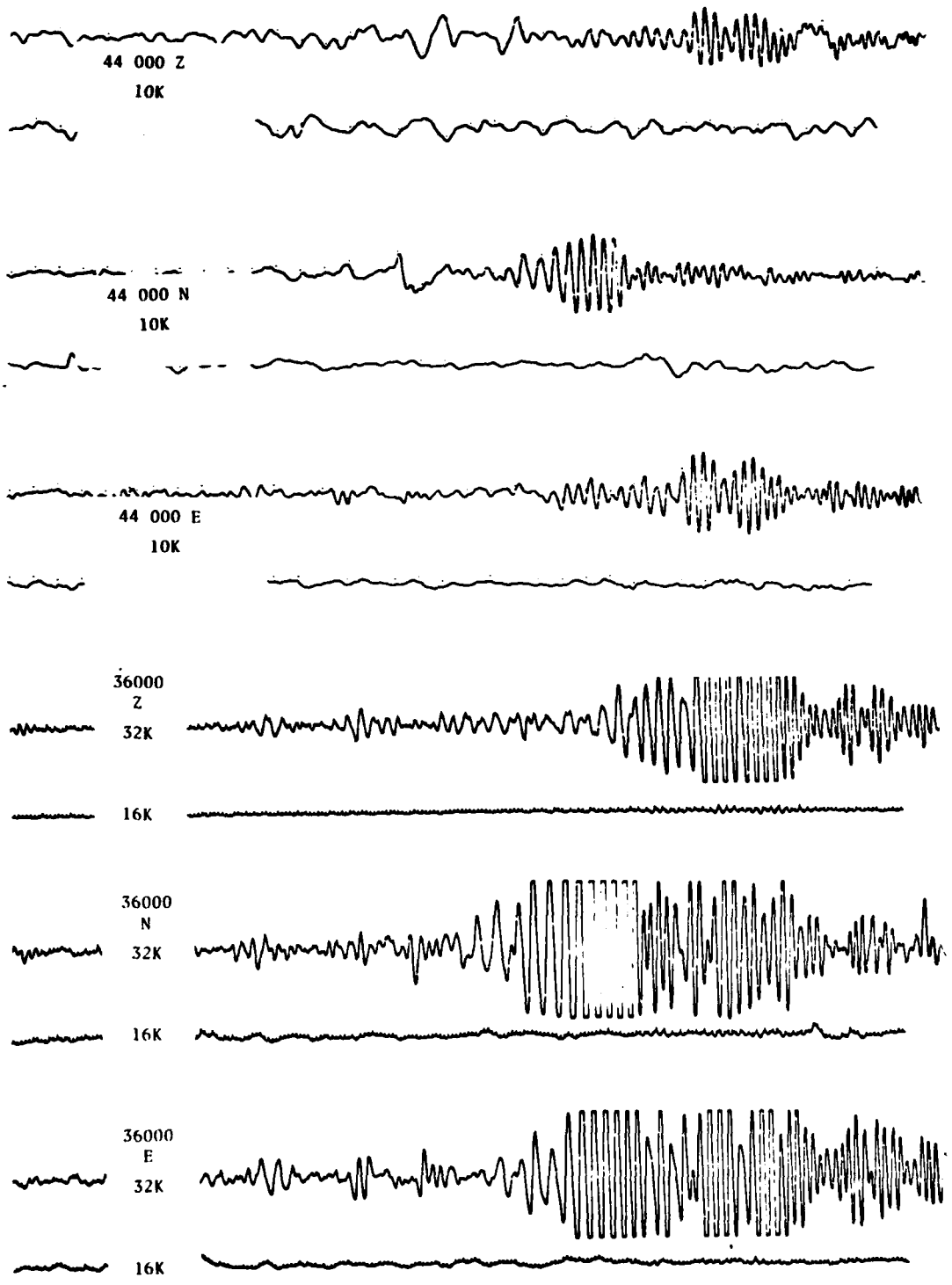

Figure 3. Comparison of 36000 and 44000 Seismometers

SEISMIC INSTRUMENTATION PROGRAM

MARTIN E. ROBINSON

Project VT/0703 Contractor: Teledyne Geotech

Task 4.2 Strain-Inertial Seismograph

Objective

The conceptual design of a strain-inertial seismograph system developed during FY79 for AFOSR will be finalized as necessary to define the required characteristics of the system. Development specifications shall be prepared for a prototype SIS system and the design of the SIS will be completed.

Two prototype SIS systems will be fabricated. These systems will include the seismometer packages, electrical cables from the seismometer to the top of the borehole, and any devices required to lock, orient, or relieve cable strain from the seismometer package.

Noise studies begun under the AFOSR program in FY79 will be extended to collect and analyze a limited amount of noise data from the Southern Methodist University (SMU) McKinney, Texas site. These data will be used to determine the composition and state of organization of the ambient earth noise field.

The results of the noise study will be incorporated into a detailed test plan for evaluating the two instruments. The test plan shall define procedures to verify that the SIS units fulfill all development specifications. An initial test facility will be prepared in Garland, Texas for use in a later feasibility evaluation of the systems.

A detailed series of tests will be conducted to critically evaluate the performance of the prototype systems under actual field conditions. The testing phase will be divided into two parts. First, the instruments will be operated at the initial test facility in Garland, Texas. The results of the initial testing will be used to finalize the requirements of the second part of the testing phase. In this part, the prototype instruments will be installed and operated at two remote sites to be determined. The first will be a quiet location where data will be gathered primarily to establish the lowest limit of ambient noise where operation of the SIS system will be effective in improving signal-to-noise ratios for various types of seismic waves. The second remote site will be chosen in an area with relatively high level ambient noise which is different in character from the Garland, Texas site.

Objective (cont.)

A package of engineering drawings used to manufacture the prototype systems will be delivered to the Government and the results of all design, development, and test efforts will be documented in a technical report.

Accomplishments

A draft of the Prime Item Development Specification for the Strain-Inertial Seismometer System Prototype (Type B1) has been completed and was submitted to the project office on 27 June 1980 for review, comment, and approval. A draft of an overall system specification for the strain-inertial seismograph system prototype (Type A) is in process.

All components and material to fabricate two vertical KS seismometer modules for use as the inertial sensor have been ordered and fabrication of machined parts has begun.

A refraction survey of the site near McKinney, Texas, where noise data will be collected, has been completed and analysis of these data is underway. The first array configuration for the noise study is being installed and will be completed during July. Twelve seismometers will be employed with six instruments installed in a north-south leg and six in an east-west leg. The instruments will be spaced 20 meters apart and will be buried approximately 1 meter deep.

A preliminary design for the strain transducer for the strain-inertial seismometer has been completed. This design has been evaluated in terms of sensitivity, linearity and impedance and meets the requirements of the draft development specifications. Detailed engineering design of the transducer commenced during the last week of June and detail drawings for the fabrication of parts for an engineering model of the strain transducer are being prepared.

A conceptual design for a strain calibrator for the strain-inertial seismometer has been generated and a detailed engineering analysis of this design is in progress.

Design of the electronics to be used for the strain channels of the strain-inertial seismograph is in progress and parts are being ordered for fabrication and testing of engineering models.

An Experimental Small Subarray within the NORSAR Array: Location of Local and Regional Events

by

Frode Ringdal and Svein Mykkeltveit

Project VT/0702/B/PMP

Contractor: NTNF/NORSAR
Post Box 51
N-2007 Kjeller, Norway

Task 5: Spatial Coherence of Seismic Phases from Regional Events

Objective

Using existing data, if available, from arrays with close spacing and a temporary seismic network to be installed in conjunction with NORSAR, a study is to be conducted to determine the effect of sensor spacing on signal coherency from regional earthquakes and explosions. This study will include the following:

5.1 Determine the signal and noise coherency at various frequencies as a function of sensor spacing.

5.2 Estimate the gain obtainable from closely spaced seismometers using standard array processing techniques.

5.3 Compare event detection and location performance at regional distances of a densely spaced array to that of a single three component short-period site.

5.4 Develop algorithms to separate and identify secondary phases using a closely spaced array and evaluate their performance on regional events.

Accomplishments

Since November 1979 one of the NORSAR subarrays (6 seismometers, each with an 8 Hz lowpass filter) has been operated with station distances

from 125 to 2051 meters. The purpose of this NORSAR Experimental Small-Aperture Subarray (NORESS) has been to obtain SP data from closely spaced sensors in order to

- Investigate noise and signal coherencies at high frequencies
- Identify P, S and Lg phases from regional seismic events
- Detect and locate regional events.

This paper describes a location procedure that has been developed for local and regional events, using NORESS. Briefly, the location algorithm consists of the following steps:

1. Identification of the P and Lg phases for each event using high-resolution frequency-wavenumber analysis
2. Manual pick of onset times for P and Lg
3. Epicenter azimuth determination based on the high-resolution analysis results
4. Epicenter distance determination using Lg-P travel time differences and a standard crustal model.

The efforts at this stage have been focused at obtaining a very simple procedure, with no attempt made to optimize location accuracy, such as might be obtained, e.g., by using azimuth-dependent travel time tables. The crustal model used for determining P wave travel times has been as follows:

Depth	P-wave Velocity
0-16 km	6.20 km/s
16-40 km	6.70 km/s
40-95 km	8.15 km/s
95- km	8.25 km/s

The group velocity of Lg has been set to 3.5 km/s, which is consistent with earlier results obtained for Fennoscandia.

The data base for the study has consisted of:

- 16 regional events from Fennoscandia
- Distance range from NORESS 200-1200 km
- Magnitude range (M_L) 2.0-3.5.

Note that 15 of the events have been located independently using the Fennoscandian seismograph network. These location estimates have subsequently been used to evaluate the accuracy of the developed location procedure.

The first step of the location procedure, the high-resolution analysis of recorded waveforms, has been conducted as follows:

- Each phase processed at 5 frequencies: 1, 2, 3, 4 and 5 Hz
- For each phase: azimuth and phase velocity is obtained from the frequency with largest signal power
- Phase (P or Lg) is then identified from the estimated phase velocity.

For further discussion of the results here, it is referred to the contribution by Mykkeltveit, Ringdal and Bungum. We note only that the 'side lobe' problem discussed there implies a need for further refinement of the sensor deployment.

With respect to the third step of the location procedure, azimuth determination, we have investigated and assessed several alternatives:

a) P_n azimuth from high-resolution analysis
b) Azimuth from 'best' P phase (P_n or P_g)
c) Lg azimuth
d) Average of P and Lg azimuths.

Selected results of the location evaluation are shown in Figs. 1 and 2 for two alternative ways of azimuth determination (using the largest P and the Lg phases, respectively). The dots on each figure correspond to

the epicenters determined via the Fennoscandian network, while the end of each arrow indicates the location obtained using NORESS alone. Best result (Fig. 1) is achieved using the azimuth computed from the largest P phase.

In Figs. 3 and 4 we compare the NORESS estimated azimuths with those corresponding to the network determinations. Similarly, in Fig. 5, the respective epicenter distance estimates are plotted against each other.

In summary, our main conclusions are:

Phase Identification

- Accurate separation has been achieved between P and secondary phases (S, Lg)
- It is difficult to distinguish S from Lg based on phase velocity alone.

Distance Estimates

- Median 'error' is 11 km using Lg-P times.
- No clear azimuth-dependent effect is apparent.

Azimuth Estimates

- From Lg phase: Median 'error' is 6^{o}.
- From largest P phase: Median 'error' is 3^{o}.

Location Estimates

- Using Lg azimuth: Median 'error' is 45 km.
- Using P azimuth: Median 'error' is 30 km.

It should be noted that the above 'errors' are relative to the location results from the Fennoscandian network, and that these locations are uncertain by typically 10-30 km or more. Thus the majority of the processed events can be located with a difference from the network location that is within the uncertainty limits of the latter.

A project has also been initiated to compare the results to those obtained from three-component recordings, in particular with respect to azimuth determination. Initial results indicate that the small array approach gives the most stable results, but more research is needed here.

Our future plans for the small aperture array developments include:

- Design array to minimize the side lobe problem
- Develop criteria for automatic identification of S and Lg phases
- Automate the picking of phase arrival times
- Refine the techniques for computing distance and azimuth from a NORESS type array
- Obtain an extended data base for evaluation
- Compare the results to those obtained using three-component location procedures, and possibly combine the two approaches.

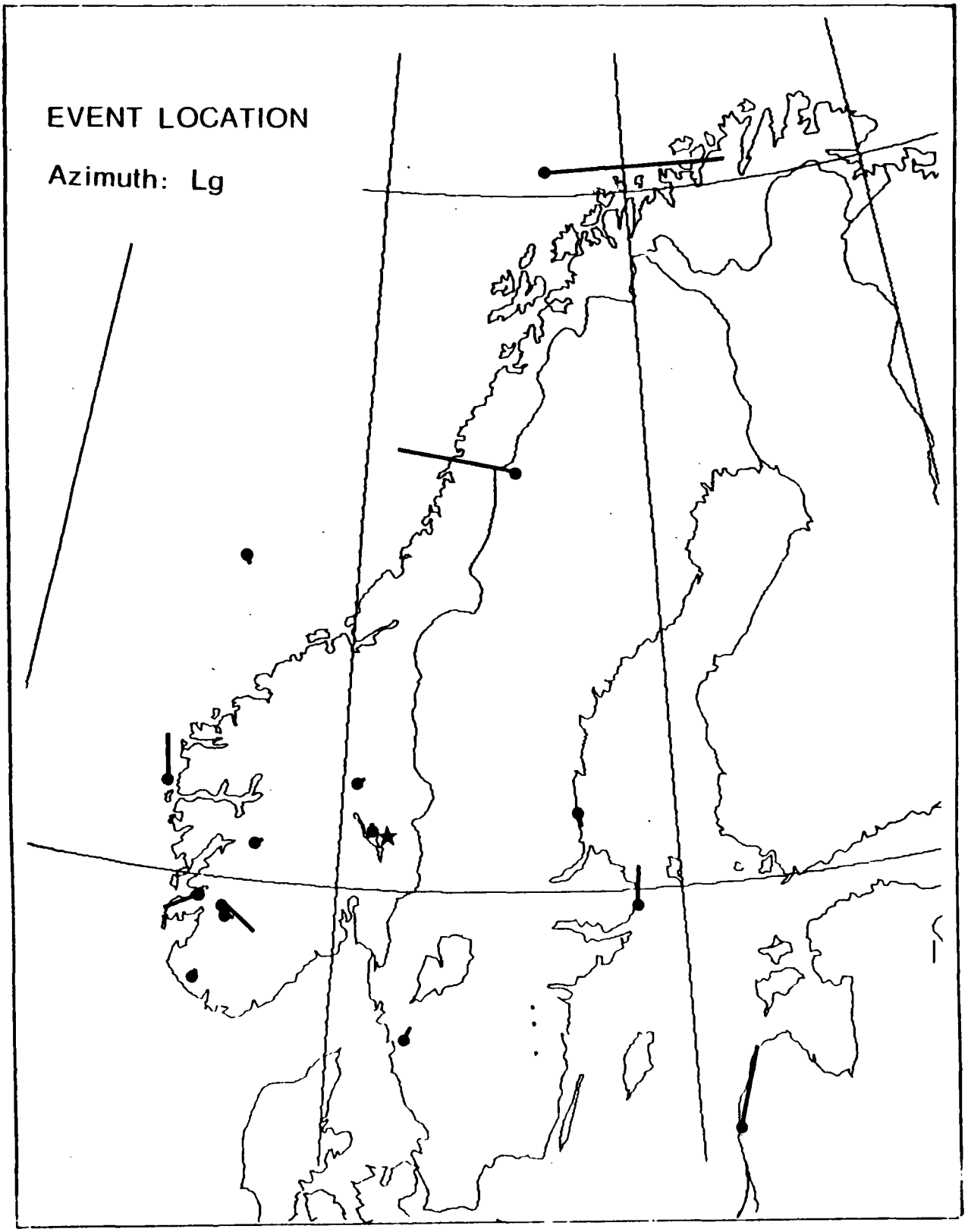

Fig. 2 Same as Fig. 1, but with NORESS location estimates based on azimuths from the Lg phase.

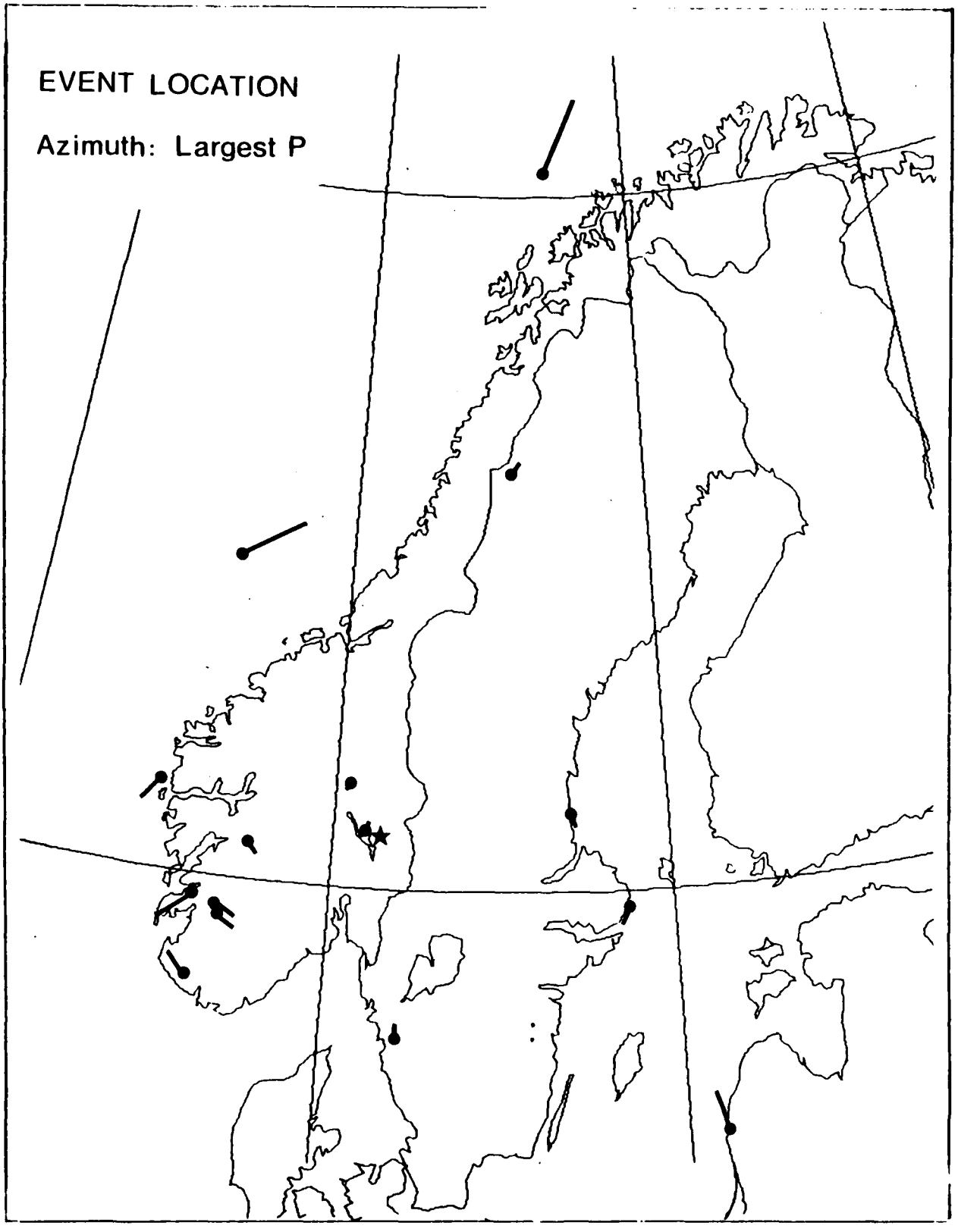

Fig. 1 Location 'errors' using NORESS (with azimuths determined from the largest P phases) for regional event location. Dots indicate epicenters determined by the Fennoscandian station network, while the end of the arrows indicate locations from NORESS processing.

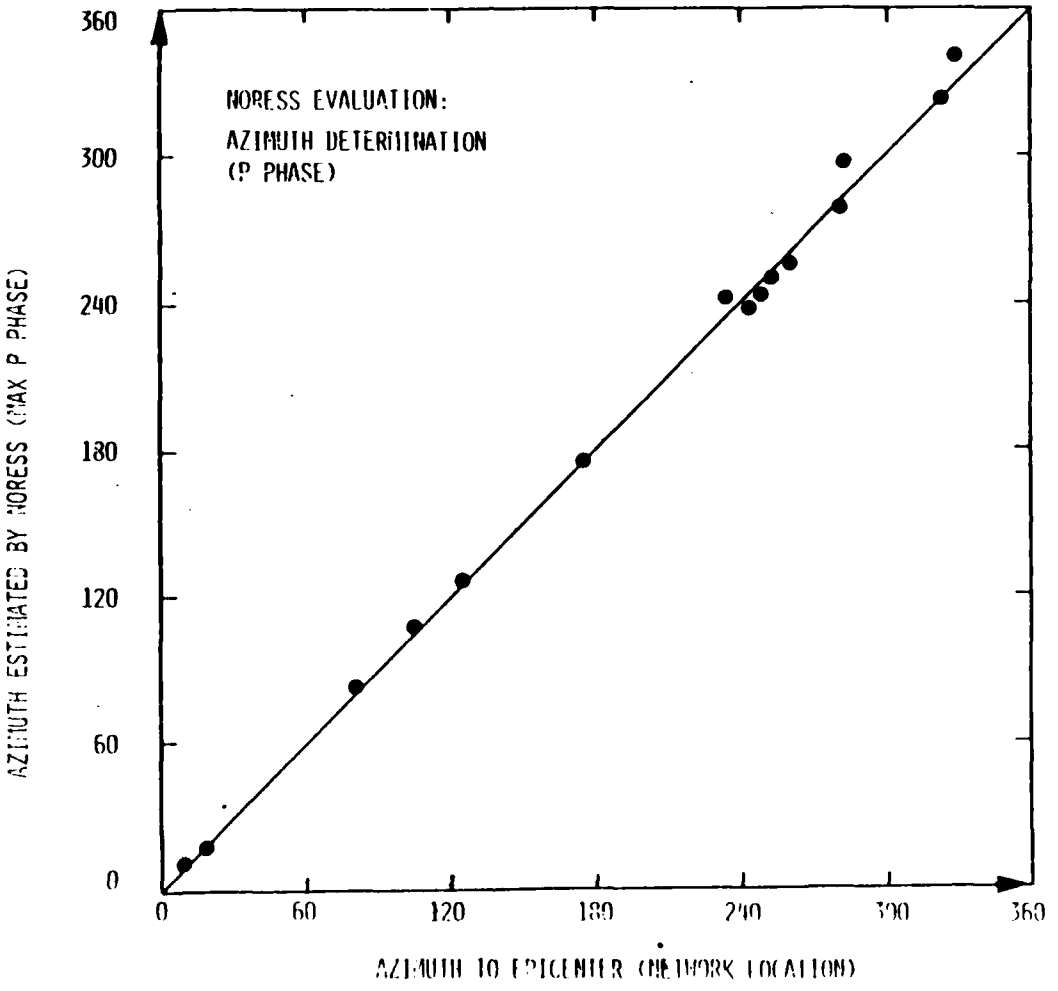

Fig. 3 Comparison of azimuths determined from NORESS processing (largest P phase) with those based on Fennoscandian network locations.

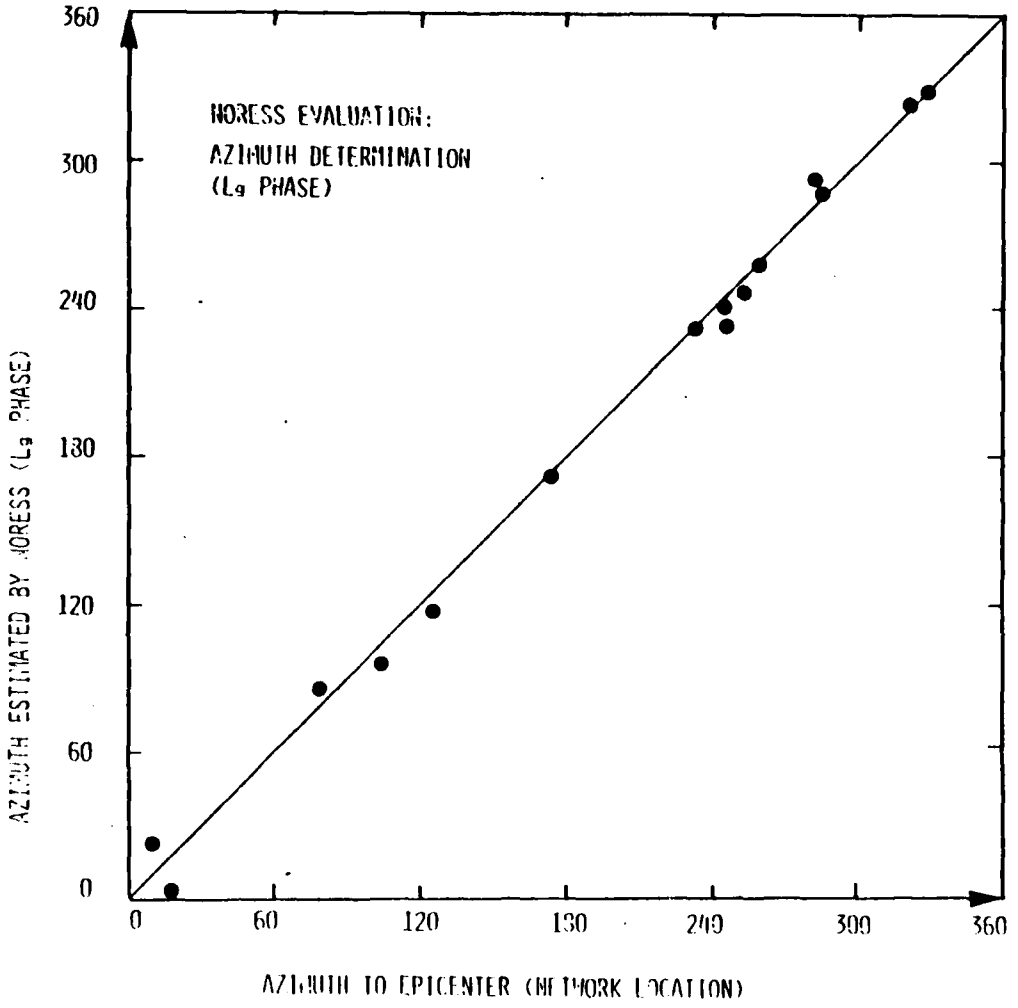

Fig. 4 Comparison of azimuths determined from NORESS processing (Lg phase) with those based on Fennoscandian network locations.

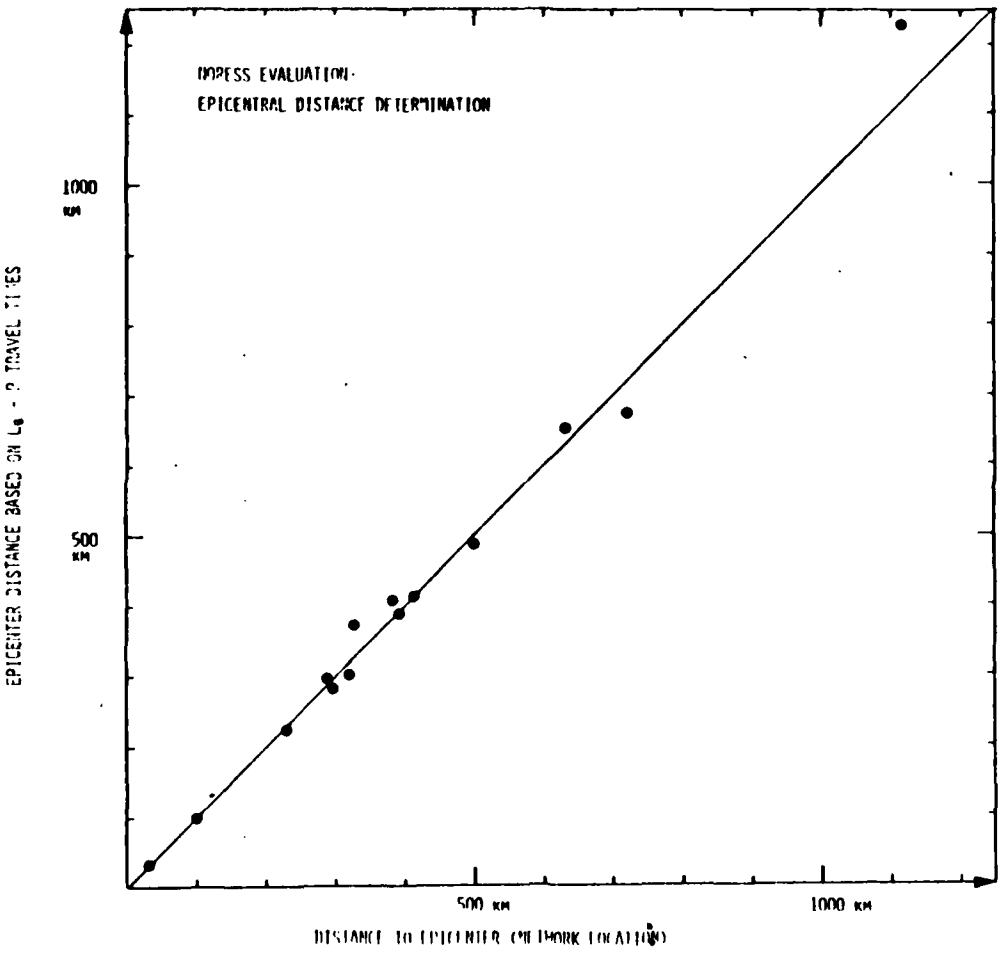

Fig. 5 Comparison between epicentral distance estimates using NORESS Lg-P travel time differences and the distance based on Fenno-scandian network locations.

An Experimental Small Subarray within the NORSAR Array: Crustal Phase Velocities and Azimuths from Local and Regional Events

by

Svein Mykkeltveit, Frode Ringdal and Hilmar Bungum

Project VT/0702/B/PMP

Contractor: NTNF/NORSAR
Post Box 51
N-2007 Kjeller, Norway

Task 5: Spatial Coherence of Seismic Phases from Regional Events

Objective

Using existing data, if available, from arrays with close spacing and a temporary seismic network to be installed in conjunction with NORSAR, a study is to be conducted to determine the effect of sensor spacing on signal coherency from regional earthquakes and explosions. This study will include the following:

5.1 Determine the signal and noise coherency at various frequencies as a function of sensor spacing.

5.2 Estimate the gain obtainable from closely spaced seismometers using standard array processing techniques.

5.3 Compare event detection and location performance at regional distances of a densely spaced array to that of a single three component short-period site.

5.4 Develop algorithms to separate and identify secondary phases using a closely spaced array and evaluate their performance on regional events.

Accomplishments

In October 1979, NORSAR subarray 06C was modified to a small aperture array - NORESS - with station distances in the range 125 - 2051 m. Fig. 1 gives the former and present configuration of 06C. All six sensors are now equipped with 8 Hz lowpass filters.

The purpose of the NORESS experiment is to obtain data from closely spaced sensors in order to

- Investigate noise and signal coherencies at high frequencies
- Identify P, S and Lg phases from regional seismic events
- Detect and locate regional events.

The first two items above are the subject of this contribution.

Both signal and noise coherencies have been evaluated for the 'new' array. An example of how the records of NORESS compare with those of an ordinary subarray at NORSAR is given in Fig. 1. For this Lg phase the waveform changes rather drastically from sensor to sensor within a 'normal' NORSAR subarray (6 top traces from subarray 02B) with a diameter about 10 km and typical sensor spacings of 3-4 km. The NORESS array proves to offer a significant improvement in this respect, as can be seen from the lower 6 traces. The epicentral distance is the same for the two subarrays.

For both signal and noise, coherencies are given in Fig. 2 at two frequencies, 2 and 4 Hz, respectively, for all station combinations within NORESS. The noise data set consists of 20 blocks each of 512 samples of 20 Hz data, amounting to a total of 8.53 minutes. This time interval was carefully selected to avoid detectable signals within it. The signal is a 12 seconds interval (1 block of 240 samples), of an Lg phase for an event about 200 km away and in appearance very similar to the one in Fig. 1. It is seen that coherency at 4 Hz is maintained at a level above 0.5 out to about 1 km and then drops to a random level. This point should serve to illustrate the need for small station separations in the study of regional Lg waves. For lower signal frequencies the coherency is maintained at a relatively high level throughout the range of NORESS station distances.

For the processing of NORESS data the high-resolution frequency-wavenumber technique has been applied to all distinct phases for a total of 16 events. For slow phases (phase velocity in the order of 3.5-4.0 km s^{-1}) and high frequencies (say 5 Hz), the corresponding wavenumber is larger than 1 km^{-1} and side lobe effects due to array response might become important. On the other hand, P phases of all frequencies (8 Hz lowpass filters applied to all channels) should have a fair chance of being correctly determined by such an array.

Figs. 3 and 4 show records from the 6 NORESS sensors for an earthquake about 300 km away together with high-resolution frequency-wavenumber plots at selected frequencies. For the P_n phase the results are shown for three frequencies in Fig. 3. According to the reporting agency (UPP), the 'true' azimuth from NORESS to the epicenter is 104^o, while the three frequencies displayed give values of 98^o, 97^o and 103^o. All wavenumber grids consist of 31 x 31 points, yielding an azimuth resolution of about $3\text{-}4^o$ for this phase. The phase velocity values fluctuate around 8 km s^{-1} and must be attributed to a P phase. For the Lg phase of the same event, the corresponding results are given in Fig. 4. The analysis of this phase serves to illustrate the side lobe problems encountered in a few cases. The frequency (3.5 Hz) corresponding to the largest power gives a maximum power in k-space which obviously results from spatial aliasing and the azimuth and phase velocity values are thus misleading. The other 4 frequencies analyzed, like 4.5 Hz (shown in Fig. 4) give, however, 'correct' values both for phase velocity and azimuth.

With the exception of a few cases for which spatial aliasing effects are easily identified, all phase velocities are plotted in Fig. 5 for the processed events. All measurements correspond to the one frequency out of five that has the maximum power. With the k-space grid that has been used, the phase velocity resolution is typically 0.3-0.4 km s^{-1}. Where more than one P phase is available, only the strongest (in terms of power) is included in this figure. On the basis of this figure, the following conclusions are readily reached.

- The P and Lg phases separate into nonintersecting phase velocity bands and a discrimination between P and Lg is possible from NORESS data.
- It is hardly possible to separate Lg from S (the S phases here are believed to be S_n) on the basis of phase velocity measurements alone.

The evaluation of the NORESS array continues and will include the following items:

- Processing of new events as they become available.
- Alteration of the array geometry to remove all side lobes from the part of the k-space corresponding to $|k| < 2\ km^{-1}$ to eliminate all spatial aliasing problems.
- Do high-resolution frequency-wavenumber analysis with a denser grid in wavenumber space for more detailed phase velocities.

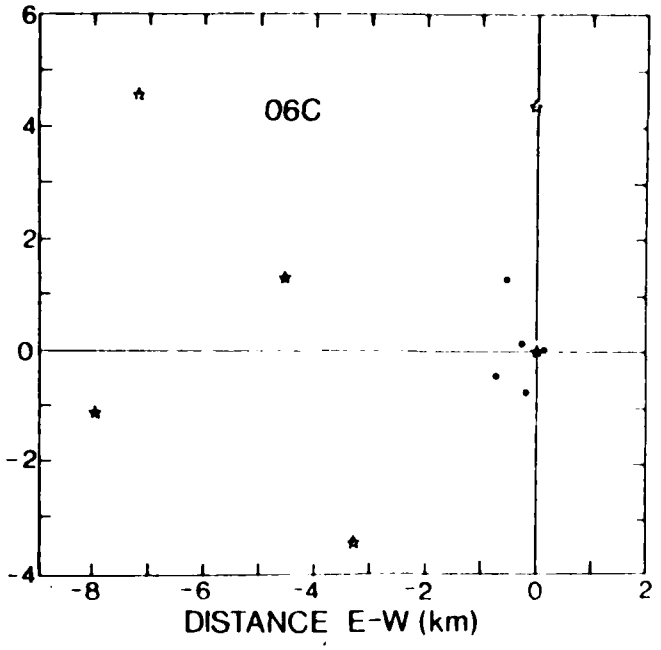

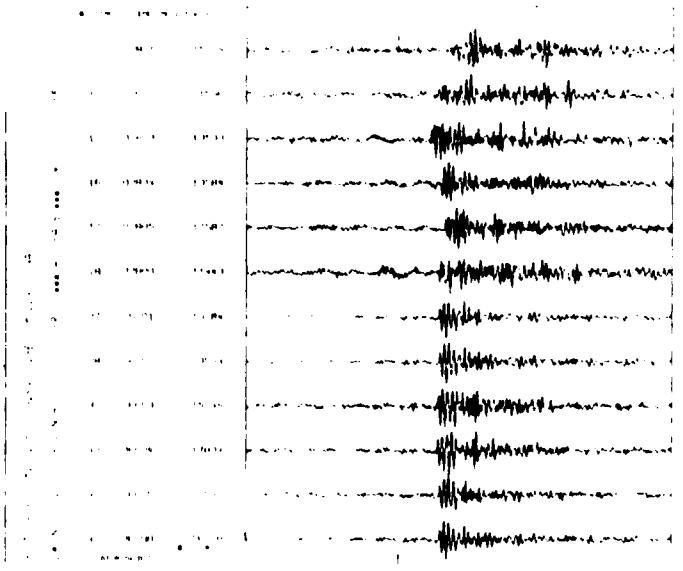

Fig. 1 NORESS geometry (top) and example of a recorded signal (bottom). In the top figure, the dots denote NORESS instrument locations, with the asterisks indicating the positions of the 'old' 06C instruments. In the bottom figure Lg waves from an explosion about 300 km away are shown. The top six traces are from standard subarray 02B, the lower six traces from NORESS. The time interval covered is 40 sec.

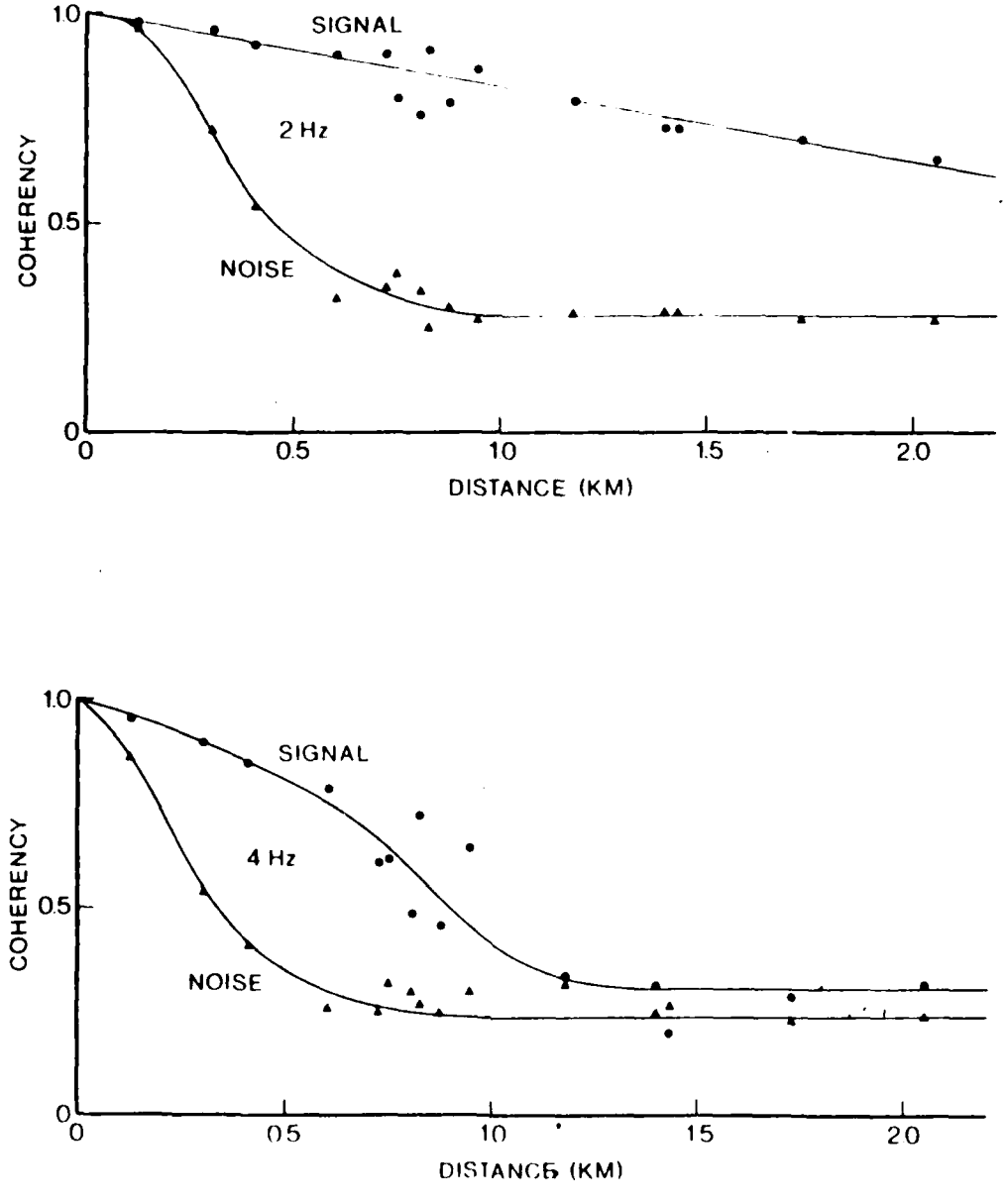

Fig. 2 Signal and noise coherencies at two selected frequencies for Lg phases as a function of sensor distance within NORESS. Frequencies shown are 2 Hz (top) and 4 Hz (bottom).

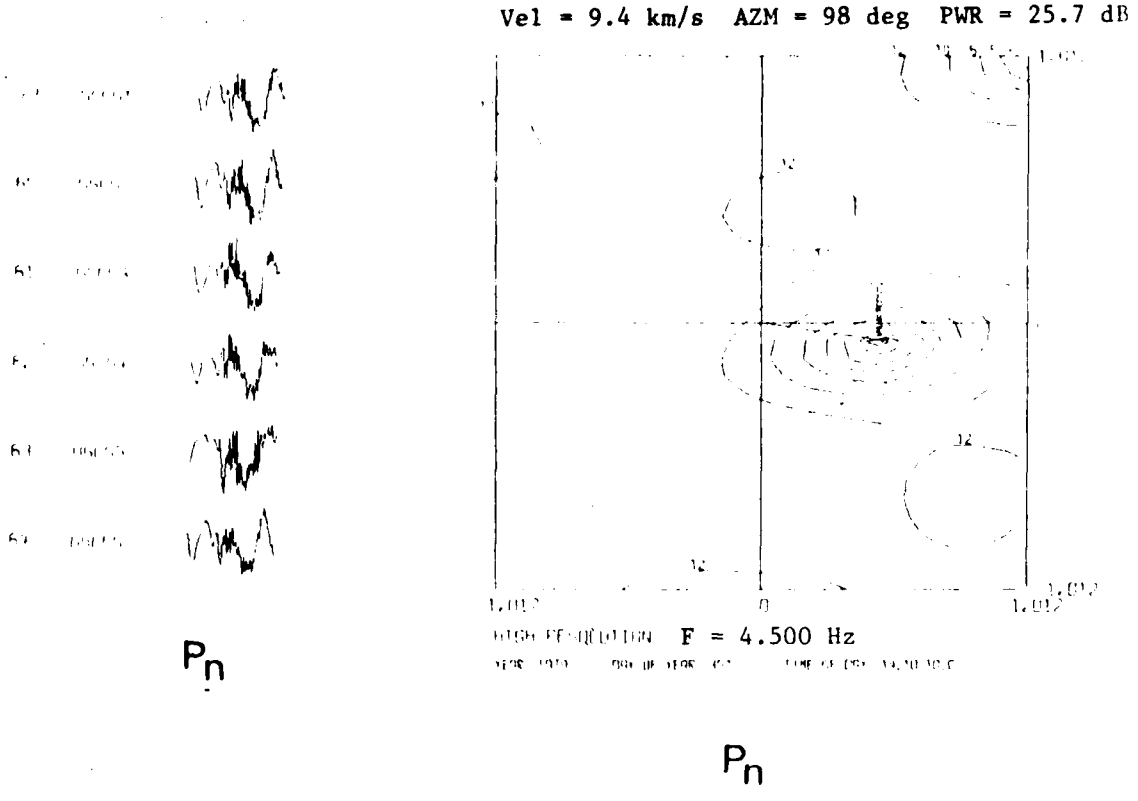

Fig. 3 High-resolution frequency-wavenumber plots at three frequencies for the 5 sec of the P_n phase shown in upper left corner.

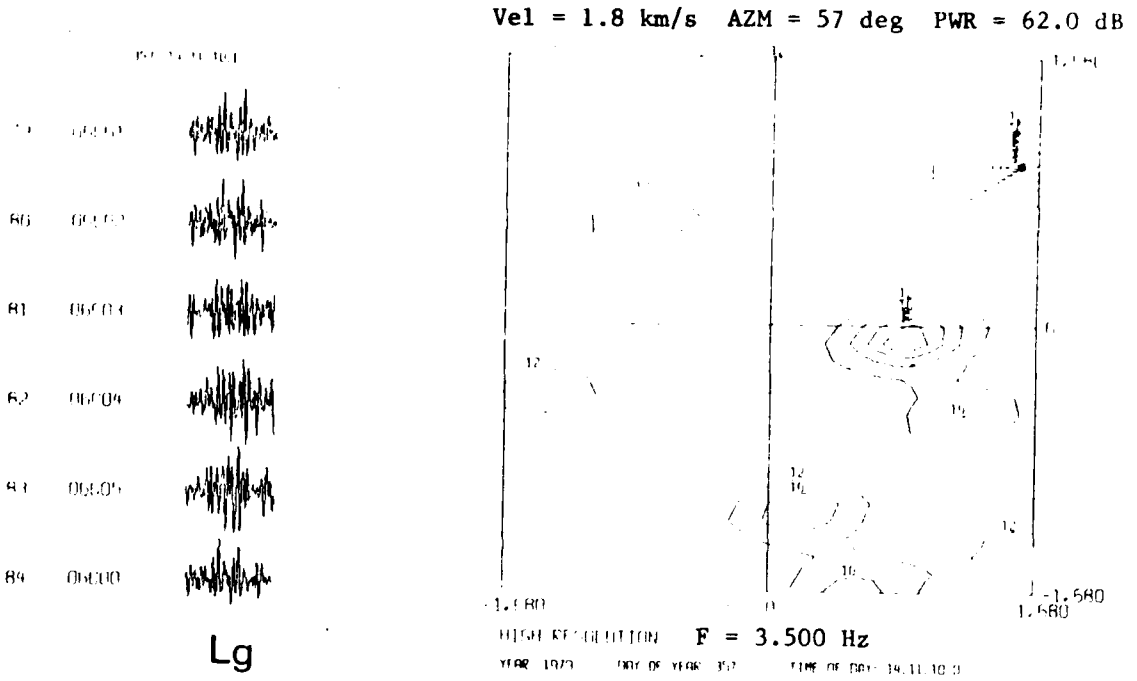

Fig. 4 High resolution frequency-wavenumber plots for the Lg phase of the same event displayed in Fig. 3. This figure illustrates the 'side lobe' problem (upper right), but in this case the proper lobe will be selected if a reasonable velocity constraint is imposed.

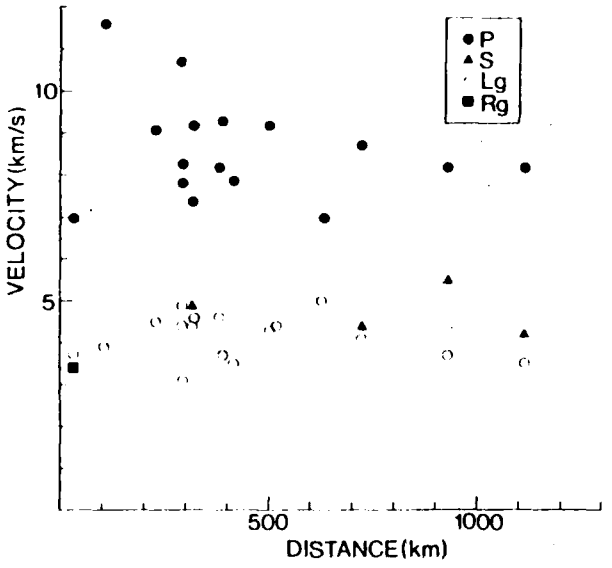

Fig. 5 Phase velocities as determined by processing of NORESS data from a set of regional events.

NORSAR System-related Research

by

Frode Ringdal, Jan Fyen and Hilmar Bungum

Project VT/0702/B/PMP

Contractor: NTNF/NORSAR
Post Box 51
N-2007 Kjeller, Norway

Task 2: NORSAR System-related Research

Objective

2.1 Complete programming effort to develop the new communications processor into a suitable replacement for the Special Processing System (SPS).

2.2 Develop the procedures so the new processor can be programmed in the future to meet AFTAC requirements; including the possibility of the deployment of a direct NORSAR-US satellite link.

2.3 Continue evaluation of the capabilities of the newly designed on-line event and detection processes; including the preparation of statistics to define the system's capability to process events under various signal-to-noise ratios and at various distances.

Accomplishments

The programming effort to develop the new MODCOMP communications processor into a suitable replacement for the Special Processing System (SPS) is continuing. By 15 July 1980 the status of this development was as follows:

- The communications protocol between the MODCOMP and the 7 NORSAR subarrays (SLEMs) has been completed.
- Interfacing between the MODCOMP and the Time-of-Day generator (TOD) at NORSAR has been completed.

- Data received by MODCOMP can be continuously read by IBM 360/40 and stored on magnetic tape in a backup mode. This transmission is now almost error-free, and it appears that the remaining problems are relatively minor ones.
- Two-way communication between MODCOMP and IBM 360/40 is still not satisfactory, but has been achieved in a test mode.
- The 230.4 kbps link between the two computers (via the IBM 2701 unit) shows high reliability.
- The filtering and subarray beamforming tasks of the MODCOMP have been programmed and tested off-line, but will need some further refinement in order to be performed in real time. The reason is that the CPU load is fairly tight, so that optimizing of some of the time-critical code will be necessary.
- Preparations have been made for programming the processor to meet future AFTAC requirements including the possibility of a direct NORSAR-US satellite link.

A very intensive effort is now being undertaken to complete the remaining MODCOMP development.

Evaluation of the capabilities of the newly designed on-line event detection processes has continued. The evaluation confirms our initial studies on this subject during FY79, and the main results are briefly summarized below:

- Detection performance of the new 7 subarray NORSAR configuration is on the average inferior to that of the earlier 22 subarray NORSAR system by about 0.2 m_b units at the 50 per cent incremental threshold level. This is close to what could be expected from theoretical considerations.
- On a regional basis, the reduction in performance is smallest for Central Asia (about 0.1 m_b unit) and greatest for the Western Hemisphere (0.3-0.4 m_b unites).

- Median NORSAR location difference for teleseismic (distance range 30^{o}-90^{o}) events relative to NEIS locations is now about 230 km. This can be compared to about 130 km when the full (22 subarray) array was in operation.
- With the reconfigured array, the best location accuracy is obtained for Central Asia (median difference 170 km), whereas the best results for the previous full array were obtained for the Japan to Kamchatka arc.

Illustrations of the above results are given in Fig. 1, which compares number of reported events before and after the NORSAR reconfiguration and in Fig. 2, which plots location differences relative to NEIS.

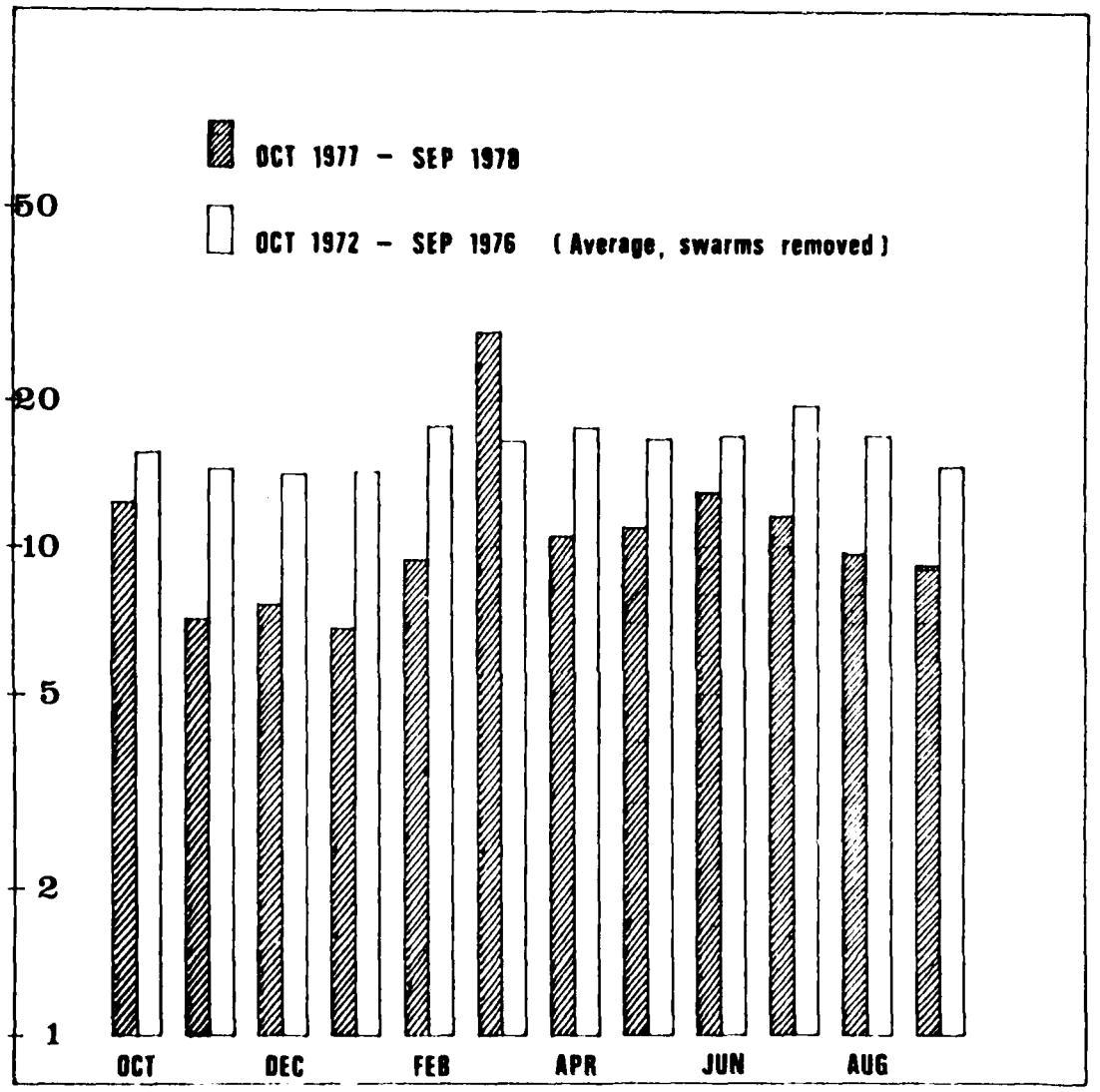

Fig. 1 Monthly averages of reported events at NORSAR before and after the reconfiguration of the array. Note that in computing the averages for the period Oct 1972 - Sep 1976 all months with significant earthquake swarms have been ignored. According to the same criterion, the month of March 1978 should be ignored when comparing the two periods.

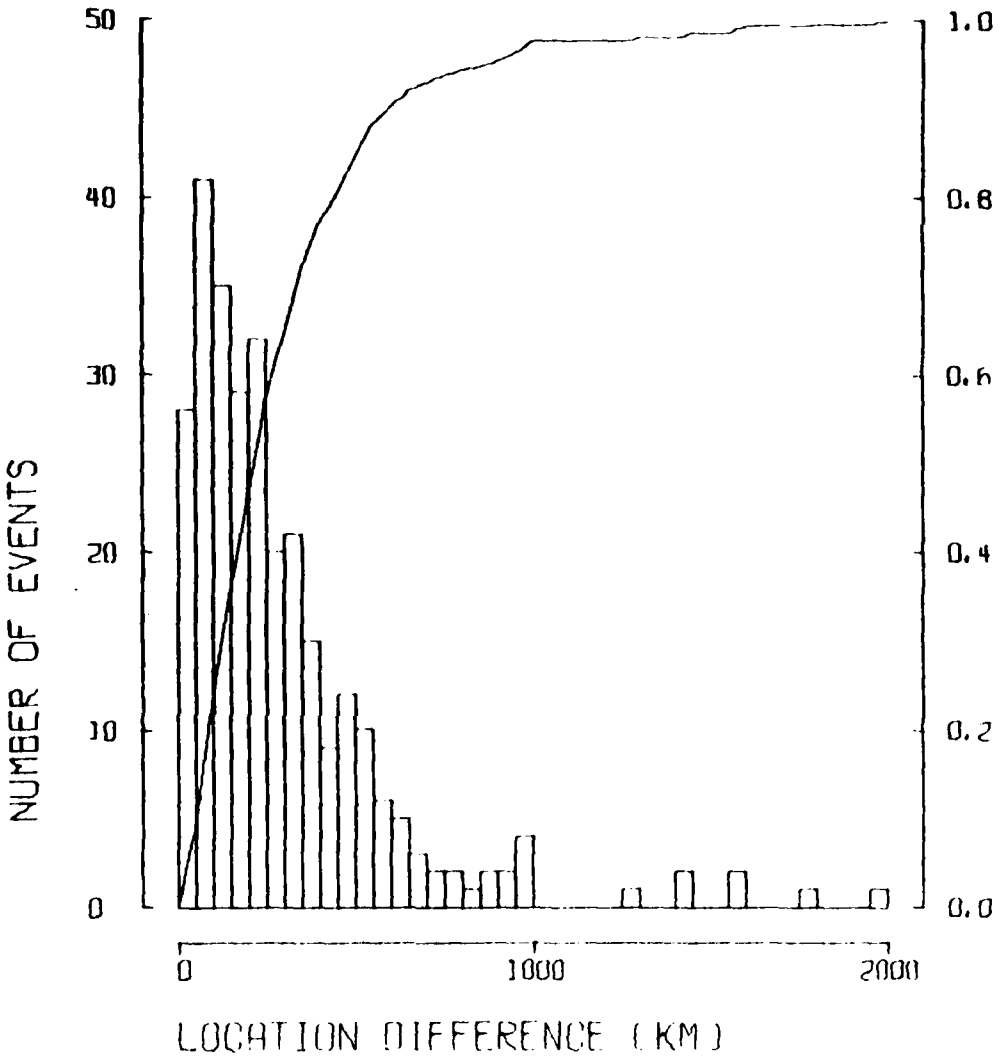

Fig. 2 Cumulative and incremental distribution of epicenter location differences between USGS and NORSAR based on 286 events during the time period Oct 77 - Dec 77.

Improvement of Visual Display of Signals

by

Jan Fyen and Frode Ringdal

Project VT/0702/B/PMP

Contractor: NTNF/NORSAR
Post Box 51
N-2007 Kjeller, Norway

Task 7: Improvement of Visual Display of Signals

Objective

As a means of improving the research capabilities of the NORSAR, investigate available graphic display systems for the replacement of the currently used pen plotters. Of prime consideration in this study should be the ability of the graphics system to display the highly complex signals from regional seismic events quickly. Procure a suitable graphics system and take the necessary steps to interface it to the NORSAR system.

Accomplishment

A study has been carried out to evaluate various means of improving the visual recordings of complex signals received at NORSAR. The conclusion is that such an improvement best can be achieved by acquiring an electrostatic printer/plotter for interfacing to the NTNF-funded interactive graphical system recently installed at NORSAR (Fig. 1). As a consequence, an electrostatic plotter of the type Versatec 1200 A has been procured, and interfacing to the NORSAR system is currently under way.

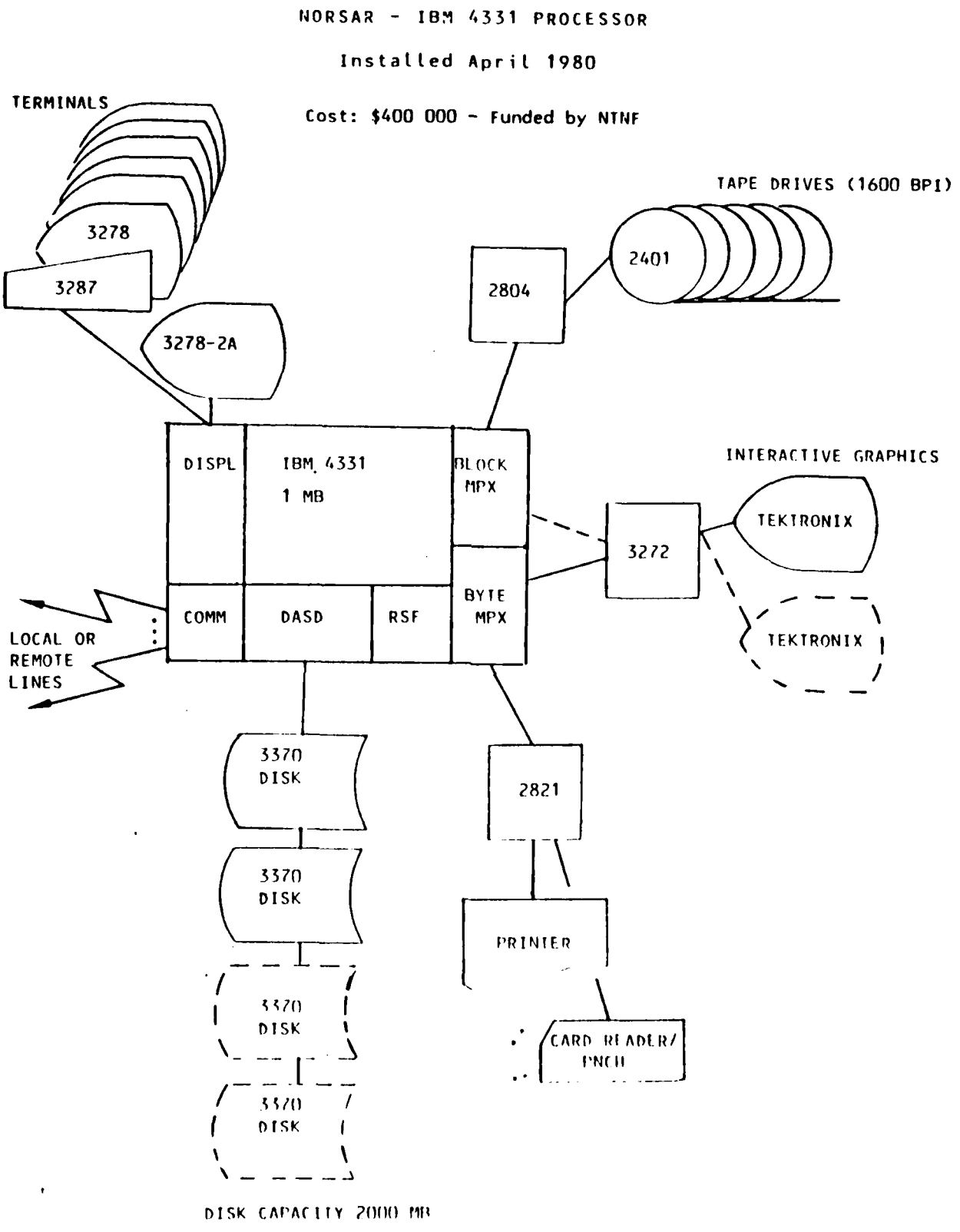

Fig. 1 The IBM 4331 research computer system at NORSAR.

AUTOMATIC ASSOCIATION (AA)

J. Goncz, R. Blandford, P. Kovacs

Project VT/0706 Contractor: Teledyne Geotech

Task 4.5.2 Automatic Association

Objective

Study the operation and processing techniques of the Automatic Association and Processing System (ADAPS) and the SDAC Automatic Association (AA) program. Determine ways in which the event formation capabilities of the two programs can be improved, and identify any post-DP processes which may be required to provide information necessary for making the improvements.

Accomplishments

Technical Report 80-2, entitled Present Status and Dynamic Planning for Automatic Association Program, was prepared for this task. Its abstract follows:

> This survey reveals that the five functioning automatic association programs existing today in the world, even though they were developed separately in independent institutions, all operate according to the same schema. Different algorithms and strategies do appear in the event refinement process, and seem to use as much of the attributes of the data as possible to exclude misassociations and false alarms. Recommendations are made for Geotech's AA and ADAPS to use as many of these algorithms as can be supported by the data.

Improvements to our current AA program were made. They consisted of:

o Obtaining local and near regional event locations by adding the TRIX algorithm to the system.

o Adding the logic to insure agreement of beam information when an arrival is associated to an event.

o Programmed a combo step in AA.

o Identifying the need for local regional discrimination and for spike discrimination in DP and guided the addition of these capabilities in DP.

o Not allowing a detection determined by DP to be a local to come from a station more than 10o from the event.

To evaluate the overall improvement in the AA from the combined effects of the improvements in DP and AA we may compare the results from running DP and AA on April 1-4, 1979 data as they were run in April of 1979, to the most recent results achieved in July, 1980. We shall use the results attained by the analyst in April of 1979 as a standard.

Teleseismic Events April 01-04, 1979

Analyst:	April 1979	76	-
DP+AA:	April 1979	29	29%
DP+AA:	July 1980	71	93%

Alaskan Regional Events April 01-04, 1979

Analyst:	April 1979	21	-
DP+AA:	April 1979	2	10%
DP+AA:	July 1980	11	52%

We see that teleseismic performance has improved from 29% to 93%; and regional performance from 10% to 52%. It is difficult to apportion the credit for this improvement as between DP and AA., they are very closely linked, each building on the strength of the other.

In the July 1980 AA runs there are an average of 27 (3)-stations events, 13 (4)-station events, and 5 (5)-station events which did not correspond to an event on the analyst's April 1979 bulletin. We know that several of these are good events. Analysis is underway on these events in order to discover their nature. Had all of the 3 and 4 station events been omitted from the printout an average of 2 analyst-produced events per day would be missed by an analyst who relied on the AA output to guide his analysis. Analysis of these latest results has revealed more ideas for improving the AA output; however these will not be implemented until the VAX version of AA is available. At present we plan to further evaluate AA on the month of April and to develop a systematic procedure by which the analyst can use this version of AA to speed analysis. Results thus far are encouraging.

AUTOMATIC SEISMIC SIGNAL PROCESSING

Project VT/0704 Systems, Science and Software

Task 4.1 Automatic Discrimination Research

Objective

The objective of this task is to develop, implement and test, on the seismic systems at the SDAC, a set of discrimination routines to be applied automatically to seismic signals. The algorithms will operate either with or without the existence of an event data file associating signals to form events. The output of the package will provide the probability that a specific event was an earthquake or explosion and the confidence level of that probability.

Body wave spectral magnitudes will be used as the primary means of performing automated discrimination. In addition, network averaged surface wave spectral magnitudes will be used in combination with averaged body wave spectral magnitudes to provide an mb-Ms discriminant to be used jointly with the variable frequency magnitude method. These measurements will be used, together with location and depth estimates when available, as discrimination methods using a multivariant approach.

Accomplishments

The choice of discrimination variables is based on previous discrimination work, including the VSC Discrimination Experiment (Savino, Archambeau and Masso, 1979 and Masso and Archambeau, 1979). In these studies it was found that the variable frequency magnitude method could be used to identify over 95% of the detected events if both regional and teleseismic stations were available (this is reduced to 90% if only teleseismic stations are used). Since the variable frequency magnitude method allows the use of single stations for discrimination, requires only single component short period seismic data and, in principle, does not require knowledge of the originating event location or depth (although rough location information is useful); it is an ideal method for automatic discrimination in view of its simplicity and effectiveness. Further, because it is a short period spectral method, it is effective to very low event magnitude levels, especially when regional data is available. It is estimated that the variable frequency magnitude method will be effective down to body wave magnitude 3.5 at the 95% level for combined regional and teleseismic data and to magnitude 4.0 at the 95% level for events with only teleseismic data.

The current VSC computer configuration is being studied to determine the optimum method of implementing these discrimination algorithms in the context of a Seismic Research Center. Some of the essential features of the proposed automatic system are:

(1) The use of a signal/event data file generated by an independent signal detection and association system. It is not assumed, however, that the file will necessarily be complete and accurate, nor that event locations and depths are included for all events.

(2) The system is structured to allow automatic event discrimination without signal associations or event locations and depth estimates, using single station and array variable frequency magnitude discrimination. This involves the use of azimuth and polarization information from arrays and three-component sensors.

(3) Formal multivariant discrimination is incorporated and may be used with single station variable frequency magnitude discriminants, with each to be treated as an independent discriminant, or it can be used with a combination of single variable frequency magnitude discriminants and network discriminants (i.e. event depth, location, network averaged mb and Ms, etc.) to provide multivariant event discrimination, where the signal associations are known along with the event location.

(4) A large signal/event file will be created, incorporating data for event signal associations, propagation path studies, detailed source characterization studies and more refined event discrimination work with events having low identification probability values.

INTELLIGENT LINE INTERFACE

E. McCoy

Project VT/0706 Contractor: Teledyne Geotech

Task 4.5.5 Intelligent Line Interface (ILI)

Objective

The purpose of this project is to develop several reliable line interface units to interface each communication line to the CCP in a buffered and uniform format. The concept is illustrated by Figure 1. Each unit performs functions unique to its line.

One objective is to test the feasibility of imbedding intelligence such as data formatting, data error detection, and seismic signal detection in a communications interface. While a formal evaluation is not being performed, information will be obtained concerning potential cost, reliability, ease of operation and systems monitoring, and flexibility for change and reconfiguration.

The design is built around general-purpose microcomputers to give flexibility for change. Figure 2 shows the internal hardware design.

Accomplishments

All systems analysis and design has been completed. The signal detection algorithm chosen is a time domain LTA/STA type of detector with additional discriminants applied.

An initial operational ILI has been installed. The signal detector and quality control features will be added upon completion of a high speed interface (illustrated by Figure 1) at the CCP to increase the input data rate sufficiently to handle the additional data generated by these functions.

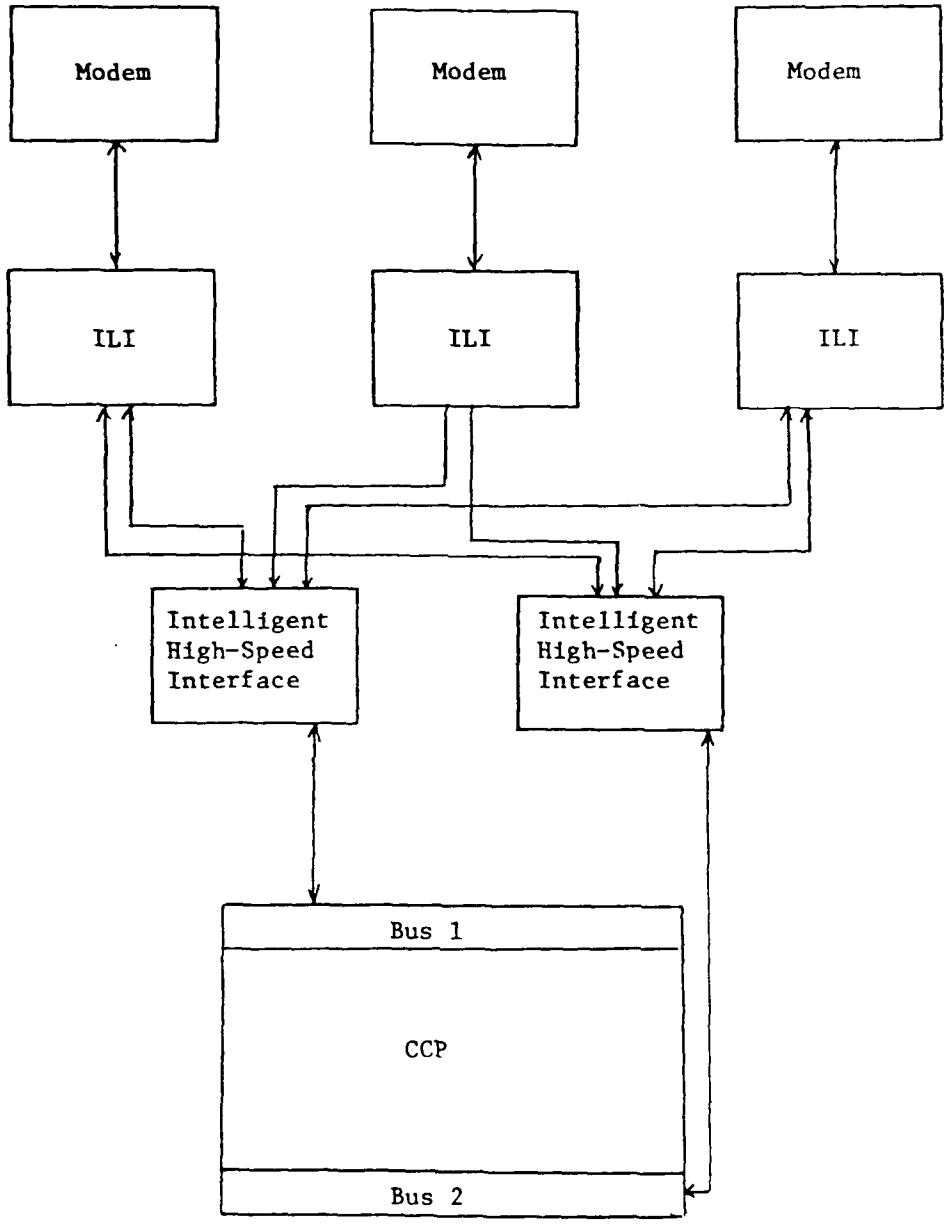

Module-Per-Line Concept

Figure 1

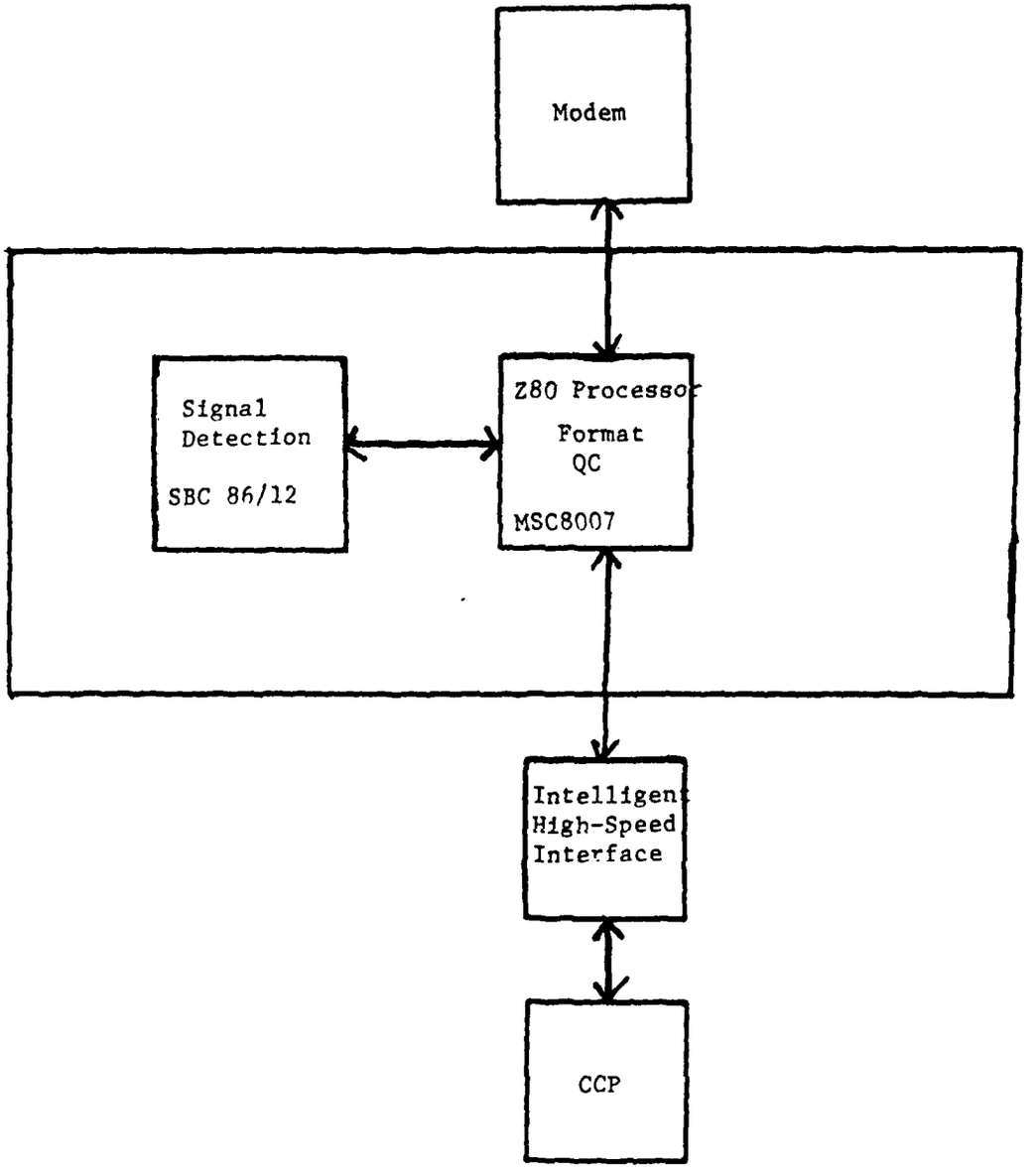

Figure 2 Internal Hardware Configuration

THE EFFECTS OF SOURCE REGION ON SEISMIC WAVEFORMS

Project VT/0710 Sierra Geophysics, Inc.

Task 4.2 Source Region Structural Influence

Objective

The object of this study is to examine the effects of shallow crustal structure and focussing on short period waveforms in the Yucca Flats region, on Pahute Mesa, on Gold Meadows Stock and at Climax Stock. The motivation for this work is the observation that events in the Yucca Flats area show significant magnitude versus yield variation which appears to be dependent upon the location of the event within the region. This study will attempt to determine if structural variations alone can account for these observations and then apply the procedures used to analyse the effects in other regions of the NTS. The analysis employs a combination of plane-layer, dipping-layer and three-dimensional wave propagation modelling techniques.

Accomplishments

Using the available geological and geophysical data for the Yucca Flats area, a three-dimensional, laterally varying impedance model has been defined. The effects of this structure on both incoming and outgoing seismic energy have been modeled using the Glorified Optics Algorithm of Hong and Helmberger (1978), with the results predicting strong waveform and amplitude variability as a function of azimuth and source or station location within the basin. However, the synthetic waveforms produced are not totally satisfactory. A weakness in the Glorified Optics Algorithm is its inability to handle diffracted energy which may play a significant role in a region such as the Yucca Valley. Currently under development is a Kirkoff Integral Technique which will include diffracted energy as well as purely geometric ray paths. Using a revised model of the Yucca Flats region, this new method will be used to determine the extent which diffracted energy influences the seismic waveforms coming from events in this region. If results are promising, the method will be applied to the Pahute Mesa area where short period magnitude biases have also been observed. Additional work will involve a detailed comparison of the Gold Meadows Stock with the Climax Stock.

THREE-DIMENSIONAL EARTHQUAKE MODELING INCLUDING NONLINEAR RUPTURE DYNAMICS

Steven M. Day

Project VT/0712

Contractor: Systems, Science and Software

Task 4.1.2 Seismic Source Calculations: Earthquake Simulation Studies Using the ILLIAC IV

Objective

The objective of this task is to investigate those aspects of source dynamics which differentiate the seismic signatures of earthquakes from those of explosions.

Accomplishments

We are using a three-dimensional finite difference method to model the features of earthquake dynamics believed to be important for predicting the teleseismic signal. The calculations have simulated inelastic response of the fault zone through nonlinear boundary conditions on the fault plane. The numerical method admits more general nonlinear material behavior, which is being incorporated as required.

Our initial numerical simulations were for a simple, constant rupture velocity, constant stress-drop earthquake model. These results show a significant influence of fault width on the slip function. For points on the fault which are more than a fault width away from the focus, the slip function is spatially quite uniform. The static slip is given by $\Delta\sigma W/\rho\beta^2$, in agreement with estimates based on elastostatic solutions. The numerical simulations predict a rise time of $W/2\beta$ and peak slip velocity of $\sqrt{2fW/\beta}\ \Delta\sigma/\rho\beta$. In these expressions, W is the fault width, $\Delta\sigma$ the stress-drop, f the maximum frequency, β the shear speed, and ρ the density.

Careful studies of the broad-band character of earthquake teleseismic signatures indicate that the relative excitation of long- and short-period waves is inconsistent with predictions from the simple model. In addition, a few isolated, severe stopping phases dominate near-field accelerograms synthesized from the simple model, in conflict with strong motion data. More complex rupture physics is required to explain the discrepancies between the model predictions and teleseismic and strong motion observations. In particular, a better physical description of the cessation of rupture growth appears necessary.

A displacement-weakening constitutive model, described by Figure 1, has been applied to simulate spontaneous rupture in the presence of both uniform and heterogeneous prestress. In this model

of failure, the shear strength of the fault zone is assumed to be a decreasing function of its deformation; energy is dissipated during rupture extension and shear stress is bounded on the fault edges. When rupture initiates in a limited region of high stress (Figure 2a), the model leads to spontaneous propagation, deceleration, and stopping of faulting. Figure 3 shows the evolution of the rupture front in this case, as well as the far-field P and S wave displacement spectra and the corresponding displacement, velocity, and acceleration pulses. In the presence of multiple high-stress regions (Figure 2b), each isolated stress concentration behaves roughly as an independent event. As shown in Figure 4, rupture velocity becomes quite irregular, and is strongly coupled to peak velocity of slip on the fault surface. Figure 5 shows the irregular rupture growth, as well as the far-field spectra and time-domain pulses which result. Predicted accelerograms are in better qualitative accord with strong motion data.

The model predicts significant consequences for the spectral and time-domain characteristics of the earthquake teleseismic signal due to the presence of stress irregularities. For example, Figure 6 compares the short-period teleseismic P-wave for the stress-concentration model with that for a uniform stress model (scaled to a source dimension equal to the dimension of the stress concentration). Both the period and amplitude of the b phase (first peak-to-trough) agree for the two models, while the stress-concentration model has twice the moment of the uniform stress model. The two events have been superimposed on an m_b versus M_S plot (from Filson and Bungum, 1972) to illustrate that the stress-concentration phenomenon enhances separation of earthquake and explosion populations.

REFERENCES

Filson, J. and H. Bungum (1972), "Initial Discrimination Results from the Norwegian Seismic Array," Geophys. J., 31, pp. 315-328.

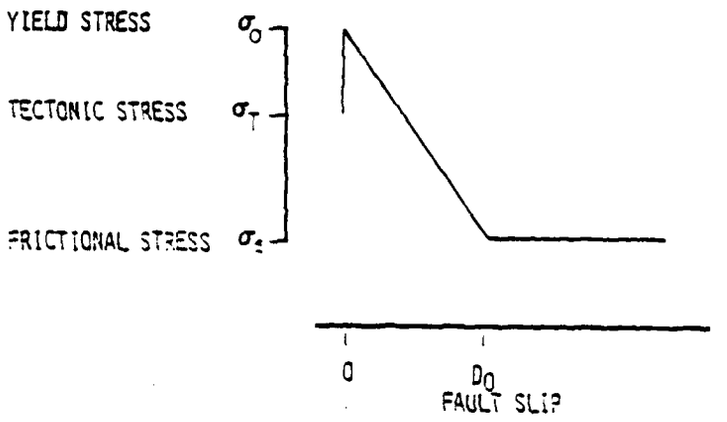

Figure 1. Displacement-weakening constitutive model for the fault zone.

a) Stress-concentration model.

b) Multiple stress-concentration model.

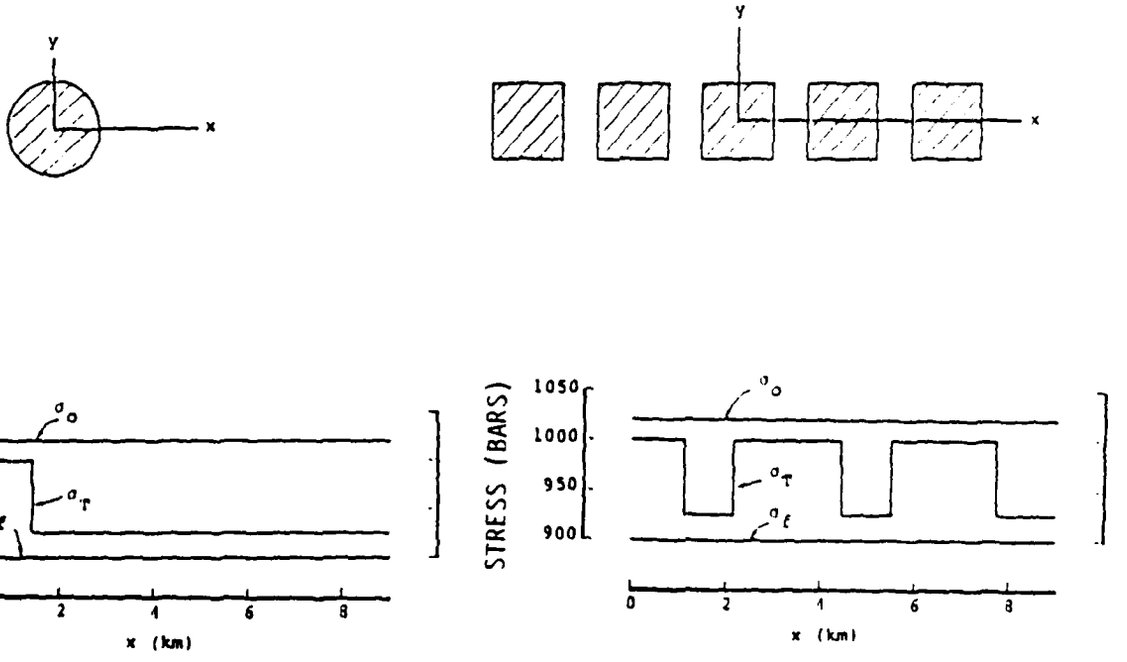

Figure 2. Stress-concentration fault models considered in this study.

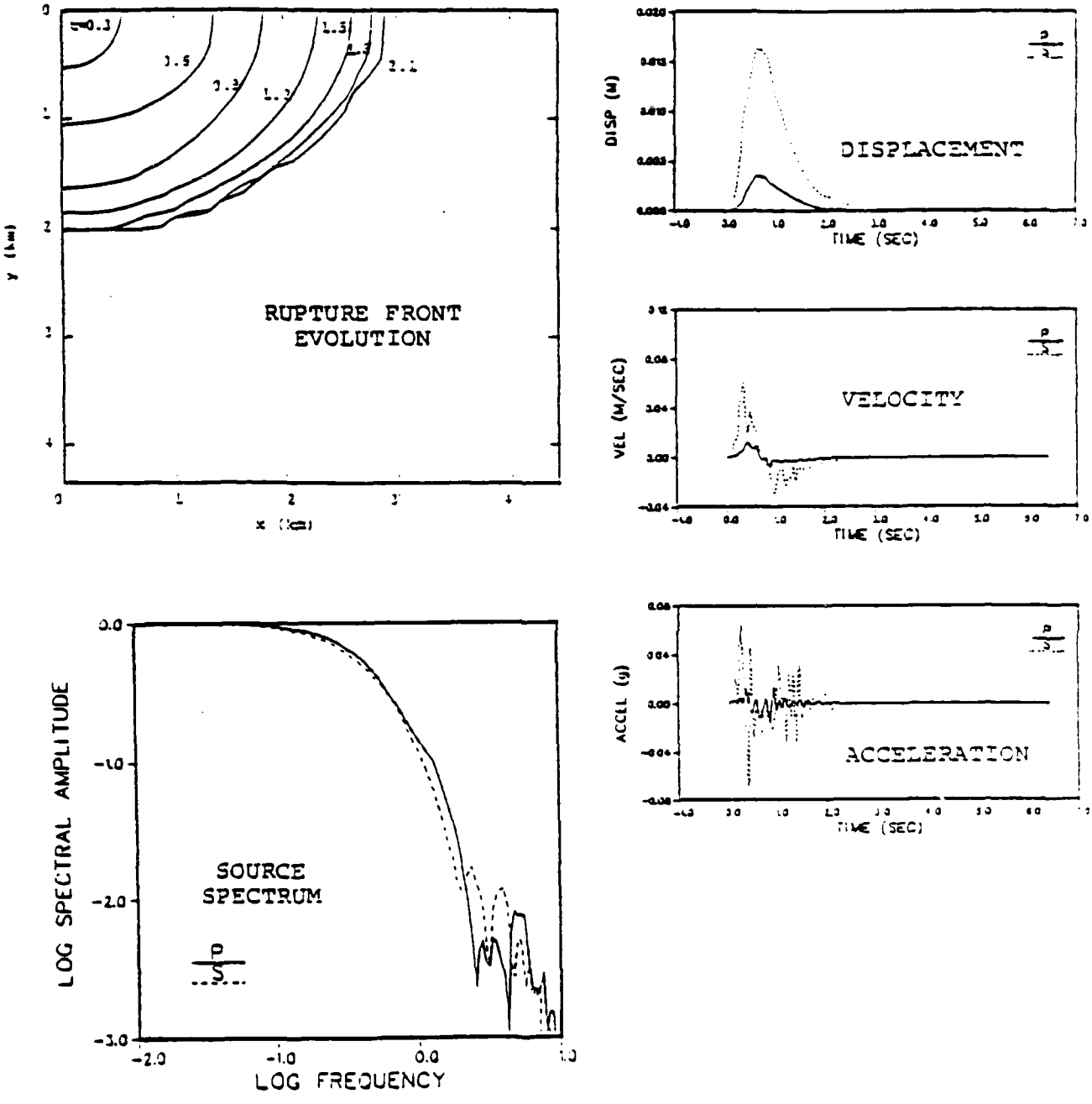

Figure 3. Rupture mechanism and far-field spectra and pulse shapes for stress concentration earthquake model at spherical coordinates $\theta = 45^{\circ}$, $\phi = 45^{\circ}$, relative to fault normal.

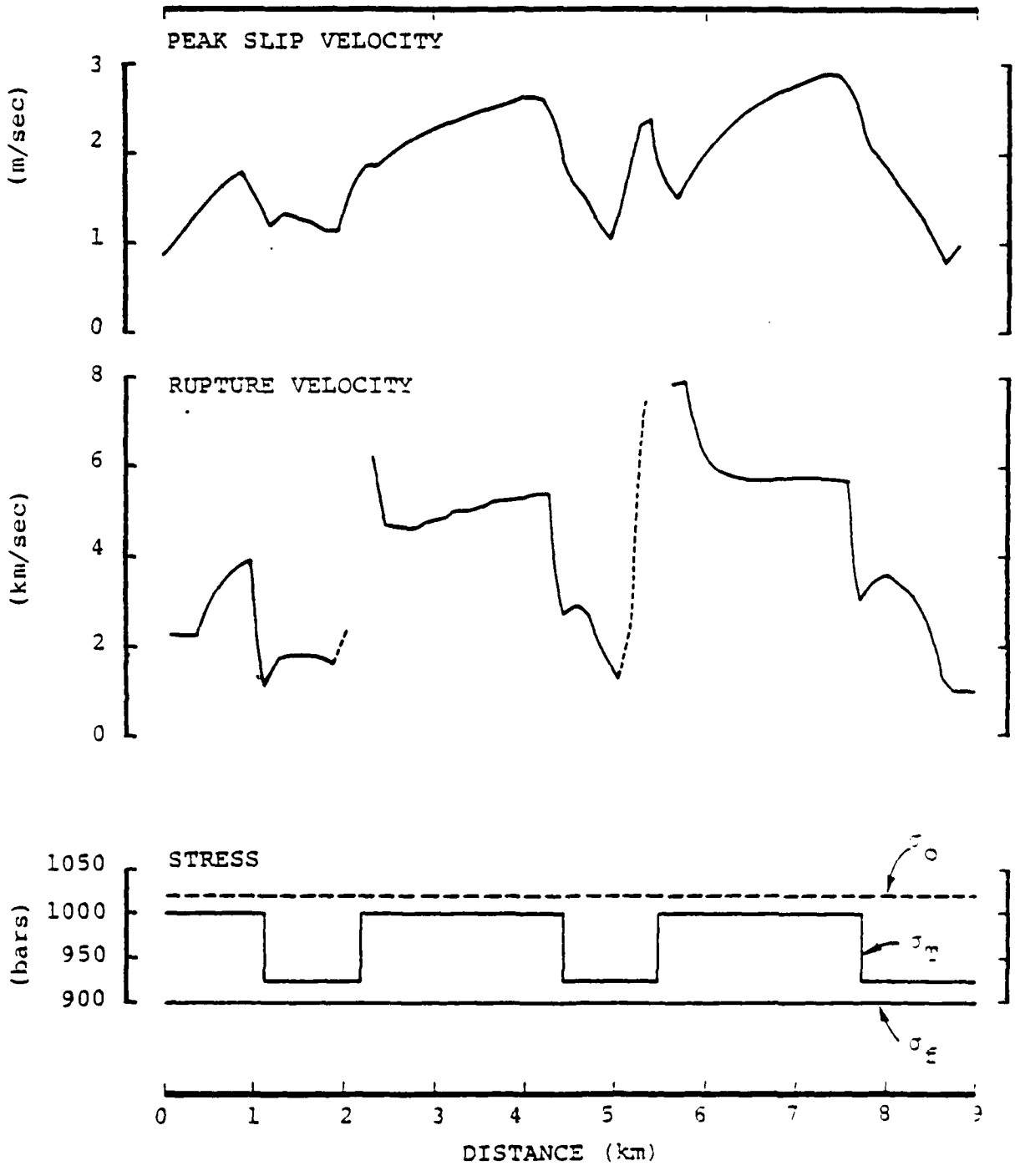

Figure 4. Peak slip velocity (low-passed, 5 Hz cutoff) and rupture velocity along the x axis, for multiple stress-concentration model. Dashed curves for rupture velocity indicate regions which ruptured out of sequence. For example, rupture occurred at x = 5.6 km while the region between 5.0 and 5.6 km was still intact.

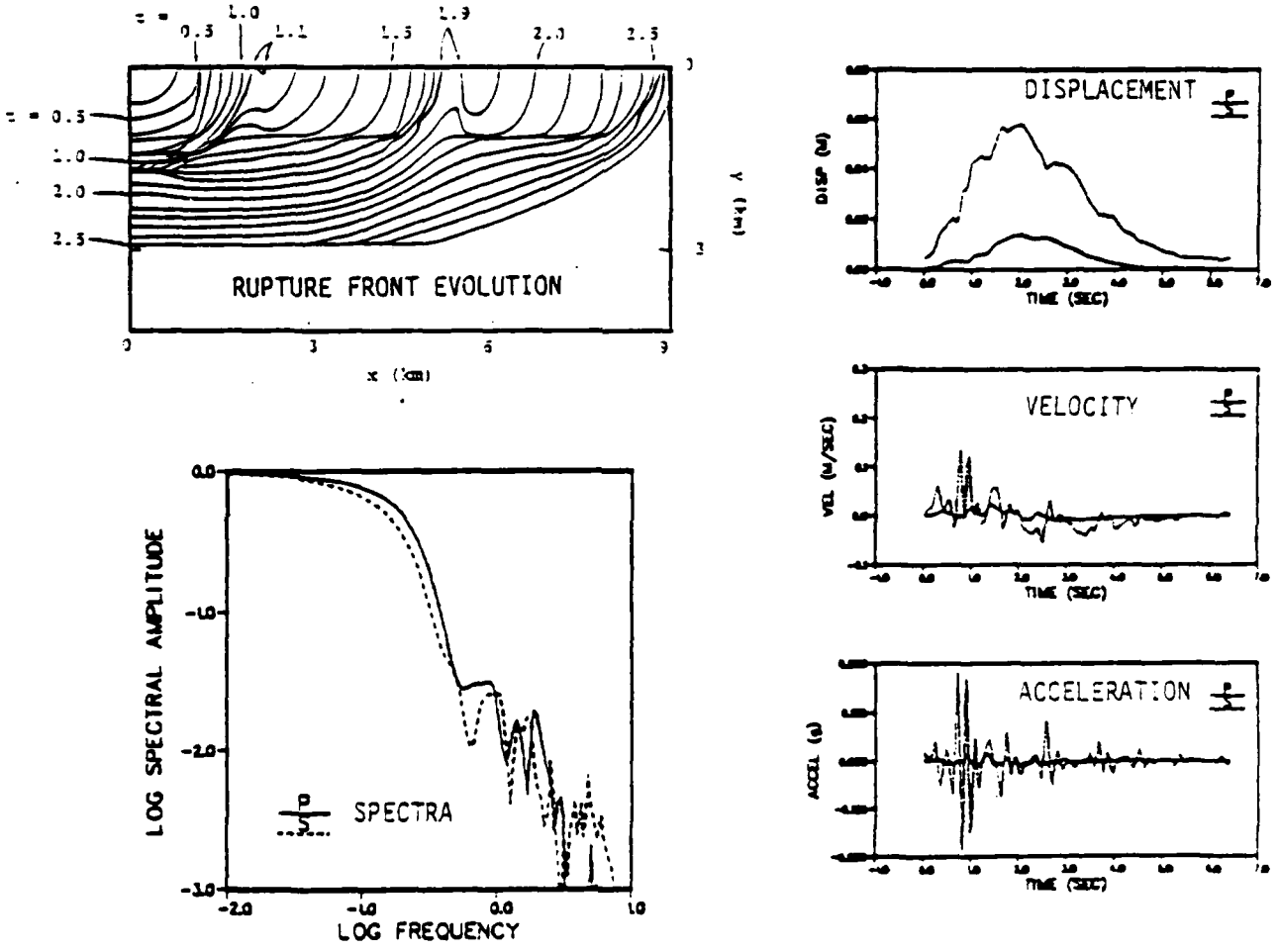

Figure 5. Rupture mechanism and far-field spectra and pulse shapes for multiple stress-concentration earthquake model (at spherical coordinates $\theta = 45^\circ$, $\phi = 45^\circ$ relative to fault normal).

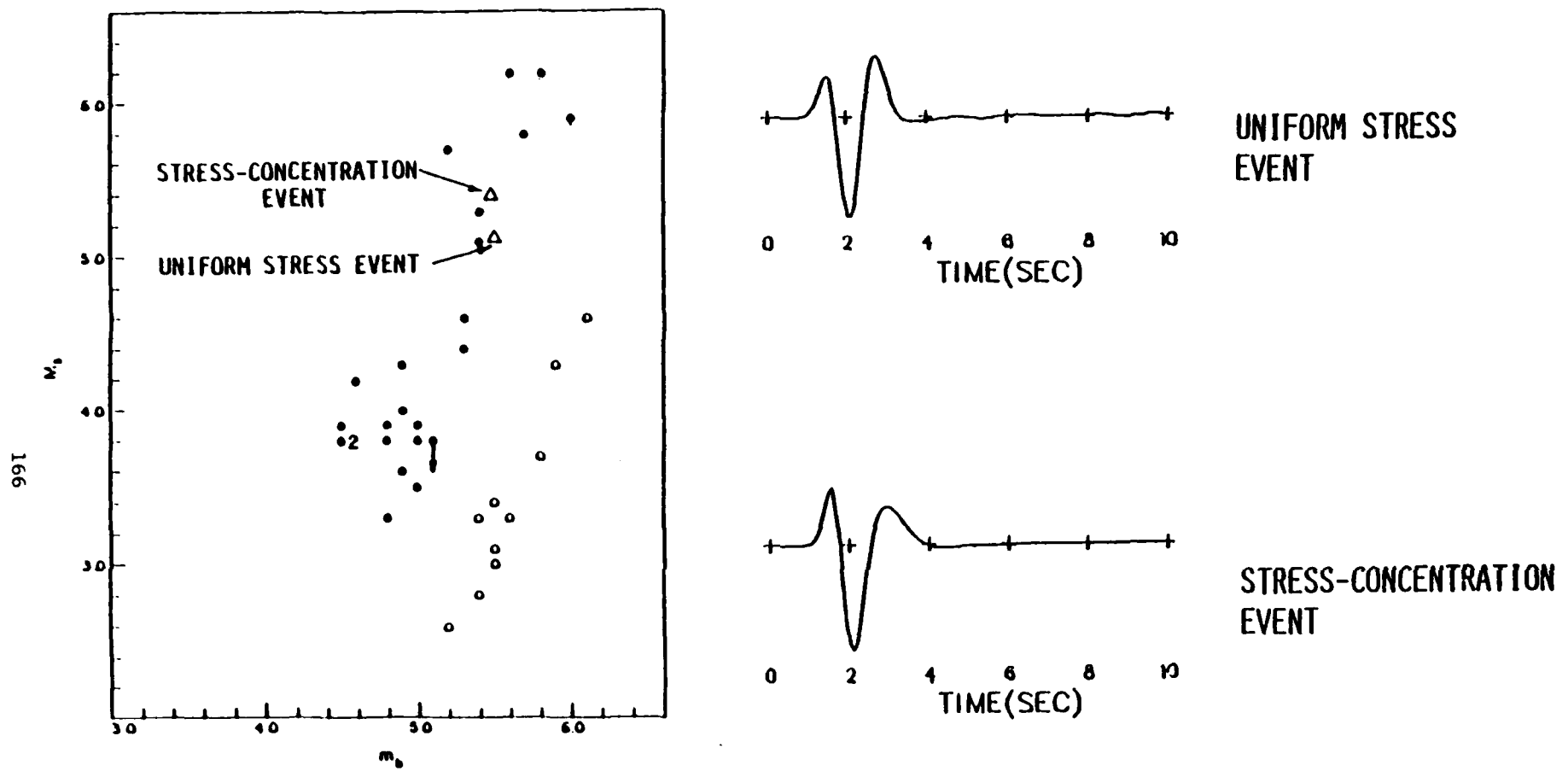

Figure 6. Short-period P-waves from uniform stress model and stress-concentration model. The two events are plotted as triangles on an m_b-versus-M_S diagram (from Filson and Bungum), in which open circles and closed circles represent presumed explosions and earthquakes, respectively.

RELATIVE RECEIVER FUNCTIONS

FOR

THREE DIFFERENT ARRAY CONCEPTS

G. M. Lundquist
G. R. Mellman
D. M. Hadley

Project VT/0710 Sierra Geophysics, Inc.

Task 4.3 Absolute Attenuation and the Role of Receiver Site Structure

Objective

The object of this study is to produce a function, R, for a given seismic station which models all near receiver contributions to observed waveforms, including crustal reverberations, acoustic impedance amplification effects, laterally refracted arrivals and variations (δt^*) in attenuation from an average earth model. As a first step toward a true receiver function, relative receiver functions (RRF's) are estimated for arrays of stations. Resolution of absolute individual receiver responses will require careful calibration of one station in the array.

Accomplishments

RRF's have been estimated for three different array concepts, including the "small" arrays, the "continental array" and the "global array." The small array, with apertures generally in the range of a few to several tens of kilometers, is typified in this study by the Yucca Flats array at NTS. The continental array studied is the Western U.S. Array, or WUSA, made up of all of the WWSSN stations west of 105° W longitude in the conterminous United States. A global array includes any seismometer or array in a usable distance range about an explosion source region. This study has concentrated, so far, on the Eastern Kazakh Global Array (EKGA).

Within an array of stations, trace deconvolutions, d_j, are computed by spectral ratio, t_j/t_o of the trace, t_j, at a secondary station to the trace, t_o, at a reference station. Because any (frequency dependent) factors common to both stations will divide out, the ratio reduces to r_j/r_o, the ratio of relative receiver

functions. The d_j are computed for each event in the data set for which both reference and secondary stations are available, and the results for each station pair are averaged in the log-frequency domain. The result is an average transfer function, $\bar{d}_j$, which permits computation of a synthetic trace from the reference seismogram.

Application of the trace deconvolution to small arrays is straightforward; since rays to both reference and secondary stations see the same source and path to within a small distance of the receivers. Though continental arrays may be thousands of kilometers across, the variation in azimuth and takeoff angle from teleseismic source regions is small enough for effective deconvolution of source and lower mantle factors. (The variation in upper mantle path, including δt^*, is a desirable part of the estimated RRF's.) Trace deconvolution of a global array relies upon approximate azimuthal symmetry of the source. Figures 1-3 show reference, secondary and synthetic traces for a selected station pair from each of the array concepts. Clearly the $\bar{d}_j$ adequately resolve the differences between receiver responses at reference and secondary stations.

The recovery of r_o, and thus r_j, from the $\bar{d}_j$ requires the imposition of an additional constraint, and we have chosen to require the r_j as a set to be as simple or "delta-like" as is consistent with the information in the $\bar{d}_j$. This is accomplished by finding a linear operator which, when convolved with the $\bar{d}_j$, will maximize the order (or minimize the entropy) in the set of estimated r_j as a whole. The procedure used is nonlinear and recursive, and the entropy minimum found is not necessarily unique. Tests show, however, that the significant information in a set of r_j determined by well constrained $\bar{d}_j$ is stable, within limits, as a function of reference station, number of stations and choice of weighting schemes. Significant information, of course, is that which affects synthetic seismograms. Figures 4 and 5 give examples of RRF's and synthetic seismograms for two choices of reference station for the WUSA array.

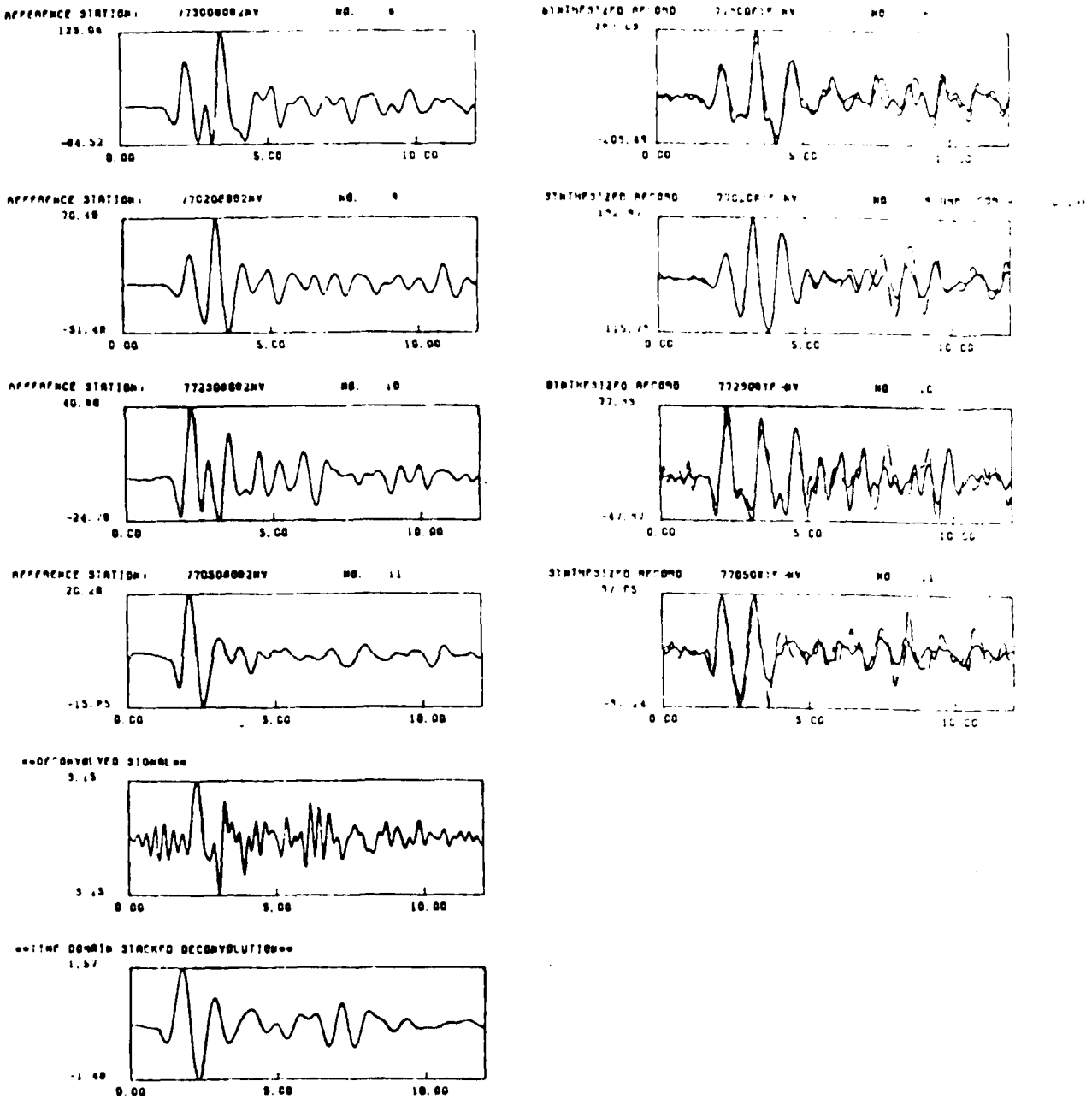

Figure 1. Observed seismograms at stations OB2NV (left) and YF2NV (right, dashed) from events to the southeast. Synthetic seismograms (right, solid) for station YF2NV produced by convolving the OB2NV observation with the YF2 receiver functions appropriate to a southeast azimuth.

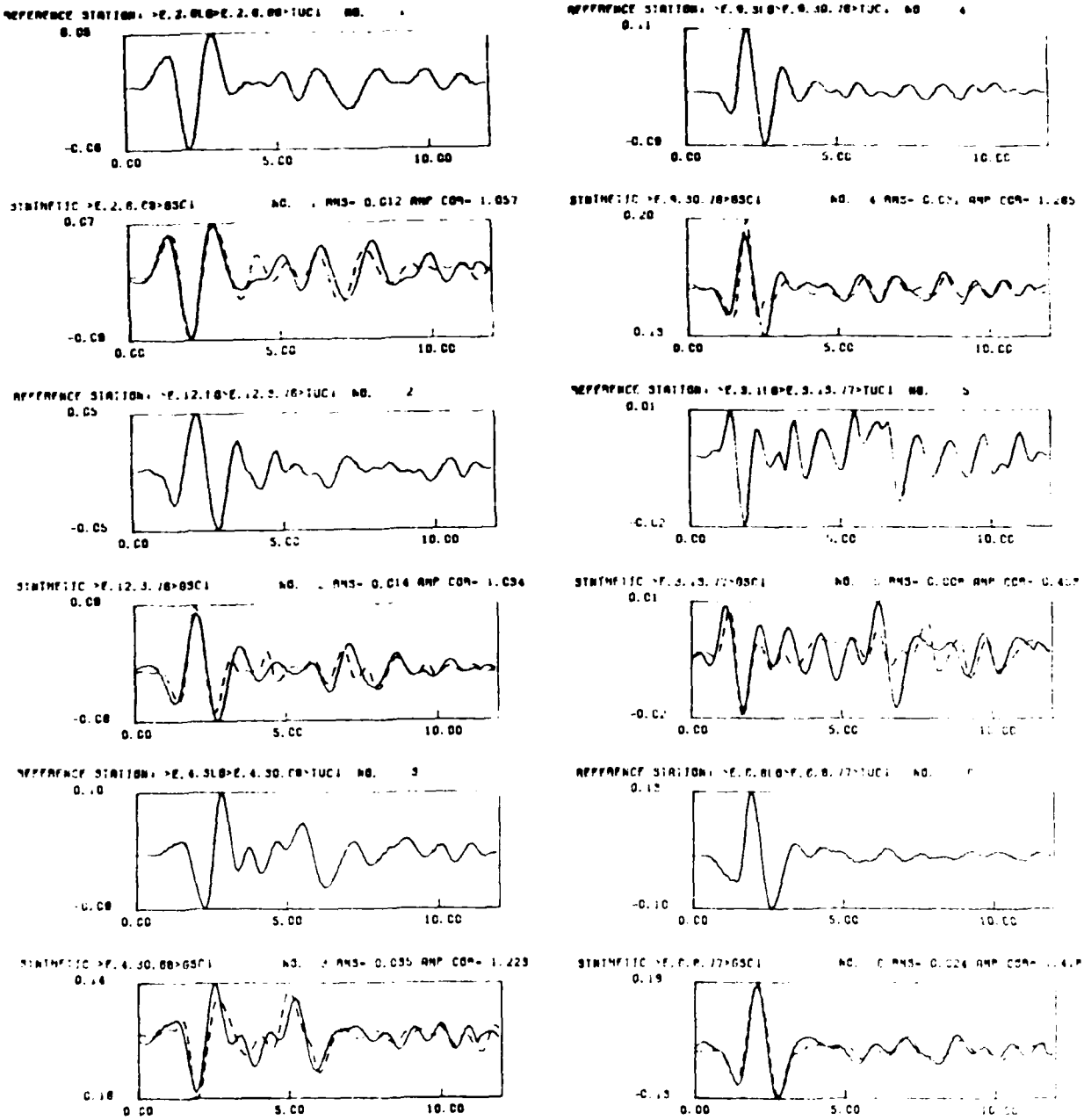

Figure 2. Data and synthetic for the station pair GSC/TUC for events from a southeastern azimuth. For each trace pair, the reference trace is plotted above, and the secondary trace (dashed line) is plotted below. Synthetic seismograms (solid line below) are produced by convolving the TUC observation with the log-spectral average of GSC/TUC deconvolutions.

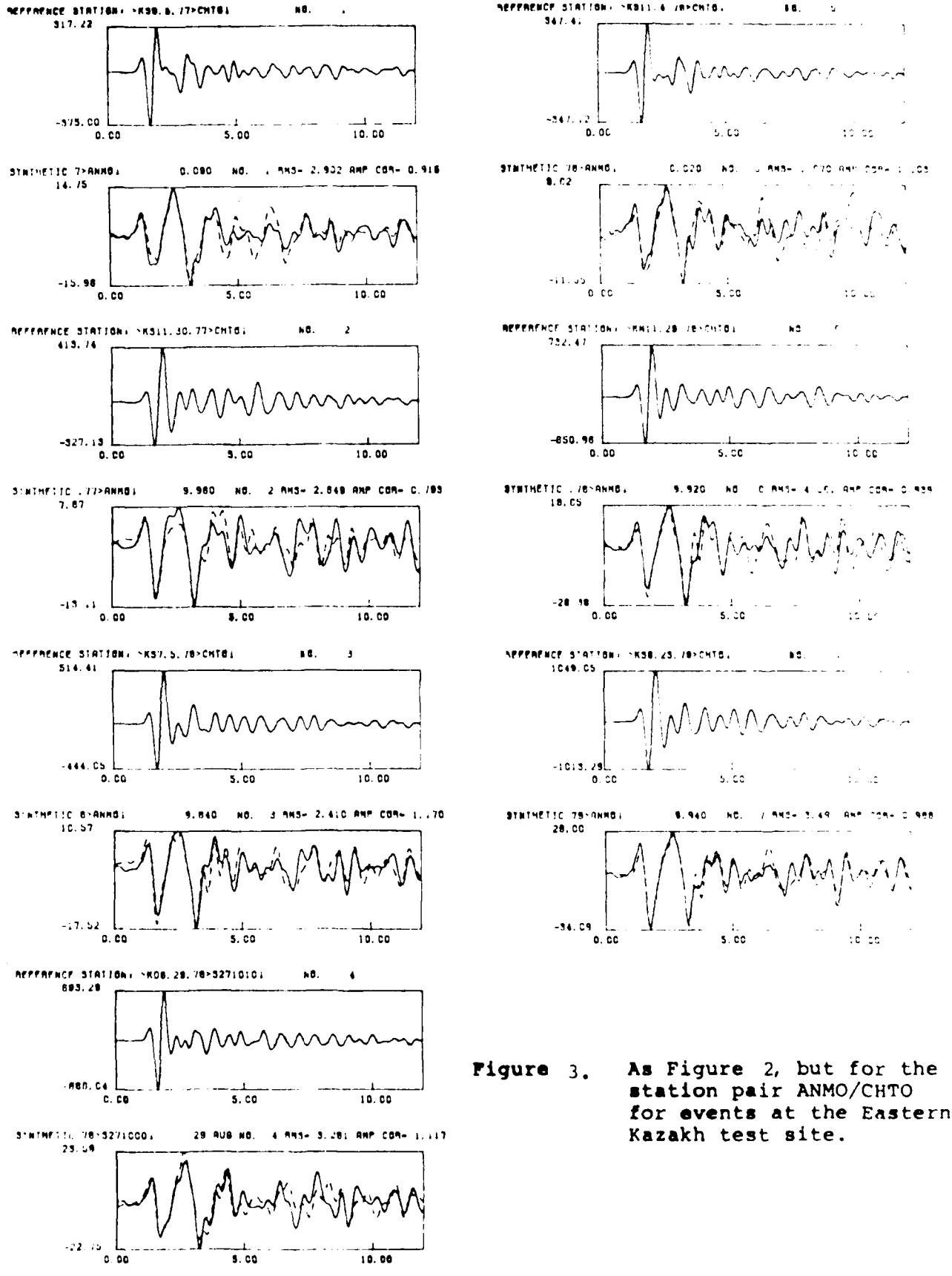

Figure 3. As Figure 2, but for the station pair ANMO/CHTO for events at the Eastern Kazakh test site.

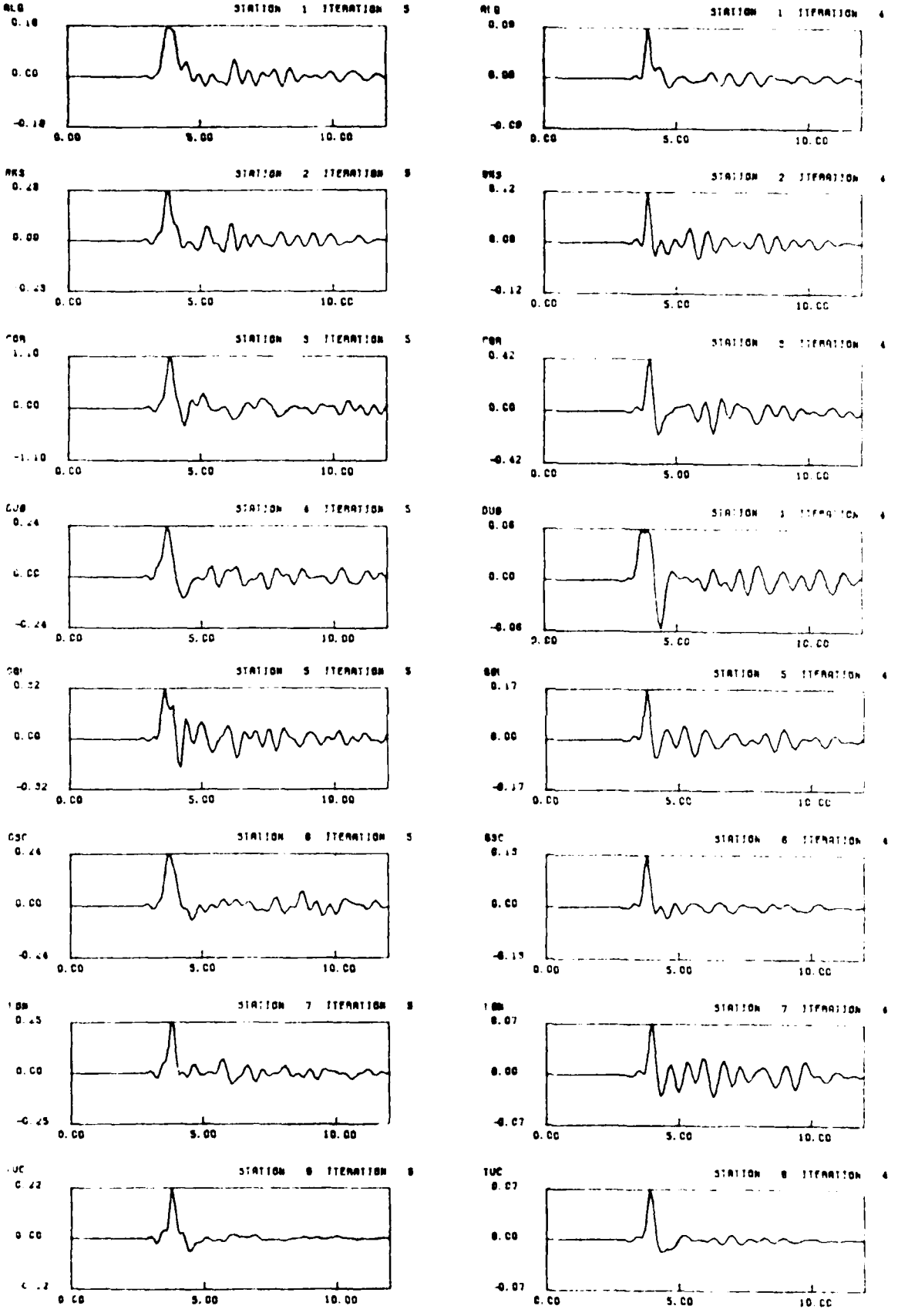

Figure 4. Estimated MED relative receiver functions appropriate for a southeast azimuth. Column at left referenced to TUC; at right referenced to GSC.

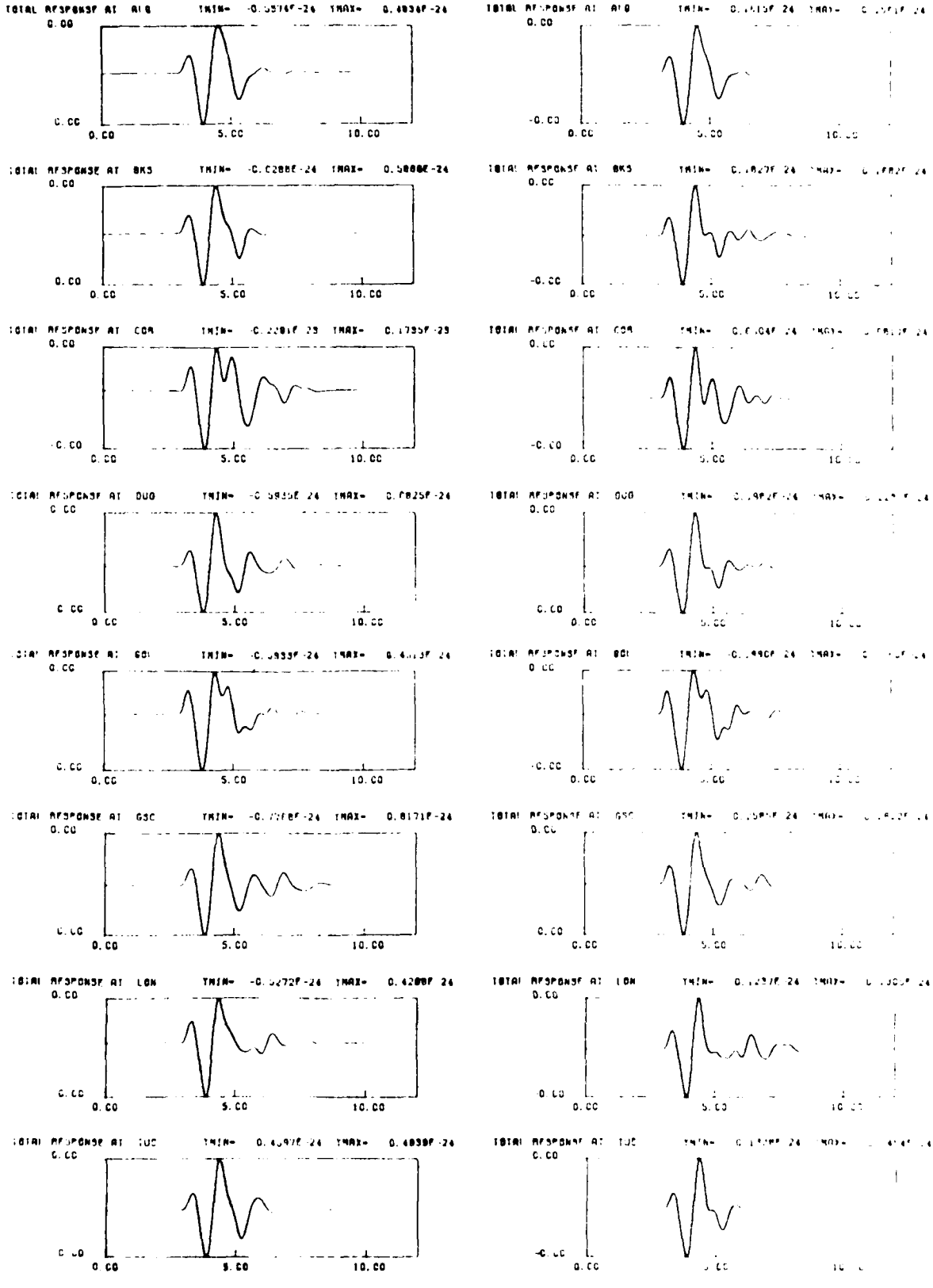

Figure 5. Synthetic seismograms computed by convolving the RRF's in Figure 4 with a simple earthquake source-time function.

AUTOMATED MAGNITUDES, $\hat{m}_b$ AND $\hat{M}_s$

T. C. Bache
B. Shkoller

Project VT/0712

Contractor: Systems, Science and Software

Task 4.4 Evaluation of Suites of Events

Objective

Evaluate the feasibility of automatic determination of body wave magnitude by the MARS process. Develop and test an analogous automatic surface wave magnitude algorithm.

Accomplishments

In FY '79 we proposed an automated magnitude measure called $\hat{m}_b$ and tested it by processing high signal/noise recordings of eleven Pahute Mesa explosions at six teleseismic stations (Bache, 1979; Bache, Day and Savino, 1979). We concluded that the $\hat{m}_b$ was at least as good a magnitude measure and yield indicator as the most carefully determined time domain m_b. The $\hat{m}_b$ algorithm used in that earlier work did not account for the presence of seismic noise, and so was viewed as primarily a demonstration of the concept.

As part of the VSC conducted discrimination experiment, algorithms were constructed to compute variable frequency magnitudes, $\bar{m}_b(f)$, at selected frequencies (Masso, et al., 1979; Savino et al., 1980). These algorithms do incorporate corrections for the presence of interfering phases and seismic noise. Otherwise the $\hat{m}_b$ used by Bache (1979) is not much different from $\bar{m}_b$ (1 Hz).

In the current contract we have implemented a new algorithm for $\hat{m}_b$ (which is essentially $\bar{m}_b$ (1 Hz)) and tested it by application to a series of synthetic seismograms which are constructed by embedding a signal of known $\hat{m}_b$ in seismic noise. The $\hat{m}_b$ has also been computed for a set of RKON recordings of Eurasian events taken from the AI data set. A similar algorithm has been implemented for computing an analogous $\hat{M}_s$, and some testing has been done.

The work accomplished in this task is summarized in an S-Cubed semi-annual technical report (Bache, et al., 1980). The most important results will be discussed in subsequent paragraphs.

Description of the $\hat{m}_b$ Algorithm

The calculation of $\hat{m}_b$ includes the following steps:

1. The seismogram is processed by MARS, which applies a suite of narrow-band filters and

constructs a table of envelope function peak amplitudes (A_c) and group arrival times (t_g).

2. The MARS detection algorithm is applied to identify an undispersed P wave arrival. This algorithm works with a "surface" like that shown in Figure 1, where the A_c are plotted versus t_g and filter center frequency, f_c. For each f_c the largest A_c is denoted by an asterisk. The relative amplitudes of the other peaks are denoted by integers, with the asterisk given the value 10. The detection algorithm searches for a "ridge" of amplitudes with nearly the same t_g to find the group arrival time, $\bar{t}_g$, of a detected P wave. The "+" and "-" symbols in the plot denote a statistically determined uncertainty window within which any A_c could be associated with the detected signal.

3. For each f_c, one A_c is chosen to define the "MARS signal spectrum." This is done by a scoring algorithm which, in its current form, works fairly well, but could probably be improved for low S/N events.

4. The A_c values about a specific f_c (e.g., 1 Hz) are fit to give a "smoothed" estimate for the spectral amplitude at that frequency. This amplitude is corrected for the presence of nearby envelope peaks and a statistical estimate of the uncertainty is made, based on the "MARS spectrum" of the ambient noise. The $\hat{m}_b$ is computed from log (A_g** ; f_c) + B, where A_g** is the noise corrected A_c and B is the usual distance correction.

$\hat{m}_b$ Algorithm Testing

In Figure 2 we show the $\hat{m}_b$ for a synthetic seismogram which has been added to a noise sample from RKON, with the ratio of peak time domain amplitudes ("Peak S/N") being scaled to 100. The $\hat{m}_b$ is 3.589, which may be compared to the time domain $\hat{m}_b$ of 3.78, computed from log(A/T) + B, with T = 0.7 seconds. Systematic differences between m_b and $\hat{m}_b$ are expected.

The same synthetic was added to various segments of noise recorded at RKON. Some examples are shown in Figure 3. Bache, et al., (1980) show fifteen such examples. The error in arrival time and $\hat{m}_b$ for these examples are tabulated in Table 1. Only when the ratio of MARS signal spectrum to MARS noise spectrum gets to be 1.5

TABLE 1

SUMMARY OF $\hat{m}_b$ TEST CALCULATIONS

Identifier	Peak Signal / Peak Noise	S/N (1 Hz)	$\hat{m}_b$	$\hat{m}_b$ Uncertainty	$\hat{m}_b$ Error	Arrival Time Error
		Noise Section 62110				
(Figure 2)	100	217	3.589	0.001	--	--
A	3	6.5	3.583	0.018	-0.006	+0.02
B	1	2.2	3.593	0.055	0.004	0.03
C	1	2.6	3.667	0.046	0.078	-0.09
D	1	2.2	3.586	0.056	-0.003	0.48
E	1	2.2	3.581	0.057	-0.008	-0.01
F	0.5	1.5	3.734	0.082	0.145	0.09
G	0.5	1.2	3.622	0.110	0.033	-0.76
H	0.5	1.5	3.708	0.088	0.119	0.14
I	0.5	1.4	3.689		Missed Signal	
		Noise Section 274110				
J	100	219	3.586	0.001	--	--
K	1	2.0	3.546	0.111	-0.05	-0.05
L	1	2.2	3.595	0.095	0.09	-0.15
M	0.5	1.1	3.583	0.226	-0.03	-0.05
N	0.5	1.0	3.548		Missed Signal	

or smaller are the errors very large. That is, even when the signals can barely be detected by eye, the $\hat{m}_b$ algorithm is able to give a good estimate for the magnitude.

$\hat{m}_b$ for Actual Data

Bache, et al., (1980) present the $\hat{m}_b$ results for Eurasian explosions and earthquakes recorded at RKON and LASA. The epicentral distances are from 53 to 94 degrees and the events have PDE magnitudes from 4.8 to 6.0. The $\hat{m}_b$ algorithm appears to give excellent results, even when the signal is difficult to detect by eye so that time domain m_b measurements would probably not be attempted.

Description of the $\hat{M}_s$ Algorithm

The $\hat{M}_s$ algorithm is nearly the same as the $\hat{m}_b$ algorithm, except that the dispersion character of the surface wave signal of interest must be specified explicitly. The t_g-f_c plane (Figure 1) is first mapped into a t_g'-f_c plane where a signal with the expected dispersion appears to be nearly undispersed. The algorithm then follows the same steps as for $\hat{m}_b$.

$\hat{M}_s$ Algorithm Testing

In Figure 4 we show an example of the $\hat{M}_s$ calculation. A synthetic seismogram was added to a long period noise segment (from LASA), with the peak signal and noise amplitudes being equal. Comparing to the $\hat{M}_s$ calculation for the synthetic itself, the 20 second arrival time error is 4 seconds and the $\hat{M}_s$ error is 0.06. This and similar calculations done with a "perfect" estimate for the dispersion of the expected signal, show that the $\hat{M}_s$ algorithm works very well. Testing with real data where the prespecified dispersion is only approximately correct has not yet been done. However, we point out that the $\hat{M}_s$ calculation only requires an accurate identification of the MARS spectrum in a narrow period band, in this case near 20 seconds.

Conclusions

The automated magnitude algorithms appear to give consistent and convenient results, though much more extensive testing with real data is required. The $\hat{m}_b$ and $\hat{M}_s$ values may be viewed as a byproduct of signal processing with the MARS program, which is also configured for signal detection and earthquake/explosion discrimination. Thus, these values can easily be catalogued when processing data with MARS for other purposes.

REFERENCES

Bache, T. C. (1979), "$\hat{m}_b$, a Spectral Body Wave Magnitude (U)," Systems, Science and Software Report SSS-CR-79-3901 submitted to AFTAC/VSC, January, 99 pages.

Bache, T. C., S. M. Day and J. M. Savino (1979), "Automated Magnitude Measures, Earthquake Source Modeling, VFM Discriminant Testing and Summary of Current Research," Systems, Science and Software Quarterly Technical Report SSS-R-79-3933 submitted to AFTAC/VSC, February, 98 pages.

Bache, T. C., J. R. Murphy and S. M. Day (1980), "Regional Detection of Decoupled Explosions, Yield Estimation from Surface Waves, Two-Dimensional Source Effects, Three-Dimensional Earthquake Modeling and Automated Magnitude Measures," Systems, Science and Software Semi-Annual Technical Report SSS-R-80-4594 submitted to AFTAC/VSC, July.

Masso, J. F., C. B. Archambeau and J. M. Savino (1979), "Implementation, Testing and Specification of a Seismic Event Detection and Discrimination System," Systems, Science and Software Final Report SSS-R-79-3963 submitted to ACDA, March, 110 pages.

Savino, J. M., C. B. Archambeau and J. F. Masso (1980), "Discrimination Results from the Priority 2 Stations," Systems, Science and Software Technical Report SSS-R-80-4566 submitted to AFTAC/VSC, July, 130 pages.

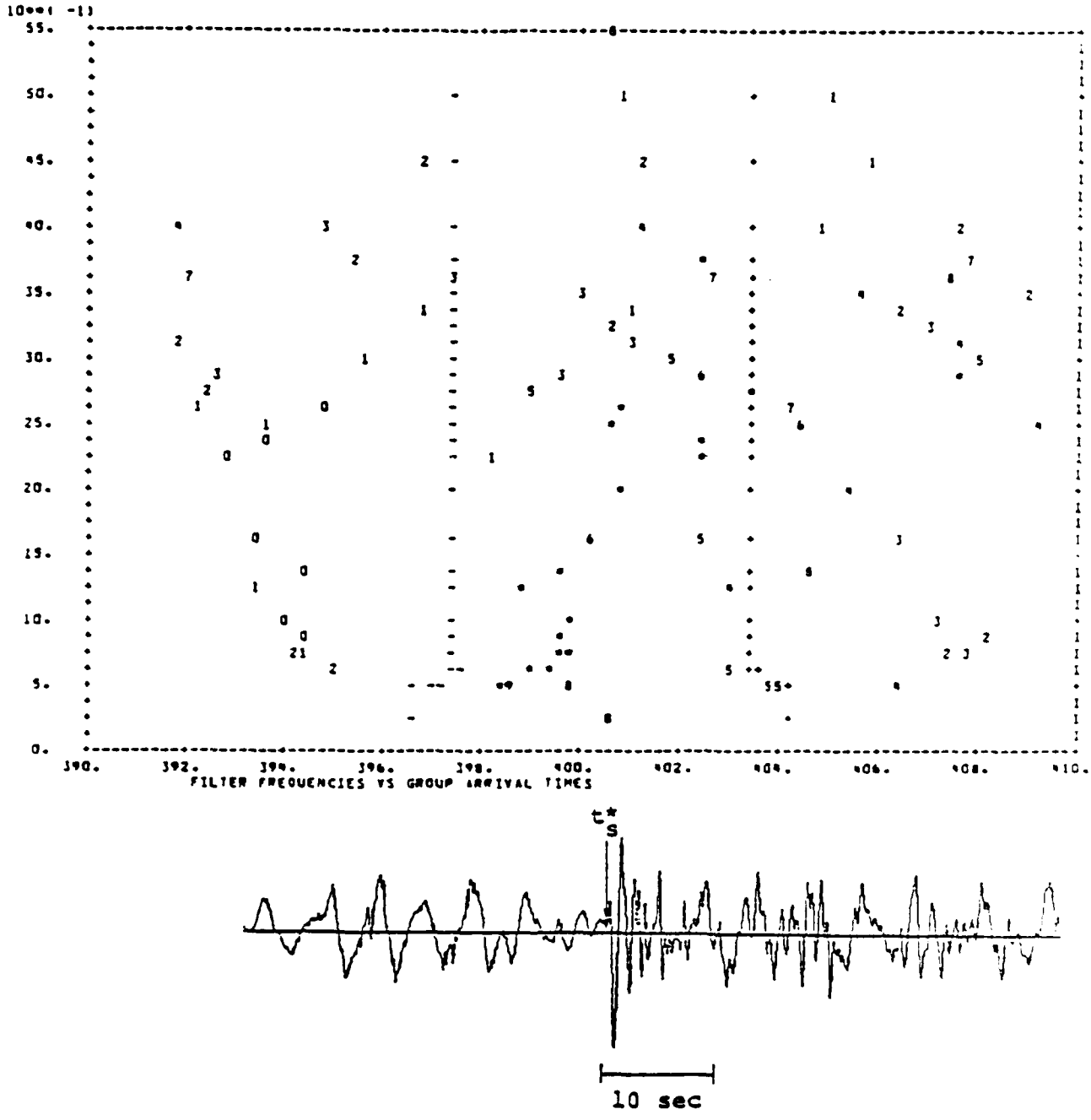

Figure 1. Bottom portion is a seismogram recorded at a station in Bluff, Alaska, from an event in the Kurils. The top half is a plot of filter center frequency versus group arrival time (sec). The t^*_s with arrow attached shows where the automated detection and first arrival algorithms picked the signal arrival time.

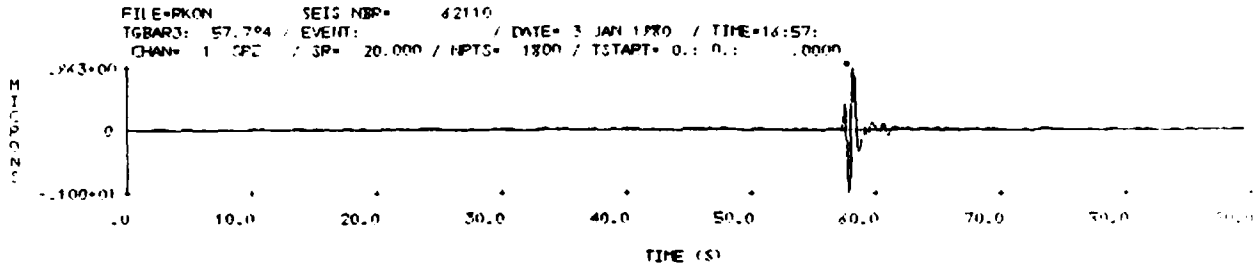

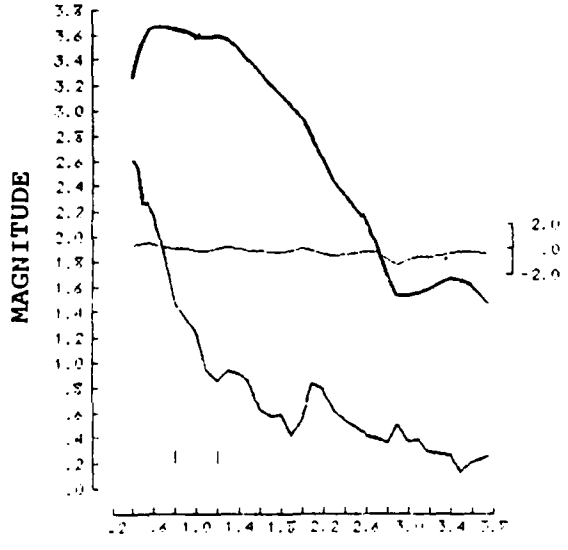

Figure 2. Calculation of $\hat{m}_b$ for a seismogram with peak synthetic/peak noise = 100. The seismogram is shown at the top with an asterisk denoting the signal arrival time $\underline{\underline{t}}_g$. The $\hat{m}_b$ calculation is shown graphically, with the heaviest line being log $(A_g^*$; $f_c)$ + B. The line of medium shade is the analogous magnitude for the noise. The light line is the t_g for each $A_g^{**}(f_c)$, with zero on the t_g scale (at right) being $\underline{\underline{t}}_g$. The $\hat{m}_b$ is computed at 1 Hz and is marked with an X. Printed above the graph are $\hat{m}_b$ (MB), the uncertainty in $\hat{m}_b$ imposed by the noise (±DMB), the noise magnitude at 1 Hz (MBNF), the mean signal/noise power over the frequency band from FLEFT to FRIGHT, and the B correction for the magnitude (BDEL).

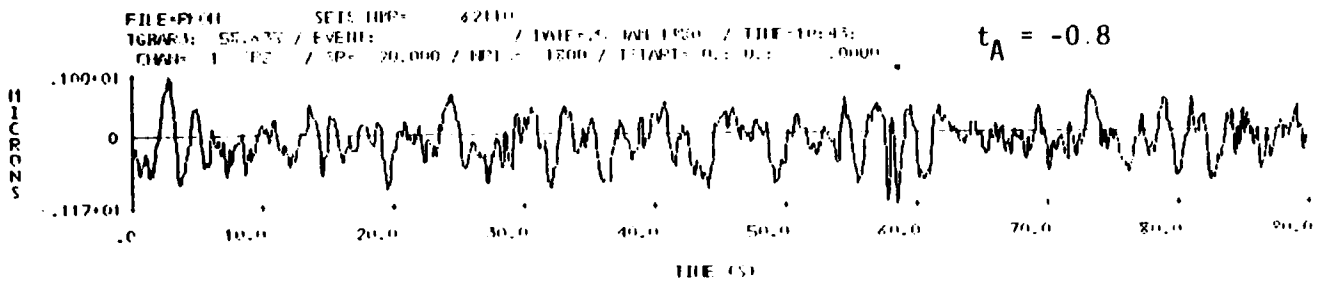

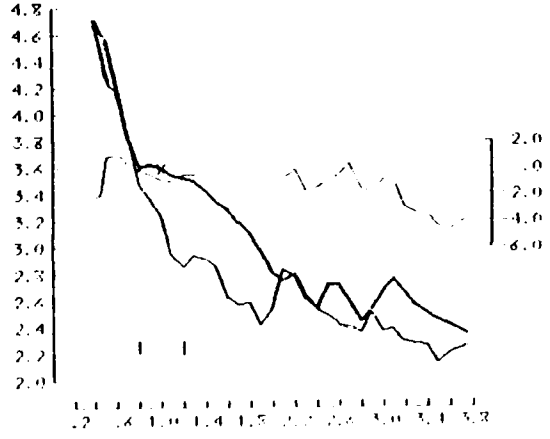

B

Peak S/N = 1

Figure 3. Test of the $\hat{m}_p$ algorithm with noise section 62110. The ratio of the peak amplitude of the synthetic to the peak noise amplitude is denoted by Peak S/N. The actual arrival time of the signal is the time of the asterisk plus t_A.

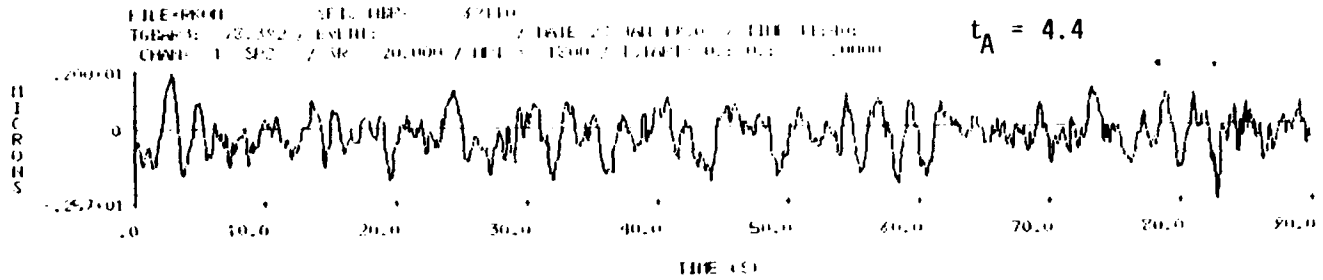

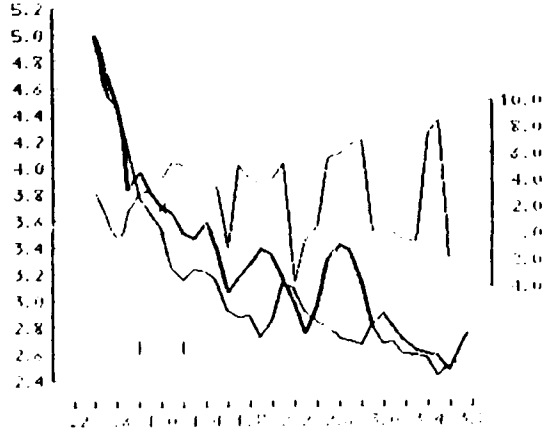

H

Peak S/N = 0.5

Figure 3 (continued)

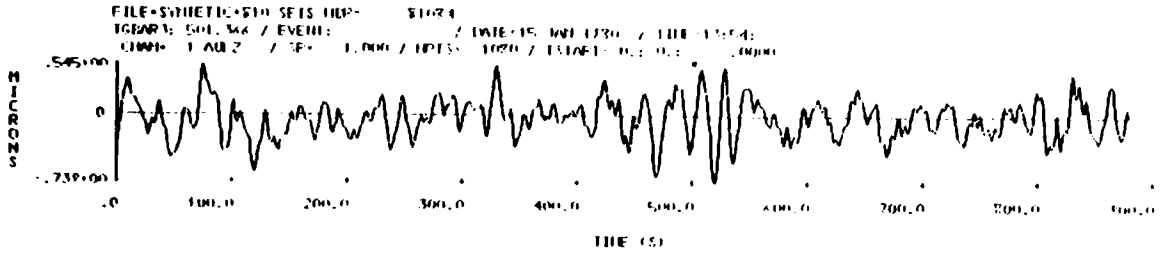

tg (20 sec) = 507.6

C

Peak S/N = 1

Figure 4. Calculation of $\hat{M}_S$ for a seismogram with peak synthetic/peak noise = 1. The reference dispersion was that of the synthetic seismogram.

Source Mechanisms - Moment Tensor Analysis

by

E.S. Husebye

Project VT/0702/B/PMP

Contractor: NTNF/NORSAR
Post Box 51
N-2007 Kjeller, Norway

Task 4: Physical Basis for Discriminants

Objective:

Obtain improved physical understanding of seismic source processes and attempt to incorporate relevant parameters into a discrimination scheme.

Accomplishments

This research task is still at an initial stage. Our research efforts so far have been tied to applying the moment-tensor approach for source characterization. Current status of the work is that initial attempts have been made of simultaneous inversion of the waveform data for the equivalent system of forces at the source and the hypocentral parameters. In the end this will hopefully lead to reliable estimates of temporal and spatial dimensions of the source region and thus also provide an improved understanding of the tectonic 'imprints' on the observed wavefield, which, of course, would constitute the very basis for seismic event discrimination. We remark that the major contributions to our research efforts here have rested with one of our visiting scientists, Dr. D. Doornbos of Utrecht University, The Netherlands, who will permanently join the NORSAR staff as of 1 September 1980.

3-Dimensional Mapping of Upper Mantle Heterogeneities

by

E.S. Husebye and J. Hovland

Project VT/0702/B/PMP

Contractor: NTNF/NORSAR
Post Box 51
N-2007 Kjeller, Norway

Task 3: Lateral inhomogeneities in the lithosphere

Objective

Use the travel time residuals for the global seismograph network, as reported by the International Seismological Centre (ISC), to estimate source and receiver corrections for this network. Based on this, estimate the extent of lateral heterogeneities in the upper mantle.

Accomplishments

Most of our research efforts have been tied to adapting the Aki, Christoffersson and Husebye (1977) inversion techniques to networks of continental size and at the same time demonstrate that this approach indeed gives rather detailed information on lithospheric tectonics. In this regard we acknowledge intimate cooperation with Dr. D. Gubbins of Cambridge University, U.K. In the following we describe briefly the work accomplished so far and also comment on work which remains.

Inversion technique for P residuals for continental networks

The method used for analysis of P residuals from subset of ISC-reporting stations is essentially an adaptation of the ACH method to arrays of continental dimensions. Major elements in the modified inversion approach is ray tracing in 3-dim. media and a grid or node representation of velocity (slowness) distribution in the upper mantle and associated cubic spline interpolation. The velocity anomaly representation is tied to the

mentioned node representation and furthermore the associated program has options for computing standard errors, resolution and variance improvements.

Applicability of method

The Central Europe seismograph network (see Fig. 1) was selected for testing the above inversion scheme. The data used were P-time residuals for teleseismic events as listed in the ISC-bulletins for 1971-1974. The events were initially grouped in 10 deg azimuth/distance areas, out of which the one or two best in the sense of many and consistent observations were selected. The above screening procedure left us with 167 events and a total of 5807 individual observations. The thickness of the anomalous zone was set at 600 km. The grid adopted had 4 (in depth) x7x7 knots. Each interpolation coefficient affects to some extent the slowness at all depths and to a horizontal distance of 4 times the knot spacing. The slowness in the depth range 0-100 km is dominated by the values at the top level of knots, for 100-300 km the second level, 300-500 km the third level and 500-600 km by the bottom level. The overall reduction in residuals achieved by our model (Fig. 3) is 11%. This is less than for NORSAR, which is closer to a 60% reduction. The total time variance reductions are respectively around 20% and 70%. The difference reflects a difference in the quality of the data and the larger area (coarser grid) in the Central European inversion. However, the RMS residual explained by the laterally varying models is the same for NORSAR as for the present model and is about 0.2 s.

Results

In Figs. 2 and 3 the estimated resolution and standard errors for the velocity perturbations associated with the knots of all 4 levels are displayed. The following comments are appropriate.

Level 1 (Fig. 2a) is representative of the uppermost 100 km and corresponds roughly to the lithosphere. The low velocity in the southern North Sea appears to be a real phenomenon required by the observations. However, its

apparent extension northeastwards is poorly resolved by data and thus should be given very little weight. There is a broad area of high velocity centered over Eastern Germany and comprising the Bohemian Massif and the eastern part of the Ardennes. The whole of the Paris Basin is low velocity while another high velocity region stretches from the Armorican Massif in Brittany to the Central Massif in Southern France. The Po Plain-N. Adriatic Sea exhibit a marked velocity high, but the area is poorly resolved which may reflect a lack of stations in Switzerland and N. Italy.

Levels 2 and 3 show features that are broadly similar to each other (Figs. 3 b&c), though the anomalies are somewhat smaller than for levels 1 or 4. Resolution is good except near the corners of the region (Fig. 2 b&c). In level 2 the dominant feature is a velocity high covering the Paris Basin and SE-France and a velocity low over most of the German-Polish Depression. As before, parts of the Pannonian Basin and (eastern) Pyrenees remain low, while the N. Adriatic Sea now is definitely high. The Paris Basin high of level 2 becomes more dominant in level 3, encompassing also the Pannonian Basin and the Appennines. Further north the German-Polish Depression area of velocity low appears to have been shifted slightly westward. Also Brittany and adjacent areas remain mostly low.

The anomalies in level 4 (Fig. 3d) are with few exceptions well resolved because there are many intersecting ray paths contributing to the values at most of the knots. The picture is very different from that in the shallower levels with pronounced highs in the German-Polish Depression, Sudetes and Southern France, and similar pronounced lows in the Paris Basin and Appeninnes-Sardinia area.

Interpretation

Level 1: The velocity anomaly map for the uppermost 100 km (Fig. 3a) shows a remarkable correlation with both available heat flow data (Fig. 4) and the tectonic features of Central Europe (outlined in Fig. 2). The most prominent feature is the large high in norhtern Germany and Poland. This region coincides with low heat flow and the Bohemian Massif and the Ardennes which are Hercynian folded units. Some rough calculations, assuming constant geotherms over the uppermost 100 km, give that for

each 10 $mW \cdot s^{-2}$ low in the heat flux the corresponding velocity anomaly would be about 1% fast. The correlation with heat flow is good. There are very few stations in the Paris Basin and so it is unlikely that the time delays are caused by the sediments, which are several kilometers thick in places, because no ray paths pass through them. The sharp low in the southern North Sea also coincides with high heat flow and besides the south end of the Central Graben. Another possible explanation for high velocity anomalies is that the rocks comprising the mentioned massifs have a higher velocity than elsewhere. An anomaly of 5% over 100 km produces a travel time anomaly of half a second. However, the Hercynian granites are probably only a few kilometers thick and thus cannot account for such a large travel time residual.

Levels 2 and 3: The anomalies in these two levels are very similar to each other and are smaller than those in level 1 and 4 (see below). This finding agrees with the general view that the material below the lithosphere lid is more homogeneous because of its lower strength. The broad high ridge trending NW-SE across the continent cannot be explained in terms of known thermal or compositional anomalies and is plausibly accounted for by variations in the depth to the phase change at about 400 km.

Level 4: The anomalies in level 4 are different from those in 2 and 3 and are larger. The resolution is good, and the anomalies may be related to variations in the depth of the 650 km discontinuity, where the P wave velocity increases by 10% from 10.2 to 11.2 $km \cdot s^{-1}$. For 3% anomalies in a 100 km thick layer this gives a depth variation of 30 km or so for the phase boundary.

Final remarks

We have shown that it is possible to use ISC-reported travel times to obtain meaningful models of lateral variations in P wave velocity in the mantle beneath Europe. In particular, the correlation between the obtained P wave velocity anomalies exhibits a remarkably good correlation with dominant tectonic features and heat flow data. In a larger perspective, the latter effects may influence profoundly the propagation efficiency of Lg phases as these waves sample various tectonic regimes more effectively than teleseismic P waves do.

Remaining work comprises studies similar to that described above for southeast Europe and parts of Central Asia. Furthermore, the ray-tracing aspects of the above inversion procedure will be expanded so as to include amplitude calculations. Studies on 2-dimensional receiver and source time and magnitude corrections have also progressed satisfactorily - current work is related to creating special disk files for ISC bulletin data for the period 1964-1977.

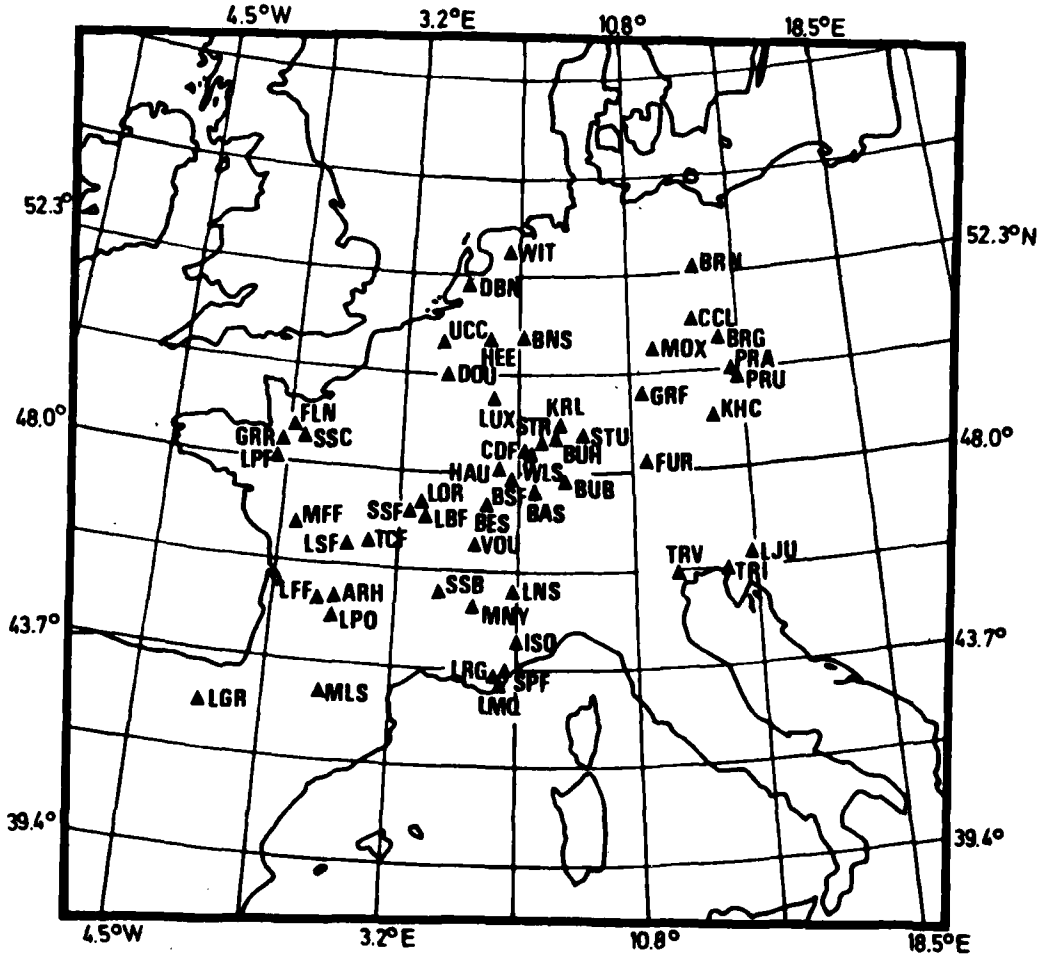

Fig. 1 Central European seismograph station network used in analysis. The intersections of the latitude/longitude grid system correspond to the nodes in the time residual inversion described in section 2.

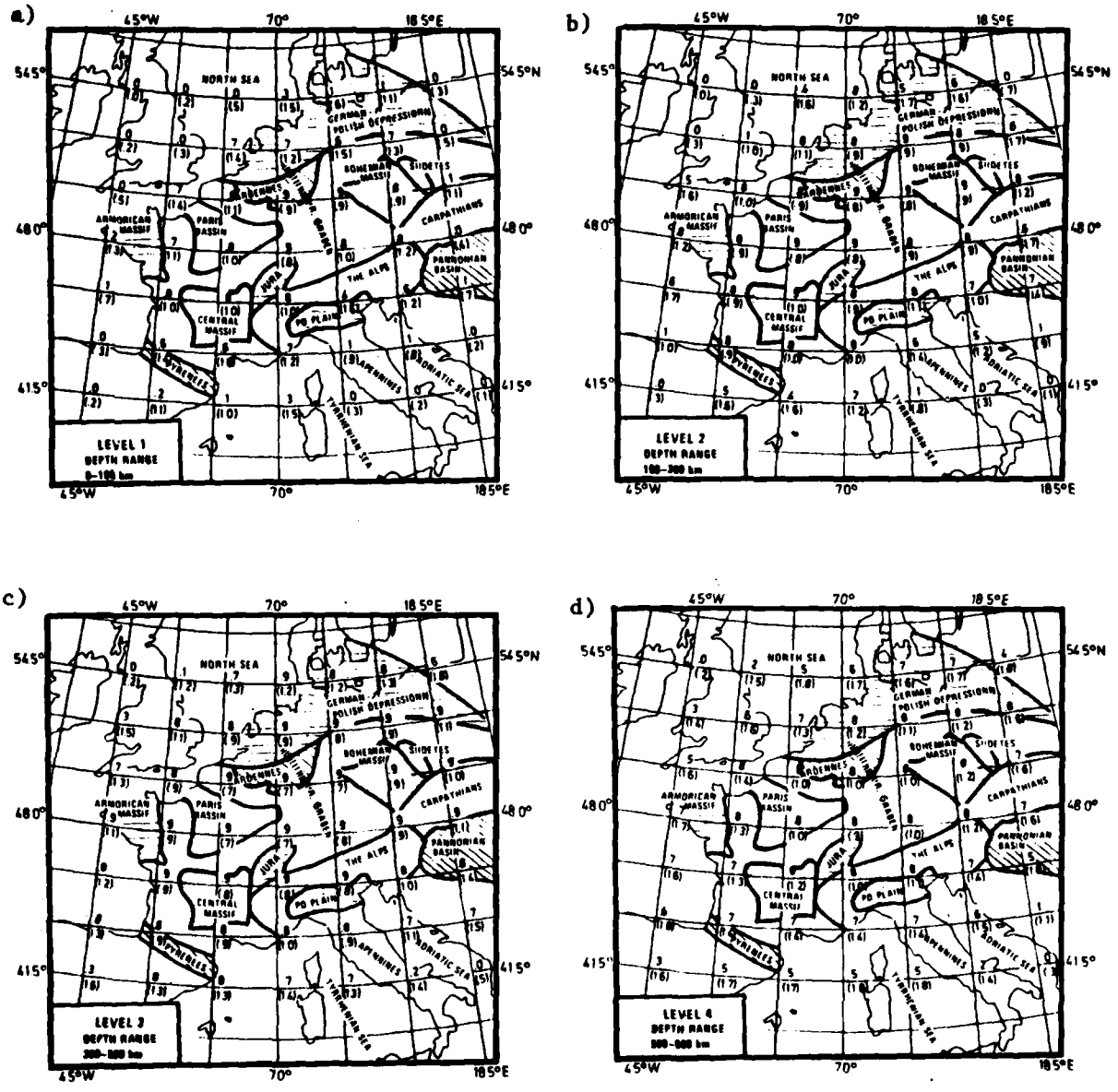

Fig. 2a Resolution and standard error (in brackets) estimates for all level 1 nodes. Geographical locations referred to in the text are also indicated.

2b. Resolution and standard error (in brackets) estimates for all level 2 nodes.

2c. Resolution and standard error (in brackets) estimates for all level 3 nodes.

2d. Resolution and standard error (in brackets) estimates for all level 4 nodes.

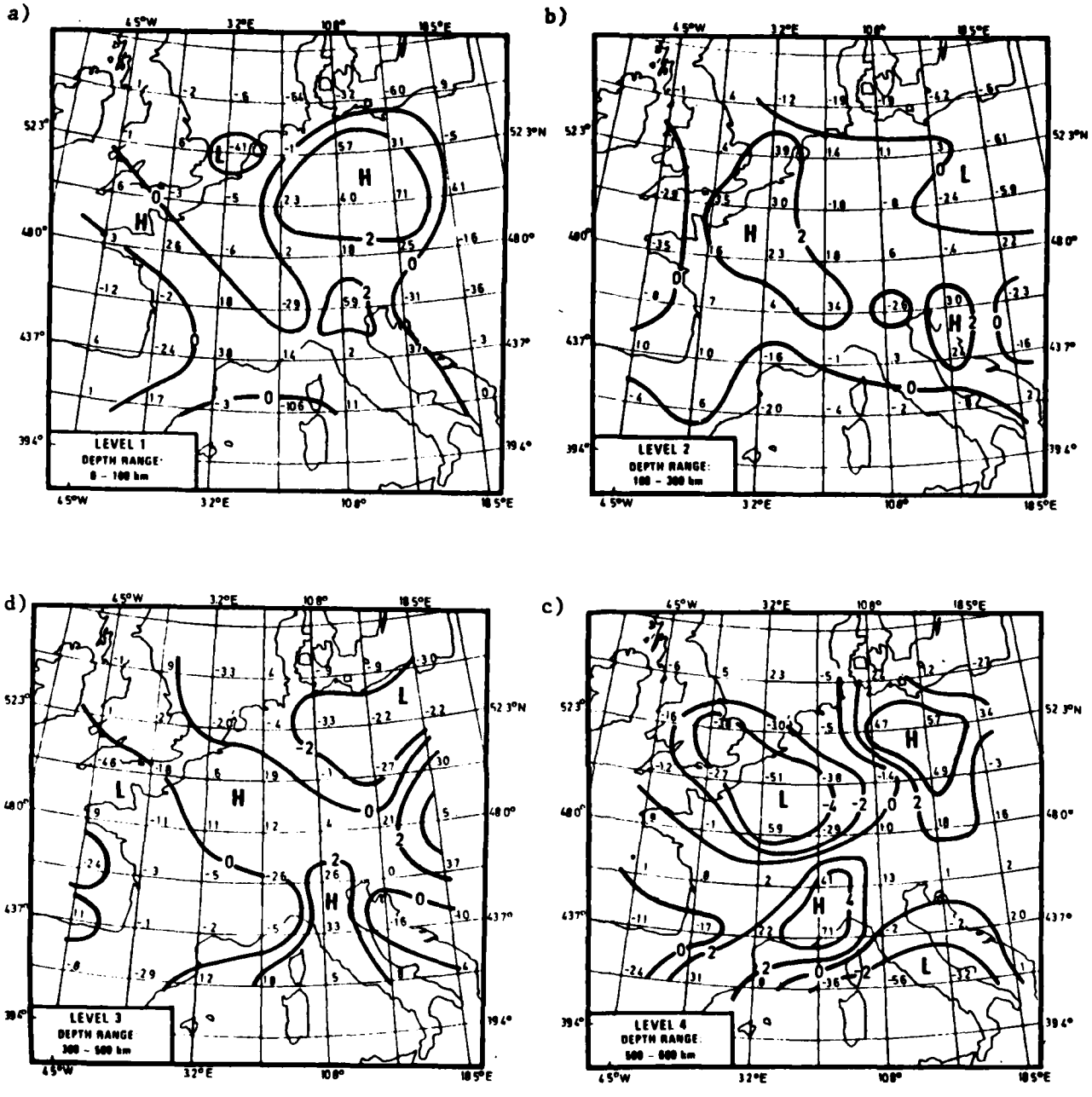

Fig. 3a Velocity perturbations (in per cent) for level 1. Areas of high and low velocities are indicated by capital letters H and L. Resolution and standard errors for all nodes are displayed in Fig. 2.

3b. Velocity perturbations (in per cent) for level 2. Otherwise caption as for Fig. 3a.

3c. Velocity perturbations (in per cent) for level 3. Otherwise caption as for Fig. 3a.

3d. Velocity perturbations (in per cent) for level 4. Otherwise caption as for Fig. 3a.

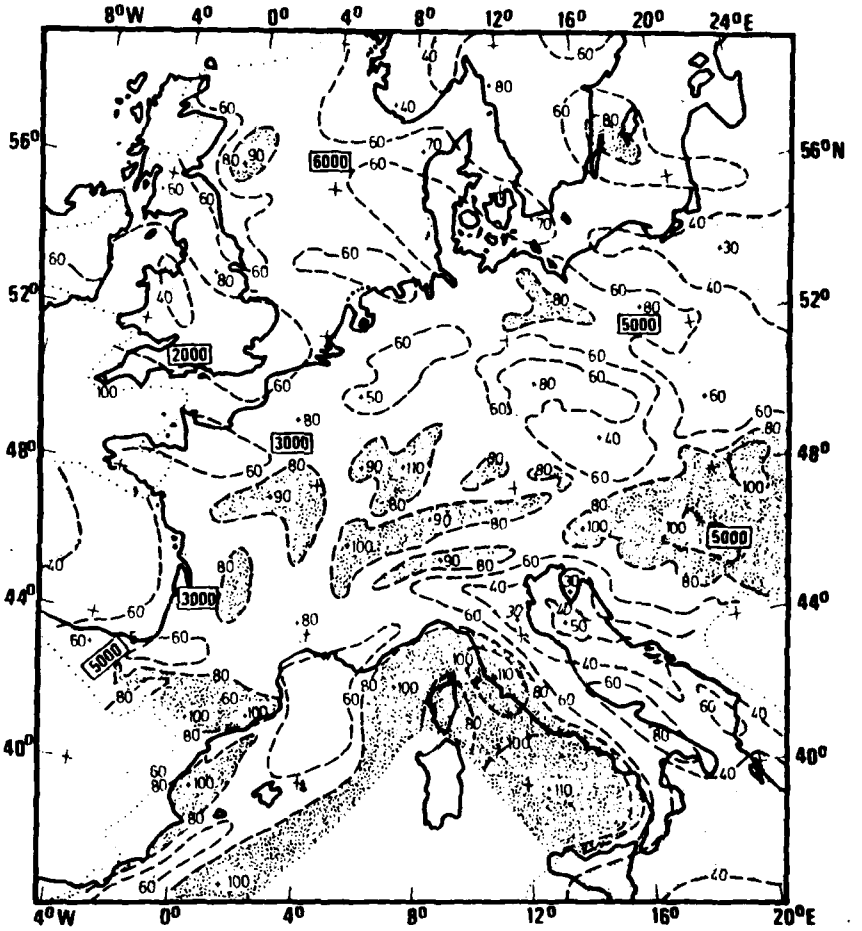

Fig. 4 Heat flow map for Central Europe (in mWm^{-2}). Number in brackets indicates upper bounds of sediment thicknesses (in meters) in basin areas.

SEISMIC INSTRUMENTATION PROGRAM

GEORGE KRAUS

Project VT/0703 Contractor: Teledyne Geotech

Task 4.1 Special Data Collection System (SDCS)

Objective

This task is a continuation of efforts initiated under the Vela program to record seismic data from underground nuclear explosions and other seismic events of special interest to ARPA and AFTAC. These data are used to evaluate the signal characteristics of explosive sources and to study the general propagation characteristics of seismic signals. Specific objectives of this project in FY80 are to deploy and operate two borehole seismograph systems that simulate the response characteristics of the National Seismic Station (NSS). The two seismographs that will be used in the evaluation are a Model 36000 instrument now being operated by Southern Methodist University (SMU) at a site near McKinney, Texas, and a similar Model 36000 seismometer that is to be installed by SMU at a very quiet site near Lajitas, Texas, in September of this year. Data from the remote sites will be digitally recorded and provided to the Seismic Data Analysis Center (SDAC) for evaluation of the NSS response characteristics in the short-period and mid-period bands. Nine remaining portable SDCS systems will be maintained in storage ready for deployment as required to support other measurement programs.

Accomplishments

The designs required to simulate the NSS Model II instrument response have been completed and materials have been ordered to fabricate this special circuitry. The standard Voltage Controlled Oscillator's (VCO's) and discriminators required to multiplex broad band data from three channels at each of two remote sites have been received.

A leased telephone circuit has been installed and checked out between the SMU long-period borehole seismometer installation near McKinney, Texas, and a Bell Telephone system exchange in Dallas, Texas. This circuit remains to be checked out between the General Telephone and Electric Co. (GTE) interchange with the Bell system and our plant in Garland, Texas.

Digital recording of the NSS short-period and mid-period response from each of the three broad band data channels from this instrument will commence as soon as the leased data circuit is installed. Two of the

Accomplishments (cont.)

Model DDS-1103 digital data acquisition and recording systems in the SDCS inventory have been modified to record the MCK site data sampled at 40 samples per second on the short-period channels and 4 samples per second on the mid-period channels. Figure 1 shows a simplified block diagram of the data acquisition and recording system for a typical site.

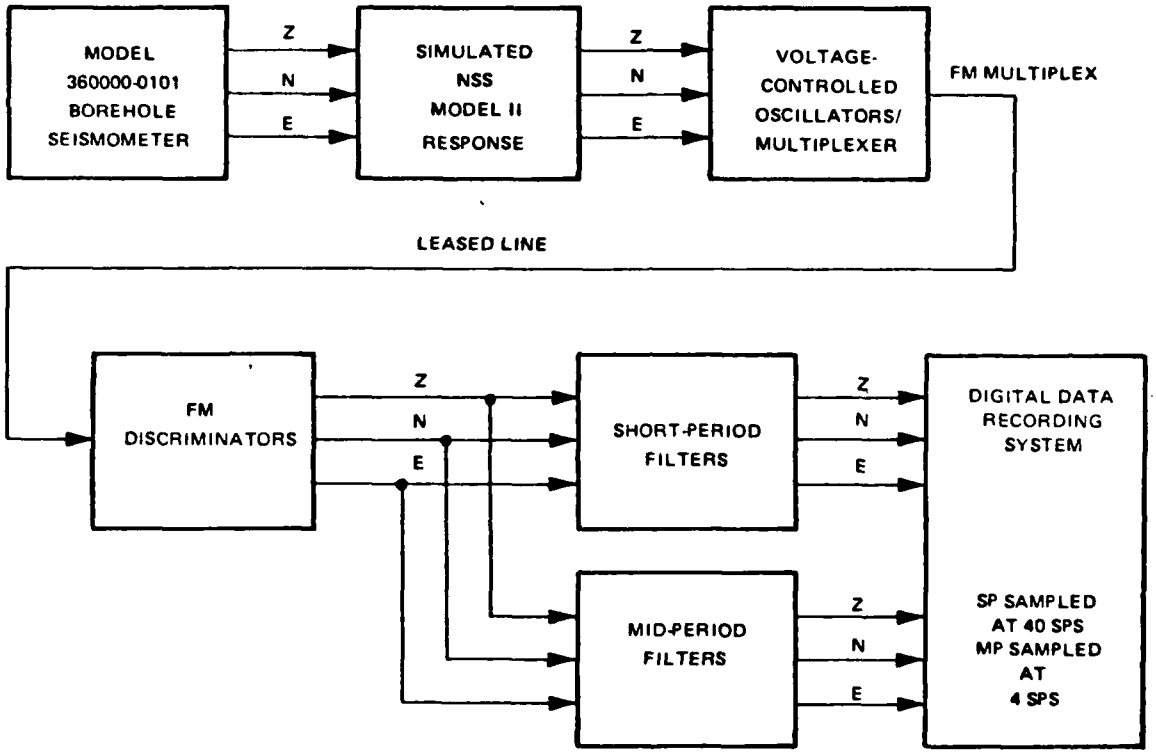

FIGURE 1. BLOCK DIAGRAM OF THE DATA ACQUISITION AND RECORDING SYSTEM FOR A TYPICAL REMOTE SITE

G 11418

REVIEW OF SEISMIC EVENT IDENTIFICATION

D. W. Rivers

Project VT/0707 Contractor: Teledyne Geotech

Task 4.1 Review of Seismic Event Identification

Objective

A comprehensive review is to be performed of the approaches to seismic event identification. This review will concentrate on evaluating the methods employed and the results obtained by the three contractors which participated in the VELA Seismological Center discrimination experiment.

Accomplishments

In 1979 the VELA Seismological Center concluded an experiment in seismic discrimination which was aimed at overcoming certain limitations of previous investigations. A data base consisting of digital seismograms recorded by seismic stations (Table 1) for 133 Eurasian events (Table 2 and Figure 1), including twenty-seven explosions, was processed. The analysis of this data base, which encompassed events with a wide range of magnitudes and in diverse tectonic environments, simulated the routine analysis which would be performed in the context of global monitoring of seismic events on a day-to-day operation basis.

The three contractors participating in the experiment analyzed a common data base of digital records, but each contractor made a different set of measurements on the signals, so three separate data bases of discriminants were created. Each contractor then applied a different statistical test to their own discriminant data base in order to classify the 133 events as earthquakes or explosions. Systems, Science and Software (S^3) passed each short-period P-wave signal through a comb of forty narrow bandpass filters. A single discriminant value was then assigned to each signal, namely the difference in m_b measured in a high-frequency and in a low-frequency passband. Each signal was classified as being explosion-like or earthquake-like on the basis of this m_b difference, and then every event was classified by averaging the classifications determined at each station. ENSCO also measured m_b by means of bandpass filtering, but the filters were of a greater bandwidth than those used by S^3. In addition, ENSCO made analogous magnitude measurements on certain seismic phases other than the P wave, and they also measured certain other time- and frequency-domain parameters (Table 3). Discriminants were formed from the differences between various magnitudes, and the discriminant data base was created by applying Ringdal's (1976) maximum likelihood estimator to the values measured at every station. The multivariate statistical technique of cluster analysis was applied to the network-averaged discriminants in order to assign each event to a cluster of either earthquakes or explosions. The approach employed by Teledyne Geotech was similar, except that magnitudes were measured in the frequency domain (i.e., directly upon the spectra, rather than on filtered traces; cf. Table 4) and the statistical technique used for discrimination was stepwise multivariate discriminant analysis.

Although it is tempting simply to compare the results obtained by the three contractors in order to determine the "best" techniques, this simple approach to evaluating the discrimination experiment is inadequate in several respects.

Task 4.1 Review of Seismic Event Identification

Accomplishments continued

For one thing, questions may be raised about the validity of certain procedures which were used in the compilation of the discriminant data bases; those questions ought to be resolved before any evaluation is attempted of the information contained within those data bases. Another point which must be considered is that there is a skewness between the earthquake and explosion populations in Table 2: the explosions are, on the whole, larger events, and the earthquakes and explosions usually occurred within different subregions of Eurasia. In light of these difficulties in evaluating the results of the experiment, we have undertaken a review of the methods employed and results obtained by each contractor, and we have identified certain items of procedure which we feel to be in need of detailed quantitative investigation. The procedural items which we have found to need further study are:

1) Seismogram editing. ENSCO and S^3 employed automation extensively in the process of editing the raw data. There are known to be in the data base many instances of misleading seismogram start times, miscalibrated gains, and mixed events; it is possible that the automatic editors, especially of long-period data, were vulnerable to errors introduced by these flaws in the data base.

2) Magnitude calculations for each signal. Conventional amplitude-distance relations, determined from unfiltered time-domain data, may be inapplicable to the spectral amplitudes and to the filtered amplitudes measured in this experiment.

3) Magnitude calculations for each event. ENSCO found that Ringdal's (1976) magnitude estimator is susceptible to systematic error at low magnitudes, and they modifed the algorithm accordingly. The modification should be subjected to more extensive testing.

4) Use of single-station and univariate discrimination. Certain previous investigations have found that discrimination should be performed on a network, rather than a station-by-station basis, and that multivariate discrimination is more powerful than the use of any single variable. The results of these investigations will be contrasted with the S^3 methodology.

5) Magnitude scaling of discriminants. ENSCO did not use the same discriminants for all events, but instead they used discriminants which varied somewhat in form as a function of event magnitude. Problems may arise in performing this scaling on account of a skewness in the magnitudes of the 133 events; the explosions were, on the average, higher magnitude events than were the earthquakes.

In order to investigate these five areas of methodology, a composite data base is being created from the measurements made by the three contractors. This data base will encompass both the final discriminant values and the raw data measurements. The compilation of this data base will evaluate the process of seismogram editing, and then the data base itself will be used in quantitative

Task 4.1 Review of Seismic Event Identification

Accomplishments continued

investigations of the other four procedural items.

A review of the results obtained by each contractor has also shown the need for three further investigations not of methodology but rather of interpretation. Investigations will be made of:

1) Anelastic attenuation of P-waves. The spectral ratios of high-to low-frequency P-wave amplitudes may be strongly affected by high-frequency attenuation, a path-dependent effect which must be distinguished from the amplitudes of the true source spectra.

2) Regionalization of discriminants. On account of differences in propagation path effects, such as attenuation, and on account of real differences in earthquake phenomenology in different tectonic environments, the earthquake/explosion discriminant may not have the same exact form in all subregions of Eurasia; this possibility must be considered in light of the fact that most of the explosions in the data base occurred in relatively aseismic regions.

3) Confidence limits. An evaluation must be made of the cumulative error in all stages of the measurement and reduction of data and of the computation of the event classification, so that a quantitative estimate can be made of the uncertainty in the identification.

In addition to these aspects of the VSC discrimination experiment which have been determined to need evaluation, certain other discrimination techniques are being evaluated by means of a literature review. Some of these additional discriminants, such as the third moment of the frequency, closely resemble those which were used in the experiment, but others, such as autoregressive models of the signals, have no close analogs in Tables 3 and 4.

Reference

Ringdal, F. (1976). Maximum likelihood estimation of seismic event magnitude from network data, Bull. Seism. Soc. Am., 66, 789-802.

TABLE 1

Stations Used in the VSC Discrimination Experiment

10 Seismic Research Observatories:

AMNO, ANTO, BOCO, CHTO, GUMO, MAIO, NWAO, SHIO, SNZO, TATO

5 Alternate Seismic Research Observatories:

CTAO, KAAO, KONO, MAJO, ZOBO

4 Large Arrays:

ILPA, KSRS, LASA, NORSAR

2 Special Data Collection Stations:

HN-ME, RK-ON

AFTAC Alaskan Stations

Atomic Energy Detection System Stations

TABLE 2 : EVENTS INCLUDED IN THE DISCRIMINATION EXPERIMENT

EVENT	DATE	ORIGIN TIME	LATITUDE	LONGITUDE
1	26 JUL 77	16 59 57.6	69.532 N	90.583 E
3	1 NOV 77	3 54 26.0	55.436 N	130.545 E
4	1 NOV 77	17 56 42.7	36.581 N	68.745 E
6	4 NOV 77	10 51 40.0	23.000 N	101.000 E
7	4 NOV 77	23 54 44.7	30.700 N	81.279 E
8	5 NOV 77	2 9 38.0	42.900 N	45.300 E
9	5 NOV 77	4 6 58.5	36.635 N	69.128 E
10	6 NOV 77	13 31 41.1	36.313 N	71.121 E
14	30 JUL 77	1 56 58.0	49.777 N	78.163 E
16	10 AUG 77	21 59 58.7	50.923 N	110.761 E
17	17 AUG 77	4 26 57.7	49.814 N	78.151 E
18	20 AUG 77	21 59 58.7	64.223 N	99.577 E
19	1 SEP 77	2 59 57.5	73.376 N	54.581 E
20	5 SEP 77	3 2 57.8	50.092 N	78.961 E
21	10 SEP 77	16 0 3.3	57.294 N	106.240 E
22	30 SEP 77	6 59 55.6	47.800 N	48.145 E
23	10 NOV 77	4 57 46.0	37.100 N	71.800 E
24	10 NOV 77	9 22 58.0	33.000 N	89.000 E
25	12 NOV 77	5 9 16.0	38.000 N	91.000 E
26	12 NOV 77	12 27 5.3	35.757 N	71.331 E
27	13 NOV 77	21 2 29.3	26.471 N	93.114 E
28	15 NOV 77	20 20 46.6	38.172 N	74.158 E
29	17 NOV 77	4 23 54.0	28.000 N	90.000 E
30	18 NOV 77	5 20 11.3	32.693 N	88.388 E
31	18 NOV 77	5 33 19.7	32.640 N	88.431 E
32	18 NOV 77	11 27 27.6	32.655 N	88.469 E
33	9 OCT 77	11 0 0.3	73.626 N	53.158 E
34	18 NOV 77	15 10 41.8	32.719 N	88.316 E
35	18 NOV 77	17 23 24.4	32.610 N	88.315 E
36	16 OCT 77	20 3 35.0	48.400 N	152.900 E
37	18 NOV 77	21 55 39.7	60.081 N	143.373 E
38	16 OCT 77	15 2 48.8	36.466 N	71.034 E
39	18 NOV 77	23 12 49.5	32.698 N	88.422 E
41	13 OCT 77	20 38 52.1	37.301 N	78.058 E
45	19 NOV 77	11 51 14.2	36.450 N	71.279 E
46	20 NOV 77	1 41 23.0	30.600 N	93.300 E
47	16 OCT 77	21 5 37.3	49.419 N	155.431 E
48	19 OCT 77	5 1 57.0	36.440 N	71.273 E
49	19 OCT 77	21 20 41.6	49.349 N	155.632 E
50	20 OCT 77	8 18 7.0	56.426 N	164.133 E
53	29 OCT 77	3 6 57.7	49.841 N	78.174 E
55	26 OCT 77	5 38 52.2	49.000 N	155.800 E
56	26 OCT 77	7 11 31.3	46.400 N	153.500 E
57	26 OCT 77	13 14 30.9	51.500 N	153.400 E
58	27 OCT 77	7 20 28.9	53.500 N	160.000 E
59	28 OCT 77	21 15 1.9	39.569 N	73.406 E
60	29 OCT 77	4 14 56.5	47.000 N	152.300 E
61	29 OCT 77	6 26 40.6	40.283 N	63.455 E
62	29 OCT 77	10 33 56.7	47.137 N	153.158 E
63	30 OCT 77	21 38 38.5	45.528 N	145.988 E
64	31 OCT 77	9 40 38.5	55.962 N	162.786 E
65	20 NOV 77	11 1 22.0	56.800 N	108.500 E
66	20 NOV 77	18 55 28.0	39.900 N	73.900 E
67	20 NOV 77	20 57 33.1	37.419 N	71.824 E
68	20 NOV 77	23 40 35.9	32.395 N	87.765 E
69	21 NOV 77	19 43 33.7	36.663 N	71.206 E
70	22 NOV 77	0 8 3.7	36.257 N	70.729 E
72	22 NOV 77	6 56 14.2	36.478 N	71.236 E
73	22 NOV 77	11 33 45.0	43.000 N	89.000 E
74	22 NOV 77	19 16 12.0	40.000 N	75.000 E
75	23 NOV 77	10 28 7.0	34.000 N	83.000 E
76	26 NOV 77	15 44 41.0	37.000 N	71.000 E
77	26 NOV 77	22 46 52.2	39.465 N	117.938 E
78	27 NOV 77	2 9 7.0	28.000 N	90.000 E
79	27 NOV 77	3 57 0.0	50.000 N	79.000 E
80	28 NOV 77	9 2 26.0	43.200 N	47.600 E
81	30 NOV 77	4 6 57.5	49.957 N	78.931 E

TABLE 2 (CONTINUED)

EVENT	DATE	ORIGIN TIME	LATITUDE	LONGITUDE
143	2 DEC 77	12 57 10.7	52.929 N	159.714 E
144	2 DEC 77	16 15 44.9	44.558 N	146.459 E
145	3 DEC 77	17 6 21.9	41.932 N	131.124 E
146	4 DEC 77	4 13 47.0	56.200 N	163.100 E
147	4 DEC 77	11 39 2.8	48.250 N	146.590 E
148	5 DEC 77	23 37 37.1	55.669 N	162.211 E
149	6 DEC 77	10 52 53.5	41.425 N	69.730 E
150	7 DEC 77	2 3 37.0	41.000 N	72.000 E
151	7 DEC 77	16 19 33.9	35.651 N	94.518 E
152	8 DEC 77	2 2 54.0	52.900 N	89.700 E
153	8 DEC 77	6 55 20.0	41.000 N	72.000 E
154	8 DEC 77	13 57 4.5	50.425 N	149.808 E
155	8 DEC 77	23 37 22.5	36.263 N	70.574 E
156	9 DEC 77	4 23 36.0	54.400 N	160.600 E
157	10 DEC 77	21 58 51.3	51.379 N	156.590 E
158	12 DEC 77	11 6 42.0	51.400 N	157.500 E
159	13 DEC 77	16 58 59.0	35.400 N	88.400 E
160	13 DEC 77	11 34 20.0	42.300 N	133.200 E
161	15 DEC 77	15 15 42.3	36.545 N	71.150 E
162	15 DEC 77	15 7 51.8	43.241 N	45.168 E
163	15 DEC 77	15 23 30.7	43.643 N	45.372 E
164	16 DEC 77	7 11 41.6	43.233 N	146.763 E
165	16 DEC 77	9 8 59.7	51.630 N	159.460 E
166	16 DEC 77	10 15 27.5	33.305 N	97.560 E
167	16 DEC 77	12 55 14.2	36.891 N	59.760 E
168	16 DEC 77	23 17 17.7	43.059 N	47.082 E
169	18 DEC 77	23 57 33.3	55.278 N	160.561 E
170	18 DEC 77	16 47 17.1	39.865 N	77.334 E
171	18 DEC 77	19 9 15.7	51.049 N	157.831 E
172	18 DEC 77	20 43 5.9	39.733 N	77.696 E
173	19 DEC 77	1 12 25.9	39.764 N	77.714 E
175	20 DEC 77	1 27 38.9	39.794 N	69.331 E
176	20 DEC 77	20 52 10.0	55.200 N	158.200 E
177	21 DEC 77	8 30 46.3	41.952 N	47.915 E
178	21 DEC 77	16 39 33.0	52.929 N	159.804 E
179	21 DEC 77	20 17 15.6	36.198 N	68.667 E
180	21 DEC 77	20 40 55.0	52.000 N	159.500 E
181	22 DEC 77	1 45 55.1	52.956 N	159.902 E
182	22 DEC 77	19 34 5.0	53.100 N	163.400 E
184	23 DEC 77	7 31 44.2	44.618 N	32.801 E
185	23 DEC 77	9 38 54.1	39.599 N	77.449 E
186	24 DEC 77	1 27 52.0	51.200 N	156.900 E
187	25 DEC 77	3 33 37.0	50.000 N	91.000 E
188	25 DEC 77	17 38 42.0	40.000 N	69.700 E
189	26 DEC 77	5 15 57.2	44.881 N	78.141 E
190	26 DEC 77	15 21.3	39.917 N	71.967 E
191	26 DEC 77	2 37 34.3	33.700 N	90.900 E
192	27 DEC 77	10 11 0.0	28.000 N	90.000 E
193	28 DEC 77	12 31 0.0	54.700 N	161.500 E
194	28 DEC 77	1 10 44.0	56.000 N	162.000 E
195	31 DEC 77	2 38.6	39.181 N	91.100 E
266	29 DEC 76	3 36.7	50.050 N	77.337 E
266	29 DEC 77	5 57 0.0	49.790 N	78.149 E
267	19 DEC 78	0.0	50.000 N	78.000 E
268	11 DEC 78	5 57 0.0	50.000 N	79.000 E
269	28 DEC 78	7 0.0	50.000 N	78.000 E
270	18 DEC 78	0.0	64.000 N	125.000 E
271	24 DEC 78	0.0	66.000 N	112.000 E
272	29 DEC 78	37 0.0	50.000 N	78.000 E
273	5 DEC 78	32 0.0	43.000 N	89.000 E
274	21 DEC 78	1 20 9.0	46.000 N	86.000 E
275	25 DEC 78	27 0.0	47.500 N	87.500 E
276	13 DEC 78	56 0.0	50.000 N	79.000 E
277	19 DEC 78	55 57.0	49.799 N	78.196 E
278	23 DEC 78	2 32 50.0	49.856 N	78.007 E
279	23 DEC 78	2 32 50.0	49.800 N	78.100 E

Figure 1. Overall view.
Location of events used in the discrimination experiment.

TABLE 3

RAW SIGNAL MEASUREMENTS

Real *4 Word	Description
	Long-Period
1	18-22 sec Vertical Log A/T *
2	50 sec Vertical Log A **
3	33.3 sec Vertical Log A
4	25 sec Vertical Log A
5	20 sec Vertical Log A
6	17 sec Vertical Log A
7	14 sec Vertical Log A
8	12 sec Vertical Log A
9	25 sec Transverse Log A
	Short-Period
10	P-wave log A/T ($\Delta<20^{o}$)
11	S-wave log A/T ($\Delta<20^{o}$)
12	Lg-wave log A/T ($\Delta<20^{o}$)
13	P-wave log A/T ($\Delta>20^{o}$)
14	0.316 Hz Vertical Log A
15	0.501 Hz Vertical Log A
16	0.794 Hz Vertical Log A
17	1.259 Hz Vertical Log A
18	1.995 Hz Vertical Log A
19	3.162 Hz Vertical Log A
20	5.012 Hz Vertical Log A
21	7.943 Hz Vertical Log A
22	Maximum mean frequency
23	Mean phase standard deviation
24	Broadband complexity
25	Minimum narrowband complexity

* Log A/T = logarithm (base 10) amplitude/period + B-factor

** Log A = logarithm (base 10) amplitude + B-factor

TABLE 4

Parameters Measured for Each Station and Each Event (Whenever Possible)

Number	Symbol	Explanation		
1	P_1	low-	frequency P	0.469 - 0.938 Hz
2	P_2	middle-		1.094 - 1.876
3	P_3	high-		2.031 - 3.438
4	$\Omega_o(-2)$	low-frequency spectral level	assuming P-wave spectrum decreases as f^{-2}	
5	$f_c(-2)$	corner frequency		
6	$t^*(-2)$	attenuation coefficient		
7	$\Omega_o(-3)$	same as 4-6, assuming P-wave spectrum decreases as f^{-3}		
8	$f_c(-3)$			
9	$t^*(-3)$			
10	$comp_1$	5-10 sec	coda interval complexity	
11	$comp_2$	5-15 sec		
12	$comp_3$	5-30 sec		
13	Lg_1	low-	frequency Lg	
14	Lg_2	middle-		
15	Lg_3	high-		
16	LP_1	low-	frequency long-period P	0.039 - 0.055 Hz
17	LP_2	middle-		0.063 - 0.086
18	LP_3	high-		0.094 - 0.188
19	LS_1	low-	frequency long-period S	
20	LS_2	middle-		
21	LS_3	high-		
22	LR_1	low-	frequency Rayleigh wave (vertical component)	0.016 - 0.031 Hz
23	LR_2	middle-		0.039 - 0.053
24	LR_3	high-		0.063 - 0.086
25	LQ_1	low-	frequency Love wave	
26	LQ_2	middle-		
27	LQ_3	high-		

MANAGEMENT OF A SIGNAL MEASUREMENT DATA BASE (SMDB)

Donald L. Dietz and Jeffrey S. Shaub

Project VT/9705/B/PMP Contractor: ENSCO, Inc.

Task 4.3.1: Data Base Transfer

Objective

The objective of this task was to transfer the Event Discriminant Data Base from the PDP-15/50 to the PDP-11/70, and to do so under the following constraints:

- Preserve the signal measurements for all event-stations processed under Contract Number F08606-79-C-0014.
- Establish an expandable and maintainable Signal Measurement Data Base (SMDB) on the PDP-11/70 that:
  - satisfies the first constraint above
  - may be updated with additional signal measurements for event-station data processed by other contractors.
- Provide FORTRAN-compatible software utilities to:
  - initialize the SMDB Directory and Free-Block File
  - update the SMDB by event, station, measurement, or contractor
  - access the SMDB for information by event, station, measurement, or contractor.
- Write selected driving programs to demonstrate an:
  - SMDB update with signal measurements discussed in the first criterion
  - SMDB access to list Directory information and signal measurements
  - SMDB access to compute unbiased network averages of signal measurements for a specified event.
- Demonstrate this software contingent on the availability of UNIX operating system utilities provided by the Government.

Accomplishments

An expandable and maintainable Signal Measurement Data Base (SMDB) program suite has been designed and compiled on the PDP-11/70 under the UNIX operating system. Tapes (from

the SDAC) which were used in the VELA-sponsored identification experiment, and which were used in the development and test of the SMDB program suite, are:

1. L22882 (IBM 360/44)
2. L13033 (DEC PDP-15/50).

These tapes can be used in future efforts to refine the SMDB program suite.

INTERACTIVE EVENT IDENTIFICATION PROCEDURES

D. W. Rivers and D. H. von Seggern

Project VT/0707 Contractor: Teledyne Geotech

Task 4.2 Interactive Event Identification Procedures

Objective

A system will be designed which will enable most seismic events to be identified routinely as either earthquakes or explosions. This system will take as input a data file of measurements made on seismograms recorded at a network of stations and will edit and pass this data file through a sequence of manipulations by means of analyst-computer interaction. The output of the system will be the cumulative probability that the unknown event which has undergone these various manipulations is an explosion.

Accomplishments

Most studies of seismic discrimination have been aimed at performing research on some general or specific features of the identification problem, and comparatively few studies have addressed the question of how discrimination ought to be performed routinely as part of a global seismic monitoring operation. In particular, most studies have evaluated only a single discrimination technique, used data recorded at a single station, and/or have concentrated on a carefully selected suite of events for which data management difficulties were minimized. One of the few studies of discrimination in an operational context was performed by Evernden (1977), who analyzed a data base of multistation, multivariate measurements made on every event which occurred within a certain time span and which exceeded a certain threshold magnitude. A principal conclusion of this study was that discrimination on the basis of hypocentral depth should be used as a first screen in any practical system, since this screen would both reduce the number of unknown events requiring further testing and identify certain earthquakes which otherwise resemble explosions.

Even Evernden's (1977) prototypical study was severely constrained, insofar as it was based on visual measurements of film records. The use of digital seismograms enables an increased volume of events to be processed since many routine measurements can be made automatically, and it also provides increased flexibility in that many additional parameters can be measured in both the time and frequency domains. Several investigations have been made into the use of automatic processing of digital data for discrimination purposes, and the culmination of these investigations was the work performed by the three participants in the VSC discrimination experiment.

We have undertaken a study of the techniques employed by all three contractors in the discrimination experiment in order to design a system which will incorporate the various discrimination techniques and utilize many of the data base management methods which were developed for the purposes of that experiment. It is assumed that various measurements will have been made on the digital seismograms, in the same way that they were made in the discrimination experiment so our system design is confined to operations which are performed upon an alphanumeric data file generated by some other system. Work which has been performed so far consists of a preliminary functional

Task 4.2 Interactive Event Identification Procedures

Accomplishments continued

design for the discrimination system.

In accordance with the conclusions reached by Evernden (1977) and by all three participants in the discrimination experiment, the first stage of the system is the identification of deep earthquakes. The conventional determination of confidence ellipsoids surrounding the event hypocenter will be used to compute the probability that the unknown event occurred at depths greater than 10 km. If this probability exceeds a certain threshold, say 95%, then the event is presumed to be an earthquake; if not, this probability is passed along through further stages in the analysis so that it may be used in the computation, via Baysian statistics, of the probability that the event is an explosion (i.e., that it satisfies the dual criteria of being shallow and exhibiting explosion-like characteristics). The confidence ellipse around the epicenter will ultimately be used to compute joint probabilities that the event is explosion-like and that it occurred within certain regions (e.g., within a known test site, on dry land, etc.).

A set of functions has been chosen to enable an analyst to edit the data file interactively so that statistical discrimination tests can be performed on those events which pass through the screening by depth. These functions consist of procedures which will enable the analyst, at his discretion, to plot map projections and cross-sections; display plots of discrimination values for selected sets of events; search through data archives to retrieve any historical events which satisfy specified indexing criteria (epicenter within a certain region, magnitude exceeding a certain threshold, low M_S-m_b difference, etc.); add or delete alphanumeric data files; isolate particular data points on a graphics display and then dump a data file corresponding to that point; flag anomalous measurements which will be referred to the signal measurement system for reprocessing; etec. The end product of this interactive editing process is a data file of both unknown and previously identified event (if any, to be used for training purposes in the classification) upon which statistical tests of similarity will be performed. Because the data base will contain both individual stations' measurements and maximum likelihood estimates of event magnitude, this editing process and the ensuing event identification can be performed, at the analyst's discretion, in either a station-by-station or a network-averaged mode. The data file can be edited to consist of an arbitrary number of discriminants; presumably this will be as many values as were measured for the unknown events under consideration. Finally, a statistical test will be run on the edited data file in order to classify the unknown events. This statistical test will be either cluster analysis or discrimination analysis; the analyst's choice of tests will be influenced by the availability in the archived data base of both explosions and earthquakes which can be used for training.

The preliminary functional design which has been performed creates constraints upon the structure of the data base, and these constraints must be satisfied by the signal measuring system which serves as input to the interactive event identification system. After the structure of the data base is

Task 4.2 Interactive Event Identification Procedures

Accomplishments continued

determined, a system design will be created to implement this functional design.

Reference

Evernden, J. F. (1977). Adequacy of routinely available data for identifying earthquakes of $m_b \geq 4.5$, Bull. Seism. Soc. Am., 67, 1099-1151.

A CONSTITUTIVE MODEL FOR SALT

J. T. Cherry
N. Rimer

Project: VT/0712

Contractor: Systems, Science and Software

Task 4.1.1 Seismic Source Calculations: One- and Two-Dimensional Explosion Calculations

Objective

Realistic decoupling scenarios in salt can be developed only after appropriate free field ground motion data in this rock are understood. Ground motion data from a number of nuclear and high explosive events in salt are available. The events include GNOME, SALMON, STERLING and COWBOY.

The SALMON event provided a large subset of this data. In addition, some of the SALMON data have been digitized. For these reasons we chose the SALMON event for the normalization of the constitutive model and then applied this model to the remaining salt events. The objective was to determine how much of the salt ground motion data a single constitutive model could explain.

Accomplishments

This procedure produced good agreement with the ground motion data from STERLING and GNOME. The predicted peak displacements for the tamped COWBOY shots were approximately a factor of two greater than those observed. However, predicted and observed peak velocities for COWBOY were in close agreement.

NORMALIZATION TO SALMON

Figure 1 shows the laboratory strength data for SALMON, GNOME and Polycrystalline salt. The curve shown in the figure fits the data for SALMON and GNOME and was used in the model for the ultimate strength of salt (Y_{lim}).

The best agreement with the SALMON ground motion data was obtained by assuming that salt work hardened to its ultimate strength. The expression used to calculate the strength (Y) as a function of the inelastic energy (E) deposited in the material during yielding was

$$Y = Y_0(1 + e_1 E - e_2 E^2) \leq Y_{lim}$$

where Y_0 is the initial (saturated) srength and e_1 and e_2 are respectively work hardening and work softening material constants.

If S_{ij} is the deviatoric component of the stress tensor and J_2' is the unadjusted second deviatoric invariant, then the increment in inelastic energy becomes

$$\Delta E = S_{ij}\,\Delta\pi_{ij} = \frac{S_{ij}\,S_{ji}}{2\mu}\quad\frac{\sqrt{3J_2'} - Y}{Y}$$

where

$$3\,J'_2 > Y^2$$

π_{ij} = the deviatoric component of the inelastic strain tensor

μ = the shear modulus.

This model is simple and easily implemented in a finite difference stress wave code. The physical basis for the work hardening aspect of the model may be an increase in effective stress, and conversely a decrease in pore fluid pressure, caused by dilatancy. If this is the case, then Y_0 is the saturated material strength. During shock loading microcracks open, the pore fluid pressure decreases and the strength increases. During release, the cracks close, pore fluid pressure increases and strength decreases. These modes of material behavior are quantitatively contained in the model with the rate of hardening and softening determined by the constants e_1 and e_2.

Figure 2 compares the calculated and observed ground motion from SALMON at a range of 620 m where the calculations were performed with the work hardening model. The emergence of a precursor with a peak velocity of approximately 0.5 m/sec is adequately modeled by assuming a saturated strength (Y_0) of 25 bars. Work hardening is required in order to match the observed pulse shape. At a radius of 967 m, the peak velocity in the calculation is determined by the precursor. Elastic material behavior occurs beyond this radius in the calculation.

Figure 3 compares calculated and observed peak velocities and peak displacements. The results of two calculations are shown in this figure; one (dashed curve) in which Y_{1im} equaled the maximum strength (0.68Kb) given in Figure 1, and the second (solid curve) in which Y_{1im} varied with stress state ($\bar{P}$) as shown in Figure 1.

Figure 4 shows the RVP spectra ($|\hat{\Psi}|$) for these two calculations. Also shown are the spectra of Springer et al. (1968), which represents an average of the free field SALMON data, and Murphy, which was obtained by scaling the spectrum of the GNOME event to the yield and depth of SALMON.

These results, involving comparisons between calculated and observed ground motions and RVP spectra indicate that the constitutive model adequately explains the SALMON data. We now apply this model to other salt events.

STERLING

Simulation of the STERLING event was accomplished by detonating 0.38 KT in the SALMON cavity. The RVP spectrum for STERLING was calculated and divided into the calculated SALMON spectra shown in Figure 4 ($Y_{lim} = Y_{MAX}$). The resulting spectral ratios are shown in Figure 5. In this figure we also show Springer's averaged spectral ratios obtained from seismic stations common to the two shots. Agreement is excellent over the frequency range analyzed by Springer.

GNOME

The GNOME event was simulated using the work hardening model. Figures 6 and 7 compare calculated and observed peak velocities and displacements for this event. The calculated elastic radius was 790 m.

Figure 8 compares the Mueller-Murphy estimate of the GNOME RVP spectrum with the calculated spectrum. Agreement is surprisingly good considering that the Mueller-Murphy spectrum was based on ground motion data at a range of 300 m, a distance well within the region of nonlinear material behavior.

COWBOY

Figures 9 and 10 compare calculated and observed peak velocities and peak displacements for the tamped shots in the COWBOY series. Agreement is good for peak velocities. However, the calculated peak displacements are a factor of two larger than those observed.

There are a number of explanations possible for this result, e.g., the COWBOY salt was not saturated, the HE was not adequately simulated, the peak displacements were not free field, the charge emplacement was not consistent with a spherically symmetric geometry, the material properties (strength and wave velocities) of the COWBOY salt are different from GNOME and SALMON.

These issues are worth pursuing, but not here. Our objective was to develop a constitutive model for salt based on SALMON ground motion data and then to determine its range of applicability for other salt events. The results of the model are consistent with data from STERLING and GNOME. They are not consistent with the data from the tamped COWBOY series.

REFERENCES

Springer, D., and M. Denny, J. Healy, W. Mickey (1968), "The Sterling Experiment: Decoupling of Seismic Waves by a Shot-Generated Cavity," J. Geophys. Res., 73, (18), pp. 5995-6010.

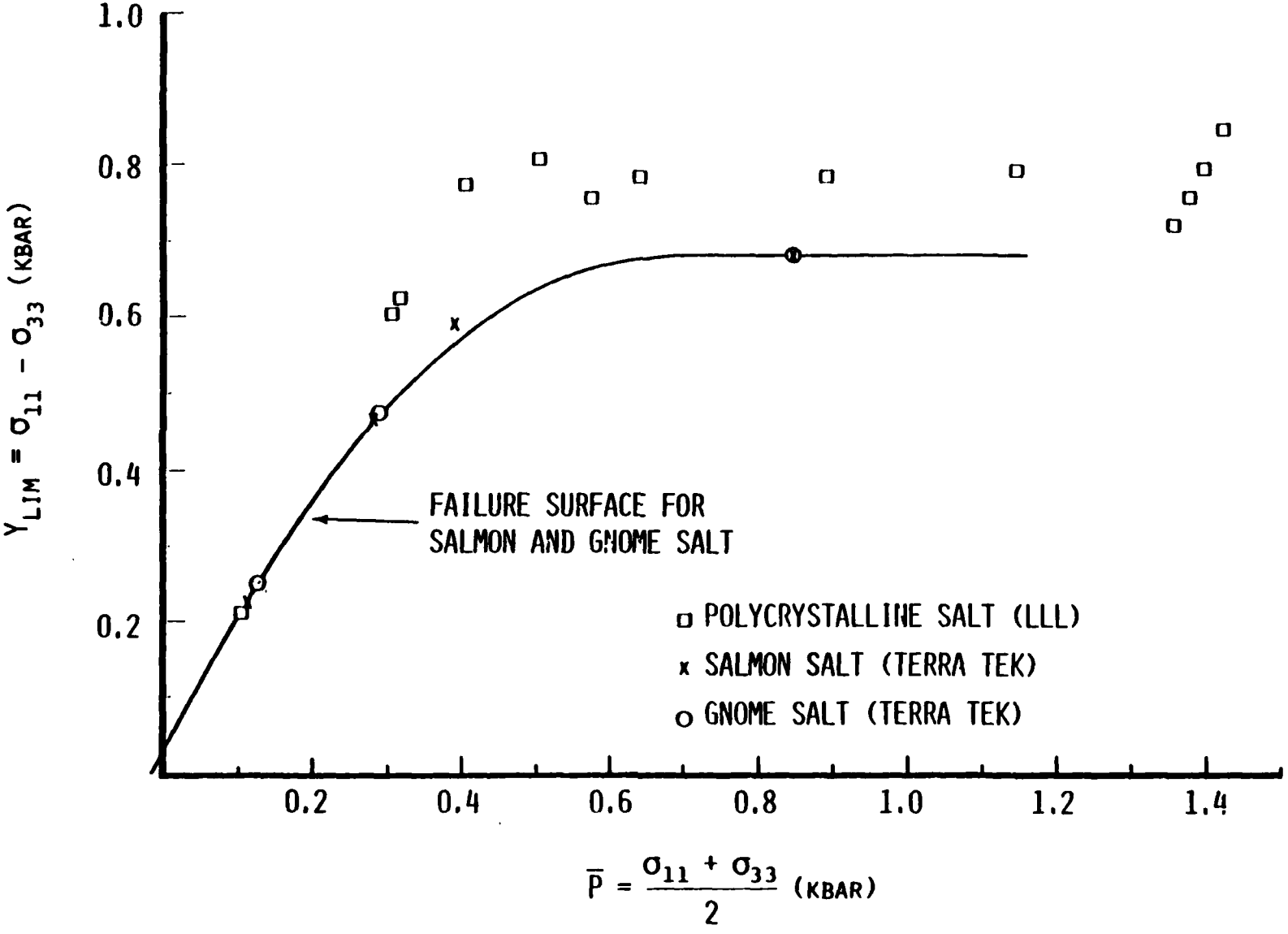

Figure 1. Strength data for salt.

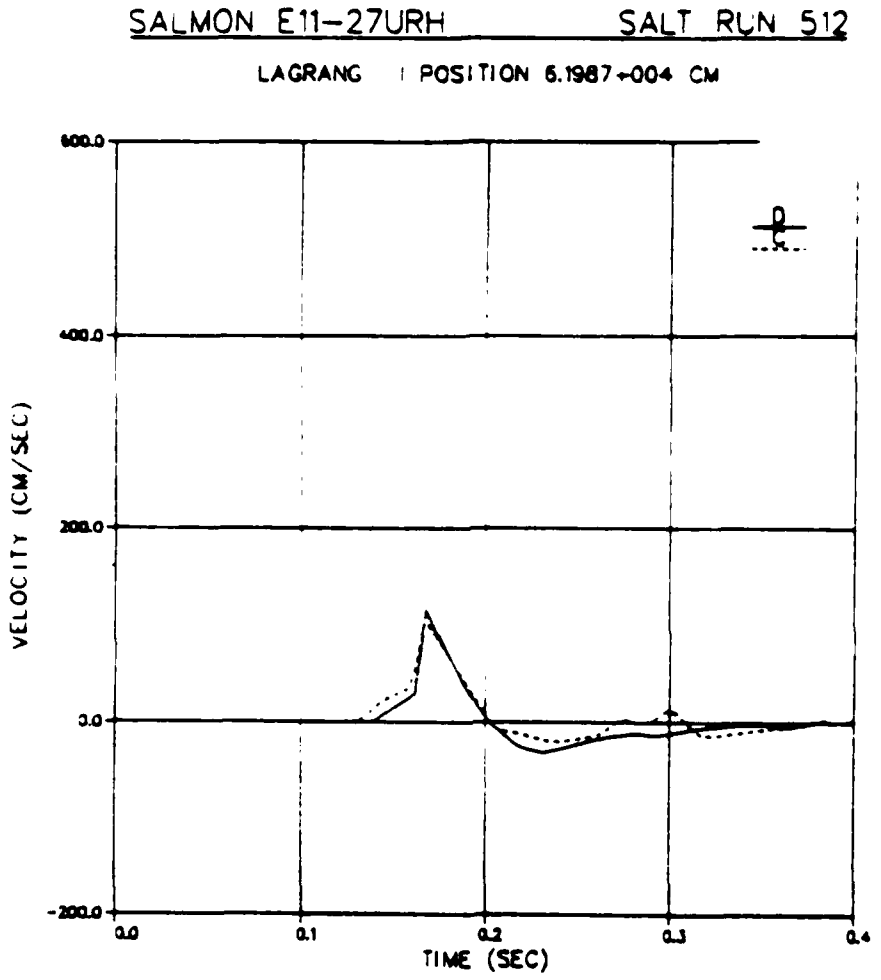

Figure 2. Comparison between calculated (dashed curve) and observed (solid curve) ground motion from SALMON at a range of 620 m.

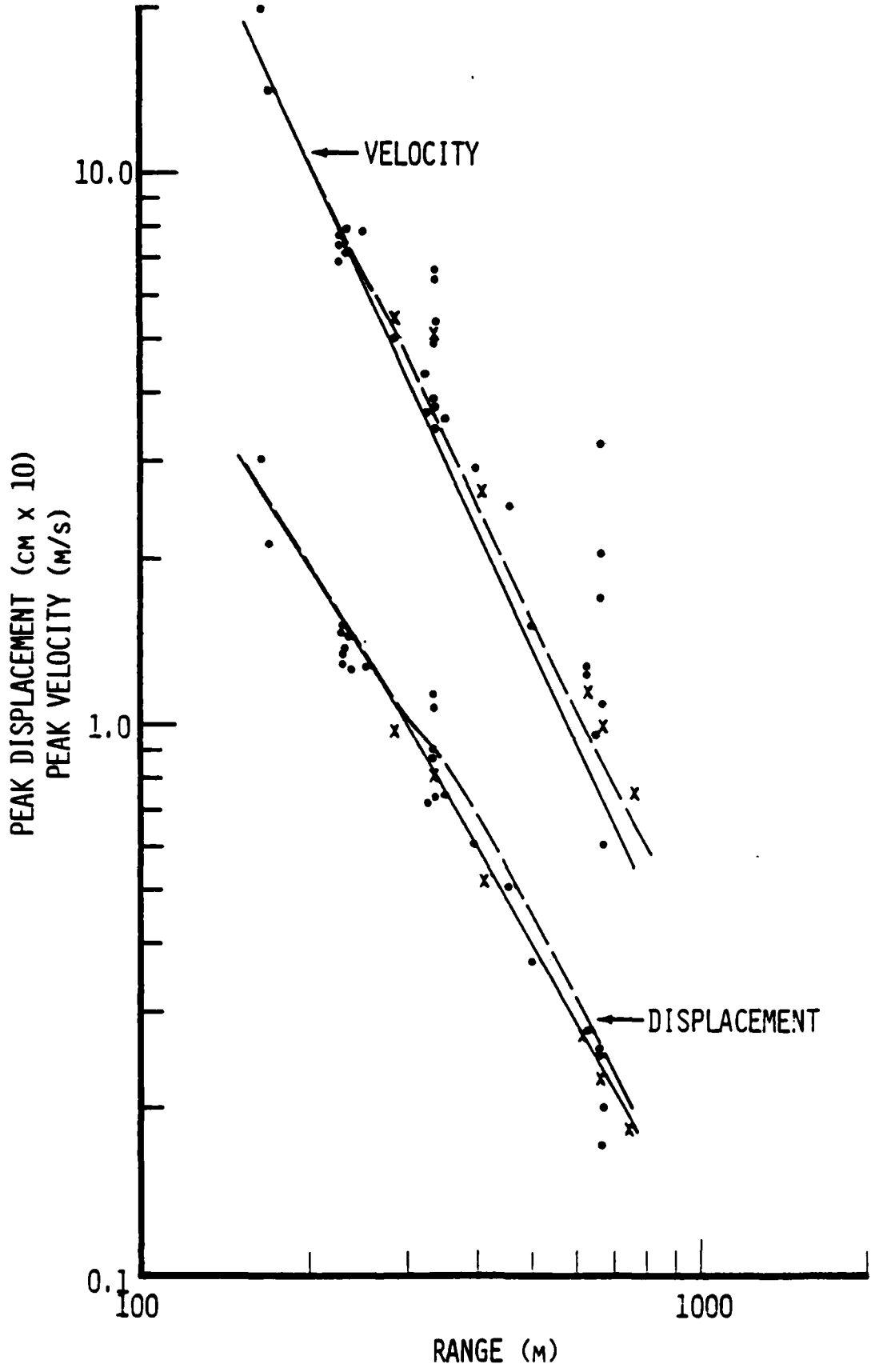

Figure 3. Comparison between calculated and observed peak velocities and displacements for SALMON.

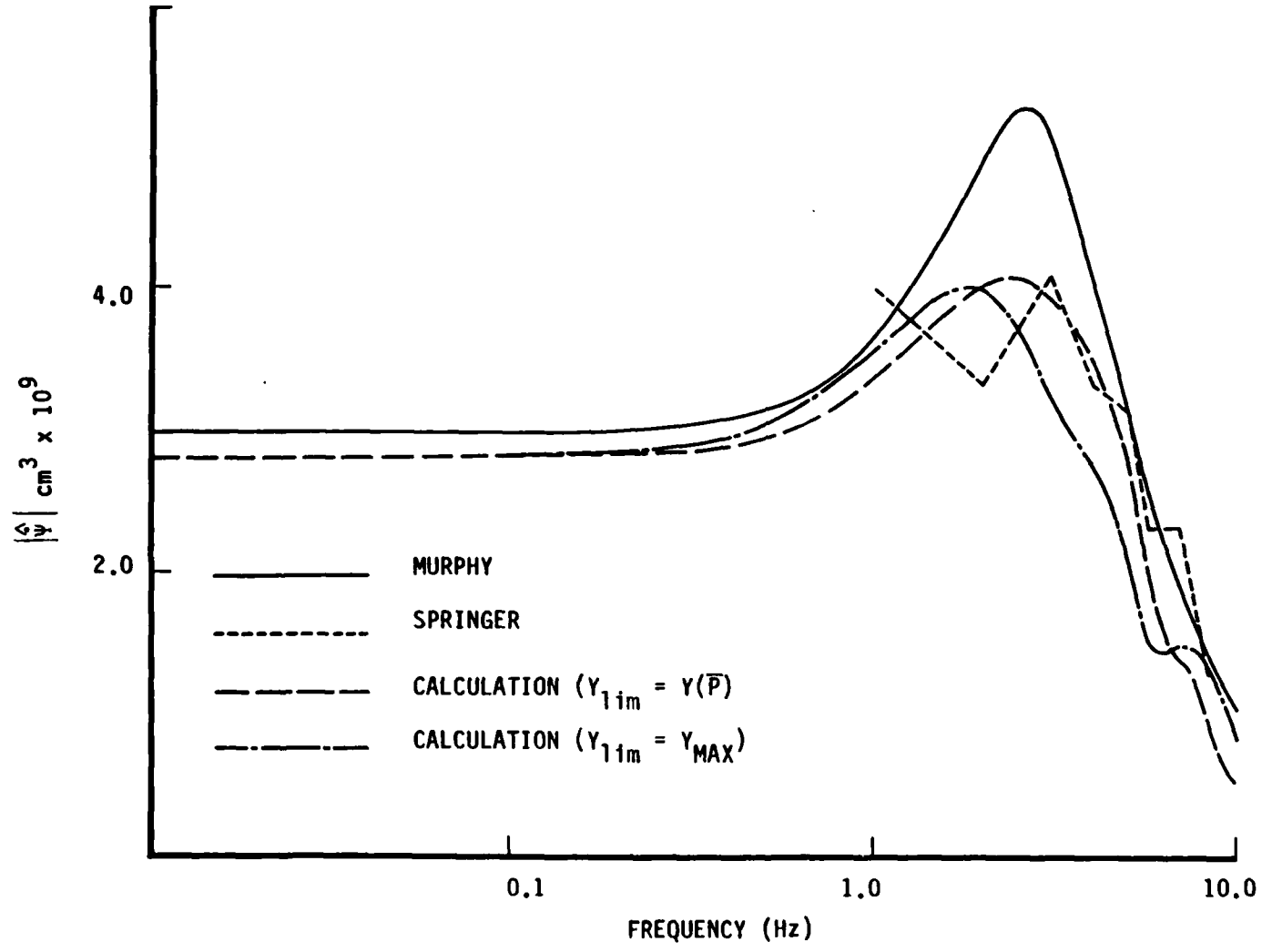

Figure 4. Comparison of calculated and observed RVP spectra for SALMON

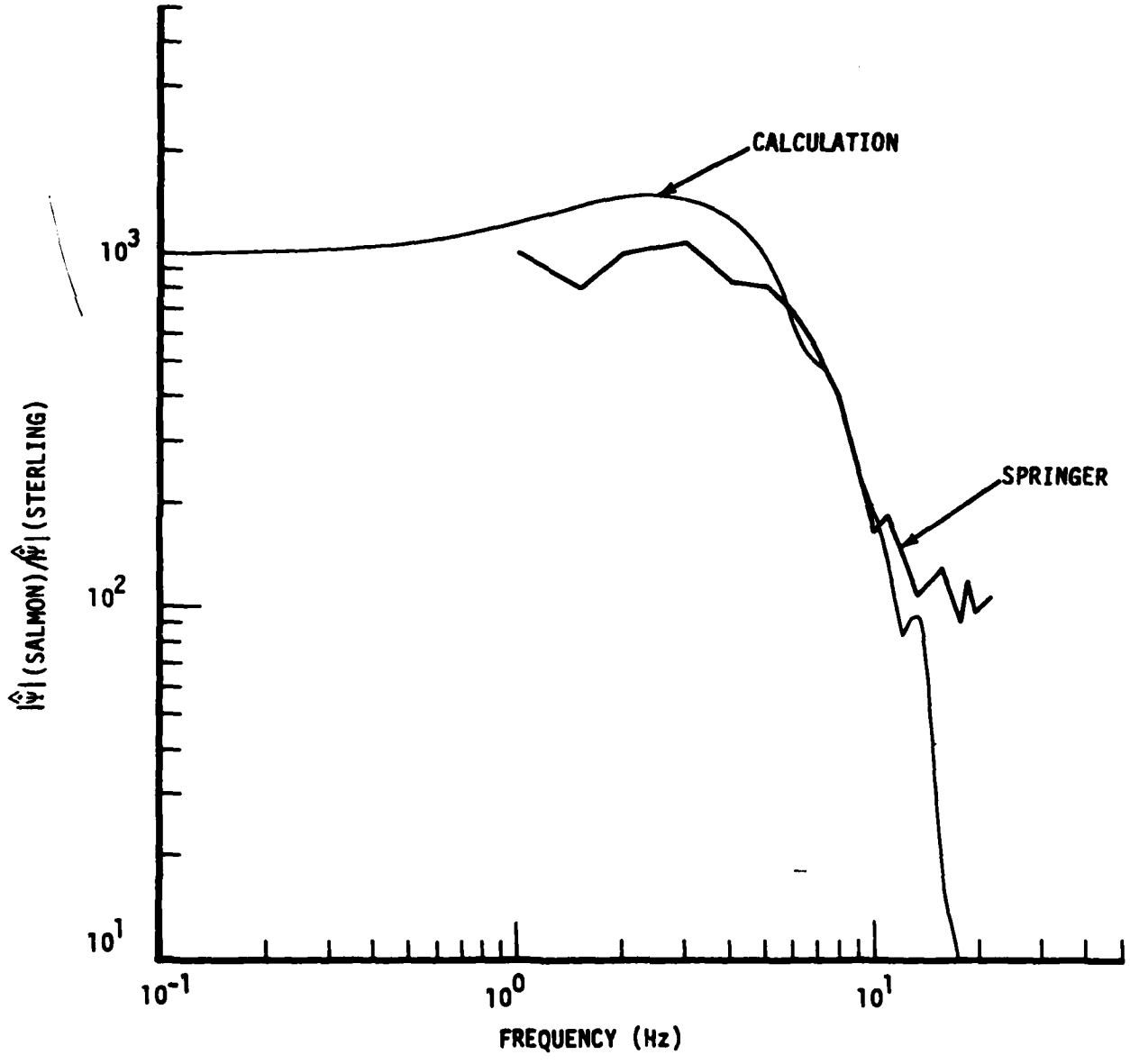

Figure 5. Calculated and observed spectral ratios for SALMON/STERLING.

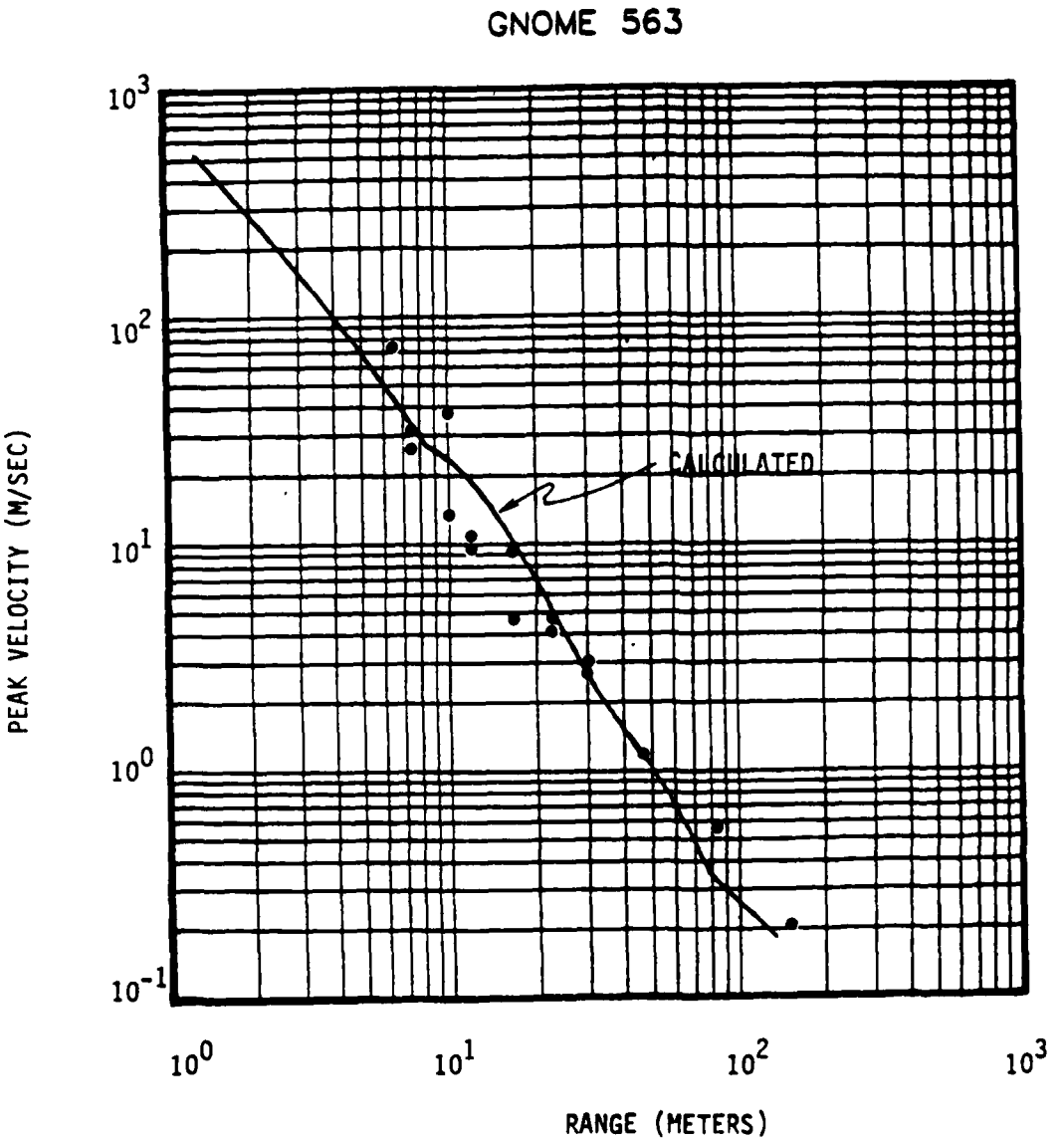

Figure 6. Comparison of calculated and observed peak velocities for the GNOME event.

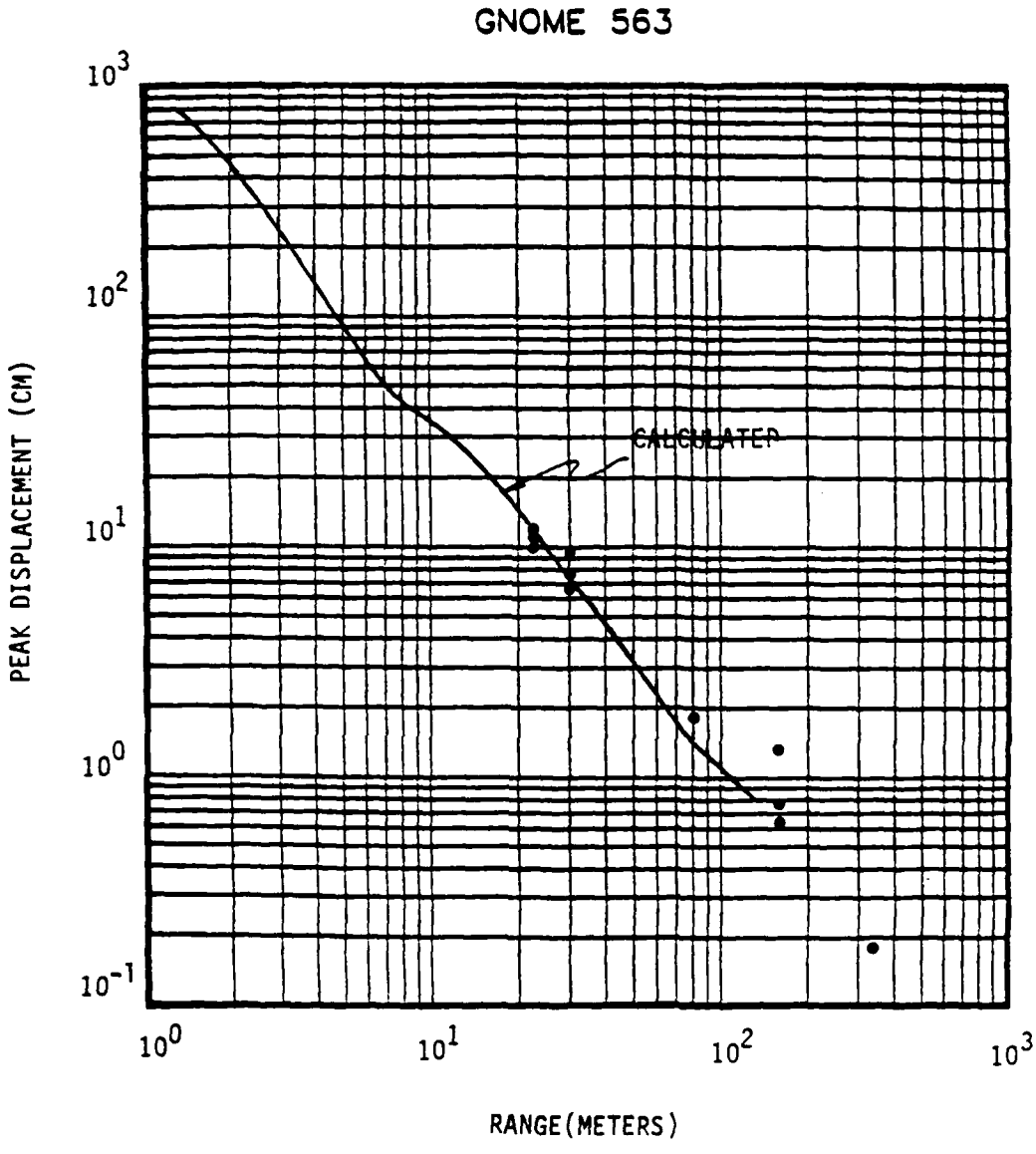

Figure 7. Comparison of calculated and observed peak displacements for the GNOME event.

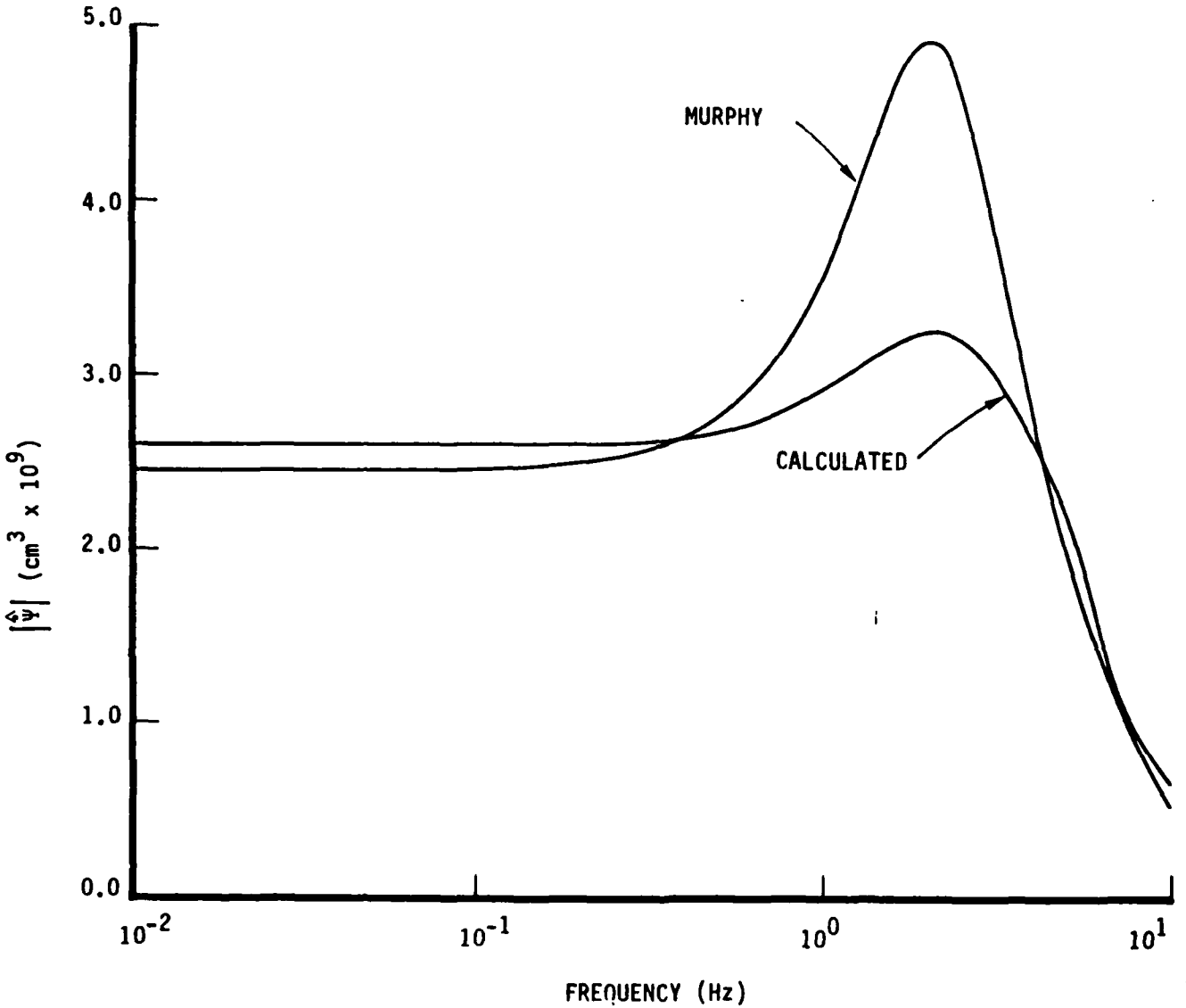

Figure 8. Comparison of calculated and observed RVP spectra for GNOME.

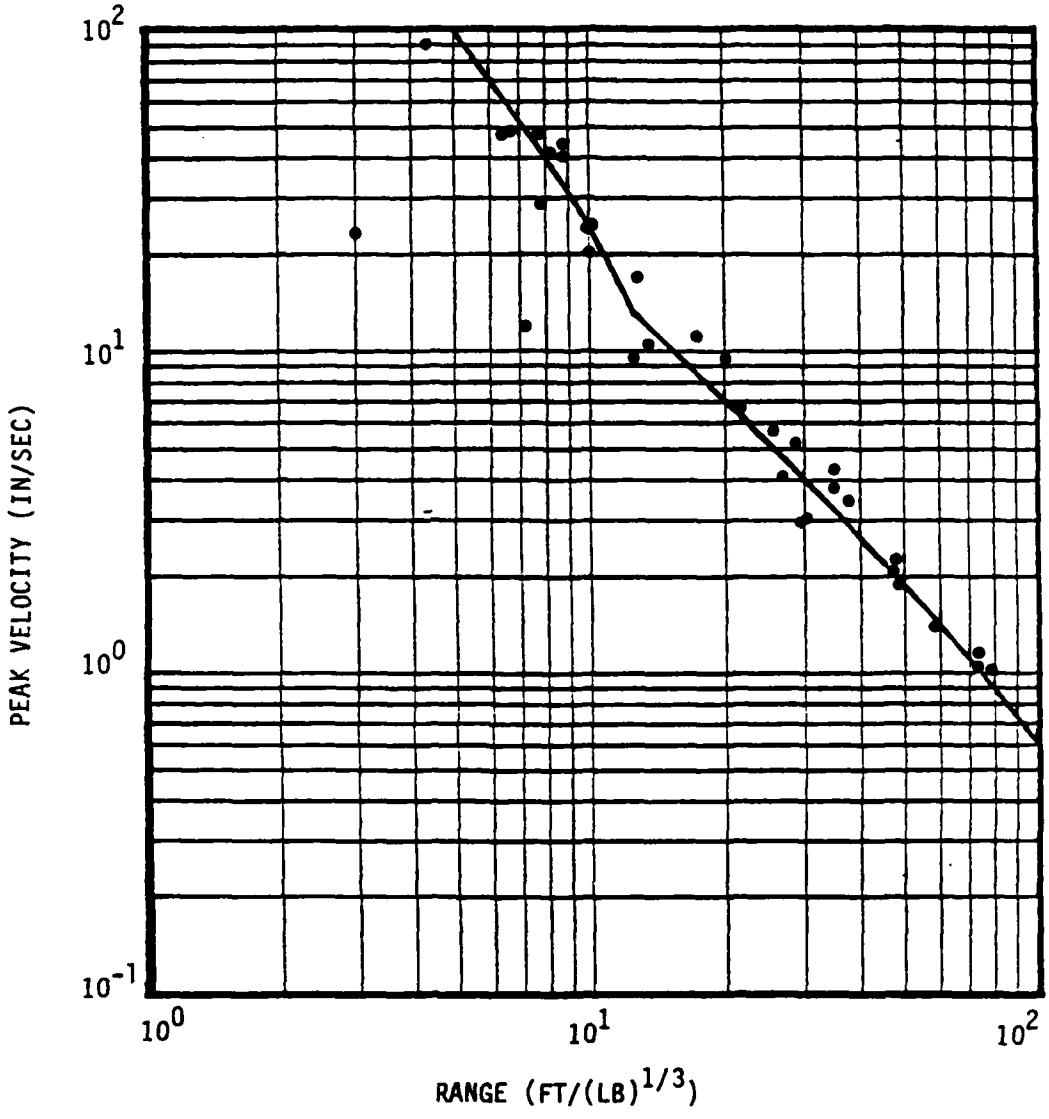

Figure 9. Comparison of observed and calculated peak velocities for the tamped COWBOY events.

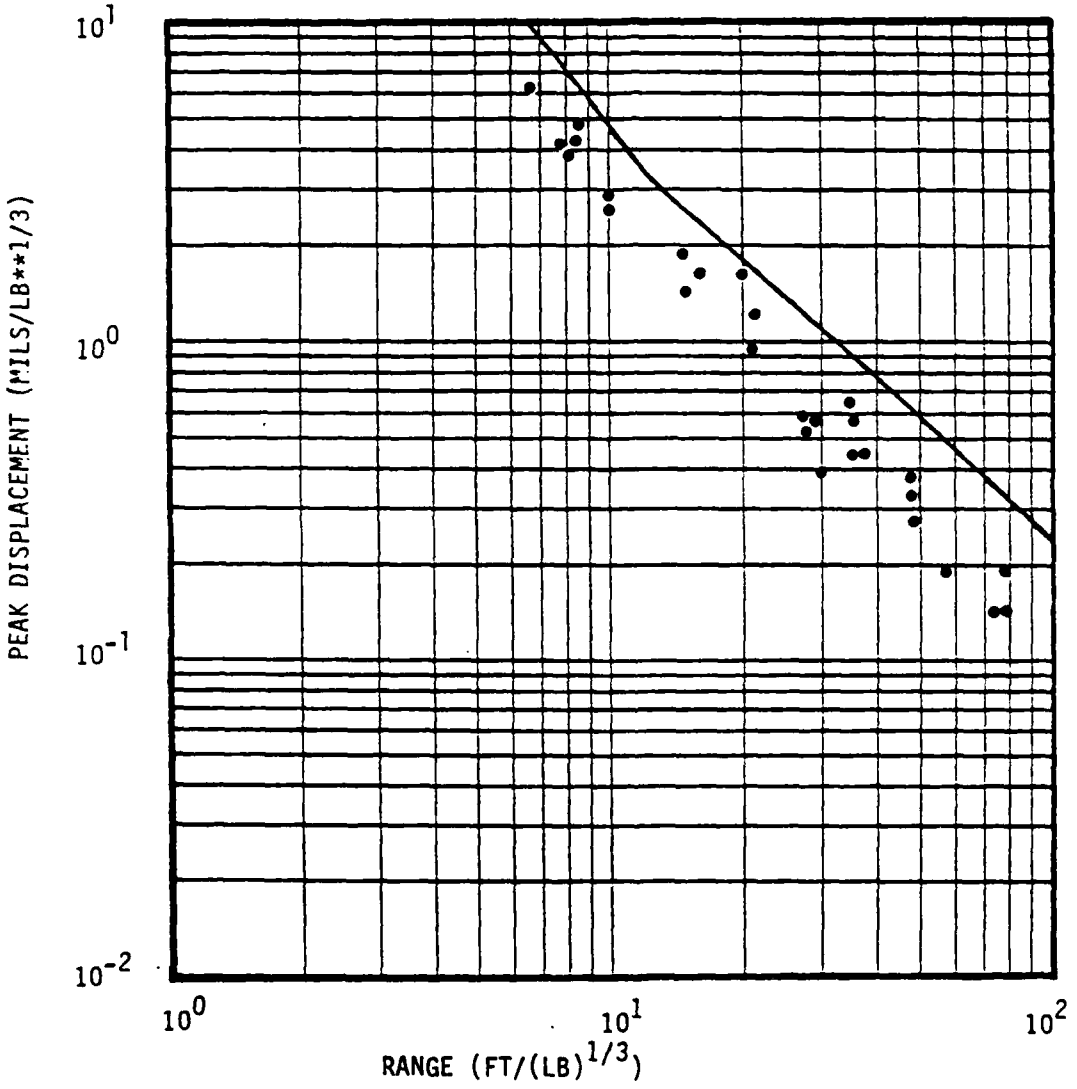

Figure 10. Comparison of observed and calculated peak displacements for the tamped COWBOY events.

THE UNDERWATER ACOUSTIC SIGNATURE OF A NUCLEAR EXPLOSION AT THE OCEAN SURFACE

T. C. Bache,
T. G. Barker
M. G. Brown (consultant)
K. D. Pyatt
H. J. Swanger

Project VT/0712

Contractor: Systems, Science and Software

Task 4.7: Acoustic Waves from Explosions in the Ocean

Objective

The objective of this task is to estimate the gross spectral character and duration of the acoustic wave signature of a nuclear explosion near the ocean surface. The explosion is assumed to have a yield of 1 kiloton and the nominal range is 6600 kilometers.

Accomplishments

The main results of this work are summarized in a report by Bache, et al., (1980). The technique was to construct theoretical pressure-time histories by convolving an elastic representation for the source with a Green's function representing the propagation. The source may include two parts. The first is the airblast loading applied to the surface and the second is the direct coupling of energy into the water. When the explosion is above a certain height, estimated to be 2.3 meters for 1 KT, the direct coupling contribution may be ignored. Thus, the calculations include the cases when the explosion is on or above the surface, though no attempt is made to account for height-of-burst effects that may become important when the (1 KT) explosion is more than 10 meters above the surface.

Both components of the source are expressed in terms of pressure-time histories, P(r,t) applied to the ocean surface. The total force applied is

$$\hat{F}(\omega) = \int_0^\infty P(r,\omega)\ J_0(\omega p r) r dr \qquad (1)$$

The spectral amplitudes of the total force for both components of the source are plotted in Figure 1 for the ray parameter (p = 0.667 sec/km) appropriate for large distances.

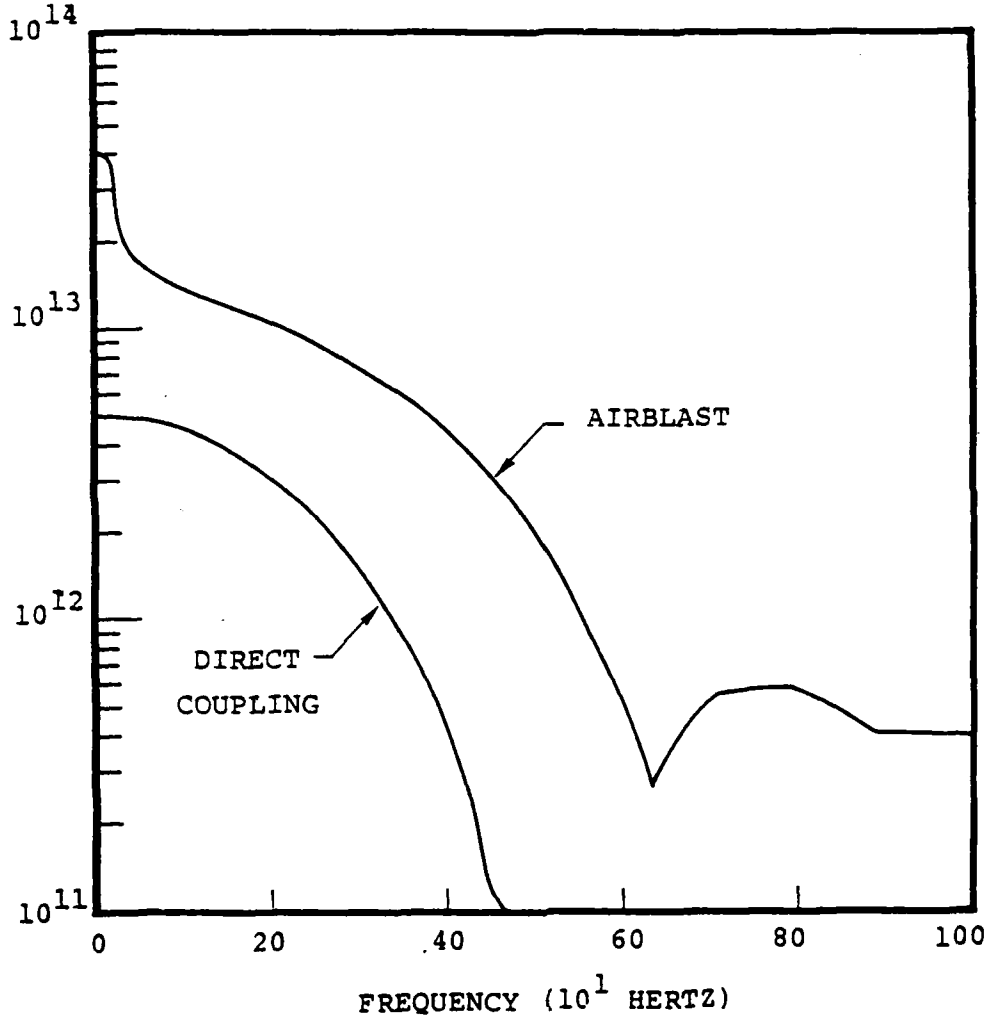

Figure 1. The explosion source spectra.

The pressure at the receiver is obtained by convolving $\hat{F}(\omega)$ with the appropriate Green's function, which is the pressure at the receiver due to a vertical point load applied at the center of the source region. The Green's functions were computed with the WKBJ seismogram method (Chapman, 1978; Brown, et al., 1980). The results turned out to be very little different from those from geometric ray theory. Then for any particular ray arrival, the spectral pressure at the receiver is approximately

$$\hat{P}_r(\omega) \approx i\,\omega\,\hat{F}(\omega) \cdot Q(\omega) \quad , \qquad (2)$$

where $Q(\omega)$ represents the frequency-dependent filter imposed by the travel path. However, at the frequencies of interest (< 50 Hz), absorption in the ocean is very small. Therefore, we assume that $Q(\omega) = 1$. The total record is a summation of many rays, leading to a total spectrum which is merely a modulated version of (2).

In Figure 2 we plot our estimates for the spectra of the pressure pulse at a hydrophone in the deep ocean at a large distance from the explosion. The direct coupling contribution is small and the spectrum is band-limited, having a peak near 22 Hertz and being down by a factor of 3 from the peak at about 4 and 50 Hz. The spectra cube-root scale with yield. That is, if the yield were 2 KT, the spectrum in Figure 2 shifts to frequencies smaller by a factor of 1.26.

To estimate the signal duration, the Green's functions were computed with WKBJ seismogram theory for a variety of assumptions about the ocean sound velocity profile. At the large ranges (> 3500 km) of interest, the main contribution is from rays that turn above the ocean bottom. For a reflection coefficient of as large as 0.98, the bottom bounces make almost no contribution because they reflect so many times.

The calculated signal duration varies widely, depending upon the assumptions about the sound velocity profile. Values from 20 to 60 seconds seem most reasonable for a range of about 6600 kilometers. The duration scales directly with range.

REFERENCES

Bache, T. C., T. G. Barker, M. G. Brown, K. D. Pyatt, and H. J. Swanger (1980), "The Underwater Acoustic Signature of a Nuclear Explosion at the Ocean Surface," Systems, Science and Software Interim Technical Report SSS-R-80-4586 submitted to AFTAC/VSC, July, 26 pages.

Brown, M. G., W. H. Munk, J. L. Spiesberger and P. F. Worcester (1980), "Long-Range Acoustic Transmission in the Northwest Atlantic," JGR, 85, pp. 2699-2703.

Chapman, C. H. (1978), "A New Method for Computing Synthetic Seismograms, Geophys. J., 54, pp. 481-518.

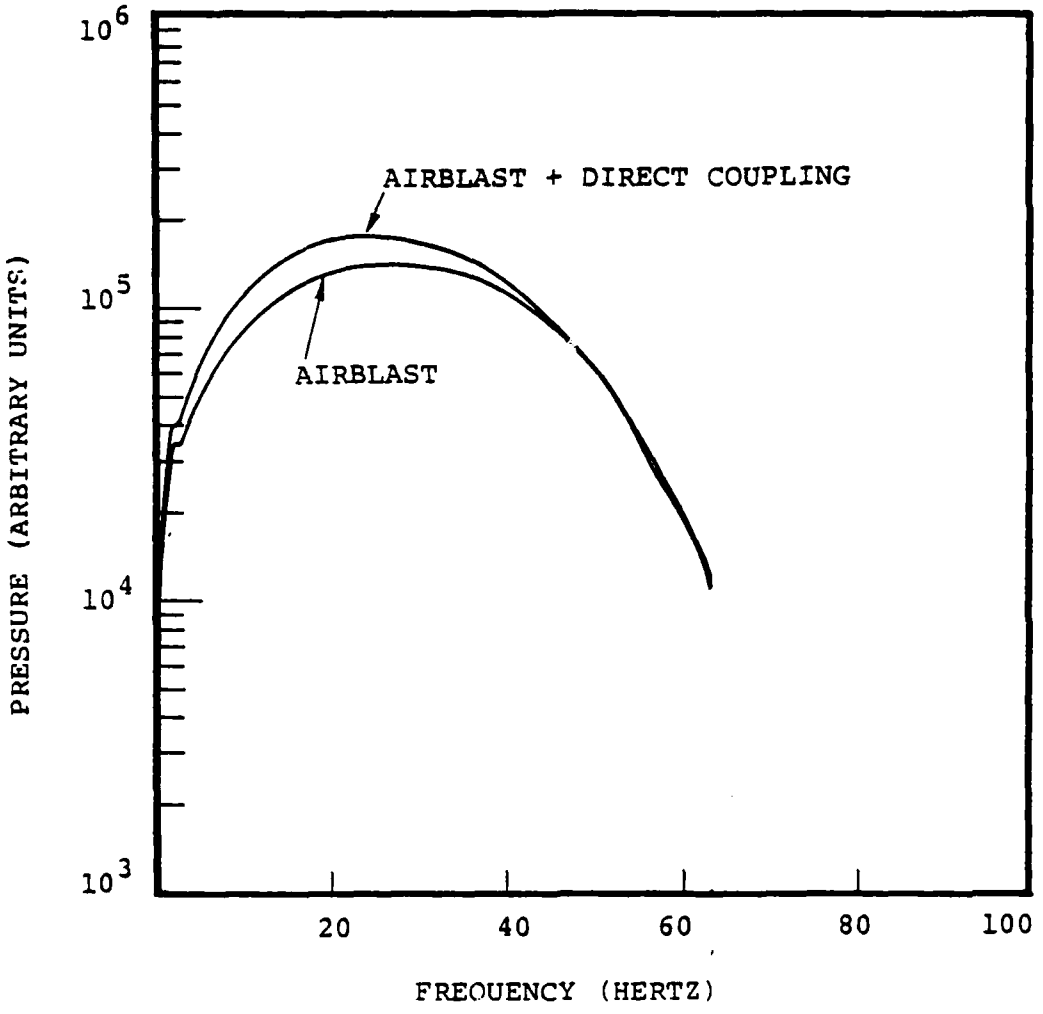

Figure 2. The spectrum of the pressure time history of a single ray arrival at a SOFAR axis receiver station. The complete signal spectrum, which is a sum of many single ray spectra, would have the same basic shape. The amplitude units are arbitrary, depending on the amplitude of the Green's function for the travel path.

ANALYSIS OF FREE-FIELD DATA FROM EXPLOSIONS IN WET TUFF AND ALLUVIUM EMPLACEMENT MEDIA

J. R. Murphy
T. J. Bennett

Project VT/0712

Contractor: Systems, Science and Software

Task 4.5 Ground Motion Analysis

Objective

The objective of this task is to compile and evaluate the near-source data recorded from underground explosions and assess their significance with respect to the definition of the nuclear seismic source functions for different emplacement media. More specifically, previously unpublished data collected from the Sandia Corporation archives are being reviewed and integrated into the previously compiled data base.

Accomplishments

Table 1 lists the events for which previously unpublished free-field data have been collected. It can be seen that data from eleven different explosions covering a yield range from about 1 to 1200 KT are being investigated. These events were detonated in wet tuff/rhyolite and alluvium emplacement media and the associated depths of burial vary by more than a factor of six. These data, together with those previously collected, are being used to assess the dependence of seismic coupling on source medium. For example, Figure 1 shows a comparison of the reduced displacement potentials (RDP's) predicted using an analytical model based on Pahute Mesa explosions in wet tuff/rhyolite with several observed RDP's from Yucca Flat events in wet tuff. It can be seen that the predicted and observed agree fairly well, which suggests that the seismic coupling properties of Yucca Flat tuff are similar to those of the Pahute Mesa volcanics. However, a very different picture emerges when this same procedure is applied to explosions in dry Yucca Flat alluvium. Figure 2 shows a comparison of the observed RDP's from four events in dry alluvium with the corresponding RDP's predicted for the same yields and depths of burial in wet tuff/rhyolite emplacement media. It can be seen that these data clearly indicate that dry alluvium is a weak coupling medium with respect to wet tuff/rhyolite, in agreement with the observed differences in the teleseismic m_b data from explosions in these two media. Thus, the available free-field data are essentially consistent with the teleseismic m_b data and, consequently, should be of use in their interpretation.

TABLE 1

NUCLEAR EXPLOSIONS FOR WHICH PREVIOUSLY UNPUBLISHED FREE-FIELD DATA HAVE BEEN COLLECTED

EVENT	MEDIUM	YIELD	DEPTH
AGILE	Wet Tuff	L-I	732 m
BOXCAR	Wet Rhyolite	1200 KT	1165 m
CALABASH	Wet Tuff	110 KT	626 m
CARPETBAG	Wet Tuff	220 KT	663 m
COMMODORE	Wet Tuff	250 KT	749 m
CYPRESS	Wet Tuff	L	411 m
DIESEL TRAIN	Wet Tuff	L	419 m
FAULTLESS	Wet Tuff	I	975 m
HUTCH	Wet Tuff	I	549 m
LANPHER	Wet Tuff	L-I	714 m
PLATTE	Tuff	1.85 KT	191 m

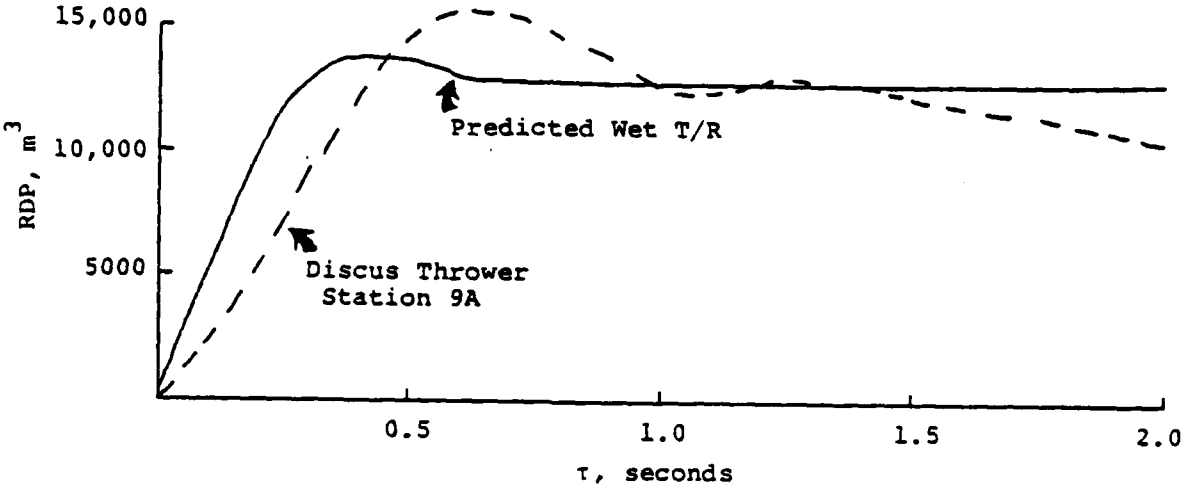

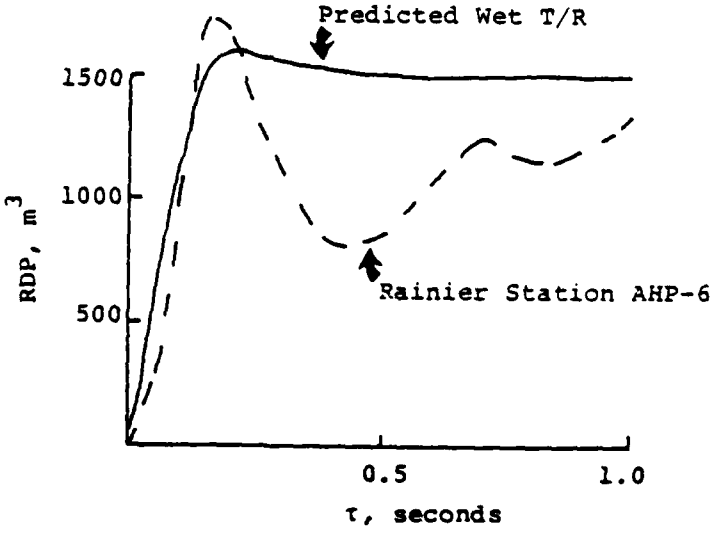

Figure 1. Comparison of observed tuff RDP's with RDP's Predicted for the same yield and depth of burial in a wet tuff/ rhyolite emplacement medium.

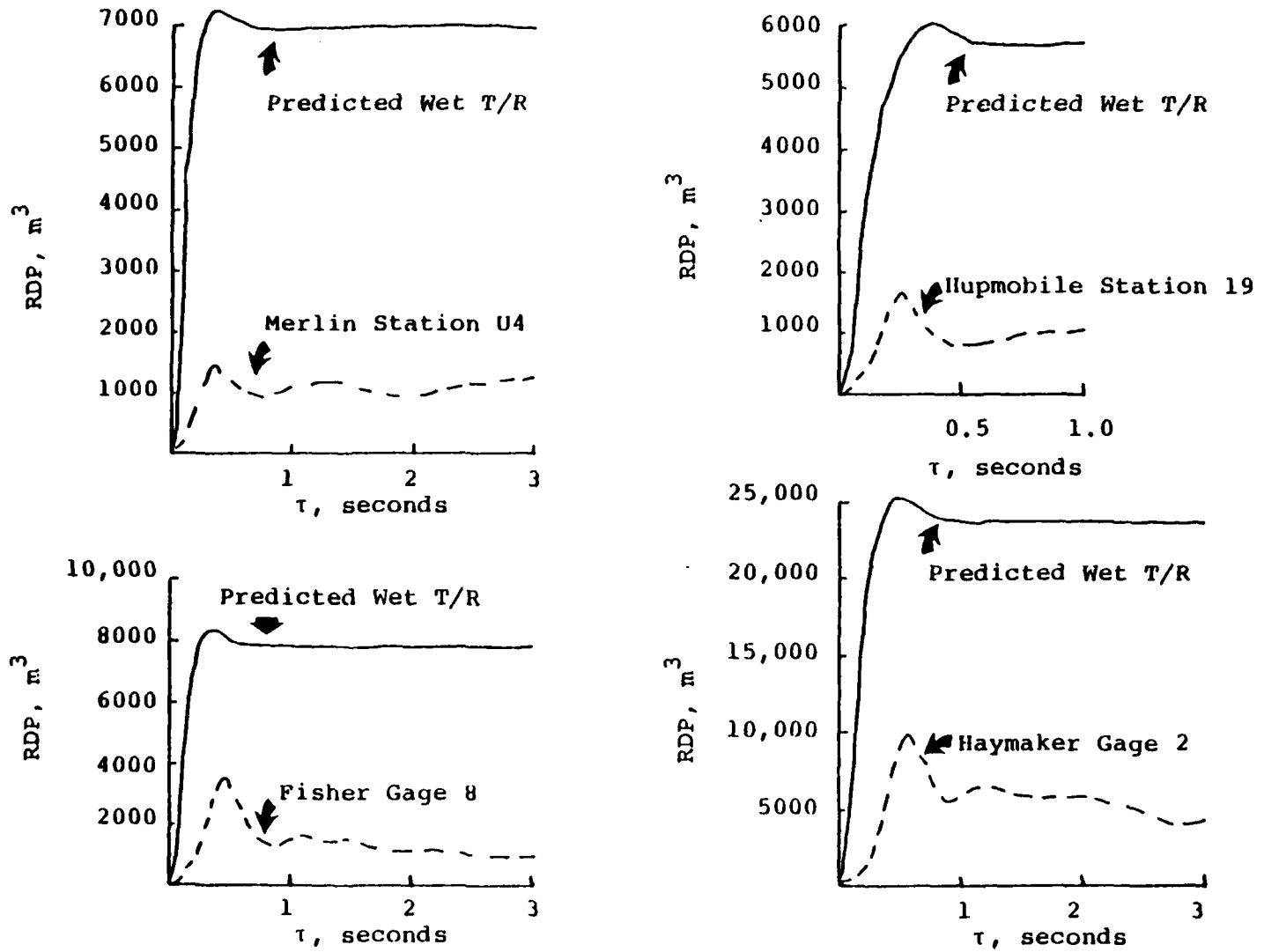

Figure 2. Comparison of observed alluvium RDP's with RDP's predicted for the same yield and depth of burial in a wet tuff/rhyolite emplacement medium.

OBSERVATIONS OF PERIODICITIES IN THE CODA OF SEISMIC SIGNALS

Robert L. Sax, Alan C. Strauss, and Theodore J. Cohen

Project VT/9705/B/PMP Contractor: ENSCO, Inc.

Task 4.2.4: Detection of Signal Periodicities

Objective

The objective of this study was to determine whether source-related effects associated with explosions produce periodicities which can be detected in signal codas. We also wanted to determine whether such periodicities, if indeed they exist and can be observed, could be related to source yield.

Accomplishments

A technique was developed for accurately detecting spectral peaks which are presumably associated with seismic sources. Tests on synthetic data indicate that the method is suitable for the unambiguous detection of spectral peaks down to a 3.2 magnitude level (to a 2.8 magnitude level with less clarity).

Observations of presumed nuclear explosion data confirm that spectral peaks presumably associated with these sources can indeed be observed. Specifically, eleven USSR presumed explosions, four USA explosions, and one earthquake were spectral analyzed. We were able to interpret the coda of eleven of the presumed explosions as containing harmonically related spectral peaks. For these events, 131 peak frequencies were measured and 123 of these frequency measurements were interpreted as possible harmonic components. Of the eight frequency measurements not so identified, all were close to expected harmonic components; these frequency peaks were not used for analysis purposes, however, because they deviated more than 5% from the expected frequency apparent spectral peaks. A possible interpretation of the data involves an ellipsoidally shaped source which is postulated to set up modes indicative of the three principal dimensions of the source. In this case, these modes are approximately in the ratio of 1.67:1.25:1.00. The observed harmonics might possibly be indicative of the linear dimensions of a contained source at scale depth in a pre-stressed medium.

One objective of this study was to examine the feasibility of detecting the spectral peaks associated with an explosion source and to use measurements of the spectral peaks to estimate the yield of the explosion. This aspect of the problem was examined by a linear regression between measurements of the base frequency of observed harmonic spectral peaks and event magnitude. This analysis indicated that larger magnitude sources correlated with lower base frequencies for coda periodicities. A relationship between yield and m_b, based on data for announced USA explosions, was substituted into the m_b-versus-frequency relationship to obtain a yield-versus-frequency measurement. This relationship, in turn, was used to estimate the yield of the explosions examined.

(U) INFORMATION ON THE SIXTEEN EVENTS FOR WHICH DATA WERE ANALYZED IN THIS STUDY

Event Designation	Date	Origin Time	Latitude (^{o}N)	Longitude (^{o}E)	m_b	Information Source
20	09/05/77	03.02.57.8	50.09	78.96	5.9	PDE
22	09/30/77	06.59.55.6	47.8	48.1	5.1	PDE
53	10/29/77	03.06.58* 03.07.03	49.84 50.06	78.17 78.9	5.5 5.6	PDE
81	11/30/77	04.06.57.5	49.96	78.93	5.9	PDE
170**	12/18/77	16.47.17	39.86	77.33	5.3	PDE
267	06/11/78	02.56.57.7	49.88	78.84	5.9	PDE
268	07/28/78	02.46.57.6	49.74	78.27	5.7	PDE
271	08/29/78	02.36.58.2* 02.37.06.5	49.84 50.01	78.01 79.00	5.0 5.9	PDE
274	04/25/75	04.59.57	47.50	47.50	4.7	Geotech/NORSAR
301 (721)	01/10/79	07.59.53	48.0	48.0	4.7	NORSAR
302 (722)	01/17/79	07.59.56	47.88	48.13	6.0	NORSAR
303 (718)	12/18/78	07.59.56	47.8	48.2	6.0	NORSAR
Greeley	12/20/66	15.30.00.1	37.30	-116.41	6.3	Dahlman and Israelson (1977)
Knickerbocker	05/26/67	15.00.00.0	37.25	-116.48	5.5	Dahlman and Israelson (1977)
Gasbuggy	12/10/67	19.30.00	36.68	-107.21	5.1	Dahlman and Israelson (1977)
Rulison	09/10/69	21.00.00	39.41	-107.95	5.3	Dahlman and Israelson (1977)

* Origin time of event analyzed
** Earthquake

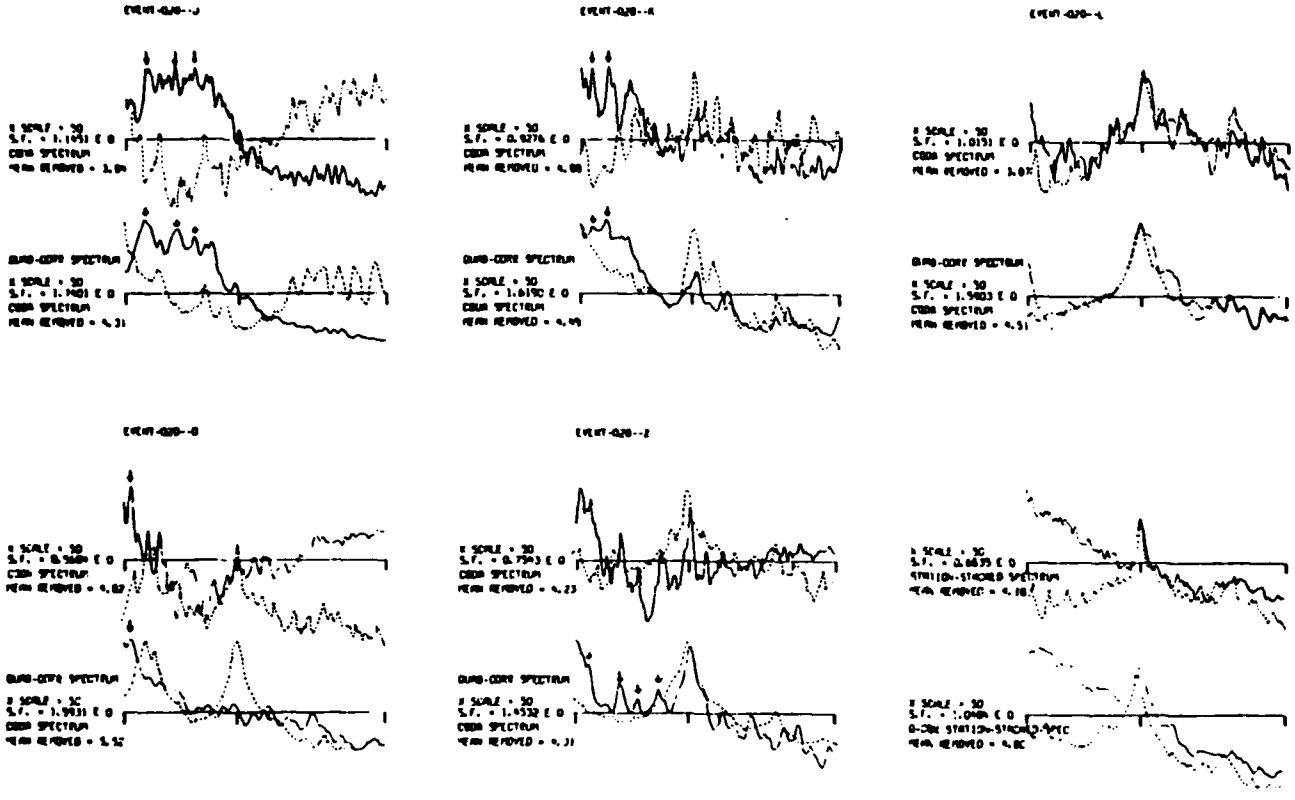

(U) THE ENHANCED CLARITY OF QUADCORRELATION SPECTRAL PEAKS WAS ACHIEVED AT THE EXPENSE OF RESOLUTION AND SENSITIVITY. ALTHOUGH SOME HIGH FREQUENCY PEAKS ARE SUGGESTED BY THE DATA, THEY ARE OF QUESTIONABLE QUALITY BECAUSE OF CORRESPONDING PEAKS IN THE NOISE, AND, PERHAPS, BECAUSE OF EFFECTS CAUSED BY UNDERSAMPLING
(NOTE: TICK MARKS ARE AT 1, 5, AND 10 Hz)
(SIGNAL, SOLID LINE; NOISE, DASHED LINE)

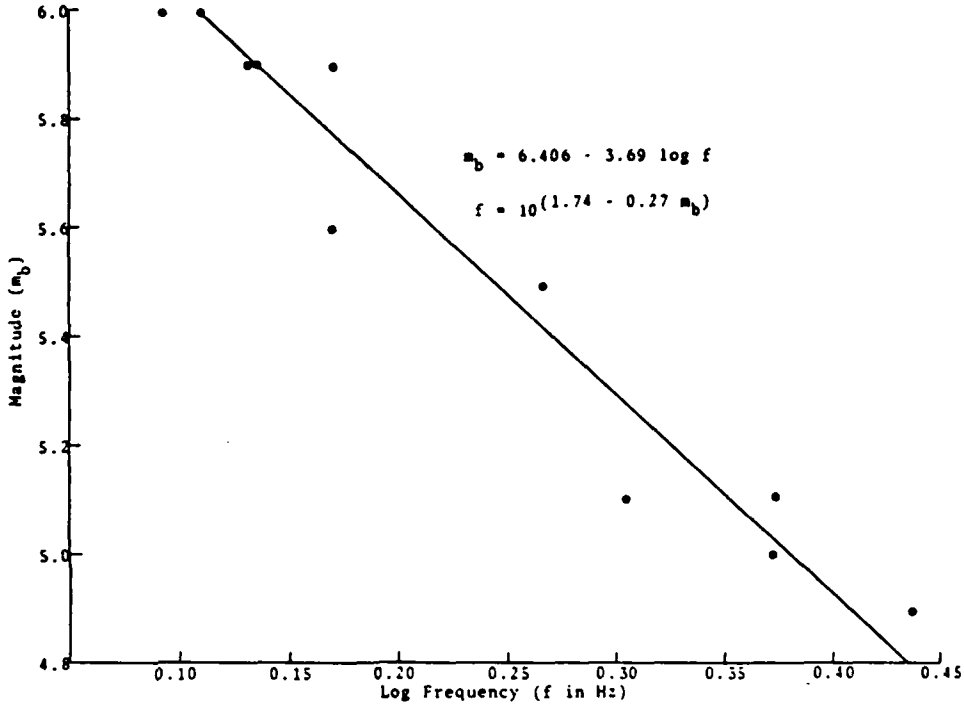

(U) m_b SCALING VERSUS BASE FREQUENCY OF CODA PERIODICITIES (VISUAL FIT)

(U) YIELD ESTIMATES FOR PRESUMED EXPLOSIONS

Event	Announced Yield (Rt)	Estimated Yield (kt)
20	--	263
22	--	18
53	--	176
81	--	266
267	--	169
271	--	17
274	--	9
302	--	333
303	--	403
Gasbuggy	29	38
Knickerbocker	71	57

ANALYSIS OF UNDERGROUND EXPLOSIONS IN SALT

R. Blandford

Project VT/0709 Contractor: Teledyne Geotech

Objective

The objective of this study is to better understand the frequency content of nuclear explosions detonated in salt. The detectability of explosions in salt is to be discussed.

Accomplishments

Several techniques for frequency domain analysis of the records of nuclear explosions have been developed at Geotech in recent years. Our first approach to this problem then involved evaluating these techniques on a salt explosion of known properties, i.e. SALMON.

In one technique it is assumed that the time delay, τ, and reflection coefficient, α, of pP are unknown, while the reduced displacement potential and absorption are known. Then, the likelihood is scanned for a maximum over a matrix of (τ, α). In Figure 1 we see that at every station except WFMN there is a maxima near $\tau = 0.5$ sec, $\alpha = -0.4$. This shows that the technique is robust at single stations. We have applied this technique, assuming the SALMON RDP, to the Azgir explosions of interest as recorded at NORSAR for those events which did not clip or have too narrow a frequency range for which $S/N > 1$. An example is seen in Figure 1. In general, the results were quite similar to those for SALMON showing that the Azgir reduced displacement potentials are not inconsistent with that of SALMON.

As the next step we planned to use the τ and α values as fixed parameters and use another program to determine the RDP. We found, however, that the answer is highly non-unique.

For example, in Figure 2 we see fits to the observed NORSAR spectrum for the overshoot parameter $B = 0.5$ (characteristic of SALMON) and $B = 3.0$. We see that there is a trade-off with other parameters such that both sets of parameters fit the data. Thus, if one of these sets of parameters were characteristic of a decoupled explosion we would not be able to tell it from a coupled explosion. Thus, the best we can hope for is to test the hypothesis that an observed signal is inconsistent with a preselected RDP; we cannot determine the RDP uniquely. Analysis will continue along a new line with five other events of interest. By the end of the contract, we plan to have tested the hypothesis that each signal at each AEDS and SRO station is consistent with the SALMON RDP, appropriately scaled. AEDS data will be very limited, it will mostly consist of North American station data. Considerable contract effort has been devoted to a systematic gathering of AEDS digital data. In general terms, the data quality, completeness, and documentation level was poor, and the return on effort in gathering this data was small. On the other

Task 4.4 Evasion Studies

Accomplishments continued

hand, the SRO data is excellent, and good results can be expected.

At NORSAR, we have found the peak in the signal to noise ratio for these salt explosions to be in the 3 to 4 Hz band as shown in Figure 3 for one of the larger events of interest, and for the smallest salt event of which we are aware. The data are from a single element of the C3 subarray at NORSAR. Thus, we see that the smallest salt explosion of which we are aware is easily detectable in the 3 to 4 Hz band at NORSAR.

The optimum detection filter for the explosions, S/N^2 where S is the signal amplitude spectrum and N is the noise amplitude spectrum, will differ according to the spectrum of the source, the noise spectrum at the receiver, the absorption along the path and the instrument response at the receiver. Using the noise just before the arrival of the salt events we have computed the appropriate filter at NORSAR and most of the AEDS stations. Figure 4 shows two examples. We see that for reasonable t* values of 0.2 to 0.4, the first filter peaks between 2 to 4 Hz and the second between 1.5 to 4 Hz.

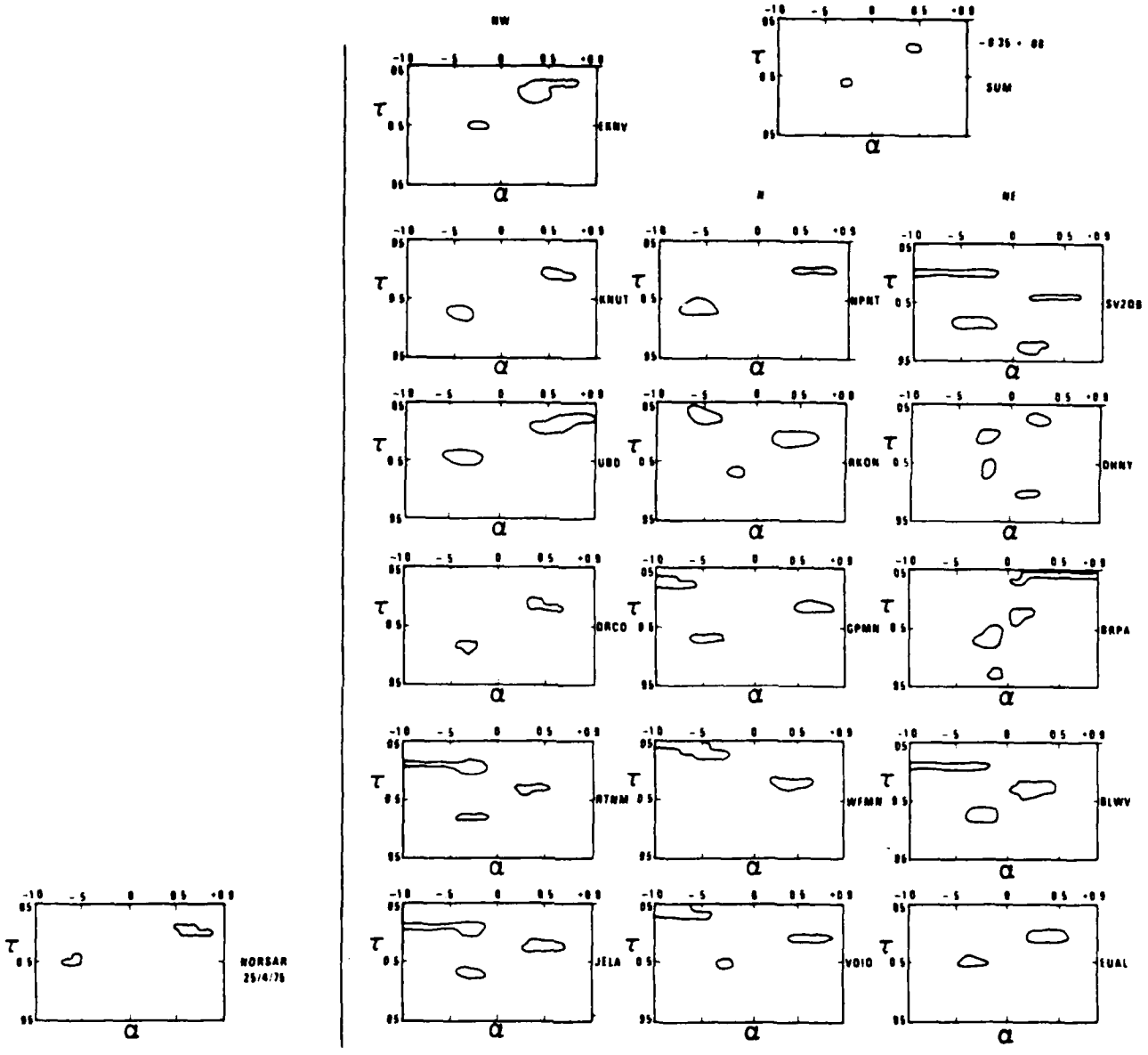

Figure 1. Likelihood as a function of a secondary arrival delay (τ) and reflection coefficient (α). We see that for SALMON there is a consistent multiple with a negative reflection coefficient with a delay near 0.5 seconds. A similar result is obtained for a single NORSAR recording of an explosion in salt.

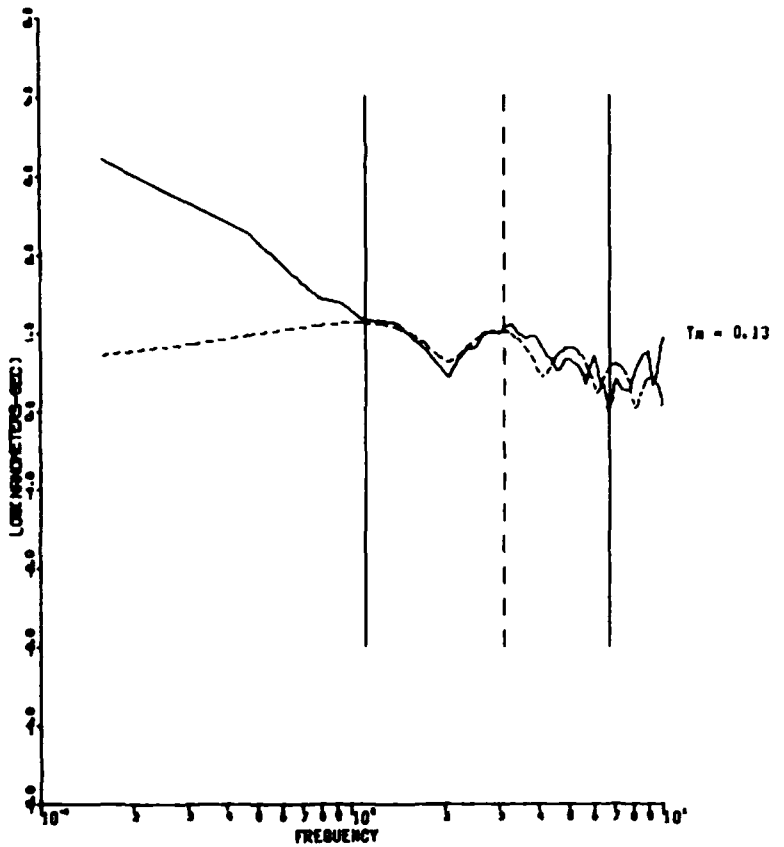

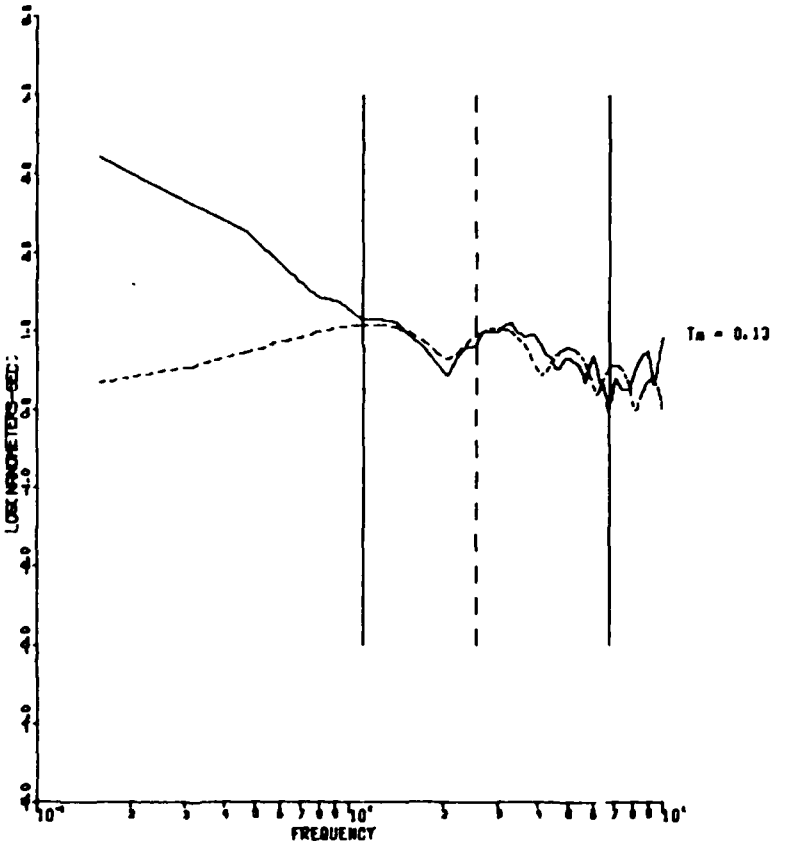

B = 0.5
Ω_0 = 8.9
k = 19.1749
0.3854

B = 3.0
Ω_0 = 3.3
k = 15.8069
0.3908

Figure 2. Fits of two greatly different source functions to the same observed spectrum as observed at NORSAR from a salt explosion. This illustrates the non-uniqueness of teleseismic determinations of the salt reduced displacement potential.

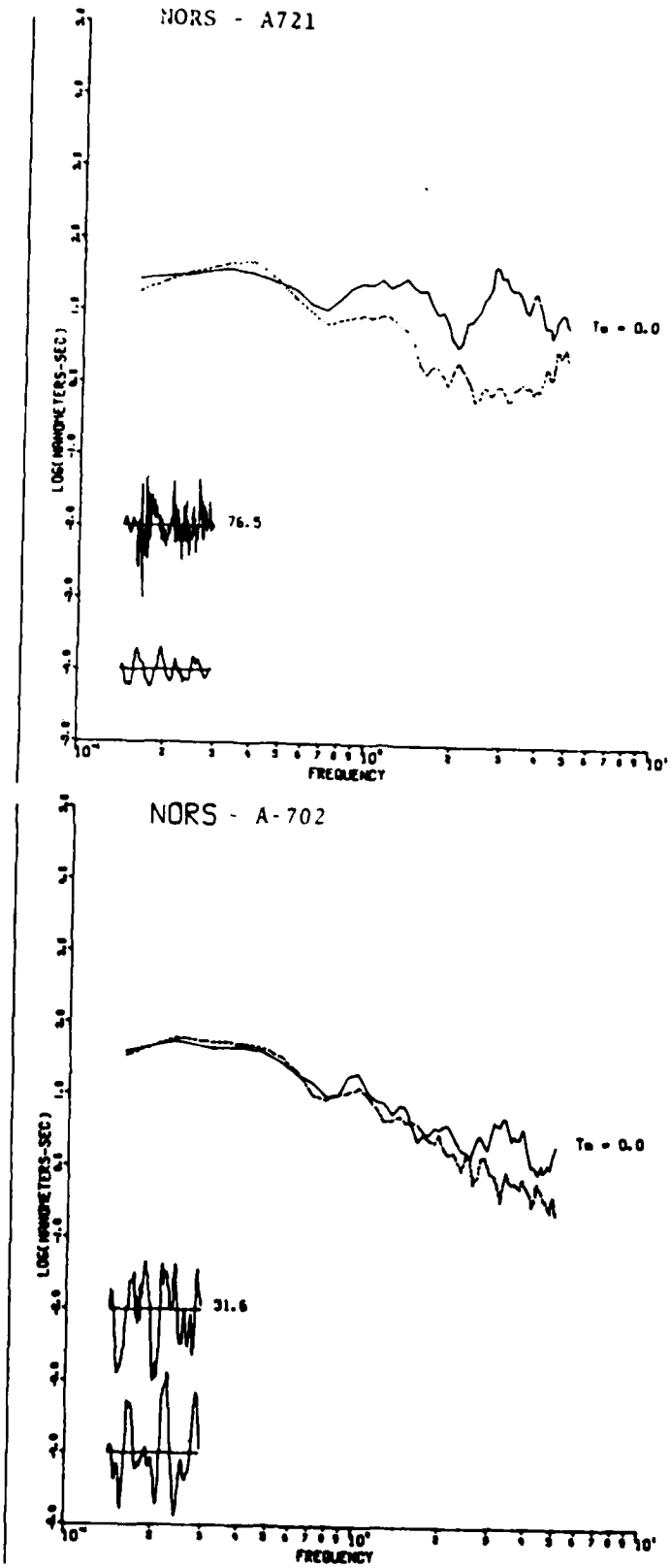

Figure 3. Illustration of the S/N ratio for a large and small salt explosion as seen at NORSAR. The peak in S/N is between 3 and 4 Hz for both events.

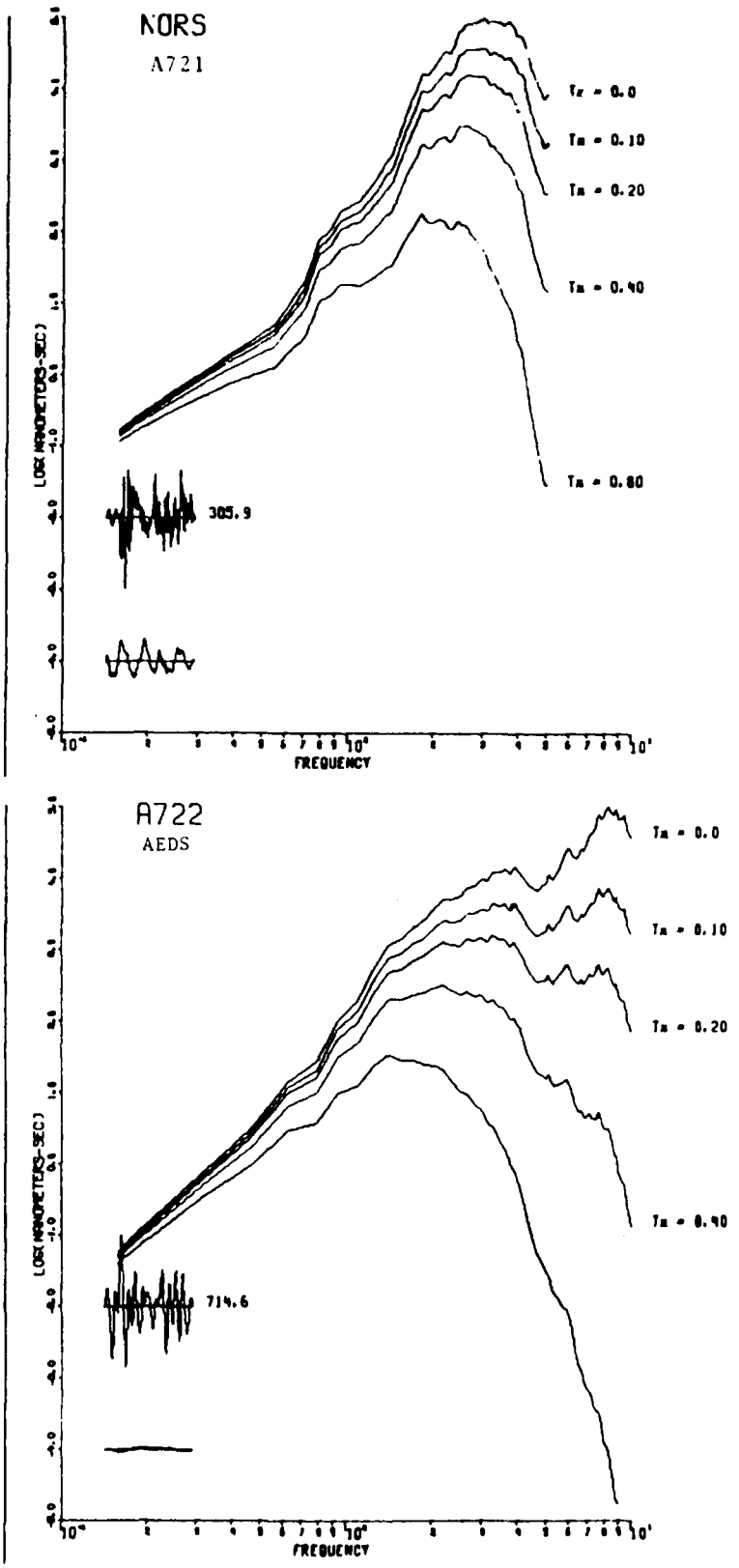

Figure 4. Optimum detection filters for slat explosions at two stations as a function of the appropriate absorption parameter for the path.

A SIMULATION STUDY OF THE DETECTABILITY OF A 5.3 KT DECOUPLED EXPLOSION AT REGIONAL DISTANCES IN THE EASTERN UNITED STATES

J. R. Murphy
T. J. Bennett

Project VT/0712

Contractor: Systems, Science and Software

Task 4.1.3 Decoupling/Evasion

Objective

The objective of this task has been to conduct a preliminary theoretical evaluation of CTBT evasion capabilities associated with the cavity decoupling evasion scenario. In particular, the investigation has focused on extending the existing regional seismic data base for explosions in the eastern United States by theoretically scaling observed SALMON data to simulate the seismograms to be expected from a hypothetical, fully decoupled 5.3 KT explosion at the SALMON shotpoint.

Accomplishments

Four eastern United States stations were selected for analysis: Eutaw, Alabama (EUAL, Δ = 246 km), Cumberland Plateau Observatory, Tennessee (CPO, Δ = 623 km), Beckley, West Virginia (BLWV, Δ = 1065 km) and Wykoff, Minnesota (WFMN, Δ = 1437 km). The locations of these four stations are indicated by squares on Figure 1 which provides a map view of the North American Stations which recorded the SALMON event (Jordan et al., 1966). The observed vertical component SALMON data recorded at these four stations have been theoretically scaled (Murphy, 1977) to the ground motion to be expected from a fully decoupled 5.3 KT explosion at the SALMON shotpoint. The selected theoretical decoupling factor (with respect to SALMON), corresponding to a simple step in pressure in a 39 m radius cavity, is shown in Figure 2. Observed SALMON vertical component seismograms recorded at stations EUAL and WFMN are shown at the top of Figures 3 and 4 respectively, where they are compared with the corresponding simulated decoupled seismograms (bottom). The simulated decoupled seismograms were obtained by convolving the observed SALMON seismograms with an operator defined by the ratio of the decoupled to SALMON theoretical source functions. The traces shown to the left of the simulated decoupled seismograms correspond to samples of the noise recorded prior to SALMON at each station, amplified so that they can be compared with the estimated decoupled signal levels. This provides a basis for assessing the detectability of the hypothesized decoupled explosion at these stations under the local noise conditions prevailing at the time of the SALMON experiment. A review of this simulated data, as well as that from the other two selected stations, indicates that, relative to

the noise background prevailing during SALMON, a 5.3 decoupled explosion would probably have been detectable on the short-period recordings from the two nearer stations (EUAL and CPO) but not from those expected at the more distant stations (BLWV and WFMN). With respect to the lower noise background expected at a modern, quiet site, the L_g phase from such a decoupled explosion would probably be detectable at all four stations, but initial P wave detection would still be questionable at the two distant stations. Furthermore, as might be expected on the basis of previous noise studies, increasing the effective bandwidth of the short-period data to encompass lower frequencies does not improve this detectability due to the fact that the noise level increases with decreasing frequency while the decoupling factor remains essentially constant. By the same argument, consideration of higher frequency data should improve detectability, at least for high Q paths. However, it has not been possible to quantitatively evalute this potential improvement using the available data set due to the relatively low sampling rate employed in the digitization.

REFERENCES

Jordan, H. N., W. V. Mickey, W. Helterbran and D. W. Clark, 1966, "Travel Times and Amplitudes from the SALMON Explosion," J.G.R., 71, No. 14.

Murphy, J. R. and T. J. Bennett, 1980, "A Simulation Study of the Detectability of a 5.3 KT Decoupled Explosion at Regional Distances in Eastern United States," Technical Memo to Major G. Wayne Ullrich, VSC, May 6, 1980.

Murphy, J. R., 1977, "Seismic Source Functions and Magnitude Determinations for Underground Nuclear Detonations," Bull. Seism. Soc. Amer., 67, No. 1.

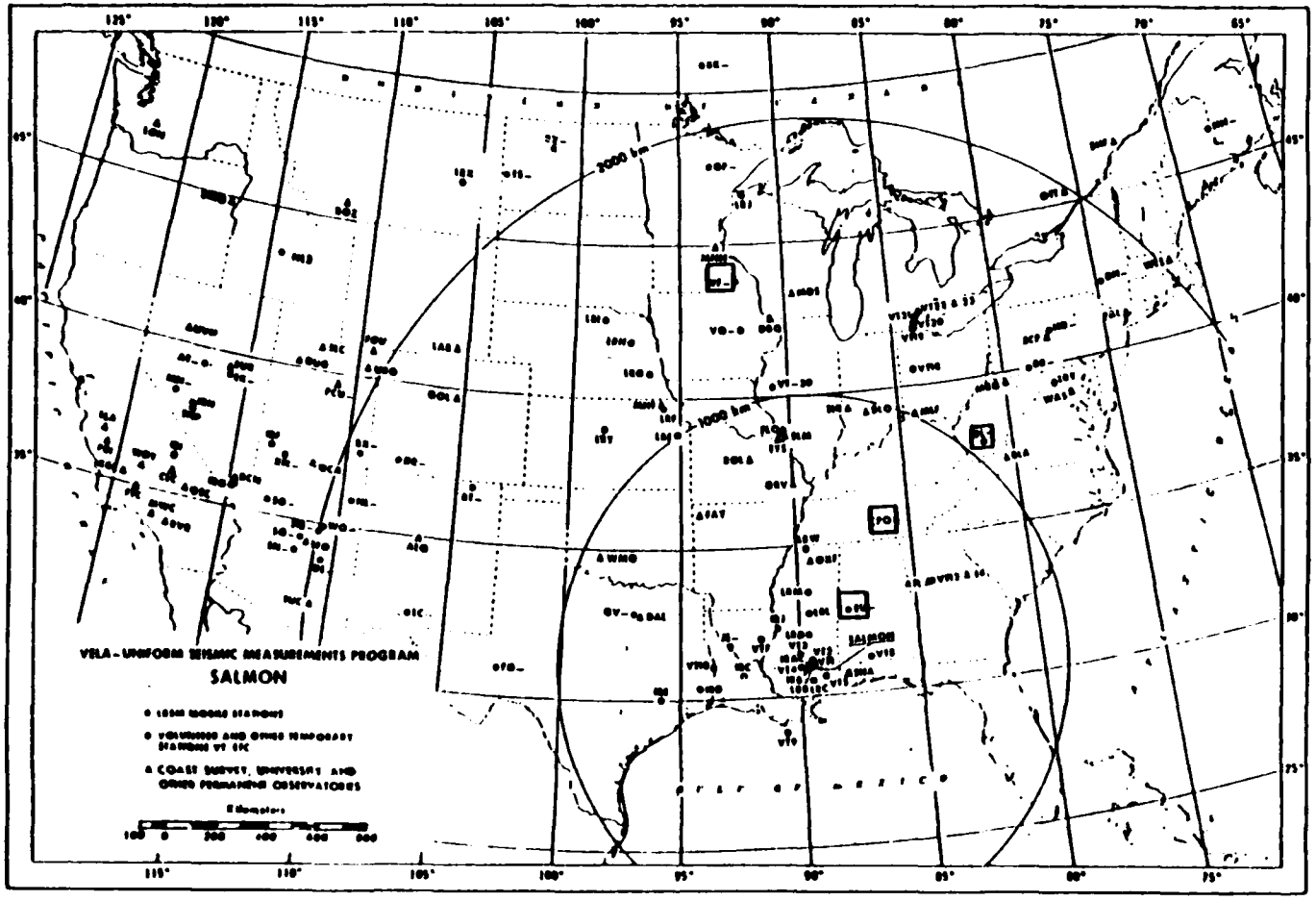

Figure 1. Map locations of regional SALMON stations (□) used in the decoupling simulation.

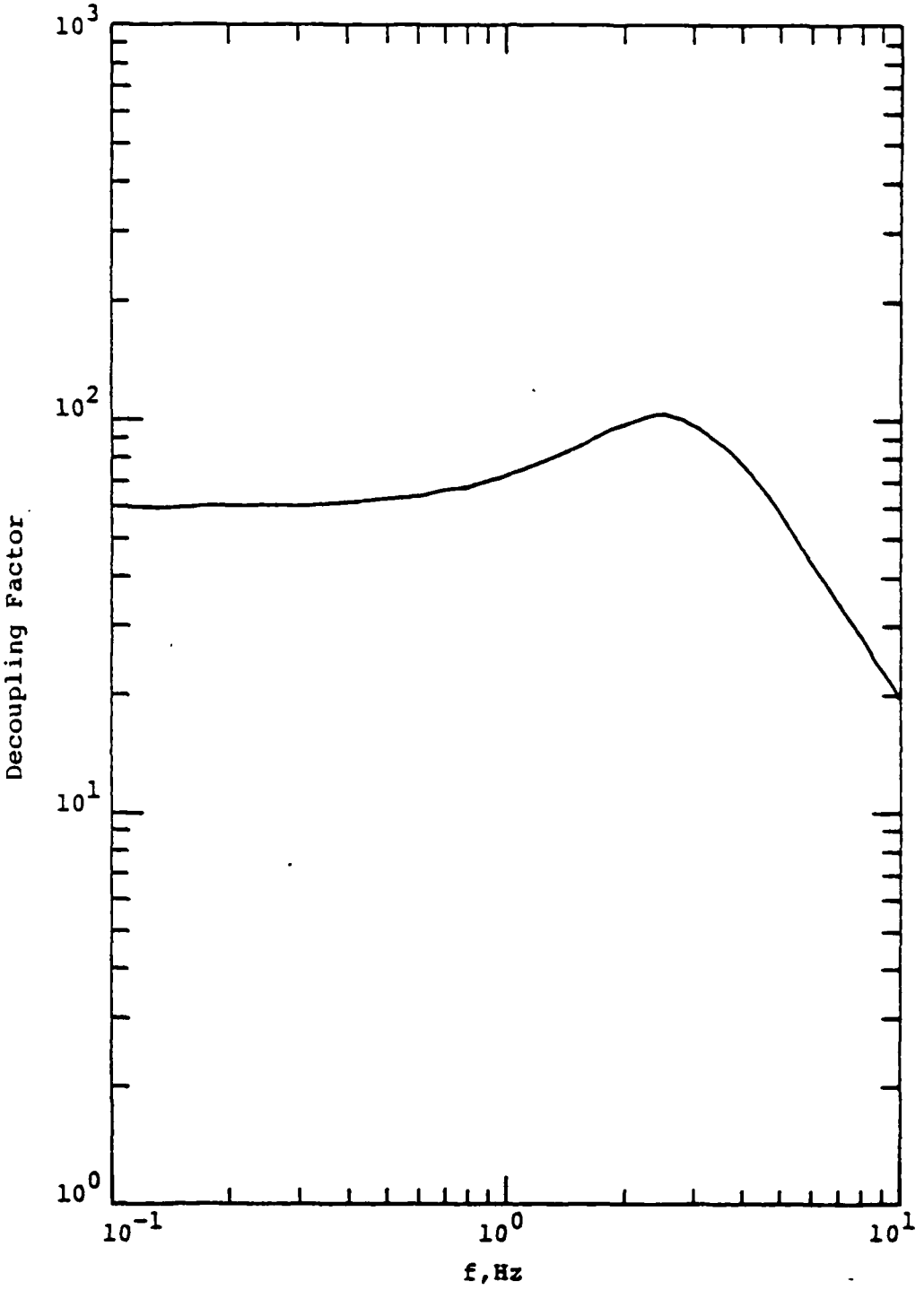

Figure 2. Theoretical decoupling factor for 5.3 KT in a 39 m radius cavity in SALMON salt.

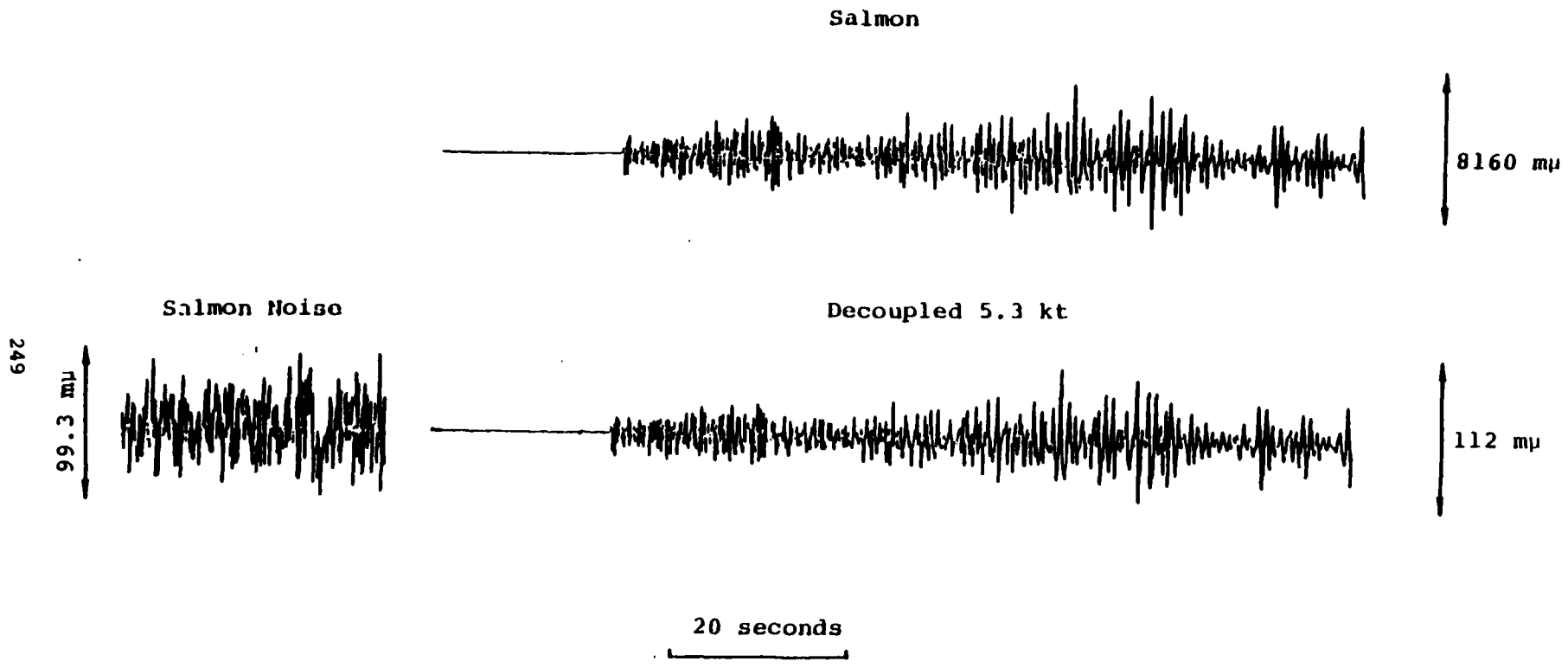

Figure 3. Comparison of observed SALMON and simulated decoupled vertical component seismograms, station EUAL.

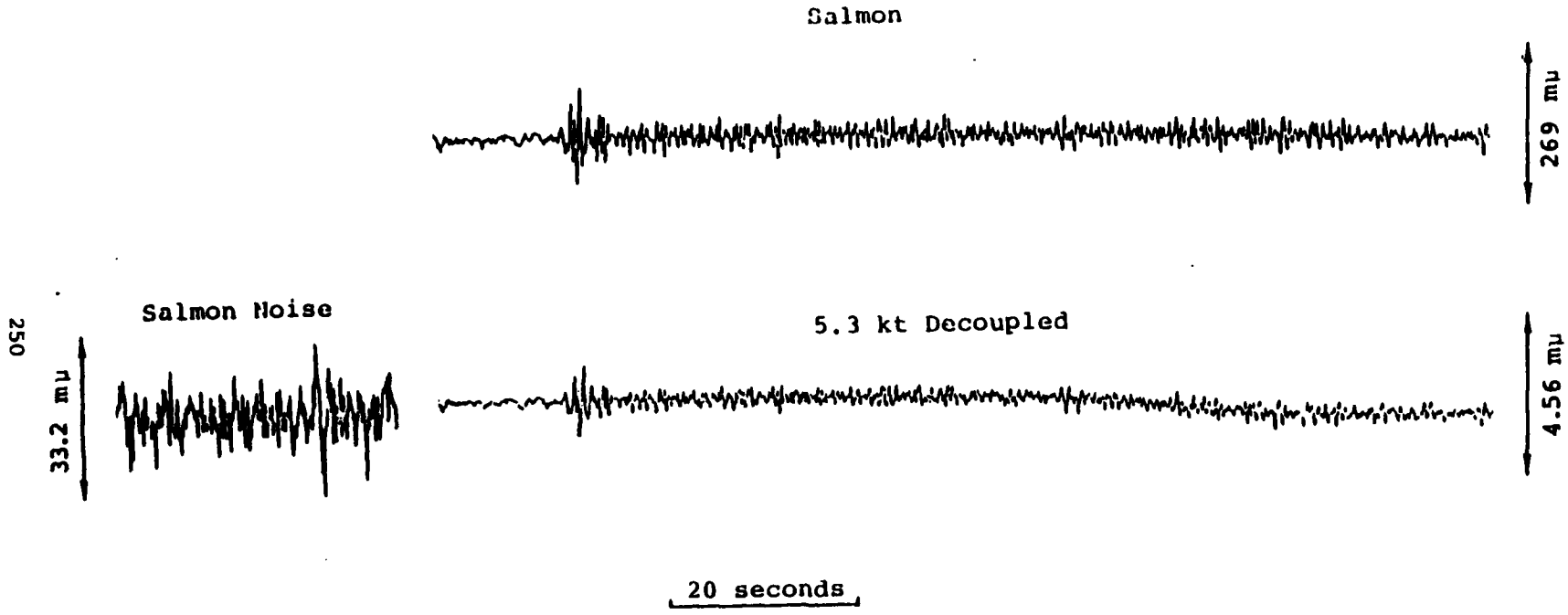

Figure 4. Comparison of observed SALMON and simulated decoupled vertical component seismograms, station WFMN.

SEISMIC VERIFICATION STUDIES

R. Blandford, Z. Der

Project VT/0709 Contractor: Teledyne Geotech

Task 4.6 Seismic Verification Studies

Objective

Perform special data analyses and theoretical research efforts on problems of seismic monitoring and related technical matters as directed by the project officer.

Accomplishments

Gain Ranging

A study has been completed and a report submitted to VSC on the subject of gain ranging and related formats. The report concluded that a suitable format for field recording and for archival storage is a 16-bit non-gain-ranged word which may be expanded to a 32-bit non-gain-ranged word in the event of large signals. A flag in the first word signifies the presence or absence of the second word.

Variability of Regional Phase Amplitudes at LASA

In earlier work using TFO recordings of 240 NTS explosions (Blandford and Klouda, 1980) it was found that log P_n and LR had a standard deviation with respect to yield of 0.35 while the standard deivation for P_g and L_g was only 0.25. The P_g/L_g discriminant ratio was found to be very stable with a standard deviation of only 0.15. Work at NTS (Barker et al, 1980) showed that there were P_g and L_g amplitudes up to 1.0 magnitude unit higher on the sediments at Yucca and Pahute as compared to on granite at the Climax stock, but that the P_g/L_g ratio did not change. Work by Chang and von Seggern (1977), used the variability of teleseismic P wave amplitudes at LASA together with a reciprocity theorem to place limits on the precision with which relative yields could be determined as a function of test-site separation were nuclear tests conducted in an area similar to LASA.

The study performed under this task is similar to the work of Chang and von Seggern except that it uses regional phases as recorded at LASA. Since this is only an exploratory study only three events were studied, all NTS explosions. The event files were scanned for the time period for which film was recorded at LASA, and events were selected for which the phases P_n, P_g, and L_g could all be read. The three possible events then were DISCUS THROWER, STODDARD, and NOOR. In Figure 1 we see the log amplitudes for DISCUS THROWER. As expected, P_n has the lowest amplitudes, P_g the highest, and L_g is intermediate. A cursory inspection also shows that P_n has the highest variance. This immediately suggests that both from a receiver point of view and by reciprocity, from a source point of view P_g and L_g would be better to use for yield estimation.

In Figure 2 we see the average root mean square variance of phase log amplitude as a function of distance between subarrays averaged over all three events. Again we see that the variance is greatest for P_n. For all three

Task 4.6 Seismic Verification Studies

Accomplishments continued

phases the variance increases with separation. These results place limits on the achievable precision which can be attained in relative yield determination by means of regional phases. To derive conclusions relative to the precision attainable by a network of regional stations it would be necessary to analyze approximately 20 events spaced azimuthally around LASA. Earthquakes would be perfectly suitable for such a study and can be measured from the film.

Excitation of Shear Waves by Shallow Events

Recent reports of the reversal of Rayleigh wave polarity from some Soviet explosions has prompted an examination of the literature and data sources on shear wave radiation from shallow explosions. Papers by such authors as Kisslinger, Aki and Toksöz have been reviewed. The mining literature for explosion in hard rock has been reviewed at Penn State, however, no relevant references or sources of data were found. Telephone conversations have been carried out with McEvilly, Stump, Drake and Leslie R. Hill at Sandia in attempts to track down sources of original data. We have received from Stump a 780 page pre-multiple burst data report (PMBII-78) with a promise to mail any digital data we might require. From Drake we have received a list of publications on the UET, MODE, JANGLE, AIR VENT, SCOOTER, PRE-GONDOLA, and CENSE test series. These test series range from the mid 1940's to late 70's. Their library in Vicksburg seems to be a good source. We have not yet been able to establish contact with LLL in reference to the data from their Rayleigh wave experimental program at Yucca Lake. Upon tabulation of these sources some data will be obtained and moment tensor inversions undertaken.

We have also examined LRSM data for Rayleigh waves from shots of interest. Investigations of long-period records for SEDAN, PAR, SCHOONER, HAYMAKER and MISSISSIPPI, nuclear explosions closely spaced in alluvium at varying depths of burial fails to reveal any difference in the Rayleigh wavetrains, the visual match at common stations is quite good. The transverse motion differs considerably though and we are planning to investigate these and the short-period records in the follow-up of this work. Inspection of records for the events analyzed by Rygg showed that the phase reversal did not occur at the MSH station, this appears to indicate a lobate radiation pattern characteristic of strain release and unrelated to the depth of burial.

High Frequency Propagation at Regional Distances

Analysis of signals from SALMON/STERLING indicated that decoupling tends to be less efficient at high frequencies. To detect such events at regional distances the propagation characteristics of high frequency energy in the crust must be well understood. We are presently conducting a literature survey of high frequency observations and at the same time cataloging and evaluating a possible data base to be used in such research. The survey of literature thus far indicates that observations of high frequency (up to 20 Hz) energy are quite common at distances of a few hundred kilometers from the source and there are reports of observations of 10 Hz at distances around 1000 km.

Task 4.6 Seismic Verification Studies

Accomplishments continued

There are also reports of Q increasing with frequency in the crust (Mitchell, 1979; Tsujiura, 1978). It appears therefore that detection at high frequencies is not as difficult as it would appear from some constant Q arguments. Some data analysis at the RKON station of the SDCS program showed considerable 6 to 10 Hz energy from about a 2.5° distance.

References

Barker, B. W., Z. A. Der and C. P. Mrazek (1980). The effect of crustal structure on the regional phases P_g and L_g at NTS, Studies of Seismic Wave Characteristics at Regional Distances, AL-80-1, Teledyne Geotech, Alexandria, Virginia.

Blandford, R. R., and P. J. Klouda (1980). Magnitude yield results at the Tonto Forest Observatory, Studies of Seismic Wave Characteristics at Regional Distances, AL-80-1, Teledyne Geotech, Alexandria, Virginia.

Chang, A. and D. von Seggern (1979). A study of amplitude anomaly and m_b bias at LASA subarrays, SDAC-TR-77-11, Teledyne Geotech, Alexandria, Virginia.

Mitchell, B. J. (1979). Frequency dependence of Q_β in the continental crust, (manuscript), Semi-annual Report for AFOSR, 1 Oct. 1978 - 31 Mar. 1979, Saint Louis University, Saint Louis, Missouri.

Tsujiura, M. (1978). Spectral analysis of coda waves from local earthquakes, Bull. Earthq. Res. Inst., Tokyo, 53, 1-48.

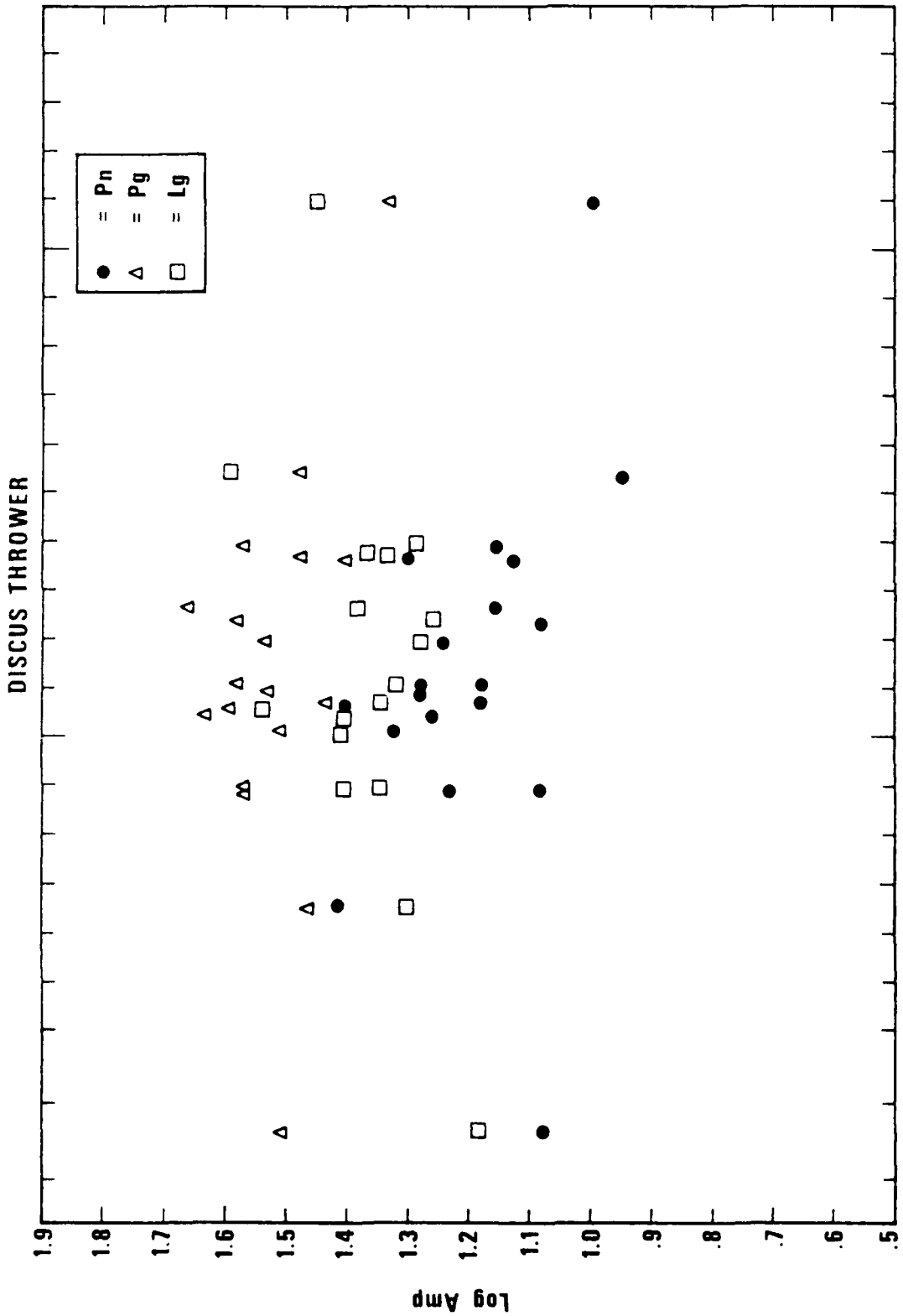
DISCUS THROWER
= Pn
= Pg
= Lg
Log Amp
1.9
1.8
1.7
1.6
1.5
1.4
1.3
1.2
1.1
1.0
.9
.8
.7
.6
.5
11
12
13
Distance from NTS to LASA subarrays (°)

Figure 1.

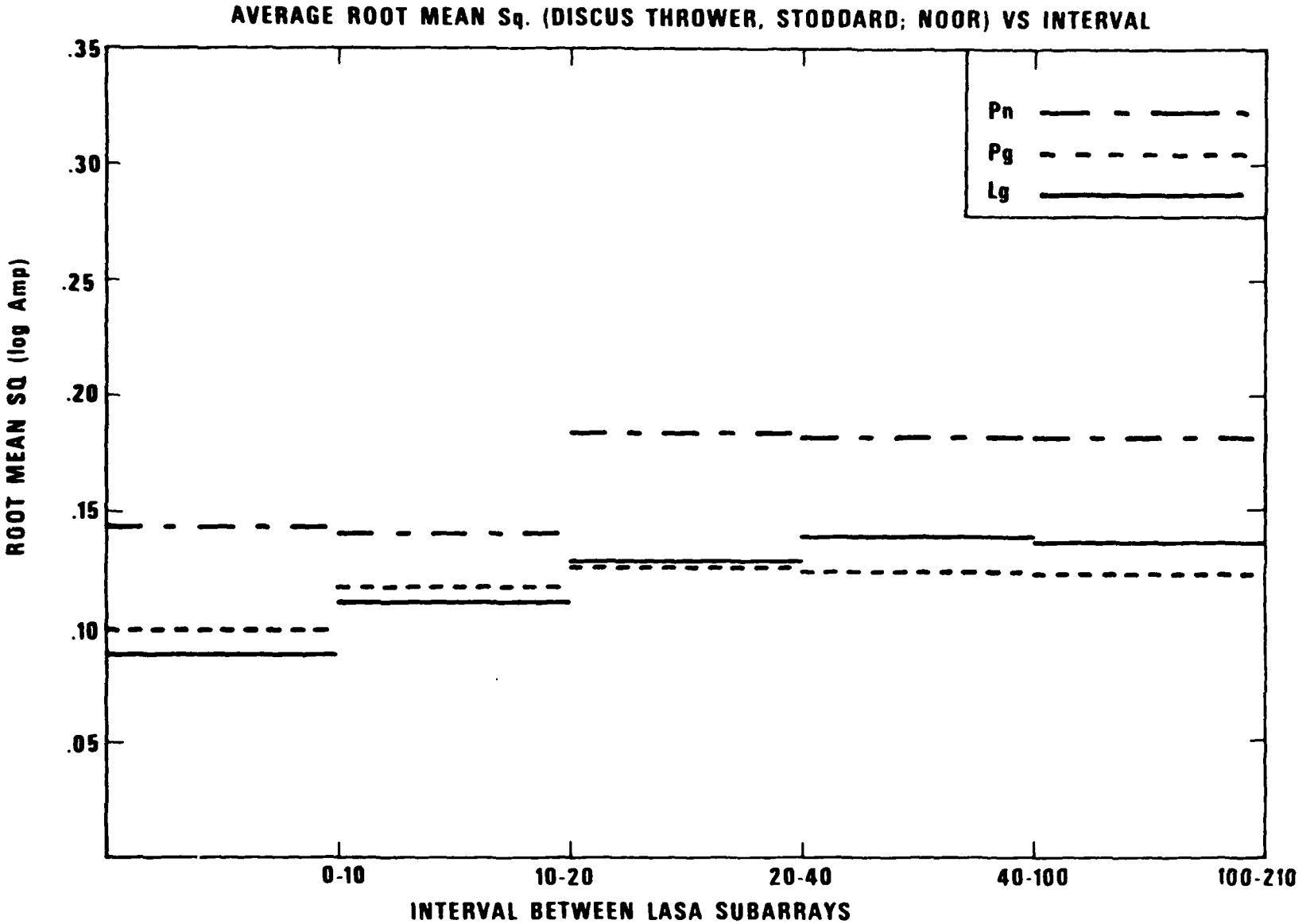
AVERAGE ROOT MEAN Sq. (DISCUS THROWER, STODDARD; NOOR) VS INTERVAL
ROOT MEAN SQ (log Amp)
.35
.30
.25
.20
.15
.10
.05
Pn
Pg
Lg
0-10
10-20
20-40
40-100
100-210
INTERVAL BETWEEN LASA SUBARRAYS

Figure 2.